



Joint Department of Naval Architecture and Marine Engineering
The Universities of Glasgow and Strathclyde

Instability of Riser Fairings in Currents

By
Mahdi Khorasanchi



UNIVERSITY
of
GLASGOW



THE
UNIVERSITY OF
STRATHCLYDE
IN GLASGOW

The Universities of Glasgow and Strathclyde
Joint Department of Naval Architecture and Marine Engineering

Instability of Riser Fairings in Currents

by

Mahdi Khorasanchi

Submitted in accordance with the requirements for the degree of
Doctor of Philosophy

September 2009

© Mahdi Khorasanchi, 2009

The candidate confirms that the work submitted is his own and that appropriate credit has been given where reference has been made to the work of others.

The copyright of this thesis belongs to the author under the terms of the United Kingdom Copyright Acts as qualified by University of Strathclyde Regulation 3.51. Due acknowledgment must always be made of the use of any material contained in, or derived from, this thesis.

Acknowledgment

This research project would not have been possible without the support of many people. It is a pleasure to convey my gratitude to them all in my humble acknowledgment.

Firstly, I would like to express my gratitude to Professor Shan Huang for his supervision, advice and constant support throughout my studies. From the very early stages of my arrival in Glasgow to the extraordinary opportunities throughout my research, his expertise, friendliness and patience, has added considerably to my graduate experience and exceptionally inspired and enriched my growth as a student and a researcher. I appreciate his vast knowledge and skill in many areas and his invaluable assistance in writing technical reports, scholarship applications and this thesis.

I would also like to thank my parents and family for the support they have provided me throughout my life. In particular, I am deeply indebted to my beloved spouse, who has always prepared the ground for my progress. Her smile and encouragement has been a constant oasis of hope and love for me.

I would like to acknowledge my dear friend, Stuart Alexander McKenna, who munificently spent his time to read this entire thesis.

I am grateful to the faculty and staff of the Department of Naval Architecture and Marine Engineering, especially Thelma Will, Fiona Cameron, David Smith and David Percival for their help and support.

I acknowledge with gratitude the financial supports provided to me by different organisations during the pursuance of my PhD. I recognise that this research would not have been possible without the PhD Studentship that The Universities of Glasgow and Strathclyde generously granted me. I must also thank them for Mac

Robertson Travelling Scholarship to attend a research project in Norway. Thanks are also due to The Institute of Marine Engineering, Science and Technology (IMarEST) for their prestigious Stanley Gray Fellowship. I am also grateful to The Aberdeen Society of Petroleum Engineers (SPE) for their valuable Bursary Award.

Finally, I sincerely thank the Almighty for his omnipresence throughout my life, in the time of hardships and loneliness as well as in the time of happiness and success.

CONTENTS

NOTATION	IX
ABSTRACT	XII
CHAPTER 1 INTRODUCTION.....	1
1.1 Need for Energy	1
1.2 The Meaning of Deepwater	2
1.3 Types of Riser.....	6
1.4 A Danger for Deepwater Risers	12
CHAPTER 2 AIMS OF THE THESIS.....	15
CHAPTER 3 CRITICAL REVIEW.....	16
3.1 Vortex-Induced-Vibration (VIV)	16
3.2 Impact on Deepwater Marine Risers	21
3.3 Methods of Mitigating VIV	24
3.4 Vortex-Shedding Suppression Devices	28
3.5 Riser Fairing.....	30
3.6 Areas Needing Research.....	44
3.7 Why ‘Instability of Fairing’ for Further Research.....	47
3.8 Research Strategy	49
CHAPTER 4 DYNAMICS OF INSTABILITY IN FAIRINGS	51
4.1 Introduction	51
4.2 Types of Fluid-Induced-Vibration.....	52
4.3 Classical Flutter	55
4.4 Differences from Classical Wing Flutter.....	59
4.5 Methodology	61
CHAPTER 5 2D THEORETICAL MODEL.....	66
5.1 Introduction	66
5.2 Governing Equations of Motion.....	68
5.3 Hydrodynamic Forces and Effect of Motion on AoA	74
5.4 Linearization.....	76
5.5 Eigenvalue Analysis	80
5.6 Dimensionless Form.....	84
5.7 Verification.....	89
5.8 Torsional Friction Damping	91
5.9 Discussion	100

CHAPTER 6 KEY PARAMETERS	105
6.1 Introduction	105
6.2 Calculation of Properties	108
6.3 Example	117
6.4 Results of Parametric Investigation	123
6.5 Summary	132
CHAPTER 7 SECTION HYDRODYNAMIC COEFFICIENTS.....	134
7.1 Introduction	134
7.2 Thick Foil and Available Methods	135
7.3 Fairing Profiles	136
7.4 Definitions	139
7.5 Discretization, Mesh Convergence and Reynolds Number	141
7.6 Summary Results.....	148
7.7 Fairing Length vs. Operational Constraints.....	163
7.8 Concluding Remarks	165
CHAPTER 8 3D THEORETICAL MODEL	167
8.1 Introduction	167
8.2 General Case.....	169
8.3 Uniform Case	190
8.4 Verification.....	194
8.5 Comments.....	200
CHAPTER 9 3D EXAMPLE AND PARAMETRIC STUDY	203
9.1 Introduction	203
9.2 An Example of the General Case	204
9.3 Parametric Study	208
9.4 Summary of Findings	222
CHAPTER 10 DISCUSSION	224
10.1 A Look Back	224
10.2 Own Contributions	227
10.3 Future Research	228
CHAPTER 11 CONCLUSION.....	230
REFERENCES.....	232
APPENDIX A: CFD RESULTS.....	240
NACA0070.....	241
Short Fairing.....	247
Guide Vane.....	253
Exxon's Fairing without Fin.....	259
Exxon's Fairing with Fin (3%).....	265
Exxon's Fairing with Fin (5%).....	271

Contents

Exxon's Fairing with Fin (7%).....	277
Fairings Offset Table.....	283

List of Figures

Figure 1-1 World Energy Consumption Over The Past Two Decades (BP, 2007).	2
Figure 1-2 Evolution of Deep Water Production Capability (Patel, 1989).	3
Figure 1-3 Bottom Supported and Vertically Moored Deepwater Systems.	4
Figure 1-4 Floating Production Systems in Deepwater.	4
Figure 1-5 Top Tensioned Risers (TTR).	7
Figure 1-6 Catenary Riser Layout.	8
Figure 1-7 Flexible Riser.	9
Figure 1-8 Flexible Riser Configurations (Bai and Bai, 2005).	10
Figure 1-9 Hybrid Riser System.	11
Figure 1-10 Hybrid Riser Main Components.	12
Figure 3-1 Single Vortex in Ideal Fluid.	16
Figure 3-2 Two Potential Vortices with Opposite but Equal Circulation (Blevins, 2001).	17
Figure 3-3 Infinite Double Staggered Row of Vortices (Blevins, 2001).	18
Figure 3-4 Bound Vortices Behind a Circular Cylinder a) Schematic b) Flow Visualisation.	19
Figure 3-5 Von Karman Vortex Street Aft of a Circular Cylinder.	20
Figure 3-6 Variation of Pressure Distribution in Vortex Shedding (Blevins, 2001).	20
Figure 3-7 Add-on Devices for VIV Suppression of Cylinders (Blevins, 2001, Kumar et al., 2008).	29
Figure 3-8 Typical Geometry of a Riser Fairing.	31
Figure 3-9 Tail-Fin Fairing (Lee et al., 2006a).	31
Figure 3-10 Ortloff et al Fairing (Ortloff et al., 1983).	32
Figure 3-11 Short Fairing (Allen and Henning, 1995b).	33
Figure 3-12 Flexible Fairing (Allen and Henning, 1995a).	33
Figure 3-13 Ultra-Short Fairings (Allen and Henning, 2001c).	33
Figure 3-14 Snap-on Rotating Reduction Fairing (Masters et al., 2002).	34
Figure 3-15 Riser Fairing at Installation, Submergence and Operation.	35
Figure 4-1 Typical Response of A System vs. Reduced Velocity.	52
Figure 4-2 Galloping (Plunge) – 2D.	54
Figure 4-3 Galloping (Torsion) – 2D.	54
Figure 4-4 Flutter – 2D.	54
Figure 4-5 Schematic Pattern of Fairing Flutter in 3D.	55
Figure 4-6 Plunge and Torsion Out of Phase in Flutter.	56
Figure 5-1 Local and Global Coordinates, Degrees of Freedom.	68
Figure 5-2 Instantaneous Angle of Attack (AoA).	75
Figure 5-3 ExxonMobil Fairing on a Rigid Cylinder.	89
Figure 5-4 Trend of Eigenvalues by Velocity Increment.	91
Figure 5-5 Effect of Considering Friction Damping.	97
Figure 5-6 Effect of Considering Friction, Coulomb Term.	99
Figure 5-7 Effect of Considering Friction, Coulomb and Hysteretic Terms.	99
Figure 5-8 Equilibrium AoA.	103
Figure 6-1 Geometry of Typical Fairing.	109
Figure 6-2 Added Polar Mass Moment of Inertia for an Ellipse.	113
Figure 6-3 Riser Fairing for SEDCO 702 (Grant and Patterson, 1977).	118
Figure 6-4 Force Coefficients of Fairing Model (Grant and Patterson, 1977).	121
Figure 6-5 Trend of Eigenvalues by Velocity Increment.	122
Figure 6-6 U_{cr} vs. Drag Coefficient.	123
Figure 6-7 U_{cr} vs. Lift Coefficient.	124

Figure 6-8 U_{cr} vs. Moment Coefficient.....	125
Figure 6-9 Trend of Eigenvalues at High Moment Coefficient.....	125
Figure 6-10 U_{cr} vs. Transverse Damping.....	126
Figure 6-11 U_{cr} vs. Torsional Damping.....	127
Figure 6-12 U_{cr} vs. A.....	128
Figure 6-13 U_{cr} vs. γ^2	129
Figure 6-14 U_{cr} vs. S_r	130
Figure 6-15 U_{cr} vs. R_r	131
Figure 7-1 Coordinate System in CFD Analysis.....	139
Figure 7-2 Computational Domain and Mesh, NACA0070.....	142
Figure 7-3 Mesh Close to The Fairing, NACA0070.....	142
Figure 7-4 Hydrodynamic Coefficients vs. Re_c , NACA0070 at 15°	147
Figure 7-5 Amplitude of Hydrodynamic Coefficients vs. Re_c , NACA0070 at 15°	147
Figure 7-6 Hydrodynamic Coefficients & Their Amplitudes vs. Re_c , NACA0070 at 15°	148
Figure 7-7 Sample Result, Time History of Lift Coefficient, NACA0070 at 0°	149
Figure 7-8 Drag Coefficients of Different Sections.....	150
Figure 7-9 Drag Coefficient Amplitudes of Different Sections.....	150
Figure 7-10 Drag Coefficients & Their Amplitudes of Different Sections.....	151
Figure 7-11 Lift Coefficients of Different Sections.....	153
Figure 7-12 Lift Coefficient Amplitudes of Different Sections.....	153
Figure 7-13 Lift Coefficients & Their Amplitudes of Different Sections.....	154
Figure 7-14 Moment Coefficients of Different Sections.....	156
Figure 7-15 Moment Coefficient Amplitudes of Different Sections.....	156
Figure 7-16 Moment Coefficients & Their Amplitudes of Different Sections.....	157
Figure 7-17 Strouhal Number of Different Sections.....	158
Figure 7-18 Effect of Adding Fin on Mean Pressure Coefficient At 0°	160
Figure 7-19 Effect of Adding Fin on Mean Pressure Coefficient At 5°	160
Figure 7-20 Necessary Conditions of Stability.....	162
Figure 7-21 Capability of Suppressing VIV at 0°	162
Figure 7-22 Modification in Circular Head of Fairing, a) Original b) Modified.....	164
Figure 8-1 Three-Dimensionality of Riser with Fairings.....	168
Figure 8-2 Free Body Diagram, 3D Model.....	170
Figure 8-3 Fairing II on The Flexible Riser Model (Braaton et al., 2008).....	194
Figure 8-4 Effect of Considering Limited Number of Modes.....	198
Figure 8-5 Threshold of Instability Onset, Test Results (Braaton et al., 2008).....	199
Figure 8-6 Frequency of Predominant Vibration, Test Results (Braaton et al., 2008).....	200
Figure 8-7 Effect of Missing Lower Modes in U_{cr}	201
Figure 8-8 U_{cr} vs. Mode Number, Uniform Case.....	202
Figure 9-1 Effect of Considering Limited Number of Modes.....	207
Figure 9-2 Trajectory of Eigenvalues, General Case, First 3 Modes.....	207
Figure 9-3 U_{cr} vs. Drag Coefficient, 3D Model.....	209
Figure 9-4 U_{cr} vs. Lift Coefficient, 3D Model.....	210
Figure 9-5 Mode Change Due to Increase of Lift Coefficient, 3D Model.....	210
Figure 9-6 U_{cr} vs. Moment Coefficient, 3D Model.....	211
Figure 9-7 Mode Change Due to Increase of Moment Coefficient, 3D Model.....	211
Figure 9-8 U_{cr} vs. Transverse Damping, 3D Model.....	212
Figure 9-9 U_{cr} vs. Torsional Damping, 3D Model.....	213
Figure 9-10 U_{cr} vs. A, 3D Model.....	214

List of Figures

Figure 9-11 U_{cr} vs. γ^2 , 3D Model.	215
Figure 9-12 Mode Change Due to Increase of γ^2 , 3D Model.	215
Figure 9-13 U_{cr} vs. S_r , 3D Model.	216
Figure 9-14 Mode Change Due to Increase of S_r , 3D Model.	216
Figure 9-15 U_{cr} vs. R_r , 3D Model.	217
Figure 9-16 U_{cr} vs. TTF, 3D Model.	218
Figure 9-17 U_{cr} vs. Flexural Factor (FF), 3D Model.	219
Figure 9-18 U_{cr} vs. Length of Coverage, 3D Model.	220
Figure 9-19 Mode Change Due to Increase of Coverage Length, 3D Model.	220
Figure 9-20 Sheared Current Profile.	221
Figure 9-21 U_{cr} vs. Bottom/Top Ratio of Current Speed, 3D Model.	222
Figure A-1 Hydrodynamic Coefficients & Their Amplitudes.	241
Figure A-2 Computational Domain And Mesh.	242
Figure A-3 Mesh Close To The Fairing.	242
Figure A-4 Pressure Coefficient At 0°	243
Figure A-5 Mean Pressure Coefficient Around The Fairing Surface At 0°	243
Figure A-6 Pressure Coefficient At 5°	244
Figure A-7 Mean Pressure Coefficient Around The Fairing Surface At 5°	244
Figure A-8 Pressure Coefficient At 10°	245
Figure A-9 Mean Pressure Coefficient Around The Fairing Surface At 10°	245
Figure A-10 Pressure Coefficient At 15°	246
Figure A-11 Mean Pressure Coefficient Around The Fairing Surface At 15°	246
Figure A-12 Hydrodynamic Coefficients & Their Amplitudes.	247
Figure A-13 Computational Domain And Mesh.	248
Figure A-14 Mesh Close To The Fairing.	248
Figure A-15 Pressure Coefficient At 0°	249
Figure A-16 Mean Pressure Coefficient Around The Fairing Surface At 0°	249
Figure A-17 Pressure Coefficient At 5°	250
Figure A-18 Mean Pressure Coefficient Around The Fairing Surface At 5°	250
Figure A-19 Pressure Coefficient At 10°	251
Figure A-20 Mean Pressure Coefficient Around The Fairing Surface At 10°	251
Figure A-21 Pressure Coefficient At 15°	252
Figure A-22 Mean Pressure Coefficient Around The Fairing Surface At 15°	252
Figure A-23 Hydrodynamic Coefficients & Their Amplitudes.	253
Figure A-24 Computational Domain And Mesh.	254
Figure A-25 Mesh Close To The Fairing.	254
Figure A-26 Pressure Coefficient At 0°	255
Figure A-27 Mean Pressure Coefficient Around The Fairing Surface At 0°	255
Figure A-28 Pressure Coefficient At 5°	256
Figure A-29 Mean Pressure Coefficient Around The Fairing Surface At 5°	256
Figure A-30 Pressure Coefficient At 10°	257
Figure A-31 Mean Pressure Coefficient Around The Fairing Surface At 10°	257
Figure A-32 Pressure Coefficient At 15°	258
Figure A-33 Mean Pressure Coefficient Around The Fairing Surface At 15°	258
Figure A-34 Hydrodynamic Coefficients & Their Amplitudes.	259
Figure A-35 Computational Domain And Mesh.	260
Figure A-36 Mesh Close To The Fairing.	260
Figure A-37 Pressure Coefficient At 0°	261

List of Figures

Figure A-38 Mean Pressure Coefficient Around The Fairing Surface At 0°	261
Figure A-39 Pressure Coefficient At 5°	262
Figure A-40 Mean Pressure Coefficient Around The Fairing Surface At 5°	262
Figure A-41 Pressure Coefficient At 10°	263
Figure A-42 Mean Pressure Coefficient Around The Fairing Surface At 10°	263
Figure A-43 Pressure Coefficient At 15°	264
Figure A-44 Mean Pressure Coefficient Around The Fairing Surface At 15°	264
Figure A-45 Hydrodynamic Coefficients & Their Amplitudes	265
Figure A-46 Computational Domain And Mesh	266
Figure A-47 Mesh Close To The Fairing	266
Figure A-48 Pressure Coefficient At 0°	267
Figure A-49 Mean Pressure Coefficient Around The Fairing Surface At 0°	267
Figure A-50 Pressure Coefficient At 5°	268
Figure A-51 Mean Pressure Coefficient Around The Fairing Surface At 5°	268
Figure A-52 Pressure Coefficient At 10°	269
Figure A-53 Mean Pressure Coefficient Around The Fairing Surface At 10°	269
Figure A-54 Pressure Coefficient At 15°	270
Figure A-55 Mean Pressure Coefficient Around The Fairing Surface At 15°	270
Figure A-56 Hydrodynamic Coefficients & Their Amplitudes	271
Figure A-57 Computational Domain And Mesh	272
Figure A-58 Mesh Close To The Fairing	272
Figure A-59 Pressure Coefficient At 0°	273
Figure A-60 Mean Pressure Coefficient Around The Fairing Surface At 0°	273
Figure A-61 Pressure Coefficient At 5°	274
Figure A-62 Mean Pressure Coefficient Around The Fairing Surface At 5°	274
Figure A-63 Pressure Coefficient At 10°	275
Figure A-64 Mean Pressure Coefficient Around The Fairing Surface At 10°	275
Figure A-65 Pressure Coefficient At 15°	276
Figure A-66 Mean Pressure Coefficient Around The Fairing Surface At 15°	276
Figure A-67 Hydrodynamic Coefficients & Their Amplitudes	277
Figure A-68 Computational Domain And Mesh	278
Figure A-69 Mesh Close To The Fairing	278
Figure A-70 Pressure Coefficient At 0°	279
Figure A-71 Mean Pressure Coefficient Around The Fairing Surface At 0°	279
Figure A-72 Pressure Coefficient At 5°	280
Figure A-73 Mean Pressure Coefficient Around The Fairing Surface At 5°	280
Figure A-74 Pressure Coefficient At 10°	281
Figure A-75 Mean Pressure Coefficient Around The Fairing Surface At 10°	281
Figure A-76 Pressure Coefficient At 15°	282
Figure A-77 Mean Pressure Coefficient Around The Fairing Surface At 15°	282

List of Tables

Table 1-1 Deepest Discovery in The Gulf of Mexico (Richardson et al., 2008).....	5
Table 7-1 Selected Fairing Profiles for CFD Analysis.....	138
Table 7-2 Effect of Mesh Convergence on Hydrodynamic Coefficients of NACA0070 at 15°.....	144
Table 7-3 Variation of Y^+ Due to Different Incidences, NACA0070.....	145
Table 7-4 Effects of Reynolds Number on Hydrodynamic Coefficients of NACA0070 at 15°.....	146
Table 8-1 Riser Model Data.....	195
Table 8-2 Faring II Data.....	195
Table 8-3 Accuracy of Calculated Mass vs. Measured Values.....	196

Notation

Abbreviations

2D	Two-dimension
3D	Three-dimension
AoA	Angle of attack
BHR	Bundled hybrid riser
CF	Cross-flow
CFD	Computational fluid dynamics
CR	Centre of rotation
deg	Degree
Dim	Dimension
DOF	Degree of freedom
GoM	Gulf of Mexico
HR	Hybrid riser
rad	Radian
SCR	Steel catenary riser
SHR	Single hybrid riser
TLP	Tension leg platform
TTR	Top Tensioned riser
VIV	Vortex induced vibration

Roman Characters

A	The inverse of mass ratio
A_b	Area of buoyancy module
A_s	Area of steel riser
A_f	Area of riser internal fluid
A_{fr}	Area of fairing
A_w	Area of entrapped water
b	Width of blunt end
d	Distance from middle of fairing to centre of rotation
c	Chord length of fairing
C_D	Drag coefficient, measured at CR with respect to chord length
C_{Dr}	Drag coefficient of bare riser, scaled to chord length
C_{Hyst}	Hysteretic damping coefficient
C_L	Lift coefficient, measured at CR with respect to chord length
$C_{M(cr)}$	Moment coefficient, measured at CR with respect to chord length

Notation

C_p	Pressure coefficient
C_y	Viscose damping coefficient, transverse DOF
C_θ	Viscose damping coefficient, torsional DOF
D	Cylinder diameter
E	Young's Modulus
f_n	Natural frequency in the mode of interest
f_s	Vortex shedding frequency
F_{int}^y	Interaction force, transverse DOF
F_{int}^θ	Interaction force, torsional DOF
I	Moment of inertia
$I_{N \times N}$	Identity matrix of size N
J	Polar mass moment of inertia
J_a	Added polar mass moment of inertia
k_y	Transverse stiffness of riser in 2D model
L	Riser length
L_{fr}	Length of fairing leeside
m	Sum of riser and fairing masses
m_a	Added mass
m_{fr}	Fairing mass
m_r	Riser mass
r_s	Outer radius of steel riser
r_f	Inner radius of steel riser
r_b	Outer radius of buoyancy module
r_t	Outer radius of total/fairing thickness, $\frac{1}{2} t$
R	Distance of reference point from CR
Re	Reynolds number
Re_c	Reynolds number based on chord length
R_r	Dimensionless form of R with respect to chord length
S	Strouhal number
S_a	Added first mass moment of area
S_r	Dimensionless distance of the gravity centre of all rotating masses
S_x	First mass moment of area
t	Thickness of fairing
t_{fr}	Thickness of fairing plate
T_a	Average tension
T_b	Bottom tension
T_t	Top tension
U	Free stream velocity
U_o	Reference velocity for a variable current profile
U_{cr}	Critical reduced velocity, $U_{ry(critical)}$
$U_{critical}$	Critical current velocity (m/s)
U_{rel}	Relative current velocity
U_{ry}	Reduced velocity of transverse motion
$U_{r\theta}$	Reduced velocity of torsional motion
V	Velocity vector
w_r	Wet weight per unit length
y	Transverse motion

Greek Characters

α	Instantaneous angle of attack
γ	Dimensionless radius of gyration with respect to chord length
Γ	Vortex circulation
θ	Distortion angle of fairing
μ	Friction coefficient
μ_{Fluid}	Dynamic viscosity of fluid
ν	Kinematic viscosity of fluid
ξ_y	Damping ratio of torsional motion
ξ_θ	Damping ratio of transverse motion
ρ	Water density
ρ_b	Buoyancy module density
ρ_f	Riser internal fluid density
ρ_{fr}	Fairing density
ρ_r	Riser density
ρ_s	Steel riser density
φ	Velocity potential function
ω_y	Natural frequency of transverse motion
ω_θ	Natural frequency of torsional motion

Abstract

Due to the growing demand for oil and gas the offshore industry has been moving its activities into deeper waters. As a consequence of this, the use of longer tubulars has become inevitable. Moreover, the move has also led to the subsea structures being exposed to more severe currents. These issues have caused an increasing concern as to how to suppress the vortex-induced-vibration (VIV) of marine risers in order to avoid their early fatigue failure.

The aims of this thesis were to investigate the mechanism of instability in riser fairings and to develop an analytical model to predict critical instabilities in the design phase. In particular the aim was to evaluate the mechanism of vortex formation, review the available methods of mitigating VIV, such as adding a vortex suppression device, and evaluate the advantages and disadvantages of using riser fairings.

Initially, an analytical model was developed for a simpler case of a two-dimensional (2D) problem. Governing equations were derived, based on Lagrange's equations, and then the hydrodynamic forces were calculated and the effect of motion in these forces was taken into consideration. The final equations were linearised and an eigenvalue analysis was employed to systematically obtain multiple solutions; to examine their stability with the emphasis on identifying the critical current speed for a given system. Some physically meaningful dimensionless parameters were defined and the characteristic equation was made dimensionless. This model was validated against the available test results and showed a good agreement. Then the impact of each dimensionless parameter in instability onset was assessed. This parametric study indicated hydrodynamic properties of fairing are very crucial to instability. Next, the behaviour of flow in vicinity of a selection of fairing profiles was evaluated, using a CFD method.

The results of this study demonstrate the effect of the section's details in hydrodynamic performance of fairing, in particular, the impacts of the angle of the leeside as well as adding fins to the trailing edge.

The next step in this research was to expand and apply the analytical 2D model to the 3D problem; a top tensioned vertical riser. A parametric study of a 3D model was carried out to assess the validity of the 2D parametric study and then to investigate the effect of the new parameters.

Overall, this study has provided riser designers with a theoretical tool to predict the instability onset in a system of riser and fairing and presented guidelines which can assist a riser engineer in impeding this destructive vibration in the event the preliminary design was diagnosed with the risk of instable behaviour.

Chapter 1

Introduction

1.1 Need for Energy

Energy has been continuously a major concern for man since the Stone Age. He has been looking for new sources of energy to move the wheel of life. Wood as fuel for fire and animals as power for agriculture were the primary types of energy throughout the early stages of human development. Due to population growth, a further demand for energy was induced and over many centuries man began to think and investigate other sources of energy. In the Palaeolithic Age wood was used for fire. Four thousand years later in the New Stone Age wood was then replaced by coal. Finally, six thousand years ago, petroleum was discovered as natural oil seeps on the ground's surface (Britannica, 2008) and became an accessible resource for ancient people.

Over the millenniums energy demand increased at a gradual rate until the late 18th century, when due to the industrial revolution, mankind's thirst for all kinds of energy intensified greatly at a rapid rate. This rapid change in human's energy consumption has never been quenched and is still rising dramatically year after year (Figure 1-1). According to the recent BP statistical report of world energy, the annual world energy consumption had about 62 percent growth over the past 26 years, a big jump from 6800 to 11000 million tonnes oil equivalent per year (BP, 2007).

Fossil fuels in general are still forming the major portion of this massive demand of energy. In particular, oil and natural gas alone provide about 60 percent of today's

world energy and this causes oil and gas to emerge as the foremost and top demanded source of energy in recent decades.

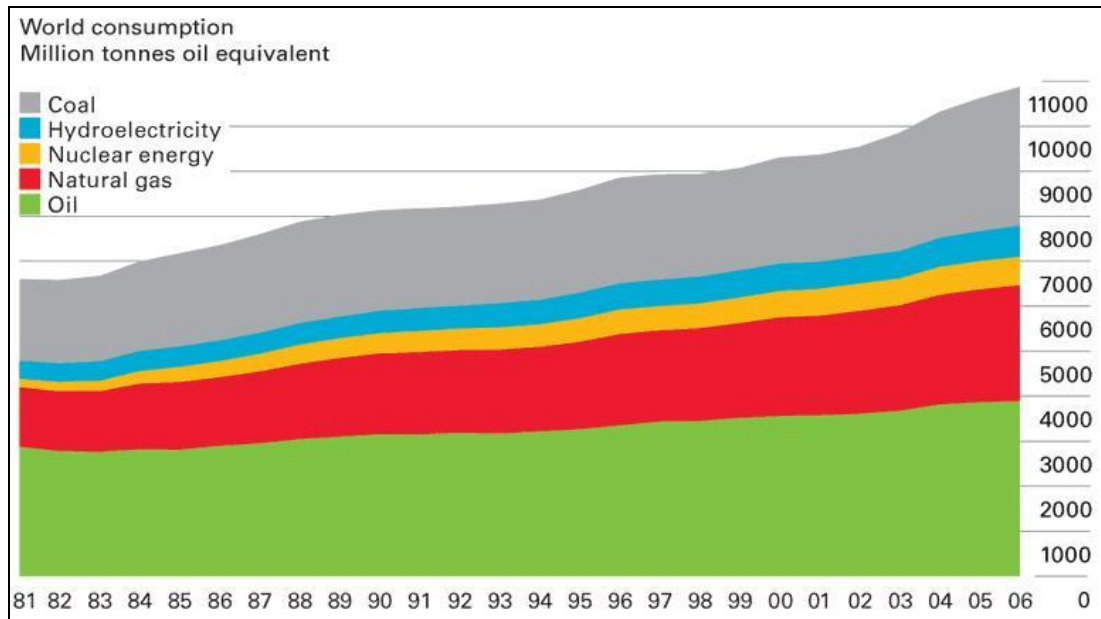


Figure 1-1 World Energy Consumption Over The Past Two Decades (BP, 2007).

Initially oil was collected from surface oil seeps. Then, people dug pits to facilitate the oil extraction. As the demand increased, surface oil collection did not yield enough supply and as a consequence of this the exploration for under-surface reservoirs started. The land-based exploration and production for crude oil was subsequently developed.

As the oil explorations were being extended, the oil pioneers of the late 1800's stepped into the sea in 1887 in California, where the first ever exploration drilling of more than a few feet of water was carried out (Patel, 1989). Since then, the trend of oil exploration and production in shallow water has gradually increased with the oil industry beginning its move offshore in the late 1940s, seeking new oil reservoirs with greater rewards (Patel and Witz, 1991).

1.2 The Meaning of Deepwater

The first offshore operations were in the United States where a gradual move was made from the swamps of Louisiana into the Gulf of Mexico (GoM). Exploration

began in shallow water of about 20 metres deep with the aid of submersible drilling units. Following the Second World War, offshore activity in GoM rapidly moved into deeper waters. By 1959, an oil production platform had been installed by Shell in 30.5 m of water.

Increasing oil prices accelerated exploration and production of deepwater installations, continuously pushing and changing the frontier of operations and definition of deepwater operations. Between 1970 and 1978, the capability of fixed platform in terms of water depth improved substantially from around 120 m through to the largest depth to date of 311 m in the GoM (Figure 1-2).

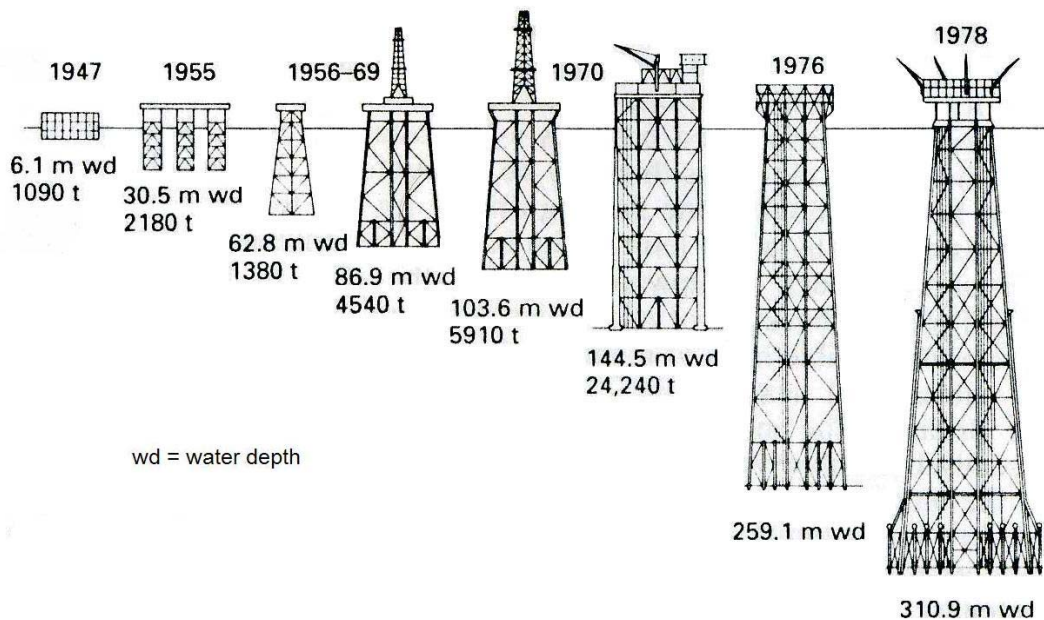


Figure 1-2 Evolution of Deep Water Production Capability (Patel, 1989).

Market demand for oil encouraged the oil industry to go deeper and deeper while fixed platforms could not be deployed in further depths. Consequently, as the meaning of deepwater was changing, the conceptual design of platforms was enhancing from fixed platform to 'Tension Leg Platform' (TLP), 'Spar platform' and finally 'Floating Production Systems' like FPSOs (Figure 1-3 and Figure 1-4).

In today's world with the recent advances in exploration and production technology the minimum water depth at which a field is classed as deepwater needs to be

redefined. However, due to its specific nature and further technological advances it is very likely that it will require a new definition in the future.

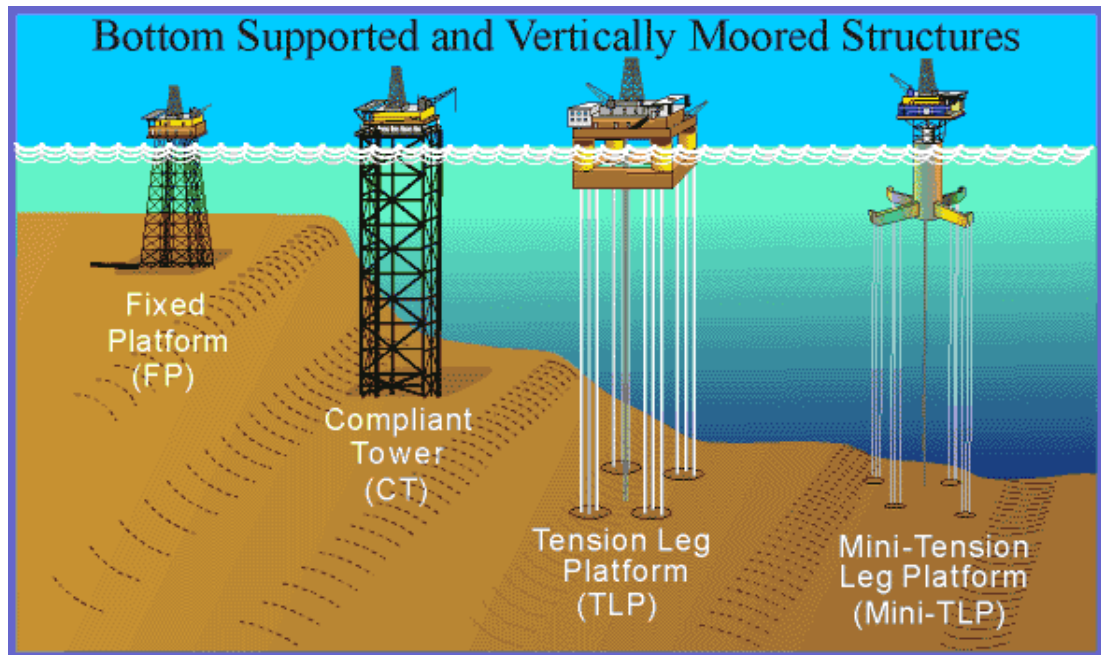


Figure 1-3 Bottom Supported and Vertically Moored Deepwater Systems.

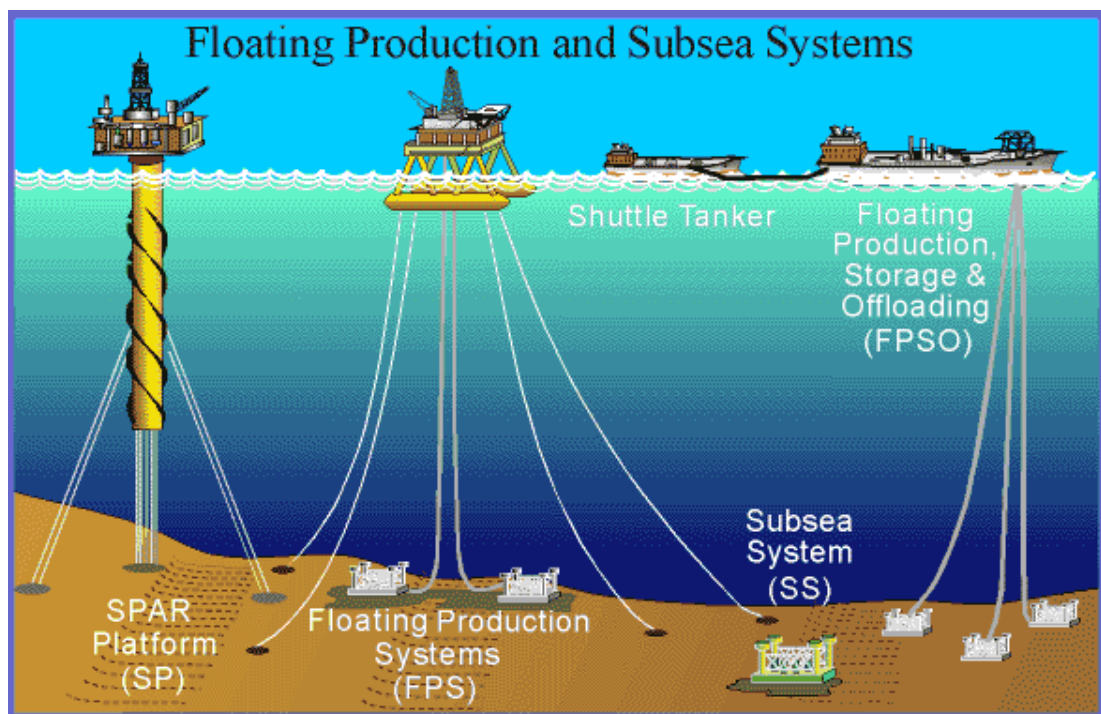


Figure 1-4 Floating Production Systems in Deepwater.

According to U.S. Department of Interior Minerals Management Services (MMS), water depth of more than 1,000 ft or 305 m is currently considered as ‘deep water’ and activities in depths of more than 5,000 ft or 1524 m is defined as ‘ultra-deep water’ (Richardson et al., 2008).

This very recent report shows that deep water has continued to be a very important part of the total GoM production. At the end of 2007, it provided approximately 72 percent of the oil and 38 percent of the gas in the region. Moreover, a record high of 15 rigs were operating in ultra-deep water. Twenty-two wells were drilled in water depths of 7,500 ft (2,286 m) or greater, representing 46 percent of all development wells drilled in 2007. This indicates the importance of deepwater operations at present. As tabulated in Table 1-1, exploration and discovery so far has been carried out in a water depth greater than 9,700 ft (2,950 m).

Table 1-1 Deepest Discovery in The Gulf of Mexico (Richardson et al., 2008).

Discovery	Water Depth (ft)	Discover year
Tiger	9,004	2004
Silvertip	9,226	2004
Tobago	9,627	2004
Stones	9,571	2005
Trident	9,721	2001

Thus, the concept of deepwater has completely changed throughout the 50-year history of offshore industry and now it is approaching the frontier of 3,000 m depth. Throughout the pioneering deep water discoveries there is one constant concept that has been always accompanying deep water production and that is the need for a tool to connect the seabed to the water surface, in other words, the need for a riser for drilling and production.

1.3 Types of Riser

A riser system essentially consists of conductor pipes connecting floaters on the surface to a wellhead on the seabed (Bai and Bai, 2005). The riser should be as short as possible to reduce the associated costs but it must have sufficient flexibility to allow for large displacement of the floater at top end.

There are generally two kinds of riser, rigid risers and flexible risers. A hybrid riser is a combination of these two.

The first generation of marine riser system was deployed on fixed platforms, normally located in shallow waters. It comprised of a continuous length of rigid pipe which was either clamped to the platform structure or put in a pre-installed guide casing. Rigid risers in deeper water, used later on, can be classified to subcategories of top tensioned riser (TTR) and catenary riser.

Top Tensioned Risers (TTRs)

TTR is used as a conduit between floating units, such as spars and tension leg platforms (TLPs), and subsea systems on the sea floor which are typically directly below the platform, allowing for vertical well access (Figure 1-5). Thus, TTR consists of vertical pipes drawn straight from seabed to sea surface. Like a cable, it is kept straight with the aid of high top tension at connection to the platform or support. TTR can serve throughout the offshore works for drilling, injection, production and export operations.

The ordinary TTR is very sensitive to heave motion of the top support due to wave or current loads because the rotation at top and bottom connection is limited. Moreover, heave motion alters the tension magnitude at the top and therefore it needs a tensioner to compensate the variation of the top tension. Lack of adequate top tension will cause larger bending moment along the riser especially if the riser is subject to harsh sea current.

In general, a TTR comprises of the following key components:

- Main body is made up of rigid segments known as joints. Steel is predominantly used in their fabrication however titanium, aluminium or composites are the other alternatives.
- Successive joints (typically of 50-ft length) are linked by connectors.
- The riser is supported at top end by a tensioning system called tensioner.



Figure 1-5 Top Tensioned Risers (TTR).

Some portions of the main body along the riser length may be covered by buoyancy modules to reduce the required tension at top end. Using buoyancy modules increases the diameter and can lead to some adverse side effects like higher drag force.

Catenary Risers

The catenary layout allows the riser to be self-compensated for the heave motion of the top end, i.e. the bottom part of riser is in contact with seabed and is lifted or lowered (Figure 1-6). The catenary riser still needs a ball/flex joint at the upper

support to provide rotational freedom. The bottom end can be smoothly laid down to the sea floor or can be connected directly to the subsea completion or wellhead through a steep wave configuration.

Steel catenary risers (SCR) are made up of steel joints. They can be assembled by welding or threading individual riser joints.

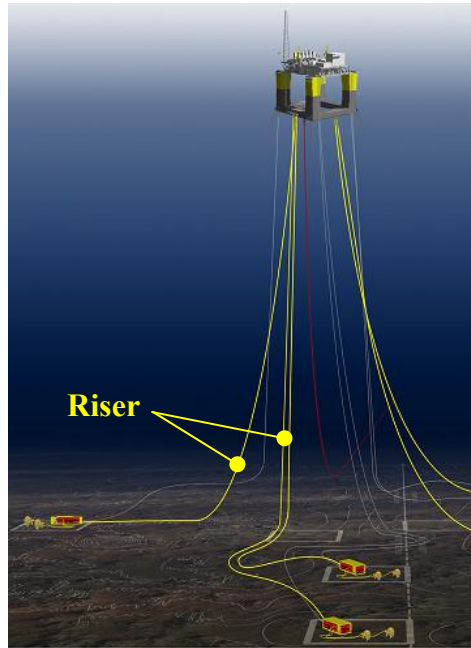


Figure 1-6 Catenary Riser Layout.

SCR in comparison with TTR can withstand larger vessel motion. Thus, it is a possible substitute to flexible riser for deepwater FPSOs (floating production, storage and offloading system) where the cost of riser system for new field development is significant compared to the total field development cost due to the number of riser lines needed. There has been an increasing interest in SCR as they are more cost effective due to the low unit cost of steel pipe compared to flexible pipe. Moreover, the possibility of selecting larger diameter for SCR is a bonus which allows higher flow rates and lower number of risers to be required.

But they are sensitive to environmental loads, e.g. wave and current because of low effective tension in the riser. The design and installation challenges of using SCR in

ultra-deepwater floating production system are primarily originated from higher hang-off tension caused by its weight.

Flexible Risers

Flexible pipes were initially used in calm weather environment in pioneering work carried out in the late 1970s (Bai and Bai, 2005). However, since then flexible pipe technology has developed rapidly and today flexible risers are employed in various projects with large vessel motions in harsh weather conditions.

Flexural flexibility of these risers (Figure 1-7) is achieved through the use of multiple concentric layers of different materials in the fabrication of pipe wall. This flexibility gives many advantages to this type of risers such as prefabrication and storage of long lengths on reel which reduces the transport and installation cost and also suitability for use in highly dynamic applications such as catenary moored vessels.

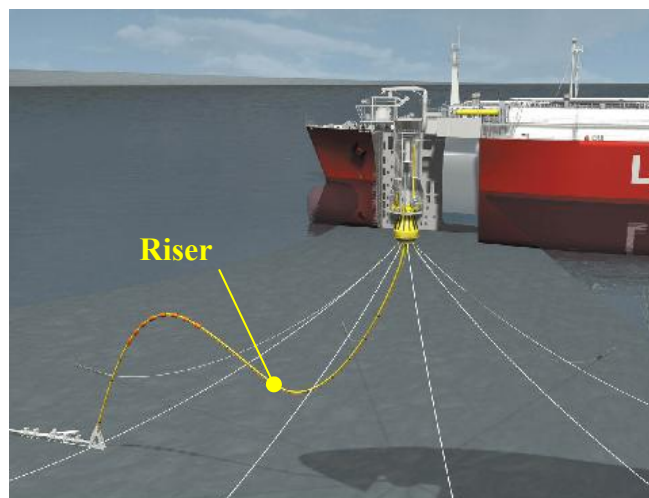


Figure 1-7 Flexible Riser.

Flexible riser configurations can be classified in six main groups as shown in Figure 1-8. The selected configuration is influenced by many parameters including water depth, host vessel access or hang-off location, field layout, environmental data and the host vessel motion characteristics.

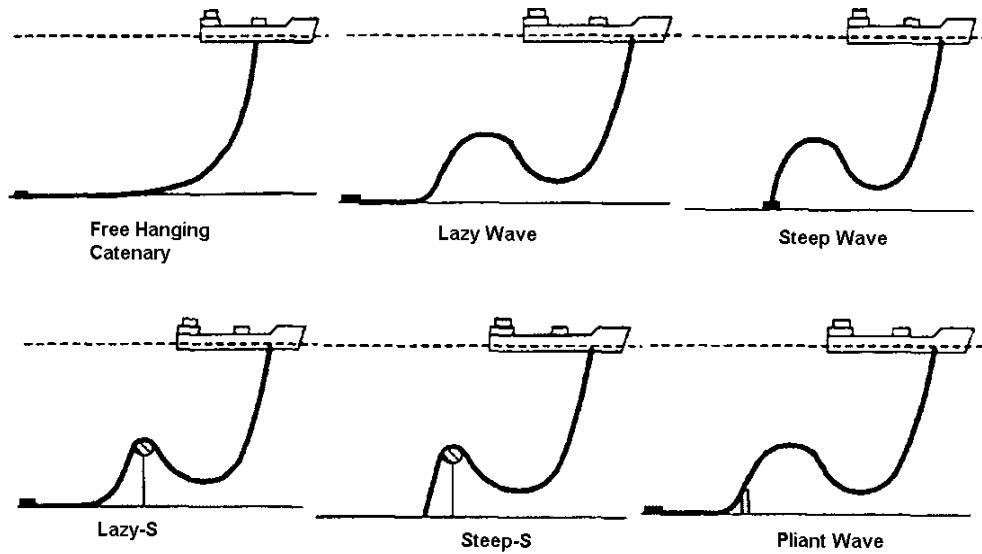


Figure 1-8 Flexible Riser Configurations (Bai and Bai, 2005).

Hybrid Risers

As the oil industry went further offshore and in deeper water, simultaneously the new concept of floating production, storage and offloading was introduced through the deployment of FPSO or semi-submersible vessels. The natural consequence of that was larger excursion of top floating structure. Thus, based on the available deepwater systems, a new riser system was devised to fulfil this need too. The single or multiple line hybrid risers (HR) aimed to de-couple the vessel motions from the vertical steel riser through the use of flexible jumpers (Figure 1-9).

The first use of hybrid risers was a single hybrid riser (SHR) installed in 1988 for production in Green Canyon by Cameron (Bai and Bai, 2005). As the hybrid risers became popular and attractive to engineers, the second generation were designed in the form of a bundled hybrid riser (BHR); fabricated at an onshore site with installation by towing out and upending for development of Total's Girassol field in West of Africa. More recently, the third generation hybrid riser was employed,

consisting of a SHR which could be installed from a drilling vessel (Bai and Bai, 2005).

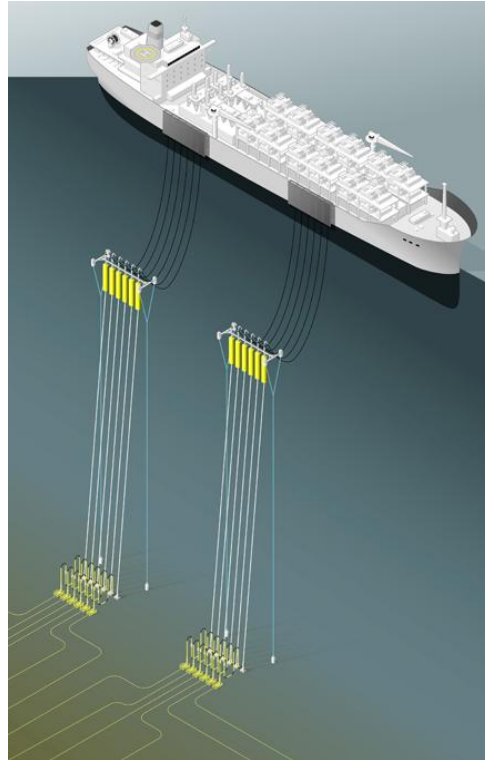


Figure 1-9 Hybrid Riser System.

One of the advantages for hybrid riser is that it facilitates the design of a clear and well-organised subsea layout on the sea floor as can be seen in Figure 1-9.

From top to bottom, a typical hybrid riser comprises of following main components (Figure 1-10):

- The flexible jumper, between the top of the riser and hang-off point in the floating vessel.
- The sub-surface buoyancy tank.
- The free standing vertical section.
- The bottom section including rigid jumper spools and connectors.
- The anchor base foundation.

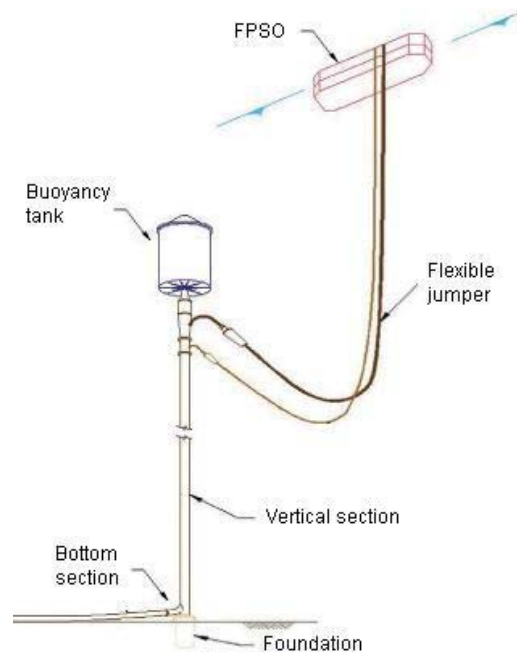


Figure 1-10 Hybrid Riser Main Components.

1.4 A Danger for Deepwater Risers

All of the above types of marine risers are being used in production of oil but prior to the phase of production in the process of exploration and development of a new offshore oil field, drilling thousands of metres beneath the seabed is one of the key and most significant stages. Drilling in deepwater and remote areas is carried out with the help of drilling risers. As the water depth increases toward ultra deep water, the integrity of drilling risers is a crucial issue and a series of integrity analysis, therefore, needs to be done to ensure the safe and smooth operation of drilling even in harsh environmental conditions. Drilling risers are classified in the category of top tensioned risers (TTR). Thus, apart from the importance of production TTRs, due to vital role of drilling riser, TTRs and associated problems have been one of the main concerns for marine riser designers.

As the oil industry targets new reservoirs in ever deeper water, with respect to TTR design, many technical issues which were already neglected in shallower waters have arisen and become a challenge for further development. For instance, high hydrostatic pressure near the seabed can cause damage to the riser and lead to the collapse of the pipe wall. On the other end of the riser, it should be able to withstand

the excessive displacement of the floating structure due to the long mooring system. Moreover, a much lengthier riser entails heavier weight which obviously demands either higher top tension or buoyancy modules. Higher top tension requires larger platforms and much more sophisticated equipments but on the other hand, the usage of buoyancy modules increases the riser diameter and naturally increases the drag force which is a pre-existing problem for the integrity of a TTR in deep water.

Above all, there is another critical problem called vortex-induced-vibration (VIV). Fatigue damage induced by this type of vibration can be detrimental to the riser and lead to early structural failure. The severity of this damage depends on a wide range of parameters and thus, to riser engineers, VIV has always been a trouble which needs extra measures and mitigation to be harnessed.

Various methods have been proposed to control this phenomenon. Among them, outfitting the riser with a VIV suppression device is one of the most prevalent techniques. These devices reduce the VIV in different ways and each has its own advantages and drawbacks. For instance, helical strakes, which may be called the first generation and perhaps the most implemented device, suffers from an increase in the drag force which is one of the problematic issues with a VIV suppression device. In light of this problem, engineers were encouraged to seek a device which was capable of mitigating VIV while simultaneously reducing drag. Thus, the concept of the riser fairing that met the necessary requirements was introduced.

However, in recent years tank tests have revealed that fairings used to mitigate VIV for a range of current velocities are exposed to severe vibrations when the current velocity exceeds the upper limit. These vibrations have different features from VIV and are generally characterised as the system being unstable. This newly emerged destructive phenomenon has led to the fairing designer having to carry out extensive model testing on the stability of each suggested fairing profile. Therefore, it is vital and beneficial to predict the instability onset condition for a given system theoretically in the design phase rather than through extensive model testing. An analytical model which had been developed for flutter type vibrations of aeroplane wings was adapted to a riser fairing case, however, it was found to have too many

assumptions which could result in errors and restrict the scope of use in a marine application.

Hence, there is a gap in industry for a more accurate and comprehensive model. This study endeavours to respond to this need by developing an analytical model to predict the instability of a riser fairing and also provide guidelines to help prevent the onset of unstable vibration.

Chapter 2

Aims of The Thesis

The targeted objectives of this project are as follows:

- a) To thoroughly research vortex-induced-vibration (VIV) and to critically review the associated mitigation methods implemented on marine risers.
- b) To develop an analytical model for instability of deepwater riser fairings and to provide designers with a theoretical tool to predict the onset of vibration.
- c) To identify the key parameters in instability onset of riser fairing and to investigate their influences through conducting a parametric study.

This chapter will investigate the concepts of vortex, vortex shedding and vortex-induced-vibration (VIV). It will then elaborate the significance of VIV in marine risers design and explain the general methods of tackling the issue. The family of riser fairings will be proposed as one of the most suitable devices of tackling the above issue and will be addressed methodically having its merits and failings discussed. Finally, the areas requiring further attention will be proposed.

3.1 Vortex-Induced-Vibration (VIV)

In an ideal fluid which in definition has no viscosity, a vortex is a type of flow in which streamlines comprise of co-centric circles. In this type of flow, fluid particles swirl in the same direction about the centre of vortex in different orbits with various velocities (Figure 3-1).

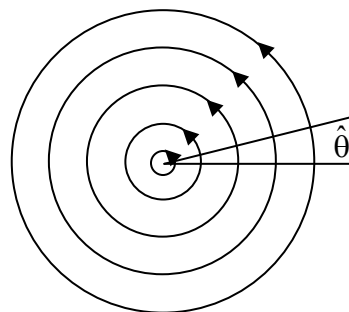


Figure 3-1 Single Vortex in Ideal Fluid.

The strength of the rotational field is measured by a parameter called ‘circulation’. Circulation, Γ , of a fluid region is defined as the line integral of velocity vector along a closed path (Blevins, 2001),

$$\Gamma = \oint \vec{V} \cdot d\vec{l} \quad 3-1$$

Where \vec{V} is the velocity vector; (\cdot) is vector dot product; and $d\vec{l}$ denotes the vector element of integration path. The equation of continuity of incompressible fluid is in the form of Laplace’s equation,

$$\nabla \cdot \vec{V} = 0 \quad 3-2$$

where ∇ is the vector gradient operator. The velocity potential function of a vortex flow is computed based on its circulation,

$$\phi = \frac{\Gamma}{2\pi} \hat{\theta} \quad 3-3$$

Since ∇ is a linear operator, it is possible to superimpose two potential flows like vortex to construct a third potential flow. Figure 3-2 illustrates two vortices with opposite but equal circulation. It is readily shown (Blevins, 2001) that these two vortices form a flow pattern in which one of the streamline encompasses both vortices, moving with a specific velocity, $\Gamma/(2\pi\alpha)$, in the direction perpendicular to the line connects the centre of two vortices. The variable α , is here the distance of two vortex centres.

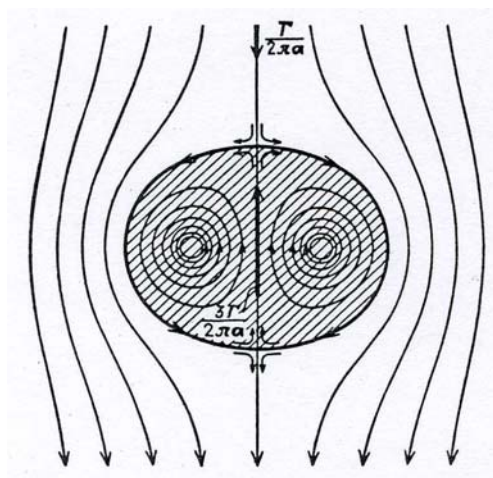


Figure 3-2 Two Potential Vortices with Opposite but Equal Circulation (Blevins, 2001).

Likewise, a number of potential vortices can be considered simultaneously. Figure 3-3 depicts an infinite double staggered row of vortices in which vortices on each row has opposite sign from those on the other row.

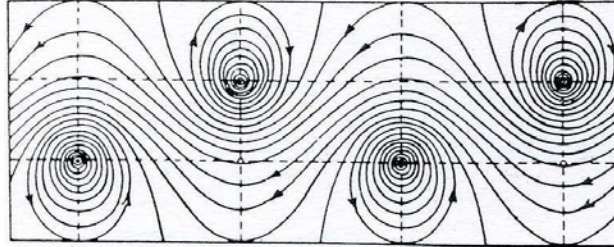


Figure 3-3 Infinite Double Staggered Row of Vortices (Blevins, 2001).

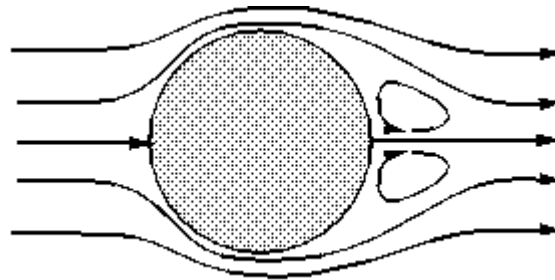
Back to the reality, in a viscous fluid like water about an obstacle, boundary layer growth and flow separation are governed by inertia of flow particle and viscosity of fluid. Reynolds number is a dimensionless parameter to show the ratio of inertial force to viscous force,

$$Re = \frac{UD}{\nu} \quad 3-4$$

where U is the free stream velocity; D is the maximum section width; and ν denotes the kinematic viscosity of fluid. As the Reynolds number rises, the inertia force becomes dominant and the flow is far more likely to separate from the back of obstacle.

As a viscous fluid particle or cell moves toward the frontal edge of a body like a cylinder, the pressure intensifies from free stream pressure to stagnation point pressure in front of the cylinder. The high pressure region in the vicinity of the leading edge pushes fluid particles about the cylinder and causes boundary layer to develop about both sides. At very low Reynolds number, e.g. $Re < 5$, the fluid flow follows the cylinder contours and the boundary layer is bound to the cylinder surface. However, high pressure is not capable of forcing the flow about the aft section of the cylinder at a high Reynolds number. Thus, at a point ahead or aft of the widest section of body, depending on the Reynolds number, boundary layers separate from each side of cylinder and build two shear layers that continues aft in the flow (Blevins, 2001). Since a particle on the inner edge of separated boundary layer,

which was in contact with cylinder surface, moves more slowly than a particle on the outer edge, which is still in contact with the free flow; both shear layers turn in behind the cylinder and fold on each other and form two discrete swirling vortices as shown in Figure 3-4.



a)



b)

Figure 3-4 Bound Vortices Behind a Circular Cylinder a) Schematic b) Flow Visualisation.

As the Reynolds number increases, the vortices become unstable and by any small perturbation, they begin to leave at the near wake of the cylinder and move downstream with the flow. When a pair of vortices or a single vortex leaves the body, the above cycle is repeated and the new vortices are formed in their place again. This phenomenon is called ‘vortex shedding’ as it looks like that the structure is shedding vortices. The train of periodically shed vortices behind the cylinder was first investigated by von Karman and is associated with his name as ‘von Karman Vortex Street’ (Figure 3-5).

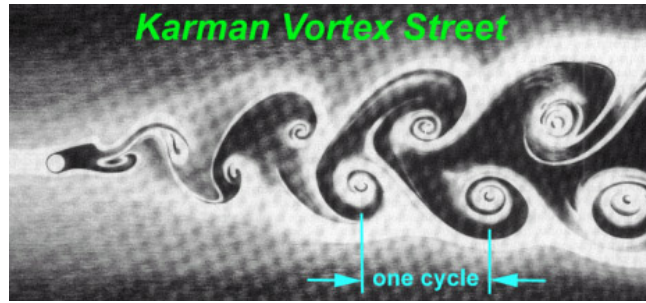


Figure 3-5 Von Karman Vortex Street Aft of a Circular Cylinder.

Bluff structures, when located in fluid flow, shed vortices and as the vortices are shed from one side and then the other, pressure distribution changes continuously over the body surface (Figure 3-6). The oscillating pressure imposes time-variant forces on structure and causes elastic structures to vibrate. This type of vibration that originates from vortex shedding is known as ‘Vortex-Induced-Vibration’ or in brief ‘VIV’.

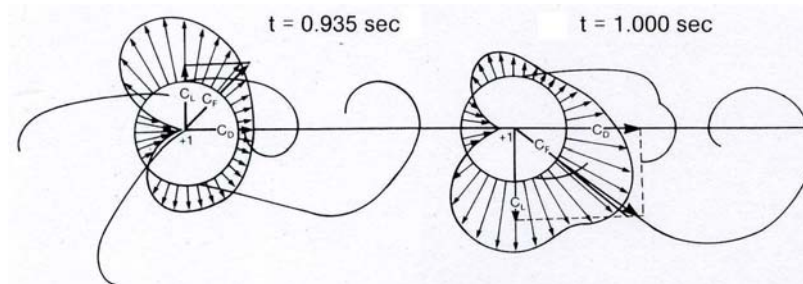


Figure 3-6 Variation of Pressure Distribution in Vortex Shedding (Blevins, 2001).

The most important VIV parameters are: the lift coefficient, the shedding frequency (Strouhal number), the shedding frequency bandwidth and the correlation length (Pantazopoulos, 1994).

The dynamic force in cross-flow direction due to shedding vortices is conventionally referred to as lift force. As was mentioned earlier, this force is a direct result of fluctuating pressure distribution. For a cylinder in steady flow, it is an alternating force that in some cases can be considered regular and periodic while in other situations its behaviour seems very complicated and rather random.

Vortex shedding frequency is often described by the Strouhal number (S), a dimensionless proportionality parameter of the form,

$$S = \frac{f_s D}{U}$$

3-5

where f_s is a frequency associated with vortex shedding in Hertz; D is the cylinder diameter; and U is the free stream flow velocity. It should be noted that the Strouhal number characterises the mean or predominant spectral frequency, f_s , and gives no detail about the range of frequencies present. The Strouhal number of a stationary circular cylinder is a function of Reynolds number and to some extent, surface roughness and free stream turbulence (Blevins, 2001).

The general description of vortex shedding so far may imply that it is a two-dimensional phenomenon. But experimental evidences from uniform and shear flows about stationary cylinders indicate that the shed vortices have a significant length in the axial (along the cylinder axis) direction, leading to term ‘vortex cell’ (Pantazopoulos, 1994). The three-dimensionality of vortex shedding can be characterised by a span-wise correlation length. The degree of correlation between vortex shedding or associated lift forces along the cylinder axis is a key factor in determining the net force, and consequently, vibration amplitude. Like the other characteristic of vortex shedding, correlation length is also dependent on Reynolds number. It tends to decrease with increasing turbulence. Typical values for stationary cylinders (Blevins, 2001) range from 100 or more diameters for laminar vortex streets at $Re = 60$ to 20 diameters at $Re = 100$ and 5 diameters for fully turbulent vortex streets at $Re = 10^4$. If the free stream flow velocity varies over the cylinder length at transitional Reynolds number, these cells also develop and vortex shedding frequency fluctuates discretely in ladder-like steps along the span with each step, spanning about 4 diameters.

3.2 Impact on Deepwater Marine Risers

Deepwater marine risers are flexible bluff structures. They are flexible because even though their diameter can reach up to 0.6 metres in steel catenary risers (SCR), the ratio of length to diameter, which is conventionally called aspect ratio, is very high and they behave like a tensioned string or wire.

They are also placed in category of bluff structures. By definition, “a bluff structure is one in which the flow separates from a large section of the structure’s surface. ... The primary purpose of these structures is not to gain lift or minimize drag ..., but rather to bear loads, contain flow ... These structures are not aerodynamically optimised. Flow-induced vibrations are usually regarded as a secondary design consideration” (Blevins, 2001).

Consequently, due to flexibility and bluntness, marine risers are one of the structures which are very much prone to vortex-induced-vibration.

The significant point here is that when the structure transforms from rigidity to flexibility, the mechanism of coupled system of structure and fluid can vary a great deal. This is due to the fact that generally, fluid flow and the flexible structure are coupled through the force exerted on the structure by the fluid and vice versa. The fluid force causes the structure to vibrate. As the structure vibrates, its orientation to the flow changes and the fluid force and behaviour may change too, in order to adapt itself to the new situation because as the fluid exerts a force on the structure in its new position, the structure exerts an equal but opposite force on the fluid.

Therefore, hydrodynamic forces on a flexible cylinder like riser, which is capable of oscillating, are much more complex than forces on a stationary cylinder due to reciprocal interaction between the oscillating cylinder and the fluid medium. In general, hydrodynamic forces on an oscillating cylinder include the added mass and the damping force in addition to lift and drag.

The motion of cylinder influences the wake, particularly vortex shedding, aft of the structure in different ways. Blevins (2001) explored many researches and summarised the effects of transverse vibration of a cylinder with frequency at or near the vortex shedding frequency in five items. According to his summary, the cylinder vibration may:

- (1) Increase the strength of vortices and alter the lift force.
- (2) Escalate the spanwise correlation of the wake.
- (3) Push the vortex shedding frequency to shift to the frequency of cylinder vibration. This state is called lock-in or synchronisation.

- (4) Amplify the mean drag on the cylinder.
- (5) Change the phase, sequence, and pattern of vortices in the wake.

The fluid forces imposed on the cylinder by vortex shedding will be a function of the cylinder's vibration amplitude and may be self-limiting at large amplitude (Blevins, 2001, Pantazopoulos, 1994). In brief, as cylinder's vibration at resonance with vortex shedding increases in amplitude, the cylinder's motion organises the wake and spanwise correlation increases. The vortex strength increases and so does the lift coefficient with it (Blevins, 2001). However, it should be noted that the relation of lift coefficient and vibration amplitude is not an endless cycle. There is a consensus in literature that lift increases with response amplitude up to a point, then decreases with further increases in amplitude (Pantazopoulos, 1994).

Now, in the design point of view, marine risers have low damping and they are subject to currents. Thus, likely resonance results in large amplitude vibration with a broad lock-in band. As flow velocity escalates, the riser passes from one resonance to another and sustains the oscillation. This type of vibration is of high importance because of its potential to lead to destructive motions and severe damage. This vibration shortens the fatigue lifespan of the riser and can end up with early fatigue failure which causes disruption in production flow and imposes higher unexpected costs on industry due to the down time loss and repair expenses.

On the other hand, the drag coefficient is mainly a function of the section shape and the dynamics of flow in terms of the Reynolds number. However, the drag can be amplified by this vibration to the extent of two or three times the normal value. High drag, however, is not as problematic in shallow water and on fixed platforms but is very difficult to deal with in deepwater. High drag results in excessive joint angle in a drilling riser and forces the rig owners to halt the drilling operation. This again imposes unforeseen costs on the industry due to the down time. The solution to high drag and its aftermath is to raise the tension of the riser, only if it can bear higher stresses. Implementation of higher tension requires larger platforms or further equipment and both of them swallow a huge amount of investor's money.

Above all, the problem of VIV in marine risers and its adverse consequences become worse as the oil industry is stepping in deeper waters. Working in extremely deep water needs longer risers. Deploying higher length of riser reduces its natural frequency and this phenomenon makes the vibration more susceptible to lock-in or synchronise with the vortex shedding. In simple terms, it raises the risk of resonance and jeopardises the durability of the riser. Moreover, a longer riser provides more structural flexibility and consequently lets the system experience a larger amplitude of vibration. This may intensify the lift and drag forces and exacerbates the conditions.

Eventually, due to the fact that VIV can be seriously harmful to marine risers and the severity of this problem increases in deeper waters, this has inspired engineers to seek for methods of mitigating these vibrations. These methods will be addressed in the next section.

3.3 Methods of Mitigating VIV

Reducing the risk of resonant vortex-induced-vibration and associated amplification of the mean drag is one of the design concerns for engineers. VIV and its consequences are a function of a combination of structural properties and flow and therefore can be substantially confined by modifying either the structure or the flow. The aim of the first two methods below is to manipulate the structural properties while the last two methods try to alter the flow in vicinity of the body.

(A) Tune Design Parameters to Avoid Resonance

If the structure is designed appropriately in order to keep the natural frequency of the structure in the mode of interest (f_n) outside of the shedding frequency bandwidth, then the risk of resonant vibration in that specific mode will diminish dramatically.

One appropriate way to achieve this is through stiffening the structure. But stiffening is usually more feasible for smaller structures. The difficulty of applying this technique to long marine risers is that they behave like a tensioned cable and the main stiffness is due to end tension and increasing the tension as earlier mentioned, if

possible, imposes higher costs. Moreover, very large values of riser length predominantly control the natural frequency.

(B) Increase Structural Damping

If the resonant VIV is not avoidable, the next method is to raise the structural damping. Then the motion will be controlled and the amplitude of vibration will abate. In particular, selecting appropriate damping could limit the peak amplitude at resonance to a value less than the deflection induced by drag (Blevins, 2001).

There are many general methods to increase the damping. They can be classified into two main areas of tuned and wide range. Most types of dampers for hydrodynamically loaded structures are heavy and mechanically complicated (Barltrop and Adams, 1991). Two tuned dampers which have been deployed in marine field are ‘chain dampers’ and ‘nutration dampers’. Chain dampers are rubber-covered chain, restricted in a container installed on the structure. Nutration dampers consist of tanks in which water sloshing dissipates energy. Drawbacks of using either one of these dampers on a marine riser include a widened projected area, an increase in the drag force and additional weight considerations. Wide frequency band damping can be produced by adding rubber or other visco-elastic materials in joints. This type of damper demands higher flexibility of structure, particularly if they are designed to damp high amounts of energy.

(C) Streamline Cross-Section

It was explained in Section 3.1 that vortices are formed aft of the structure when the flow is separated from the body surface. Consequently, if the separation from the structure can be minimised, then the vortex formation followed by vortex shedding can be minimised too and drag will decline accordingly. To achieve that, the leeside of a structure needs to be streamlined. To be effective, a streamline cross section should be in the form of a taper of a 6 longitudinal for each unit lateral or an included angle of the taper less than 8 to 10 degrees (Blevins, 2001, Ericsson and Reding, 1980, Grimminger, 1945, Hoerner, 1965). This restriction elongates the section length which may be not acceptable for a set of risers in operational conditions,

unless a blunt end section is used. Moreover, streamlining is most practical when the direction of current is fixed relative to the structure and the structure is stiff enough not to undergo flutter type instability which will be explained later in Chapter 4.

Thus, this method is not deployable for marine risers which experience currents from various directions across their service life, unless the streamlining shield is free to rotate and align itself to current. This became the concept for introduction of a VIV suppression device, called ‘fairing’, which will be presented in detail in Section 3.5.

(D) Add a Vortex Suppression Device

The purpose of installing a vortex suppression device is to control or manipulate the flow in the neighbourhood of the body, in order to disrupt or prevent the formation of an organised vortex street with long correlation length.

For better understanding and phenomenological explanation of the mechanism of suppressing vortices, it is necessary to clarify two concepts, ‘entrainment layer’ and ‘confluence point’ (Zdravkovich, 1981). The entrainment layers supply the irrotational fluid necessary for the growth of vortices in addition to rotational fluid in separated shear layers. The confluence point shows the region where the two entrainment layers from opposite sides of the cylinder converge and interact. The timing of vortex shedding is governed by the switch of the confluence point from one side of the wake axis to the other. Therefore, it can be expected that vortex shedding is quelled by interfering with shear layers or entrainment layers, or on the other hand, by preventing the confluence-point switch.

To achieve this goal, there is a wide range of VIV suppression devices which fall into two groups of active and passive. Most of them are classified in the latter group which can be sub-divided further to reflect the function and method of suppression. Passive devices are categorised in three subgroups of ‘topographical devices’, ‘shrouds’ and ‘near-wake stabilisers’ (Zdravkovich, 1981).

A topographical device is any device which modifies the cylinder’s contour without being located mainly in the wake of cylinder. It suppresses the vibration through impact on shear layers separation and accordingly on the formation of vortices.

These devices are usually multi-directional and can be effective. But the tendency to increase drag is their main shortcoming. They include strakes, fins, studs and semi-sphere bumps.

Shrouds are, by definition, devices situated with a gap from cylinder's surface such that it accommodates a flow of fluid in this gap. They suppress the vibration in two ways. The boundary layer separation is disrupted by leading section and the vortex growth and shedding are influenced by trailing section of shroud. Shrouds are multi-directional but may not be quite as effective if their design is not appropriate (Barltrop and Adams, 1991). Shrouds have the advantage over topographical devices that the drag penalty is not as great. Shrouds can be produced in different forms including perforated, gauze, axial rods and axial slats.

Near-wake stabilisers are devices designed to be located predominantly in the wake of a cylinder. They mitigate the vortex shedding by affecting the switch of the confluence point. In other words, the wake of a cylinder shedding vortices is unstable and asymmetric; these devices help to stabilise the wake and remove the asymmetry of the wake. They are also capable of hindering the formation of vortices by extending the shear layers downstream and preventing the entrainment of fluid across the wake of cylinder. As they should always lie in the wake, they are conceptually unidirectional but if due to variation of current direction, the wake is not fixed, they should be free to rotate about the cylinder. Therefore, their multi-directionality requires firstly their ability to rotate and secondly their capability to align themselves to current direction and wake. If so, these devices can be very effective at reducing both drag force and vortex-induced vibration. Lengthy chord is the drawback which can be crucial for a set of risers in operational conditions. Fairings, splitter plates and guide vanes are the traditional examples of these means.

Active devices, as implied from the classification, need motive power to disturb the flow and eliminate vortex shedding. They can be subdivided into blowing or suction devices. Blowing devices generate columns of air bubbles or water jets around the cylinder to interfere with flow and prevent the mechanism of vortex formation. Suction devices do this by entraining the water. Active devices can be used multi-directionally. They work well if the length of excitation is limited (Barltrop and

Adams, 1991). Such system is difficult to be implemented on a long riser. In addition, it requires pumps and power and can be not as cost effective as passive devices.

Generally, vortex-shedding suppression devices are widely used for deepwater marine risers and hence will be elaborated in the next section.

3.4 Vortex-Shedding Suppression Devices

In Section 3.3, four methods of mitigating VIV were introduced and the associated penalties were explained. As was alluded, the first three methods are mainly related with design parameters which are not very flexible in marine risers. Consequently, the last method, addition of a vortex-suppression device, is often deployed if VIV is a concern in the riser design.

A wide range of VIV suppression means has been devised to date that each of them falls in a group of classification presented in the previous section. Blevins (Blevins, 2001), Zdravkovich (Zdravkovich, 1981) and Rogers (Rogers, 1983) summarised the main tools with associated merits and drawbacks. These devices, as shown in Figure 3-7, include (a) helical variations (protrusions, strakes or grooves), (b) different types of shroud, (c) axial slats, (d) spoiler plates, (e) stepped cylinder or semi-spheres bumpers, (f) ribbon or hair cables, (g) splitters, (h) pivoted guide-vanes or (i) streamlined fairings and finally active devices such as bubble jet, water jet or suction.

Among these techniques, helical strakes are first-generation technology and apparently the most prevalent device for inhibition of VIV on risers, pipelines and other tubulars offshore. Helical strakes typically have three different raised sections or protrusions around the circumference of a column, much like a screw, with a pitch of several times the diameter of the cylinder and height of approximately ten percent of the diameter.

Because they are wrapped helically, helical strakes shorten the correlation length of the vortices. Vortices are shed in finite cells and finite lengths from helical strakes and the shorter the vortices, the weaker they are. The principle is similar to that of the helical protrusions on industrial chimneys, first seen in the early 1950s.

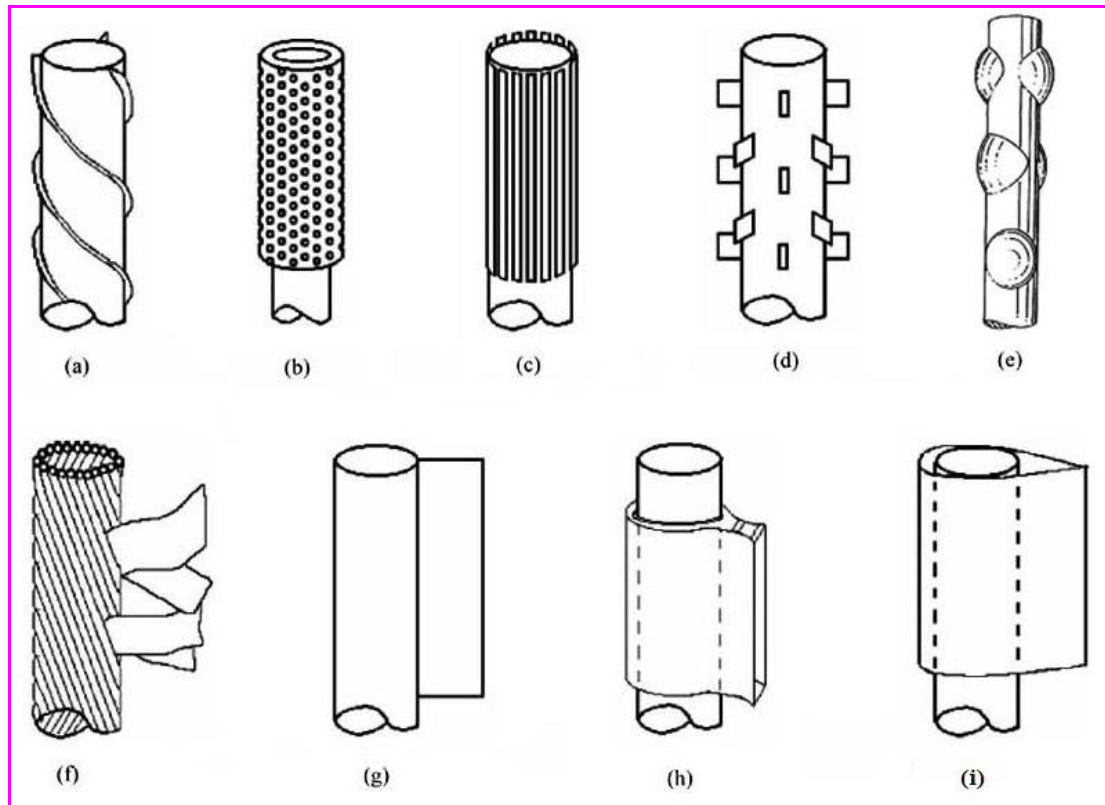


Figure 3-7 Add-on Devices for VIV Suppression of Cylinders (Blevins, 2001, Kumar et al., 2008).

Helical strakes have the advantage that they are effective irrespective of the direction of current. They also have high VIV suppression efficiency, typically the VIV response amplitude is reduced by 80% (Rogers, 1983). However this VIV suppression comes with a detrimental side effect in the form of increased drag. The drag on the bare risers, even without the increase, is already extremely difficult to deal with in deep waters. With the increase, the problem is further exacerbated.

Helical strakes increase drag because they cause early separation of the flow around a tubular and amplify C_d (Shell Global Solutions' website). Moreover, they widen the effective frontal area as well.

Another problem associated with helical strakes on subsea pipelines and risers is that their efficiency is reduced by increased water drag, which results from build up of marine growth (Armstrong, 2004a). In other words, marine growth on helical strakes degrades their VIV suppression capability. It requires underwater cleaning

technology or anti-fouling coating to retard marine growth (Shell Global Solutions' website).

The other shortcoming of deploying helical strakes on marine risers is that they are substantially reduced in VIV suppression when they are on a downstream (or down current) tubular (Allen et al., 2008).

Large drag of helical strakes was a great challenge for industry. Therefore, the attentions turned into a device which can simultaneously suppress VIV as well as reduce the drag. To this end, fairings became an option. The "teardrop" profile of the fairings could reduce drags and eliminate VIV.

Fairings are relatively a new field in marine risers VIV and will be discussed in more details in the next section.

3.5 Riser Fairing

(A) Description

Outfitting all or some portions (often the upper joints) of the riser with fairings is relatively a common method and maybe the most effective and best field-proven solution to both drag and VIV (Barltrop and Adams, 1991, Cuming-Corp.). As mentioned earlier in Section 3.3, fairings are classed in the subgroup of 'near-wake stabilisers' and they reduce both drag and motion by streamlining the fluid current round the riser and consequently weakening the vortices shed aft of the body. Thus, they need to be in the form of a streamlined profile.

Fairings are typically of 'teardrop' geometry, varying in terms of the chord length, nose thickness, span length and tip and tail details. Figure 3-8 illustrates the most common types of fairing which are generally specified in terms of the ratio of chord length (c) to thickness (t). The face of fairings is usually either convex or flat in the leeside. The trailing edge can vary from a sharp point end to rounded or even flat blunt end. The fairing tail may be equipped with a pair of wedges, rounded bumps or perpendicular fins to enhance the performance. It is usual to have blunt trailing edge with some out-turn of the plates to provide stability (Gardner and Cole, 1982). The

in-line fins have been also implemented in some other cases. Fairings are also generically closed sections, fully encapsulating the riser. The space within the fairing can be used for buoyancy material. But, a derivative of this scheme is to allow flow between the two side plates in an open section in which the fairing consists of a fin portion only, strapped to the riser length at discrete points (Figure 3-9). The plates may be shorter than those of a fairing and the buoyancy material can be included (Bartrop and Adams, 1991, Grimminger, 1945, Lee et al., 2006a).

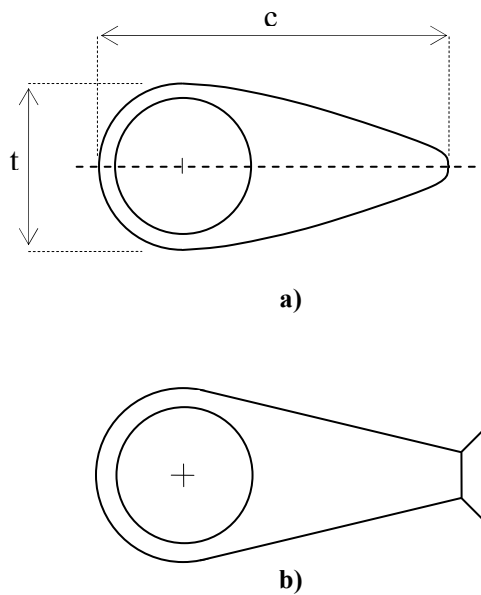


Figure 3-8 Typical Geometry of a Riser Fairing.

a) Convex Face with Rounded Tail, b) Flat Leaside, Blunt End with Fins.



Figure 3-9 Tail-Fin Fairing (Lee et al., 2006a).

Ortloff et al. from Exxon Production Research Company patented one of the earliest fairings in 1983 (Ortloff et al., 1983) which had the ordinary shape of convex face

with a blunt edge fitted with a pair of perpendicular plate fins (Figure 3-10). In addition to that, there are also a number of other profiles that have been introduced and patented as riser fairing. In 1995, Allen and Henning from Shell Oil Company introduced the concept of the short fairing for the first time (Allen and Henning, 1995b). Short fairing as shown in Figure 3-11 with c/t ratio in the range of 1.25 to 1.5 was patented as a non-rotatable device. Later that year, the inventors proposed the flexible fairing (Allen and Henning, 1995a) which in fact was comprised of a deformable shroud (Figure 3-12), capable of adjusting itself in response to changes in flow direction. It was claimed that they would be tolerant of marine life growth. A modified design of quasi-fairing showed good VIV suppression performance (Brown and King, 2008). Six years after introducing the short fairing, Allen et al. modified and promoted the idea again and announced the ultra-short fairing (Allen and Henning, 2001c). According to their definition, “the ultra-short fairing has a leading edge substantially defined by the circular profile of the marine element for a distance following at least about 270 degrees thereabout and a pair of shaped sides departing from the circular profile of the marine riser and converging at a trailing edge” (Figure 3-13). The chord to thickness ratio (c/t) of such a section should be between about 1.10 and 1.20. One year later, Masters et al. patented a completely new design named ‘a dual-fin splitter’ (Figure 3-14). The new design was found to have very good VIV suppression quality while at the same time having its drag very low (Masters et al., 2002, Spencer et al., 2007).

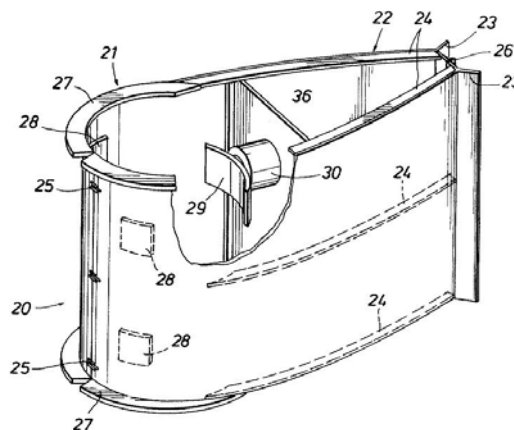


Figure 3-10 Ortloff et al Fairing (Ortloff et al., 1983).

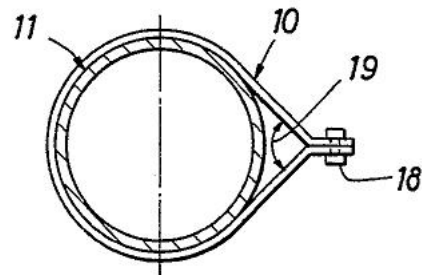


Figure 3-11 Short Fairing (Allen and Henning, 1995b).

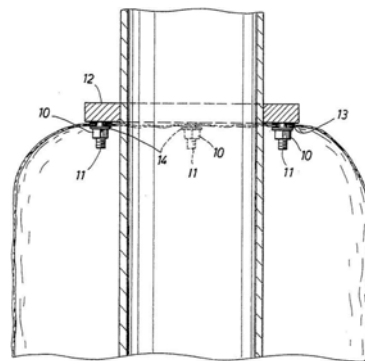


Figure 3-12 Flexible Fairing (Allen and Henning, 1995a).

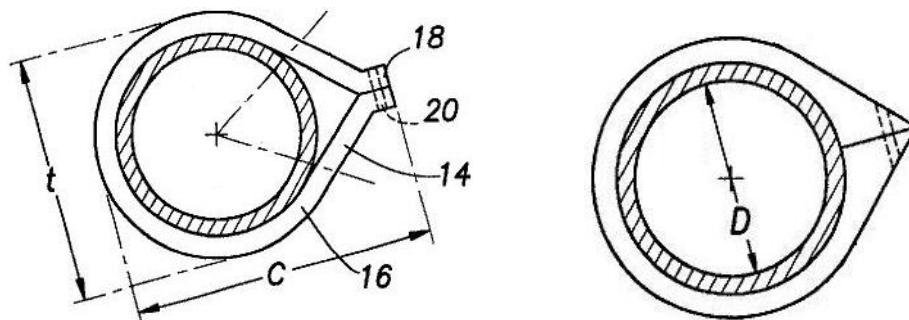


Figure 3-13 Ultra-Short Fairings (Allen and Henning, 2001c).

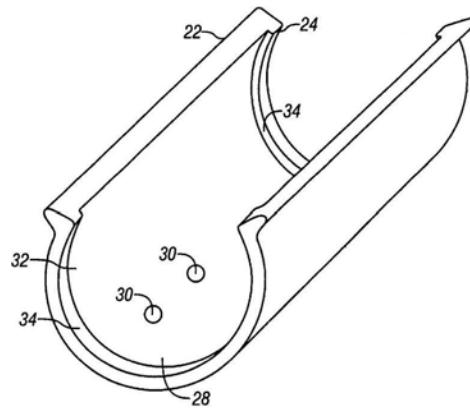


Figure 3-14 Snap-on Rotating Reduction Fairing (Masters et al., 2002).

Due to operational constraints, generally the chord length must be relatively short and thus, the fairing typically resembles a very thick foil. However, as the ocean currents can come from any direction, the fairing differs from a fixed foil or wing in the sense it is free to swing about the central riser. Moreover, in the spanwise direction the fairing is not continuous along the riser length; rather it is made of many finite but contiguous segments.

Regardless of section profile, Figure 3-15 shows schematically a fairing in three successive stages, i.e. installation, submergence and operation. Installation and retrieval is one of the challenging aspects and therefore, many fairings have been developed and patented which are quite different with respect to the installation method and apparatus (Denison et al., 2000a, Denison et al., 2000c, Denison et al., 2000b, McMillan and Allen, 2006, McMillan et al., 1999, Ortloff et al., 1983, Sweetman, 1998). Allen and Henning also suggested a staggered fairing system consisting of an array of non-rotative fairings with different orientations along the axis of marine element (Allen and Henning, 2001b) to protect it from VIV over an extended range of angles of attack. They also expanded the scope of fairing application to spars and developed a spar-fairing and accordingly designed the necessary installation method (Allen and Henning, 2001a).

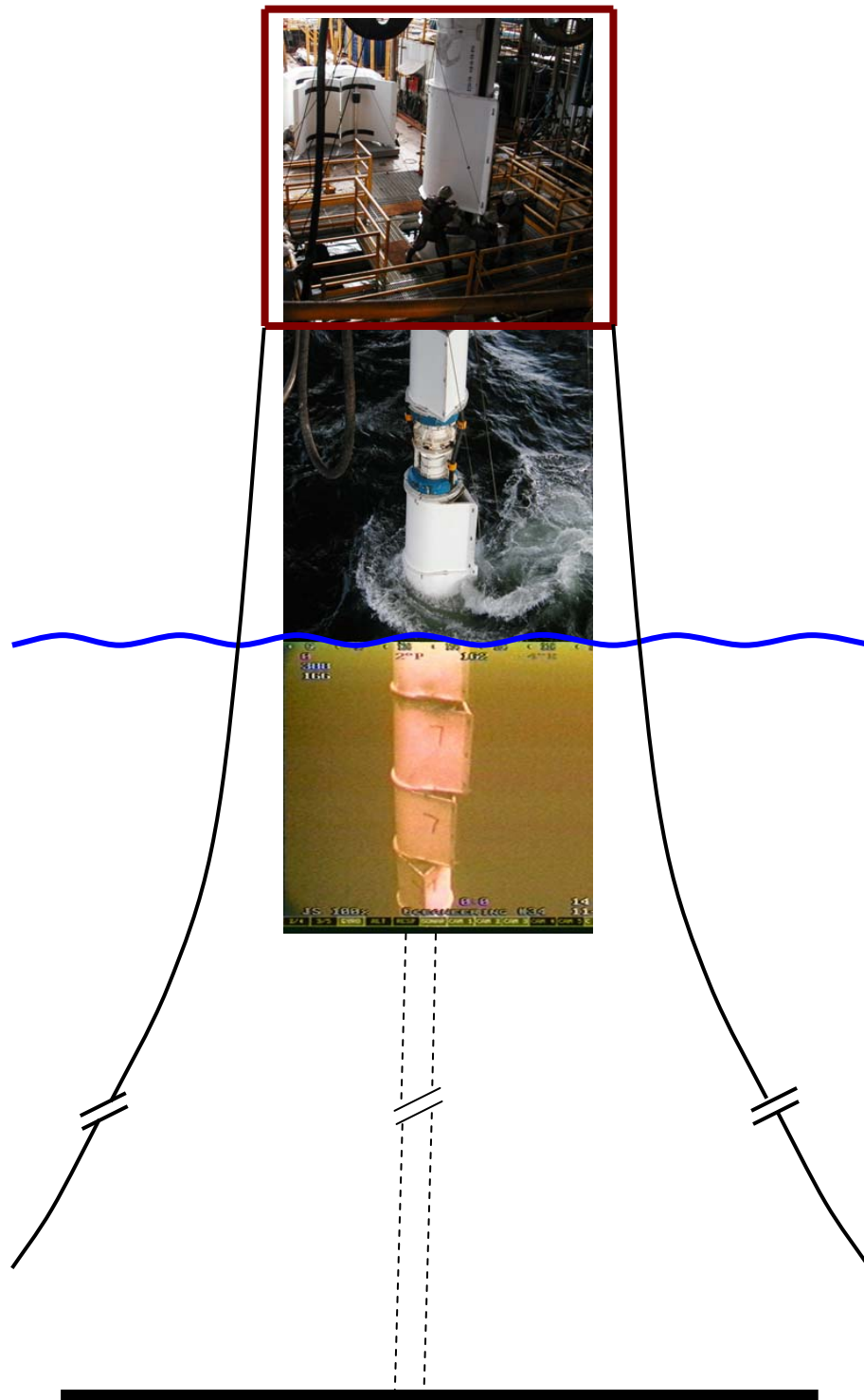


Figure 3-15 Riser Fairing at Installation, Submergence and Operation.

(B) Scope of Application

Fairings operate most efficiently while the riser is in a near vertical configuration (Bai and Bai, 2005). Thus, they are typically used on vertical or near-vertical risers. They have been successfully deployed on upper catenary section of SCRs, drilling risers and top tensioned risers including Auger, Mars, Ursa, Brutus and Na Kika.

The use of fairings in a marine application had been even greater than risers and spars. In the late 1970s/early to mid 1980s, a number of studies commenced to develop designs of faired cables (Nair and Hegemier, 1979, Nair and Hung, 1984, Wingham, 1983, Wingham and Keshavan, 1978, Vandiver and Mazel, 1976). At the time, faired cables with $4 < c/t < 10$ were successfully deployed for towing underwater objects, however, some instabilities in the form of divergence at low speeds and flutter at high speeds were reported too (Nair and Hung, 1984, Nair and Hegemier, 1979). Faired cables were typically continuous and the faired part was not free to rotate. More significantly, they were still far thinner than the riser fairing.

In seeking the behaviour of a typical riser fairing, as a fairing looks like a foil, either an airfoil or hydrofoil, its characteristics may be initially assumed to be like those of foils. Foils have been investigated quite well in aerodynamics (Fung, 2002, Abbott and Von Doenhoff, 1959, Anderson, 2007, Bertin and Smith, 1998, Dowell et al., 1995) and hydrodynamics (Newman, 1999, Breslin and Andersen, 1994, Saunders, 1956). Many experimental works has been carried out on various sections in different conditions and based on these findings several theoretical methods have been established to predict the dynamics of foils. Most of these theories are on the basis of inviscid flow which is not applicable in dynamics of fairings in seawater. Moreover, they assume foils to be thin; which is completely different from riser fairings with the thickness to chord ratio of several times larger. It should be noted that thickness can play an important role in determining hydrodynamic properties of fairings; firstly, it raises the drag, secondly, it makes vortex shedding more likely due to resembling a bluff section, thirdly, a higher thickness could lead to early separation, stall phenomena and alter the slope of lift coefficient curve adversely, and finally, a higher thickness results in a higher Reynolds number and different governing conditions.

All in all, riser fairings demonstrated different features and were not comparable to thin foils typically used in aviation or the marine industry. They needed separate investigation and many experimental studies therefore have focused on their merits and drawbacks as follows.

(C) Merits

Like helical strakes, fairings are an omnidirectional device, but in regard to merits, fairings are a lower-cost alternative to them (Allen and Allen, 2008) with a number of other advantages.

Firstly, they are generally considered to be more effective solution to deepwater VIV of marine risers (Armstrong, 2004a, Rogers, 1983). They also benefit from lower drag coefficient relative to a bare cylinder. The drag coefficient for such a device, provided that it is continuous and based on the full width, is about 0.3. However, if the fairings are in short sections it will be significantly higher, for example $C_d = 1.0$ for a cylinder and spaced fairings at a Reynolds number of 10^5 (Bartrop and Adams, 1991). In general, excellent VIV suppression performance and drag reduction of various fairing sections have been reported in many references (Lee et al., 2004a, Allen et al., 2007a, Gardner and Cole, 1982, Ikeda et al., 2003, Lee et al., 2006a, Grant and Patterson, 1977, Grimminger, 1945).

It should be noted that suppression effectiveness is a function of the chord to thickness ratio (c/t) (Allen and Henning, 2008); however, c/t is not sufficient for determining fairing performance. There are other significant parameters which should be taken into account including detailed design of fairing geometry (face and tail), centre of mass and centre of lift (Slocum et al., 2004, Miyazaki et al., 2008). Nevertheless dynamic characteristics such as the location of the centres of mass, pressure and rotation plus lift and moment coefficients, though vital, are often not reported (Lee and Allen, 2005, Lee et al., 2004a, Lee et al., 2005, Lee et al., 2004b, Slocum et al., 2004). The hydrodynamic forces, their trend versus variation of angle of attack and the location of hydrodynamic centre were addressed for a few given sections (Allen, 2003, Calkins, 1984, Grant and Patterson, 1977, Ikeda et al., 2003).

These parameters are relatively difficult to calculate accurately due to lack of information about the detailed design of a fairing in literature.

The second advantage is that when located on downstream tubulars, fairings have a significantly lower drag and suppress VIV more effectively than helical strakes (Armstrong, 2004a, Lee et al., 2006b, Allen et al., 2008).

Thirdly, their VIV suppression performance is less sensitive to their exterior being covered with marine growth and will continue to mitigate VIV more effectively over time (Armstrong, 2004a, Allen et al., 2008).

An added benefit of introducing fairings for VIV suppression is that they not only minimise the vortex excitation, but also generate large hydrodynamic damping in the range of 0.10 to 0.18 (Lee et al., 2004b). It should be noted that test results on small fairings are very conservative for determining the resulting displacements for a real pipe with fairings because fairings on longer spans will additionally reduce the pipe vibration due to damping of adjacent sets of fairings (Allen et al., 2007a).

Fairings can be designed to have neutral buoyancy in water as well.

(D) Difficulties

Chord Length

In the process of selecting a fairing for a given riser, one of the controversial issues is how to determine the appropriate chord length. On the one hand, clearance margins with the guidelines, capital and running time cost considerations and the desire to minimise weight all point towards a short and stubby fairing. On the other hand, the relationship between performance and chord length point toward a longer fairing (Grant and Patterson, 1977).

Fairings with longer chords (about $2.3D$ and longer) have been known to often suppress VIV quite effectively, but are also prone to a type of instability called flutter. While flutter can be minimised by careful design of the fairing, these design changes can be expensive to implement. Moreover, these expensive longer chord fairings, which are heavier, entail higher installation costs too. This means long

chord fairings should only be used when other, more economical, alternatives have been exhausted (Allen et al., 2007a).

Coverage Length

The next design parameter to be selected is the necessary length which should be fitted with fairing and its location along the riser. If the current profile is not uniform, naturally fairings are at least required in those parts that experience the highest current speeds.

According to the observations, there is no necessity to cover the entire riser with fairings. It has been reported that fairings can be effective even if they only cover 25% to 50% of the cylinder length provided that they are split into short lengths and that the gap between the length is not greater than a few diameters (Barltrop and Adams, 1991). In fact fairings can be very effective even if they only cover the anti-node area of vibration (Allen et al., 2007a). But if the flow region is long, or the vibration modes are high, the effects of fairings is more localised and more fairings are needed to achieve the VIV suppression objective (Lee et al., 2004b).

Test data confirmed that fairings have a strong local presence, consisting of a large reduction in the exciting lift forces together with significant damping. It means if a cylinder has a significant fairing coverage, the VIV will be dominated by excitation from currents outside of the fairing segment (Allen et al., 2007b, Lee et al., 2005). This test data revealed that the effectiveness of fairings in VIV suppression increases with increased fairing density until a density of 70% is obtained. Beyond that, increases in fairing coverage do little to reduce the vibration. Hence, risers in the field can be fitted with less than full coverage of fairings if the fairings cover the region experiencing the highest velocities.

In general, the VIV behaviour of a marine riser is very much dependent on the total length of coverage with fairings and also the arrangement/distribution of fairings along the riser length. This makes the VIV modelling of such riser more complicated and demands extensive test data and model calibration (Lee and Allen, 2004, Lee and Allen, 2007).

Installation and Costs

Following design, installation and cost are the other significant points. They include material cost and weight, installation time and cost, and ability to retrofit. One of the important considerations is quick and easy assembly to speed installation on the riser in the moonpool, and robust construction to withstand wave action during riser service life (Cumming-Corp.).

Fairings are relatively easily installed in the yard, during pipe lay operations or via retrofit (Armstrong, 2004a). Nevertheless, special methods may be required for each case (Armstrong, 2004c, Armstrong, 2004b, Armstrong, 2006, West et al., 2007). Fairings have been fitted in many locations in severe environments, such as deepwater currents in the Gulf of Mexico, including on the MARS and URSA tension leg platforms. A deepwater spar in a case study demonstrates the feasibility of retrofit and replacement of high-drag helical strakes with fairings.

The decision to run fairing on drilling risers is critical in terms of the additional cost to run fairings versus downtime cost from suspended operations due to current conditions causing excessive flex-joint angles. Balch et al discussed the appropriate conditions for using fairing. They developed a systematic approach to determining the requirements for fairings in drilling program (Balch et al., 2003).

A way of minimising fairing cost is to use tailfin fairing. It can be very light and fast to install, with potentially less material cost than a full fairing (Allen et al., 2007a, Lee et al., 2006a). Tail fairings are very effective at suppressing VIV and rival full fairings and helical strakes in their VIV suppression ability (Lee et al., 2005).

Marine Growth

Like the helical strakes, durability and the continuance of good performance after installation is the next concern. There exists a possibility that marine growth gradually degrades the fairing performance and threatens its function.

It is clear that if the current is variable, fairings must rotate freely without inducing torque on the main structure. This requires that fairings be provided with low-friction bearing surface and designed to generate sufficient turning moment to guarantee

accurate ‘pointing’ (minimum angle of attack) into the current. Therefore, their ability to weathervane reliably over long periods is vital to their performance in most offshore locations, particularly tidal zones.

The question is whether fairings will continue to swing freely on risers over time to align with current. Fairings have been shown to move freely about tubulars without need for cleaning. On the MARS tension leg platform, for example, the fairings installed on production risers in 1996 continue to move freely. Moreover, copper rings have been incorporated on thrust collars to retard marine growth and to keep fairings weathervane (Shell Global Solutions’ website).

It has been reported that the presence of surface roughness on the exterior surface of a fairing can reduce its effectiveness in streamlining the flow. Moreover, fairings with large hard marine growth are not as effective on a downstream cylinder as when on an upstream cylinder (Allen, 2003, Allen and Allen, 2008). But they still have substantial VIV suppression capability relative to the bare pipe. Short fairing has shown excellent performance with surface roughness (Lee and Allen, 2005). Short fairings performance was investigated more profoundly in terms of suppression capability, and how it is influenced by other parameters, e.g. upstream tubulars, marine growth, Reynolds number and aspirated section (Allen, 2003, Pontaza and Menon, 2008).

Misalignment

Eventually, there remain two main concerns including misalignment and instability which demand special attention. Each of them can lead to malfunction of fairing and causes fairing to jeopardise the riser instead of protecting it.

Fairings are designed to streamline the flow around the riser. The best performance occurs when they are in line with coming current and the more distortion from this position happens, the more deterioration of performance is expected. Thus, one of the characteristics of an ideal fairing is the ability to align itself to current accurately. However, for some fairings it was observed that the fairing did not point itself into the current properly (Grant and Patterson, 1977, Calkins, 1984, Meyer et al., 1995).

An angle of attack of zero was not a stable equilibrium orientation because if it represented a stable equilibrium configuration, then any disturbance from that position would produce a moment tending to bring it back while quite the reverse was documented. Any small angle of attack set up a moment forcing the fairing to rotate more. Misalignment or equilibrium orientation at an angle rather than zero increases both the drag force and the risk of vortex shedding from the leeside of the fairing which both are in contradiction to the defined goals of using fairing. Moreover, it introduces dual equilibrium positions on the two sides of zero angle of attack and small oscillations between these positions were observed. These small amplitude oscillations or so called ‘fishtailing’ may be controlled by adding appropriate trailing-edge fins or bumps but the mechanism is not yet clear.

This problem should be assessed in the light of section hydrodynamic characteristics but it has been reported that this problem is more common for some specific fairings. Particularly fairings with a very short chord, 1.10D to 1.25D, do not all align perfectly with the flow even at high speeds (Allen et al., 2007a). Therefore, there is a lower limit for chord to thickness ratio in an effective fairing.

Instability

The more important and major concern is that in the model test of some fairing designs, researchers have observed instability at higher Reynolds numbers.

Some designs demonstrated typical VIV response meaning that these sections, though streamlined to some extent, were still experiencing vortex shedding and associated vibrations while some other designs exhibited self-induced oscillation or dynamic instability characterised by the increase of responses upon excitation (Ericsson and Reding, 1980, Ikeda et al., 2003, Lee and Allen, 2005, Meyer et al., 1995, Slocum et al., 2004). The frequency of this vibration was reported to be less than the frequency of corresponding vortex shedding (Braaton et al., 2008).

Dynamic instability, defined in a classical sense, is the fact that response of a system increases with time which is caused by negative damping in the system (Lee and Allen, 2005). Lee and Allen expound that in the context of VIV, dynamic stability

can be described otherwise. As the flow speed increases the VIV motion of a cylinder rises to a certain level, and then the motion interferences with the vortex shedding process and begins to break up the symmetric pattern of alternate vortices. The motion magnitude does not increase even if the flow speed continues to rise, thus the process is self-limiting. When the cylinder is fitted with VIV suppression devices, such as fairing, the dynamic properties may change. Fairings, if not properly designed, can rotate and form a dynamically unsymmetrical section which entails lift force and may amplify the vibration beyond that of a bare riser. This type of vibration is not self-limiting anymore.

Some researchers tried to explain the source of the problem through early separation of boundary layer and stall (Calkins, 1984, Ericsson and Reding, 1980). Accordingly, it was recommended to reduce the angle of fairing contour in the leeside to match the fairing design to the flow regime (Ericsson and Reding, 1980, Grimminger, 1945). Qualitatively, the onset of instability due to stall at low Re and subsequent restoration of stability with increasing Re is consistent with movement of the separation point away from the pivot point as Re is increased.

Meyer et al argued that observed instability was due to the fact that the centre of rotation of the fairing was located behind the aerodynamic centre (Meyer et al., 1995). They proposed a few methods to rectify the problem including effectively moving the centre of rotation closer to the leading edge by lengthening the fairing and also moving the lift vector to the trailing edge by contouring the fairing shape. Meyer et al and Calkins advised to reduce the high pressure on the upper surface of the fairing near the trailing edge by adding vortex generators (Meyer et al., 1995, Calkins, 1984). They along with other researchers suggested to employ trailing-edge wedge or fin to tackle the problem of instability and misalignment by creating additional moment to counter the unstable moment (Calkins, 1984, Grant and Patterson, 1977, Meyer et al., 1995, Gardner and Cole, 1982).

An analytical model was also proposed to explain the instability. This model was based on a simple two-dimensional model of airfoil flutter to predict the threshold velocity at which large oscillations had been observed in tank tests (Slocum et al., 2004). The model estimated the critical current velocity for the simple cases but was

unable to explain the evolution of motion thereafter and why the observed motion reached steady-state amplitude. The model did not provide a basis for prediction of this speed limit for other modes or other riser configurations and did not include the effect of friction damping or hydrodynamic damping.

On the other hand, it has been emphasised that short fairings produce responses for operational conditions that can be characterised as both low and dynamically stable (Lee and Allen, 2005). In fact, the dominant suppression mechanism may be due to large hydrodynamic damping that they generate (Lee et al., 2004b). This large damping can be a key reason to prevent the instability of short fairings response. Short fairing was further assessed in terms of motion trajectory of the midpoint of the riser (Lee et al., 2004a). A new design called ‘a dual-fin splitter’ is claimed to be significantly more stable (with no tendency to flutter) than short (1.5D) or long (2.5D) fairings (Spencer et al., 2007).

In summary, important issues with respect to the use of riser fairings include ease of installation, hydrodynamic performance and long-term reliability/durability. Drag reduction is the key to extending the operability window. Extending operability will increase the risk of VIV and VIV will naturally increase the drag. Use of fairings, although reducing the drag, introduces an additional risk associated with instability. Fairings also impact the operability window due to increased run/retrieve time. It follows that there exists a trade-off between improved hydrodynamics and durability/installation issues.

3.6 Areas Needing Research

The ultimate goal of designing an optimum fairing is to develop a section with as short as possible length that gives stable performance, high level of suppression, low drag coefficients, and is more easily handled and fitted offshore. This goal has been and is still of interest to oil companies and is forming many researches.

For instance in late 2004, Shell published the results of some of the ongoing tests on fairing performance, with or without stabilisers and surface roughness, and also the impact of coverage length (Allen and Lee, 2004). At the time, fairing design

including hydrodynamic performance and stability was one of the future interests to BP (Sworn, 2004). Both samples disclose the significance of the issue to industry.

Despite the research interests and all studies carried out to date, this literature survey uncovers the following areas which suffer from lack of sufficient clarity and need further investigation.

(A) Misalignment and Fishtailing

According to reports, some fairings fail to orient themselves to current or undergo fishtailing. It was also documented that adding fins or wedges to the trailing edge can improve the fairing performance and control this phenomenon. The roots of the problem are not clear and the mechanism in which fins stabilise the fairing needs to be probed. Moreover, as fishtailing oscillations are seemingly similar to other types of vibration, sometimes it is confused with them. Further investigations are required to distinguish fishtailing and its causes from other vibrations.

(B) Instability

Many studies on riser fairings have depicted oscillations with monotonic growth of vibration amplitude with velocity increment. This is the characteristic of an instability rather than VIV. Thus, while complete removal of vortex shedding remains a concern for fairing design, the mechanism of stability should be separately regarded in fairing analysis as well. To this end, more test data is needed to confirm the mechanism. On the other hand, a dynamic model should be developed to establish the criteria governing the onset and mechanism of fairing instability. The available simple analytical model suffers from some imperfections and does not consider all parameters involved in the stimulation of instability or its confinement. It has limitations and simplifying assumptions which can cause errors. Hence, making definitive predictions possible necessitates a comprehensive, reconstructed and improved model. In this analytical model, the influence of body velocities on angle of attack must be considered. Moreover, the effects of different types of damping including hydrodynamic, friction and structural damping which were ignored in the existing model must be added as well.

(C) Damping

Positive damping inherently dissipates energy and alleviates dynamic motions of a system. It can also control the unstable oscillations and confine the vibration amplitude. The important question is whether this is the case for fairings too. Many studies have stipulated that adding fairings to the riser not only suppresses the vortex shedding but also increases the damping of the system greatly. In fact this question may be raised as to whether this is merely large damping of the fairing which mitigates the violent vibrations of vortex shedding and also prevents instability alone. This can be a reasonable scepticism because tests revealed that some types of fairing were still shedding vortices while they suppressed the vibrations as well. For instance, the computational simulation of a riser fairing showed that the VIV suppression was caused by the rapid wagging of the fairing tail (Chen et al., 2006). Moreover, fairings featured with large damping capability were reported to have no tendency to flutter instability. Besides, such a high level of damping could originate from or be a combination of various parameters. For instance, contribution of rotational friction is indeterminate. Some studies state that the rotational friction between fairing and riser can be very high and this may have contributed to its suppression efficiency. Thus, further tests are required to focus on the level of damping and the mechanisms generating it in order to have better understanding of the role of different damping.

(D) Mechanism of Suppression

In general, fairings are expected to streamline the flow and prevent the boundary layer from separation from the fairing circumference as the primary element of vortex shedding. Thus, the suppression performance of a fairing can decline rapidly due to flow separation in a specific range of Reynolds number as some studies reported. Consequently, the prospective investigations should explore the relationship between flow attachment/separation and Reynolds number for various fairing designs with a range of c/t , face and tail details. It is also necessary that physical testing, supported by CFD or theoretical analysis, should be planned to discover the mechanism of VIV suppression particularly for shorter fairings.

(E) Interference Effects

It has long been recognised that in steady flow, vortices shed from one cylinder onto a second parallel cylinder can have a very marked effect on its dynamic forces (Barltrop and Adams, 1991). There are also some observations on the effect of one helical strake on another helical strake located in downside. Thus, this important issue must be addressed for fairings too. The suppression performance of fairings fitted to downstream risers in arrays can be influenced by the presence of upstream fairings. The role of riser spacing and fairing geometry is not well assessed for a wide range of configurations (Lee et al., 2006b) and needs further theoretical developments and physical testing investigations to validate the theory.

3.7 Why 'Instability of Fairing' for Further Research

Indeed the outstanding advantage of fairings, i.e. drag reduction, apart from other superiorities to many suppression devices particularly helical strakes remains no doubt that fairings in general are the ideal available tool.

On the other hand, the literature review in this chapter revealed that most of the studies accomplished to date are based on experimental methods. They are usually either industry-ordered tests or experiments for commercial purposes. They typically contain data acquired from sophisticated tests followed by explanations for observations. Each individual study concludes that for specific conditions, their design is the suitable solution. In other words, they mainly endeavour to fulfil industrial needs and rectify their problems.

For instance, installation and associated costs is one of the operational concerns and many methods have been established to answer that and facilitate operation. Another example can be the observation of misalignment. This problem was also resolved experimentally and it was qualitatively advised to implement fins to the trailing edge.

Besides, there is a tendency or, to put it more simply, a competition of developing new patented designs and proving through tests that they show good performance in VIV suppression and drag reduction with no susceptibility to instability for a wide range of current velocities. While velocity may not be the only measurable criterion

for the onset of unstable oscillations there, in fact, exists a combination of parameters governing or endangering the fairing stability.

In contrast, very little work attempted to analytically address the roots of instability and to develop a thorough model to make the definitive prediction possible. In other words, analytical approach to the fairing's problem was removed from the prevalent methodology sphere. If the problem is supposed to be solved once and for all it demands reverse engineering. What this means is instead of running many tests to conclude the stable conditions, the governing mechanism along with parameters involved must be firstly discovered and then an analytical model ought to be set up to anticipate the threshold of problem occurrence and finally the importance and influence of each components should be clarified. Such model needs to consider the role of effective components as below.

The Role of Structural Properties

Structural properties of riser and fairing form one of the key elements in stability of the system. Their contribution to stiffness hinders the instability while their damping dissipates absorbed energy from outside and relieves any external excitation prone to lead to excessive oscillations. Riser properties include material, dimensions (length and diameter), damping, tension and its variation due to weight. Fairing has also similar structural variables plus the length of riser fitted with fairing (coverage length) and its position. Moreover, riser and fairing constitute an integrated system and their interaction produces rotational friction which can help the stability. Besides, a remarkable challenge is that such a theoretical model should provide a method of how to calculate these parameters.

The Role of Fairing Hydrodynamic Characteristics

Hydrodynamic characteristics of fairing are in the focal point of attention. They can lead to instability as much as they can suppress vortex-induced-vibration. Assessment of the following issues is essential in analysing the hydrodynamic performance of a fairing. They include potential of separation and vortex shedding, hydrodynamic coefficients, pressure distribution and the location of centre of pressure, added mass and so on. Variation of some parameters with fairing

orientation relative to current is a significant point and needs to be studied. In addition, the effect of adding fins or blunt end on pressure distribution and hydrodynamic coefficients should be investigated too.

The Role of Ocean Current

Ocean current is the external element which inputs forces into the system. It can also play the role of a damper depending on whether that specific area is fitted with a fairing or is bare. Current velocity may vary along the riser length in different forms. Moreover, the important point is the real velocity that a system experience. The real velocity and its orientation are influenced by system motion relative to current.

Clearly, the best analytical model for prediction of likely instability must be based on a combination of the above groups of parameters. With this in mind, a successful approach needs to be able to tackle the problem from a variety of perspectives. In fact, as mentioned above, the majority of existing approaches are experimental and tend to concentrate attention mainly on the velocity as the measurable and critical variable with little or no attention being paid to the role of other elements. There is therefore a need for a more comprehensive and holistic analytical model. The present study will focus on this issue.

3.8 Research Strategy

This study has targeted the investigation of riser fairing performance and theoretical prediction of likely instability. Firstly, this research will seek a more comprehensive understanding of the mechanism of instability and possible methods of approaching the issue. Secondly, an analytical model will be established initially for a simple case of two-dimensions (2D) and subsequently be expanded to the comprehensive case of a three-dimensional (3D) riser fairing. Finally, the role of the significant parameters will be assessed and analysed. On this basis, the present study comprises of the key steps below.

Step 1: Provide a clear perception of the mechanism of instability and methodology.

Step 2: Develop the analytical model for 2D case.

Step 3: Identify the key parameters playing a significant role.

Step 4: Assess the hydrodynamic coefficients as a key variable for a few fairings.

Step 5: Expand the developed analytical model to 3D case.

Step 6: Application of model to examples and parametric study.

The rest of this documented research will follow in the above step-wise structure.

Dynamics of Instability in Fairings

This chapter will first explore the types of fluid-induced-vibration and will then compare the attributes of fairing instability with the characteristics of these vibrations to identify the type of instability and associated possible causes. Afterwards, it will explain what method of approaching this problem suits the purpose of developing an analytical model for this phenomenon and what consequences selection of this method entails in terms of assumptions and limitations.

4.1 Introduction

The philosophy of using fairings as a VIV suppression device is to hinder the large amplitude oscillations, however, literature surveys revealed that at a higher Reynolds number, or in simple terms higher current velocity for a given section, the structure again encountered cross-flow vibration which could lead to instability. The characteristic of vibration, in this case, was different from that of VIV because the VIV was self-limiting and the amplitude of oscillation did not increase when the current velocity exceeded a certain level. Instead, the reverse of the above was observed and the amplitude increased along with the velocity. Figure 4-1 shows the behaviour of system against the increase in current speed (Blevins, 2001). The first peak in the vibrations is caused by vortex shedding aft of the bare riser. The second peak at higher reduced velocity is associated with the instability of a riser fitted with fairings. Thus, vortex-shedding does not play the main role in this oscillation and the source of problem is different from VIV with self-limiting attribute.

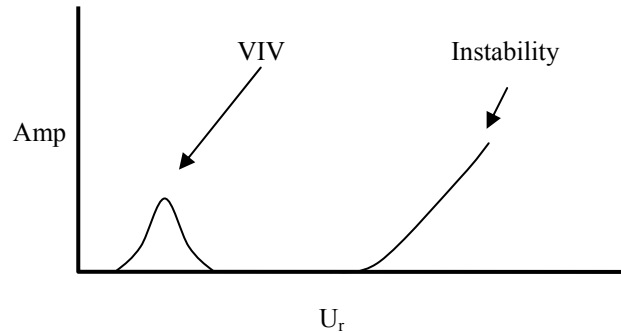


Figure 4-1 Typical Response of A System vs. Reduced Velocity.

To discover the element causing this sort of unstable oscillation in riser fairings, different types of fluid-induced-vibration are discussed in the following. Their causes and characteristics will be scrutinised as well to find the best match.

4.2 Types of Fluid-Induced-Vibration

The first type of fluid-induced-vibration is VIV. In brief, it was mentioned that bluff structures when located in a stream shed vortices alternately from each side of the body. This induces a periodic force in the direction perpendicular to the line of current motion and the body wobbles back and forth. If the frequency of vortex-shedding is close to the natural vibration frequency of the body, resonance and subsequent large-amplitude oscillations will set in. The considerable feature of VIV is that the process is self-limiting.

A different type of vibration is the ‘galloping’ of transmission lines during a sleet storm. The cause of galloping has been shown to be a cross section formed by ice. Such a section is unstable in wind and means the aerodynamic force exerts a negative damping component so that once the oscillation is started it will continue to build up. Flow about circular cylinder with perfect symmetry will not trigger galloping, a general prerequisite for which is some asymmetry in the aerodynamic forces associated with the cross flow (Dowell et al., 1995).

In general, a structure with noncircular cross-section is subject to a fluid force that varies with orientation to the flow. As the structure oscillates, its orientation changes and so does the fluid force. If the oscillating fluid force tends to synchronise itself with vibration and consequently increase the amplitude of vibration, the structure is dynamically unstable and can end up with very large-amplitude vibration. All noncircular cross-sections are susceptible to this sort of vibration which can be divided into two groups, i.e. ‘galloping’ and ‘flutter’.

Differences between galloping and flutter lie in the historical usage of the terms. ‘Galloping’, as illustrated in Figure 4-2 and Figure 4-3, is the term used by civil engineers for one degree of freedom instability of bluff structures in winds and currents (Blevins, 2001). Similar to VIV, galloping is characterised by a separated flow in the rear of the body, i.e. a flow that does not follow the contour of the solid body (Fung, 2002).

‘Flutter’ is aerospace terminology for coupled pitch-plunge instability of airfoils (Figure 4-4). Flutter is another type of self-excited oscillation which does not necessarily involve flow separation. The best example occurs in the field of aeronautics where streamlining is a rule and flow separation is avoided. But in cases that separation may happen over part of the body, it is called ‘stall flutter’.

As the literature survey confirms, the characteristic of fairing vibration best matches an instable behaviour rather than VIV. Moreover, observations in a tank tests have indicated that the system experiences coupled transverse-torsion motion in 3D space as shown in Figure 4-5. Thus, it can be concluded that the instability of system should be in the form of ‘flutter’.

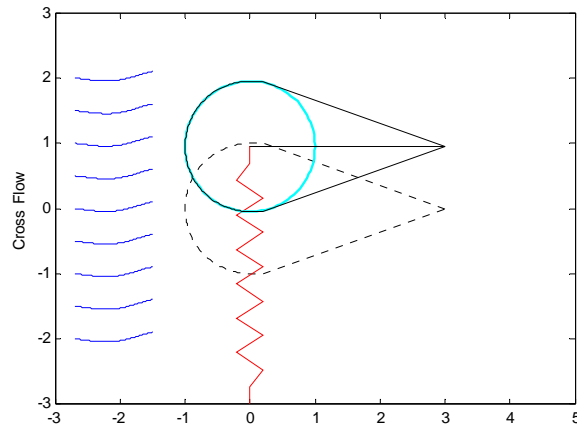


Figure 4-2 Galloping (Plunge) – 2D.

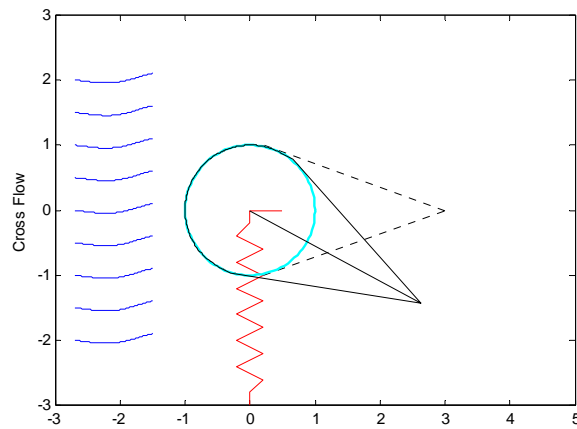


Figure 4-3 Galloping (Torsion) – 2D.

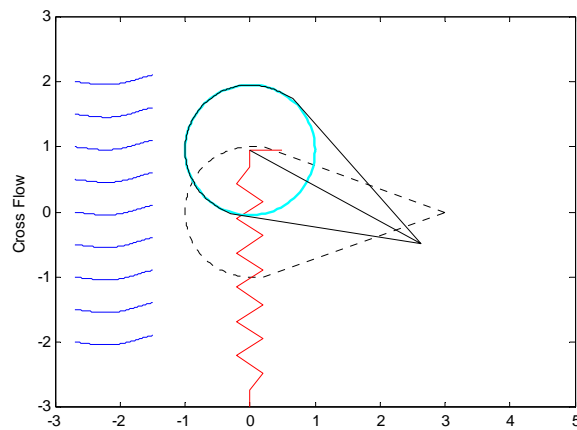


Figure 4-4 Flutter – 2D.

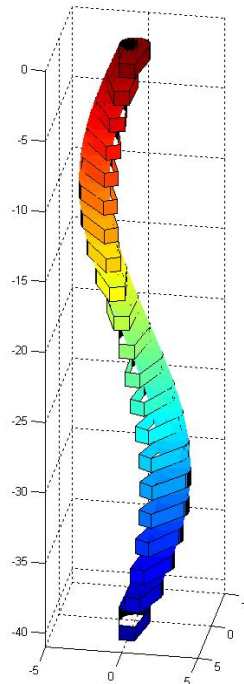


Figure 4-5 Schematic Pattern of Fairing Flutter in 3D.

4.3 Classical Flutter

To describe the physical phenomenon of foils flutter, consider a simple foil mounted in a wind tunnel at small angle of attack like a cantilever beam (Fung, 2002). When there is no flow in the wind tunnel and the model is disturbed, say by a poke with a rod, oscillation sets in which is damped gradually. When the speed of flow in the wind tunnel gradually increases; the rate of damping the oscillation first increases. With further increase of the flow speed, however, a point is reached at which the damping rapidly decreases. At the critical flutter speed, an oscillation can just maintain itself with steady amplitude. At speeds of flow above the critical, a small accidental disturbance of the foil can serve as a trigger to initiate an oscillation of excessive violence. In such circumstances, the foil suffers from oscillatory instability and is said to flutter. Experiments show that the oscillations are self-sustained, i.e. no external oscillator or forcing source is required.

Flutter Mechanism

The oscillatory motion of a fluttering foil has both flexural and torsional components. A rigid foil so constrained as to have only flexural degree of freedom (DOF) does not experience flutter. In general, coupling of several DOFs is an essential feature for flutter. The steady oscillations that occur at the critical speed is harmonic. A three-dimensional experiment of a wing shows that the flexural movements at all points across the span are approximately in phase with one another, and likewise the torsional movements are in phase too, but the important point is that the flexure is 90° out of phase from the torsional movement (Figure 4-6). It is this phase difference that induces the flutter (Fung, 2002). It has been shown in aerodynamics that flutter occurs because the speed of flow affects the amplitude ratio and phase shift between motions in various DOFs in such a way that energy can be absorbed by foil from the stream passing by.

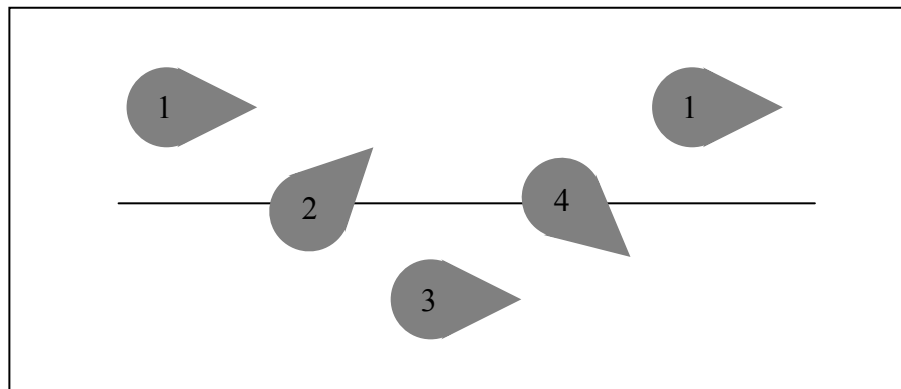


Figure 4-6 Plunge and Torsion Out of Phase in Flutter.

Flutter Theories

Many efforts have been accomplished to set up a theoretical model for analysis of wing flutter and its causes. The coupled interaction of wing motions and flow response and associated forces causes tremendous complication. Governing equations are comprised of terms representing structural characteristics and motions of wing as well as aerodynamic forces which are dependent on the wing motions.

Thus, the aerodynamic forces should be calculated along with solving the equations of motion. To this end, many have tried to establish a method to find the fluid force term and replace it in governing equations.

The most recent method introduces sophisticated computational fluid dynamics (CFD) in order to solve the complicated Navier-Stokes equations for which it is not inherently possible to find an analytical solution in a general case. But few years before, when numerical methods were not so popular and feasible, several analytical methods were developed for special cases with the aid of simplifying assumptions.

Frequently simplifying assumptions are made with respect to the spatial or temporal dependence of the aerodynamics forces. There are two widely used approximations for spatial dependence, i.e. ‘Slender Body’ and ‘Strip Theory’ (Dowell et al., 1995).

The first approximation based on spatial consideration is possible when the airfoil is of high aspect ratio or one is dealing with slender body. In such cases the chordwise spatial derivatives (rates of change) may be neglected compared to spanwise rates of change and hence the chordwise coordinate effectively becomes a parameter rather than an independent coordinate. It is useful as an asymptotic check on numerical methods for slender bodies and high aspect ratio wings.

In strip theory approximation, one employs the known results for two-dimensional flow (infinite span airfoil) to calculate the aerodynamic forces on a surface of finite span. The essence of the approximation is to consider each spanwise station as though it was a portion of an infinite span wing with uniform spanwise properties.

With the aid of using strip theory method, the three-dimensional (3D) problem is simplified to two-dimensional (2D) case. Then there exists three simplifying assumptions to calculate the aerodynamic force exerted on a 2D airfoil, i.e. ‘Theory of Wing-section’, ‘Linearised Thin-airfoil Theory’ and ‘Quasi-steady Assumption’.

Theory of wing section dates back to the 1930s when Theodorsen gave an exact treatment of the problem of determining the 2D potential flow around wing section of any shape (Theodorsen, 1933, Theodorsen and Garrick, 1934, Abbott and Von Doenhoff, 1959). In this method, viscosity is neglected and the potential flow

conditions hold and in the light of that, it is tried to transform the potential flow around an airfoil to potential flow around a circle which is easily calculated. It is based on the theorem of conformal representation stated by Riemann almost two centuries ago. Thus, the aerodynamic forces are known in an analytical form and they can be replaced by the force term in governing equations of body motion. Eventually, it results in an analytical solution for airfoil flutter in inviscid flow (Theodorsen and Garrick, 1940, Theodorsen and Garrick, 1942, Theodorsen, 1935).

Linearised thin-airfoil theory is also based on potential flow in inviscid fluid. It says that if a steady 2D flow stream passes an airfoil, disturbances are imposed into the flow in such a manner that the resultant flow is tangent to the airfoil. According to the aerodynamic theory, the thin airfoil can be replaced by a continuous distribution of vorticity. The total lift force is the sum of contribution of each individual vorticity. In addition, for a thin enough airfoil of small camber, the surface of the airfoil differs only infinitesimally from a flat plate. The induced velocity over the airfoil surface, to the first order of approximation, can be calculated by assuming the vortices to be situated on the chord axis (Fung, 2002). Through these simplifying assumptions, aerodynamic forces can be calculated analytically.

Quasi-steady assumption was introduced in order to make the analysis of a moving airfoil simple. It states that the aerodynamic characteristics of an airfoil whose motion consists of variable linear and angular motions are equal, at any instant of time, to the characteristics of the same airfoil moving with constant linear and angular velocities equal to the actual instantaneous values.

The strip theory approximation, to change a 3D problem into 2D case, is clear and its meaning is generally accepted but this is not true for the quasi-steady assumption. Its qualitative meaning is generally accepted, i.e. one ignores the temporal memory effect in the aerodynamic model and assumes the aerodynamic forces at any time depend only on the motion of airfoil at that specific time and are independent of the motion at earlier times. That is, the history of foil motion is not taken into account as far as determining aerodynamic forces (Dowell et al., 1995). As a result, the viscose fluid force can be measured in wind-tunnel tests on stationary models held at various angles.

Nevertheless, most galloping and flutter analysis utilises quasi-steady fluid dynamics (Blevins, 2001). In general, the quasi-steady assumption is valid only if the frequency of periodic component of fluid force, resulted from vortex shedding, is well above the vibration frequency of structure, $f_s \gg f_n$, so that the fluid responds quickly to any structural motion. This requirement is often met at higher reduced velocities such that $(U/f_n \cdot D) > 20$. Below this limit, the quasi-steady assumption is questionable and for galloping-like instabilities of bluff structures, VIV may occur simultaneously. In this case, both vortex shedding and instability can excite the vibration. Then the structure responds to vortex shedding near the vortex resonance, $U/f_y D \approx 5$, and to instability at higher reduced velocity $U/f_y D > 5$. In such conditions, the predictions of instability theory become relatively poor because the quasi-steady forces induced by changes in angle of attack are obscured by unsteady vortex shedding forces acting at the same or similar frequencies.

4.4 Differences from Classical Wing Flutter

The observations of wing flutter and fairings instability are in conformity and therefore it can be deduced that the governing mechanism is the same. However, when it comes to the stage of setting up an analytical model to explain and predict these phenomena, a number of subtle distinctions emerge which do not let the researcher apply available flutter theories to fairing instability blindly. Existing analytical theories for flutter as discussed have been developed for thin airfoils.

The essential assumptions of thin-airfoil theory are (1) that the lifting characteristics of an airfoil below stall are negligibly affected by viscosity, (2) that the airfoil is operating at a small angle of attack, and (3) that the resultant of the pressure forces (magnitude, direction, and line of action) is only slightly influenced by the airfoil thickness, since the maximum mean camber is small and the ratio of maximum thickness to chord is small (Bertin and Smith, 1998). Typically, airfoil sections have a maximum thickness of approximately 12% of the chord. Thus thin airfoil relative to chunky fairing and inviscid flow relative to viscous seawater are two major assumptions which differentiate fairing instability from classical flutter. The main

differences between fairing instability and classical flutter in developing an analytical model can be outlined as follows.

(A) Viscosity

The effects of viscosity on hydrodynamic forces of foil are to produce two types of drag as follows (Anderson, 2007). (1) Skin friction drag, that is, the component in the drag direction of the integral of the shear stress over the body. (2) Pressure drag due to separation, that is, the component in the drag direction of the integral of the pressure distribution over the body. The occurrence of separated flow over an aerodynamic body not only increases the drag but also results in a substantial loss of lift.

(B) Thickness

Thickness plays a critical role in hydrodynamic characteristics of a foil because thickness causes the flow in vicinity of the foil to change behaviour and thus the pressure distribution over the foil contour will alter. Eventually, the resultant of the pressure forces will be quite different for foils with different thickness. For instance, the centre of pressure of a thick foil moves with variation of foil orientation (angle of attack) (Grant and Patterson, 1977) whereas it is assumed to be fixed in classical flutter analysis. In addition, the net vertical force on structure is the vector sum of lift and drag in the vertical plane. For thin airfoil at small angles of attack, the lift is much larger than drag. So the vertical force is almost entirely due to lift. But this is not true for bluff structures and thick foils like fairing.

(C) Torsional Stiffness

A wing of an airplane is a continuous structure which can be modelled as a cantilever beam with both flexural and torsional stiffness. Torsional stiffness provided by structure is advantageous in controlling the flutter. But, riser fairings are designed to freely swing about the riser and therefore, there exists no torsional stiffness to restore a distorted fairing to initial condition except the torsional stiffness generated by hydrodynamic forces. Consequently, the absence of torsional stiffness of structure

and replacement of its role with hydrodynamic stiffness results in an influential difference from classical flutter.

(D) Frictional Damping

An oscillation is called dynamically unstable if the oscillating body extracts energy from the flow in completing a cycle. If the oscillating body has neither external excitation nor internal friction, then the dynamic instability can be identified with flutter. Internal friction dissipates energy and modifies the kinematic relations (the amplitude ratio and phase relationship between various DOF) of the oscillation of an elastic system. Hence, when there is internal friction, the dynamic instability alone cannot be directly identified with flutter (Fung, 2002).

All above distinctions between fairings instability and classical flutter of airfoils imply that dealing with fairing instability requires further attention and classical flutter theories cannot be employed directly. Thus, there exists a need to set up a new and holistic model for fairings instability.

4.5 Methodology

The purpose of this study is to investigate the flutter type instability of fairing analytically in order to set up the governing criterion for instability onset. It seeks an analytical model that can describe the physical mechanisms causing instability and determine how it is related to the characteristics of system. Such a model should provide some guidance on design changes that may remove the instability or hinder its onset to a higher threshold speed and provide a basis for determining whether instable behaviour observed in tests is common to all fairing designs or it is limited only to fairings with particular design characteristics. Establishing such model needs governing equations and forces to be derived.

Equations of motion will be in the form of structural terms representing body motion and also terms indicating hydrodynamic forces. Hydrodynamic forces are dependent on the body motion and therefore they are coupled and interrelated with other terms. Thus, to solve such problem, hydrodynamic forces should be first defined with respect to body motion.

To this end, the exact solution of governing Navier-Stokes equations ends up with sophisticated numerical work and requires the method of computational fluid dynamics (CFD). Consequently, the main analytical features are masked by the calculative complications which are not compatible with primary defined goal. Thus, using simplifying approximations, both spatial and temporal, to find an analytical answer is inevitable.

To remove the effect of three-dimensionality on hydrodynamic forces, ‘strip theory’ approximation is deployed. Thereby, it is assumed that hydrodynamic characteristics of a 3D fairing are equal to that of a 2D section and spanwise variations of force are negligible.

Now, the question is how to define hydrodynamic forces of a 2D moving fairing. Fairings resemble a typical foil but as was earlier mentioned, the theory of wing-section with analytical solution for forces and centre of pressure is not applicable due to assumption of inviscid fluid and potential flow. Likewise, the thin-foil theory, linearised or unsteady, cannot be employed either because of its associated assumptions that are not valid here.

The last remaining method is to seek a solution under the assumption of quasi-steady dynamic derivatives. The quasi-steady assumption introduces important simplifications that one will have no difficulty in carrying through a detailed analysis explicitly. Therefore, it seems advantageous to use the quasi-steady theory for this study.

Therefore, based on the details explained thus far, the general approach to model the instability of riser fairing will be in the form of first, identifying all degrees of freedom. Then the equations of motion will be derived through using Lagrange’s equation. The force term will be replaced with hydrodynamic forces obtained under the assumptions of quasi-steady condition and strip theory. Last step is to assess the stability of assembled equations against infinitesimal disturbance from equilibrium position. It will be done through eigenvalue analysis.

With regard to assessing stability against infinitesimal disturbance, it should be noted that in a large proportion of all cases, an adequate definition of flutter properties of a system can be obtained by studying the stability of infinitesimal motions (Bisplinghoff et al., 1996). It is then sufficient to analyse the vibration with exponential time dependence e^{pt} (p complex), since all other small motions can be built up therefore by superposition. If slight deformation is unstable, it is an undesirable situation regardless of the stability of the bigger ones. On the other hand, the larger displacements are usually stable if the small ones are. In fact, they may have much greater stability, as in the case of amplitude limitation due to stalling on the flutter oscillations, which is often observed on very flexible aero-elastic models in the wind tunnel.

Assumptions

The development of the analytical stability model discussed in the following chapters is based on few assumptions outlined below:

- Fairing segments are installed on a vertical top tensioned riser.
- Individual fairing segments are rigid structures and do not experience any deflection.
- Fairing segments are free to rotate about the riser and there is no structural torsion-stiffness.
- Entrapped water within the fairing shell moves with the fairing as a rigid body.
- ‘Strip theory’ approximation is employed to reduce the three-dimensionality of hydrodynamic characteristics of fairing to a two-dimensional section.
- ‘Quasi-steady’ assumption is considered and the effect of flow history is eliminated.
- As observed in the tank tests, motion in-line with the current direction is of very limited amplitude in comparison with cross-flow translation, e.g. 0.6D

against 4D (Braaton et al., 2008), and has negligible effect on flutter-type instability.

- Any disturbance or motion from equilibrium position at the instability onset is of small amplitude.
- Lift, drag, moment and added mass (for all degrees of freedom) are the hydrodynamic forces taken into account.
- According to quasi-steady assumption, lift, drag and moment are functions of instantaneous angle of attack (AoA). But the effects arise from cross-flow translation as well as influences due to time variation of AoA (torsional velocity) are to be considered.

These assumptions impose some limitations on the application of this model which will be discussed in the following.

Limitations

This model will be helpful in determining the threshold velocity at which the instability can occur for a given system of riser and fairing, however, it is not capable of explaining the evolution of unstable motion and its development in subsequent stages. Whether the amplitude of this unstable motion continues to increase or is interrupted later by other events is out of the scope of this model.

The other major limitation of the theory outlined so far is that the hydrodynamic coefficients are assumed to vary only with angle of attack, but experience shows that the coefficients are affected by turbulence and vortex shedding. Turbulence in the mean flow can either reduce or increase the tendency toward instability (Blevins, 2001). On the other hand, the quasi-steady assumption employed in this method requires that the vortex shedding frequency be well above the natural frequency of structure. It should be noted that as the fairing is devised to remove vortex shedding, such a situation is not very likely but just in case the fairing still experiences some vortices, this condition should be assessed too.

It should be mentioned that all research discussed in this study is based on linearization of hydrodynamic forces. Since real physical phenomenon are not linear, the question always arises how good the linearised theory is as an approximation to the real case, and to what extent of magnitude of the variables concerned is linearised theory valid. Unfortunately, so little is known about the nonlinear case that the question raised cannot be answered. At present, it can only be said that experimental observations show the linearised theory of flutter type instability represents fairly closely the real situation in the neighbourhood of the critical instability speed, provided that the amplitude of motion remains small (Fung, 2002).

In the next chapter, the analytical model will be developed within this framework for the simple case of two-dimension to identify the role of parameters involved. It will be expanded to three-dimensional case later.

2D Theoretical Model

This chapter focuses on developing an analytical model for simplified case of a two-dimensional (2D) problem. It explains how to eliminate the third dimension, riser's length, and elaborates the process of modelling the mechanism of system instability step by step. Finally, the established model is verified against available experimental data.

5.1 Introduction

A system of riser and fairing in practice consists of a vertical top-tensioned riser (see Section 4.5) which can deform due to its flexural stiffness and also a set of fairings attached to the riser and free to rotate about it while moving with it transitionally.

In general, such a system of a continuous elastic body/riser plus fairings has infinitely many degrees of freedom (DOFs). However, owing to its particular construction, if the elastic deformation of fairing cross-section is negligible relative to other deformations and the fairing being treated as a rigid body, then regardless of negligible stream-wise displacement, the system motions in any section along the riser length can be described with sufficient accuracy by two quantities: the deflection at centre of rotation as a reference point and the angle of rotation about that point, i.e., the flexural and the torsional deformations, respectively. A flutter-type mode is comprised of these two elements.

The motion of such 3D dynamic system looks at the first glance too complicated to be evaluated analytically. In order to decompose this complexity into several simpler problems it seems suitable to remove the third dimension by considering its effect on a 2D model. This simplified model provides the ground to easily and without any confusion identify the key parameters.

To reduce the full problem to a 2D case, it is required to pick a section along the riser length including one of these fairings and remove the rest of the system, however, in order to analyse the selected section or fairing individually, it is necessary to take the influence of the removed part into account.

Thus, the simplified 2D model should be made of a riser, a fairing surrounding it, as well as a combination of transverse stiffness and transverse-torsion damping, which represents the effect of a riser in the third dimension. Such a model can also simulate the case consisting of a set of fairings installed on a rigid riser supported with springs at two ends.

This chapter will be limited to two-dimensional coupled transverse-torsion dynamics of this system. In the following, based on the assumptions described in Section 4.5, the degrees of freedom and corresponding hydrodynamic forces are identified first. The equation of motion will be established using the Lagrange's equations. As was mentioned earlier, the hydrodynamic forces are functions of the system motion and the effect of the fairing's motion therefore will be considered next. The resultant equations are linearised and an eigenvalue analysis is carried out to find the situation at which a system goes unstable. The obtained criterion is converted into dimensionless form through defining meaningful dimensionless parameters. Eventually, the developed 2D analytical model will be used to predict the instability onset condition for a tank test. This comparison helps to verify the level of model agreement with what happens in reality. Later on, the influence of friction damping is further discussed.

5.2 Governing Equations of Motion

Before proceeding to set up the governing equations, it is first necessary to identify the system in terms of the degrees of freedom for each body and associated external or interactional forces. Suppose a cross-section of a riser fitted with fairings as shown in Figure 5-1. The sea current flows in this plane in X direction from left to right.

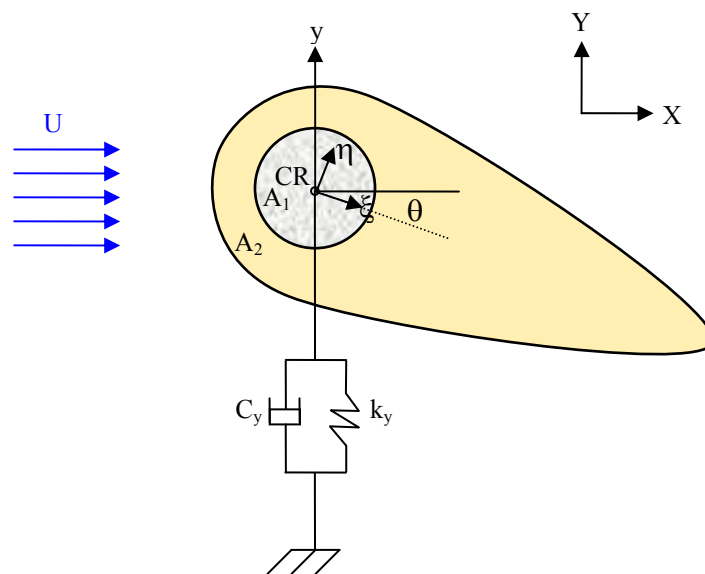


Figure 5-1 Local and Global Coordinates, Degrees of Freedom.

A riser is a pipe, possibly covered by buoyancy module, filled with fluid and is supported by a spring in cross-flow (CF) direction which depicts the contribution of the rest of the riser. Moreover, the rest of the riser can dissipate energy through oscillation in CF direction. This phenomenon is simulated by a damper, shown by a dash-pot. As the test reports showed large amplitude vibration in CF direction, it is assumed that the negligible motion in line with the current is unimportant in comparison with CF oscillation (see Section 4.5). With this in mind, the riser has only translational DOF and merely moves transversely, $y(t)$. The riser also interacts with the fairing which results in transverse and torsional forces, F_{int}^y and F_{int}^θ respectively. What should be noted is that the goal in fabrication of the fairing is that

it experiences as little torsional friction as possible to easily align itself to current. Therefore, it can be deduced that this friction force can affect the rotational freedom of fairing and induces no tangible deformation in the riser, hence, meaning there is no need to consider another DOF for torsion of the riser.

On the other hand, a fairing is a teardrop-shape shell which is believed to be constructed robust enough not to bear any structural deformation induced by hydrodynamic forces (see Section 4.5). It embraces the riser in the nose and follows its transverse motion. In addition, it is designed to weathervane about the riser (see 4.5). Consequently, the fairing has two DOFs and while moving transversely with the riser $y(t)$, it rotates independently $\theta(t)$. As mentioned above, the riser and fairing impose mutual forces at their interface, i.e. F_{int}^y and F_{int}^0 . More importantly, the interaction of the system with the surrounding fluid and current is through fairing and associated hydrodynamic forces. The hydrodynamic forces which have components in the direction of fairing's DOFs consist of lift, drag, moment and added mass. The resultant component for corresponding DOF will be derived later. It should be noted that the fairing may be filled with buoyancy material which is rigid and behaves as a part of the fairing. Nevertheless, there are other types of fairings which are hollow and the sea water penetrates into them. The entrapped water within the fairing's shell is assumed to follow its motion and thus the entrapped water is treated as a rigid body like the previous case, i.e. a solid fairing (see Section 4.5).

A very effective method for deriving equations of motion for dynamic systems is to use Lagrange's equations. These equations state that,

$$\frac{d}{dt} \left(\frac{\partial L}{\partial \dot{q}_i} \right) - \frac{\partial L}{\partial q_i} = Q_i \quad 5-1$$

where the superscript dot denotes the derivative with respect to time and,

$L = T - V$, Lagrangian

T = Kinetic energy

V = Potential energy

Q_i = generalised forces

q_i = generalised coordinates

In this case, as was explained earlier, the motion of whole system requires two independent DOFs, $y(t)$ and $\theta(t)$, to be fully described. So, these DOFs can be used as the generalised coordinates. The convention of positive direction for them is as illustrated in Figure 5-1, i.e. upward for $y(t)$ and clockwise for $\theta(t)$.

Prior to applying the Lagrange's equations to this problem, a coordinate system needs to be defined in order to specify the displacement and motion of each point. The local coordinate system (ζ, η) is fixed on the fairing, moving and rotating correspondingly with it (Figure 5-1). Its origin is located at the centre of rotation (CR), i.e. centre of riser. The global coordinate system is fixed on the platform (in the plane of cross-section). Consequently, the global coordinates (X, Y) of any point on the fairing and riser have three terms, local coordinate plus transverse and angular displacements of the origin of local coordinate system.

$$\begin{aligned} X &= 0 + \xi + \eta\theta \\ Y &= y + \eta - \xi\theta \end{aligned} \quad 5-2$$

The velocity of each point in the global coordinate system is easily obtained.

$$\begin{aligned} \dot{X} &= \eta\dot{\theta} \\ \dot{Y} &= \dot{y} - \xi\dot{\theta} \end{aligned} \quad 5-3$$

The kinetic energy of the whole system is composed of two parts, energy of solid bodies, i.e. riser (T_1) and fairing (T_2), and energy of fluid motion (T_3) induced by moving body. Taking the interaction forces between riser and fairing into account, let's derive the equation of motion for each of them separately.

Kinetic energy of the riser is,

$$T_1 = \frac{1}{2} m_r \dot{y}^2 \quad 5-4$$

where m_r is the mass of riser.

Potential energy is accumulated in the spring,

$$V = \frac{1}{2} k_y y^2 \quad 5-5$$

The influence of CF damping is presented in the conventional form of a non-conservative viscose damping force, $-C_y \dot{y}$, where C_y is the damping coefficient of riser.

The other forces imposed on the riser come from the interaction interface with the fairing and as was described in the system identification contain F_{int}^y and F_{int}^θ for transverse and torsional DOFs respectively.

By substituting these variables in Lagrange's Equations (5-1) and taking $y(t)$ as the only DOF or generalised coordinate, q_i , it gives,

$$L = T - V = \frac{1}{2} m_r \dot{y}^2 - \frac{1}{2} k_y y^2$$

$$\frac{d}{dt} \left(\frac{\partial L}{\partial \dot{y}} \right) - \frac{\partial L}{\partial y} = m_r \ddot{y} + k_y y = Q_y = -C_y \dot{y} + F_{int}^y$$

Eventually, the governing equation of motion for riser CF transition can be written,

$$m_r \ddot{y} + k_y y = -C_y \dot{y} + F_{int}^y \quad 5-6$$

The fairing is in contact with the riser on the inner side and interacts with fluid and current on the outer side. As it moves or swings, it pushes fluid particles and thus, the kinetic energy of the system comprises of two parts, one from the fairing's body (T_2) and one from fluid (T_3). By integrating the kinetic energy of a particle on the fairing, it renders,

$$T_2 = \frac{1}{2} \int_{A_2} (\dot{X}^2 + \dot{Y}^2) \rho_{fr} d\xi d\eta = \frac{1}{2} \int_{A_2} (\eta^2 \dot{\theta}^2 + \dot{y}^2 - 2\xi \dot{y} \dot{\theta} + \xi^2 \dot{\theta}^2) \rho_{fr} dA =$$

$$= \frac{1}{2} m_{fr} \dot{y}^2 + \frac{1}{2} J \dot{\theta}^2 - S_x \dot{y} \dot{\theta} \quad 5-7$$

where m_{fr} , S_x and J are the mass, first mass moment of area and polar mass moment of inertia for fairing respectively.

$$m_{fr} = \int_{A_2} \rho_{fr} dA$$

$$J = \int_{A_2} (\eta^2 + \xi^2) \rho_{fr} dA$$

$$S_x = \int_{A_2} \xi \rho_{fr} dA$$

The kinetic energy of fluid domain is obtained by integrating the kinetic energy of a fluid particle over the whole domain,

$$\begin{aligned}
 T_2 &= \frac{1}{2} \int_{\text{fluid}} \left[\left(\dot{y} u_x^{\dot{y}} + \dot{\theta} u_x^{\dot{\theta}} \right)^2 + \left(\dot{y} u_y^{\dot{y}} + \dot{\theta} u_y^{\dot{\theta}} \right)^2 \right] \rho dA = \\
 &= \frac{1}{2} \int_{\text{fluid}} \left[\dot{y}^2 \left(\left(u_x^{\dot{y}} \right)^2 + \left(u_y^{\dot{y}} \right)^2 \right) + \dot{\theta}^2 \left(\left(u_x^{\dot{\theta}} \right)^2 + \left(u_y^{\dot{\theta}} \right)^2 \right) + 2\dot{y}\dot{\theta} \left(u_x^{\dot{y}} u_x^{\dot{\theta}} + u_y^{\dot{y}} u_y^{\dot{\theta}} \right) \right] \rho dA = \\
 &= \frac{1}{2} m_a \dot{y}^2 + \frac{1}{2} J_a \dot{\theta}^2 - S_a \dot{y}\dot{\theta} \tag{5-8}
 \end{aligned}$$

where $u_x^{\dot{y}}$ denotes the velocity of a fluid particle in x direction induced by unit velocity of the fairing in y direction ($\dot{y}=1$). Interestingly, m_a , J_a and S_a are the conventional and well-known parameters so-called added mass. They are respectively the added mass parameters for CF transition, angular motion and their mutual effects on each other.

$$m_a = \int_{\text{fluid}} \left(\left(u_x^{\dot{y}} \right)^2 + \left(u_y^{\dot{y}} \right)^2 \right) \rho dA$$

$$J_a = \int_{\text{fluid}} \left(\left(u_x^{\dot{\theta}} \right)^2 + \left(u_y^{\dot{\theta}} \right)^2 \right) \rho dA$$

$$S_a = - \int_{\text{fluid}} \left(u_x^{\dot{y}} u_x^{\dot{\theta}} + u_y^{\dot{y}} u_y^{\dot{\theta}} \right) \rho dA$$

It should be noted that no potential energy is reserved in the fairing as it is free to rotate.

Forces exerted on the fairing come from two different sources. One group arises from interface with the riser and includes $-F_{\text{int}}^y$ and $-F_{\text{int}}^\theta$. $-F_{\text{int}}^\theta$ represents the torsional friction resulted from angular oscillation of the fairing against the riser. This friction absorbs energy and works as a damper. For simplicity, this non-conservative force is modelled here with a viscous type damping term and will be discussed later in Section 5.8.

$$-F_{\text{int}}^\theta = -C_\theta \dot{\theta}$$

The other group of forces is hydrodynamic forces which have components in the direction of both DOFs/generalised coordinates. So, the resultant forces are,

$$Q_y = [\text{Hydrodynamic Force}]_y - F_{int}^y \quad 5-9$$

$$Q_\theta = [\text{Hydrodynamic Force}]_\theta - C_\theta \dot{\theta} \quad 5-10$$

By substituting Equations (5-7) and (5-8) in Lagrange's Equation (5-1), Lagrangian will be,

$$L = T - V = \frac{1}{2}(m_{fr} + m_a)\dot{y}^2 + \frac{1}{2}(J + J_a)\dot{\theta}^2 - (S_x + S_a)y\dot{\theta}$$

By taking both DOFs of $y(t)$ and $\theta(t)$ as the generalised coordinates and replacing the corresponding forces from Equations (5-9) and (5-10), the Lagrange's equation gives two coupled equations for transverse and torsional motions of the fairing respectively,

$$(m_{fr} + m_a)\ddot{y} - (S_x + S_a)\ddot{\theta} = [\text{Hydrodynamic Force}]_y - F_{int}^y \quad 5-11$$

$$(J + J_a)\ddot{\theta} - (S_x + S_a)\ddot{y} = [\text{Hydrodynamic Force}]_\theta - C_\theta \dot{\theta} \quad 5-12$$

In summary, the governing equations of the riser's CF transition as well as the fairing's both transverse and torsional motions have been derived. To remove the term of internal force, F_{int}^y in Equation (5-11) is substituted from Equation (5-6),

$$(m_{fr} + m_a)\ddot{y} - (S_x + S_a)\ddot{\theta} = [\text{Hydrodynamic Force}]_y - m_r \ddot{y} - k_y y - C_y \dot{y} \quad 5-13$$

By re-arranging the Equations (5-12) and (5-13), the final equations of motion of the whole system are obtained,

$$(m + m_a)\ddot{y} + C_y \dot{y} + k_y y - (S_x + S_a)\ddot{\theta} = [\text{Hydrodynamic Force}]_y \quad 5-14$$

$$-(S_x + S_a)\ddot{y} + (J + J_a)\ddot{\theta} + C_\theta \dot{\theta} = [\text{Hydrodynamic Force}]_\theta \quad 5-15$$

where

$$m = m_r + m_{fr}$$

The next step is to calculate the hydrodynamic forces acting on the fairing at an instantaneous position during the vibration.

5.3 Hydrodynamic Forces and Effect of Motion on AoA

In general, a fairing like any other foil when exposed to a current feels hydrodynamic forces which include drag, lift, moment and added mass. The latter has already emerged through the process of deriving equations of motion. A fairing is a three-dimension body which swings in the fluid and the associated hydrodynamic forces therefore inherit this characteristic. As was explained in Section 4.5, if the spanwise length of the fairing is adequately long, the ‘Strip Theory’ approximation can be deployed to eliminate the effect of third dimension along the riser and reduce the problem to a 2D case in the plane of the fairing cross-section.

However, it is quite obvious that although the direction of current is constant, the fairing still oscillates in this plane and like any foil such as airplane’s wing, the hydrodynamic forces depends on the position of the fairing relative to the current direction, or in other words angle of attack (AoA). More significantly, sea water is a fluid and not a rigid body. So, its reaction, to any disturbance caused by the fairing’s motion, does not respond in a prompt manner. To put it more simply, the hydrodynamic forces at a specific time not only depend on AoA but also they may be influenced by the history of fluid’s motion. This adds to the complexity of the issue and makes the analysis face some difficulties. To tackle this issue, it was elaborated in methodology (see Section 4.5) as to why it is necessary to use the ‘Quasi-Steady’ assumption and remove the flow history. As a result, hydrodynamic forces of the fairing depend on only instantaneous AoA, α .

Prior to writing down the equations of hydrodynamic forces, there exists another key phenomenon which needs serious attention and should never be neglected. By considering the ‘Quasi-steady’ assumption, the hydrodynamic forces become a function of instantaneous AoA, but as the fairing is swinging in the constant sea current, its transverse and torsional velocities have effect on relative flow velocity, U_{rel} . In other words, what a moving fairing experiences at a distortion angle of say θ is quite different from what a fixed fairing feels at the same angle of θ . As shown in Figure 5-2, it is due to the fact that the fairing’s velocity has components inline and perpendicular to current velocity and therefore they change the vector of relative current velocity. Accordingly, the instantaneous angle of attack, α , is not equal to the

instantaneous distortion angle, θ . It should be noted that as explained in Section 4.5, since the motion in-line with the current direction is of small amplitude compared with CF oscillation, the associated effect on AoA is therefore ignored.

When the fairing moves upward in $+y$ direction, what the fairing feels is a current flowing downward in $-y$ direction. Thus, with reference to Figure 5-2, the instantaneous AoA may be written as,

$$\alpha = \theta - \beta \tag{5-16}$$

where

$$\beta = \arctan\left(\frac{\dot{y} - R\dot{\theta}}{U}\right) \tag{5-17}$$

R is the distance of a reference point from the centre of rotation. It is used to describe the resultant of variations of the AoA over the fairing's circumference which are induced by the angular velocity, $\dot{\theta}$. In fact, angular velocity generates a vertical component of velocity vector which varies over the section by horizontal distance from pivot point. It will be further clarified later in Section 6.1. If $R > 0$, by convention the reference point is located aft of the CR.

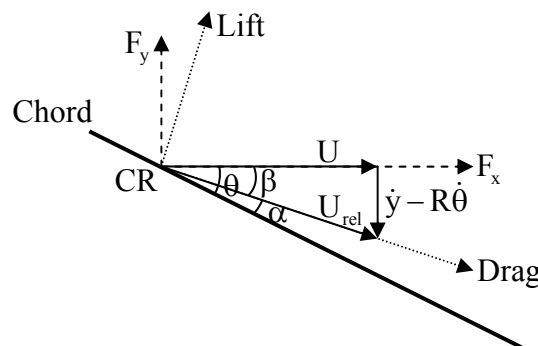


Figure 5-2 Instantaneous Angle of Attack (AoA).

Now, the force components arising from hydrodynamic forces should be derived for each DOF. Suppose a fairing at an instantaneous distortion angle of θ (see Figure 5-2). In these circumstances both lift and drag have a component in the direction of

y. In addition, there exists a moment striving to turn the fairing about the pivot point. All these forces are calculated based on the relative current velocity, U_{rel} , and instantaneous incidence angle of α . If it is assumed that the hydrodynamic coefficients have been measured at the centre of rotation (CR), then the hydrodynamic force for each degree of freedom consists of,

$$\begin{aligned} [\text{Hydrodynamic Force}]_y &= (\text{Lift}) \times \cos \beta - (\text{Drag}) \times \sin \beta = \\ &= \frac{1}{2} \rho U_{rel}^2 c C_L|_{\alpha} \times \cos \beta - \frac{1}{2} \rho U_{rel}^2 c C_D|_{\alpha} \times \sin \beta \end{aligned} \quad 5-18$$

$$[\text{Hydrodynamic Force}]_{\theta} = \frac{1}{2} \rho U_{rel}^2 c^2 C_{M(cr)}|_{\alpha} \quad 5-19$$

where C_D , C_L and $C_{M(cr)}$ are drag, lift and moment coefficients respectively, measured at CR with respect to chord length, c .

If the moment coefficient (C_M) is measured at a point aft of the centre of rotation for a distance w , then C_M should be modified by following equation,

$$C_{M(cr)}|_{\alpha} = C_{M(w)}|_{\alpha} - (w/c)(C_L|_{\alpha} \cos \alpha + C_D|_{\alpha} \sin \alpha) \quad 5-20$$

By substituting these force terms in Equations (5-14) and (5-15), the final form of equations of motion will be as below,

$$(m + m_a)\ddot{y} + C_y \dot{y} + k_y y - (S_x + S_a)\ddot{\theta} = \frac{1}{2} \rho U_{rel}^2 c (C_L|_{\alpha} \cos \beta - C_D|_{\alpha} \sin \beta) \quad 5-21$$

$$-(S_x + S_a)\ddot{y} + (J + J_a)\ddot{\theta} + C_{\theta} \dot{\theta} = \frac{1}{2} \rho U_{rel}^2 c^2 C_{M(cr)}|_{\alpha} \quad 5-22$$

5.4 Linearization

This study as was expressed in objectives (see Chapter 2) is seeking the onset condition for instability of the riser fairing. In other words, it tries to discover the condition at which a fairing that has been aligning itself to the current suddenly loses its stability and any small distortion from equilibrium position, i.e. zero AoA, may develop subsequently and the amplitude of vibration escalates instead of dissipating to its normal state.

To this end, the appropriate approach is to give the system an infinitesimal disturbance from equilibrium position (Section 4.5) and then track down the trend of

oscillation's amplitude to see what conditions makes it rise or descend. The postulate of very small amplitude vibration at instability onset provides the ground to reasonably assume that the variation of hydrodynamic forces is linear in this interval.

Thus, for a small AoA of α , the hydrodynamic coefficients at this angle can be expanded in Taylor's power series about the equilibrium position and the non-linear terms are removed,

$$C_L|_{\alpha} = C_L|_{\alpha=0} + \alpha \left. \frac{\partial C_L}{\partial \alpha} \right|_{\alpha=0} + O(\alpha^2) \quad 5-23$$

$$C_D|_{\alpha} = C_D|_{\alpha=0} + \alpha \left. \frac{\partial C_D}{\partial \alpha} \right|_{\alpha=0} + O(\alpha^2) \quad 5-24$$

$$C_{M(cr)}|_{\alpha} = C_{M(cr)}|_{\alpha=0} + \alpha \left. \frac{\partial C_{M(cr)}}{\partial \alpha} \right|_{\alpha=0} + O(\alpha^2) \quad 5-25$$

where $O(\alpha^2)$ means terms proportional to α^2 and higher powers of α have been neglected. It should be noted that for a section symmetric about the stream direction, e.g. fairings, lift and moment coefficients at rest ($\alpha = 0$) are zero in these equations.

The variable α in the above equations is itself a function of velocities. With this in mind, this variable also needs to be expanded in Taylor's series similarly. With reference to Equations (5-16) and (5-17), it can be easily written as,

$$\beta = \arctan\left(\frac{\dot{y} - R\dot{\theta}}{U}\right) = \left(\frac{\dot{y} - R\dot{\theta}}{U}\right) + O\left(\left(\frac{\dot{y} - R\dot{\theta}}{U}\right)^2\right) \quad 5-26$$

$$\alpha = \theta - \beta = \theta - \frac{\dot{y}}{U} + R \frac{\dot{\theta}}{U} + O\left(\left(\frac{\dot{y} - R\dot{\theta}}{U}\right)^2\right) \quad 5-27$$

Now it is time to linearise the hydrodynamic forces in equations of motion. The process is to substitute Equations (5-23) to (5-27) in Equations (5-21) and (5-22) and keep the terms containing DOFs (y , θ and their derivatives) up to only first order. To remove the ambiguity which may arise in the midway of process, it is carried out here step by step for the first one. It will be the same for the second one.

First the drag and lift coefficients in the right-hand side of Equation (5-21) are replaced by Equations (5-23) and (5-24). Then the variable α is substituted from Equation (5-27) and the result is rearranged. This will give,

$$\begin{aligned} \frac{1}{2}\rho U_{rel}^2 c(C_L|_{\alpha} \cos\beta - C_D|_{\alpha} \sin\beta) &= \frac{1}{2}\rho U_{rel}^2 c\left(\cancel{C_L|_{\alpha=0}} \cos\beta - C_D|_{\alpha=0} \sin\beta\right) + \\ &+ \frac{1}{2}\rho U_{rel}^2 c\left(\frac{\partial C_L}{\partial \alpha}\Big|_{\alpha=0} \cos\beta - \frac{\partial C_D}{\partial \alpha}\Big|_{\alpha=0} \sin\beta\right)\theta \\ &- \frac{1}{2}\rho \frac{U_{rel}^2}{U} c\left(\frac{\partial C_L}{\partial \alpha}\Big|_{\alpha=0} \cos\beta - \frac{\partial C_D}{\partial \alpha}\Big|_{\alpha=0} \sin\beta\right)\dot{y} \\ &+ \frac{1}{2}\rho \frac{RU_{rel}^2}{U} c\left(\frac{\partial C_L}{\partial \alpha}\Big|_{\alpha=0} \cos\beta - \frac{\partial C_D}{\partial \alpha}\Big|_{\alpha=0} \sin\beta\right)\dot{\theta} \end{aligned}$$

With reference to Figure 5-2, the trigonometric terms are equal to

$$\cos\beta = \frac{U}{U_{rel}}$$

$$\sin\beta = \frac{\dot{y} - R\dot{\theta}}{U_{rel}}$$

Substitution of these two terms results in,

$$\begin{aligned} \frac{1}{2}\rho U_{rel}^2 c(C_L|_{\alpha} \cos\beta - C_D|_{\alpha} \sin\beta) &= \frac{1}{2}\rho U_{rel} c\left(-C_D|_{\alpha=0} (\dot{y} - R\dot{\theta})\right) + \\ &+ \frac{1}{2}\rho U_{rel} c\left(\frac{\partial C_L}{\partial \alpha}\Big|_{\alpha=0} U - \cancel{\frac{\partial C_D}{\partial \alpha}\Big|_{\alpha=0} (\dot{y} - R\dot{\theta})}\right)\theta \\ &- \frac{1}{2}\rho U_{rel} c\left(\frac{\partial C_L}{\partial \alpha}\Big|_{\alpha=0} - \cancel{\frac{\partial C_D}{\partial \alpha}\Big|_{\alpha=0} \left(\frac{\dot{y} - R\dot{\theta}}{U} - \frac{R\dot{\theta}}{U}\right)}\right)\dot{y} \\ &+ \frac{1}{2}\rho RU_{rel} c\left(\frac{\partial C_L}{\partial \alpha}\Big|_{\alpha=0} - \cancel{\frac{\partial C_D}{\partial \alpha}\Big|_{\alpha=0} \left(\frac{\dot{y} - R\dot{\theta}}{U} - \frac{R\dot{\theta}}{U}\right)}\right)\dot{\theta} \end{aligned}$$

The cross-lined terms are of second order or higher. Therefore, their very small influence is negligible and they should be omitted. By rearranging the terms, it leads to,

$$\begin{aligned} \frac{1}{2}\rho U_{\text{rel}}^2 c \left(C_L|_{\alpha} \cos \beta - C_D|_{\alpha} \sin \beta \right) &= \frac{1}{2}\rho U_{\text{rel}} c \left(\left. \frac{\partial C_L}{\partial \alpha} \right|_{\alpha=0} U \right) \theta \\ &\quad - \frac{1}{2}\rho U_{\text{rel}} c \left(\left. \frac{\partial C_L}{\partial \alpha} \right|_{\alpha=0} + C_D|_{\alpha=0} \right) \dot{y} \\ &\quad + \frac{1}{2}\rho R U_{\text{rel}} c \left(\left. \frac{\partial C_L}{\partial \alpha} \right|_{\alpha=0} + C_D|_{\alpha=0} \right) \dot{\theta} \end{aligned}$$

Since relative velocity (U_{rel}) in the above equation is multiplied by terms of first order, in order to finally reach the linear terms, the constant term in relative velocity should be kept only. It means,

$$U_{\text{rel}} = U \sqrt{1 + \left(\frac{-\dot{y} + R\dot{\theta}}{U} \right)^2} \approx U \left(1 + \frac{1}{2} \left(\frac{-\dot{y} + R\dot{\theta}}{U} \right) \right) \approx U$$

Using this, eventually the right-hand side of Equation (5-21) will be in the form of,

$$\begin{aligned} \frac{1}{2}\rho U_{\text{rel}}^2 c \left(C_L|_{\alpha} \cos \beta - C_D|_{\alpha} \sin \beta \right) &= \frac{1}{2}\rho U^2 c \left(\left. \frac{\partial C_L}{\partial \alpha} \right|_{\alpha=0} \right) \theta \\ &\quad - \frac{1}{2}\rho U c \left(\left. \frac{\partial C_L}{\partial \alpha} \right|_{\alpha=0} + C_D|_{\alpha=0} \right) \dot{y} \\ &\quad + \frac{1}{2}\rho R U c \left(\left. \frac{\partial C_L}{\partial \alpha} \right|_{\alpha=0} + C_D|_{\alpha=0} \right) \dot{\theta} \end{aligned} \tag{5-28}$$

Similar process for Equation (5-22) will render,

$$\begin{aligned} \frac{1}{2}\rho U_{\text{rel}}^2 c^2 C_{M(\text{cr})}|_{\alpha} &= \frac{1}{2}\rho U_{\text{rel}}^2 c^2 \left(\cancel{C_{M(\text{cr})}|_{\alpha=0}} + \alpha \left. \frac{\partial C_{M(\text{cr})}}{\partial \alpha} \right|_{\alpha=0} \right) = \\ &= \left(\frac{1}{2}\rho U_{\text{rel}}^2 c^2 \left. \frac{\partial C_{M(\text{cr})}}{\partial \alpha} \right|_{\alpha=0} \right) \theta + \\ &\quad - \left(\frac{1}{2} \frac{\rho U_{\text{rel}}^2 c^2}{U} \left. \frac{\partial C_{M(\text{cr})}}{\partial \alpha} \right|_{\alpha=0} \right) \dot{y} + \left(\frac{1}{2} \frac{\rho R U_{\text{rel}}^2 c^2}{U} \left. \frac{\partial C_{M(\text{cr})}}{\partial \alpha} \right|_{\alpha=0} \right) \dot{\theta} \\ &= \left(\frac{1}{2}\rho U^2 c^2 \left. \frac{\partial C_{M(\text{cr})}}{\partial \alpha} \right|_{\alpha=0} \right) \theta + \\ &\quad - \left(\frac{1}{2}\rho U c^2 \left. \frac{\partial C_{M(\text{cr})}}{\partial \alpha} \right|_{\alpha=0} \right) \dot{y} + \left(\frac{1}{2}\rho R U c^2 \left. \frac{\partial C_{M(\text{cr})}}{\partial \alpha} \right|_{\alpha=0} \right) \dot{\theta} \end{aligned} \tag{5-29}$$

By replacing the hydrodynamic force terms in Equations (5-21) and (5-22) with linearised terms from Equations (5-28) and (5-29) and re-arranging the result, the equations of motion will finally be in the following form,

$$\begin{aligned} (m + m_a) \ddot{y} + \left(C_y + \frac{1}{2} \rho U c \left(\left. \frac{\partial C_L}{\partial \alpha} \right|_{\alpha=0} + C_D \Big|_{\alpha=0} \right) \right) \dot{y} + k_y y - (S_x + S_a) \ddot{\theta} + \\ - \frac{1}{2} \rho R U c \left(\left. \frac{\partial C_L}{\partial \alpha} \right|_{\alpha=0} + C_D \Big|_{\alpha=0} \right) \dot{\theta} - \left(\frac{1}{2} \rho U^2 c \left. \frac{\partial C_L}{\partial \alpha} \right|_{\alpha=0} \right) \theta = 0 \end{aligned} \quad 5-30$$

$$\begin{aligned} - (S_x + S_a) \ddot{y} + \left(\frac{1}{2} \rho U c^2 \left. \frac{\partial C_{M(cr)}}{\partial \alpha} \right|_{\alpha=0} \right) \dot{y} + (J + J_a) \ddot{\theta} + \left(C_\theta - \frac{1}{2} \rho R U c^2 \left. \frac{\partial C_{M(cr)}}{\partial \alpha} \right|_{\alpha=0} \right) \dot{\theta} + \\ - \left(\frac{1}{2} \rho U^2 c^2 \left. \frac{\partial C_{M(cr)}}{\partial \alpha} \right|_{\alpha=0} \right) \theta = 0 \end{aligned} \quad 5-31$$

The behaviour of the obtained equations is to be investigated and the amplitude of oscillation induced by an infinitesimal distortion should be tracked down in the next stage.

5.5 Eigenvalue Analysis

The purpose of this step is to assess the trend of amplitude variation through time when a small disturbance from equilibrium position occurs due to any instantaneous external excitation, e.g. abnormality in flow or so on. This analysis reveals what conditions makes the system suddenly switch the response from a diminishing oscillation to an increasing vibration and lose its stability.

The equations of motion are two coupled homogenous linear differential equations of second order. To reduce the order of equations to first order, it is necessary to define two auxiliary variables for derivatives of first order (Harris and Stocker, 1998),

$$\hat{Y} = \dot{y} \quad 5-32$$

$$\hat{\Theta} = \dot{\theta} \quad 5-33$$

By substituting them in equations of motion and rearranging the terms, it gives,

$$\begin{aligned}
 (m + m_a) \dot{Y} - (S_x + S_a) \dot{\Theta} = & -k_y y - \left(C_y + \frac{1}{2} \rho U c \left(\frac{\partial C_L}{\partial \alpha} \Big|_{\alpha=0} + C_D \Big|_{\alpha=0} \right) \right) \hat{Y} + \\
 & + \left(\frac{1}{2} \rho U^2 c \frac{\partial C_L}{\partial \alpha} \Big|_{\alpha=0} \right) \theta + \frac{1}{2} \rho R U c \left(\frac{\partial C_L}{\partial \alpha} \Big|_{\alpha=0} + C_D \Big|_{\alpha=0} \right) \hat{\Theta} \quad 5-34
 \end{aligned}$$

$$\begin{aligned}
 -(S_x + S_a) \dot{Y} + (J + J_a) \dot{\Theta} = & - \left(\frac{1}{2} \rho U c^2 \frac{\partial C_{M(cr)}}{\partial \alpha} \Big|_{\alpha=0} \right) \hat{Y} + \\
 & + \left(\frac{1}{2} \rho U^2 c^2 \frac{\partial C_{M(cr)}}{\partial \alpha} \Big|_{\alpha=0} \right) \theta - \left(C_\theta - \frac{1}{2} \rho R U c^2 \frac{\partial C_{M(cr)}}{\partial \alpha} \Big|_{\alpha=0} \right) \hat{\Theta} \quad 5-35
 \end{aligned}$$

Equations (5-32) to (5-35) can be easily re-written in the matrix form,

$$\underbrace{\begin{bmatrix} 1 & 0 & 0 & 0 \\ 0 & (m + m_a) & 0 & -(S_x + S_a) \\ 0 & 0 & 1 & 0 \\ 0 & -(S_x + S_a) & 0 & (J + J_a) \end{bmatrix}}_{\underline{\underline{A}}} \underbrace{\begin{Bmatrix} \dot{y} \\ \dot{Y} \\ \dot{\theta} \\ \dot{\Theta} \end{Bmatrix}}_{\underline{\underline{X}}} = \underbrace{\begin{bmatrix} 0 & 1 & 0 & 0 \\ -k_y & - \left(C_y + \frac{1}{2} \rho U c \left(\frac{\partial C_L}{\partial \alpha} \Big|_{\alpha=0} + C_D \Big|_{\alpha=0} \right) \right) & \left(\frac{1}{2} \rho U^2 c \frac{\partial C_L}{\partial \alpha} \Big|_{\alpha=0} \right) & \frac{1}{2} \rho R U c \left(\frac{\partial C_L}{\partial \alpha} \Big|_{\alpha=0} + C_D \Big|_{\alpha=0} \right) \\ 0 & 0 & 0 & 1 \\ 0 & - \left(\frac{1}{2} \rho U c^2 \frac{\partial C_{M(cr)}}{\partial \alpha} \Big|_{\alpha=0} \right) & \left(\frac{1}{2} \rho U^2 c^2 \frac{\partial C_{M(cr)}}{\partial \alpha} \Big|_{\alpha=0} \right) & - \left(C_\theta - \frac{1}{2} \rho R U c^2 \frac{\partial C_{M(cr)}}{\partial \alpha} \Big|_{\alpha=0} \right) \end{bmatrix}}_{\underline{\underline{B}}} \underbrace{\begin{Bmatrix} y \\ \hat{Y} \\ \theta \\ \hat{\Theta} \end{Bmatrix}}_{\underline{\underline{X}}} \quad 5-36$$

Or in short form,

$$\underline{\underline{A}} \cdot \underline{\underline{\dot{X}}} = \underline{\underline{B}} \cdot \underline{\underline{X}} \quad 5-37$$

A general solution in exponential form is assumed,

$$\underline{\underline{X}} = \underline{\underline{a}} e^{\lambda t} \rightarrow \underline{\underline{\dot{X}}} = \underline{\underline{a}} \lambda e^{\lambda t} \quad 5-38$$

where \underline{a} is a vector of constants. It is substituted in Equation (5-37), resulting in,

$$\underline{\underline{A}} \cdot \underline{a} \lambda e^{\lambda t} = \underline{\underline{B}} \cdot \underline{a} e^{\lambda t} \quad 5-39$$

Or by rearranging, it is simplified to,

$$\left[\underline{\underline{A}} \lambda - \underline{\underline{B}} \right] \cdot \underline{a} = \underline{0} \quad 5-40$$

This matrix equation needs to have non-trivial solution to illustrate the response of system to a disturbance. More significantly, this response should be stable. In summary, the following conditions should be regarded in solving the above matrix equation,

- (1) having non-trivial solution: $\underline{a} \neq \underline{0}$
- (2) stability of response ($\underline{X} = \underline{a} e^{\lambda t}$)

This linear homogenous equation has non-trivial solutions only if the matrix is singular which requires the matrix determinant to be zero. Moreover, the stability of system dictates that the amplitude of response should decline and the vibration should abate through the time. This means the real part of power in assumed exponential solution should be negative. Consequently, to satisfy the above conditions, it necessitates having,

- (1) $\left[\underline{\underline{A}} \lambda - \underline{\underline{B}} \right] = \text{singular} \rightarrow \det \left[\underline{\underline{A}} \lambda - \underline{\underline{B}} \right] = 0$
- (2) $\text{Real}(\lambda) < 0$

Setting the determinant to zero gives,

$$\det \left[\underline{\underline{A}} \lambda - \underline{\underline{B}} \right] = \begin{vmatrix} \lambda & & & \\ & -1 & & \\ & & 0 & \\ & & & 0 \end{vmatrix} \\ \begin{vmatrix} k_y & (m + m_i) \lambda + \left(C_y + \frac{1}{2} \rho U c \left(\frac{\partial C_l}{\partial \alpha} \Big|_{\alpha=0} + C_D \Big|_{\alpha=0} \right) \right) & - \left(\frac{1}{2} \rho U^2 c \frac{\partial C_l}{\partial \alpha} \Big|_{\alpha=0} \right) & - (S_x + S_s) \lambda - \frac{1}{2} \rho R U c \left(\frac{\partial C_x}{\partial \alpha} \Big|_{\alpha=0} + C_D \Big|_{\alpha=0} \right) \\ 0 & 0 & \lambda & -1 \\ 0 & - (S_x + S_s) \lambda + \left(\frac{1}{2} \rho U c^2 \frac{\partial C_{M(\alpha)}}{\partial \alpha} \Big|_{\alpha=0} \right) & - \left(\frac{1}{2} \rho U^2 c^2 \frac{\partial C_{M(\alpha)}}{\partial \alpha} \Big|_{\alpha=0} \right) & (J + J_s) \lambda + \left(C_0 - \frac{1}{2} \rho R U c^2 \frac{\partial C_{M(\alpha)}}{\partial \alpha} \Big|_{\alpha=0} \right) \end{vmatrix} \\ = 0 \quad 5-41$$

If the above equation is expanded, it renders a characteristic equation in λ which in this case is a polynomial of fourth degree,

$$\sum_{i=1}^4 c_i \lambda^i = 0 \quad 5-42$$

where the coefficients c_i as anticipated in Section 3.7 are functions of three categories of variables, i.e. structural properties of the riser and fairing, hydrodynamic characteristics of the fairing and finally current velocity. Therefore, for a given system of a riser and fairing, current velocity is the only variable which governs the instability onset.

$$c_4 = \left[(m + m_a)(J + J_a) - (S_x + S_a)^2 \right]$$

$$c_3 = \left[\left(\frac{1}{2} \rho U c^2 \frac{\partial C_{M(cr)}}{\partial \alpha} \Big|_{\alpha=0} - \frac{1}{2} \rho R U c \left(\frac{\partial C_L}{\partial \alpha} \Big|_{\alpha=0} + C_D \Big|_{\alpha=0} \right) \right) (S_x + S_a) + \left(C_y + \frac{1}{2} \rho U c \left(\frac{\partial C_L}{\partial \alpha} \Big|_{\alpha=0} + C_D \Big|_{\alpha=0} \right) \right) (J + J_a) + \left(C_\theta - \frac{1}{2} \rho R U c^2 \frac{\partial C_{M(cr)}}{\partial \alpha} \Big|_{\alpha=0} \right) (m + m_a) \right]$$

$$c_2 = \left[k_y (J + J_a) - \left(\frac{1}{2} \rho U^2 c^2 \frac{\partial C_{M(cr)}}{\partial \alpha} \Big|_{\alpha=0} \right) (m + m_a) + \frac{1}{2} \rho U c \left(\frac{\partial C_L}{\partial \alpha} \Big|_{\alpha=0} + C_D \Big|_{\alpha=0} \right) C_\theta + C_y C_\theta - \left(\frac{1}{2} \rho U^2 c \frac{\partial C_L}{\partial \alpha} \Big|_{\alpha=0} \right) (S_x + S_a) - \left(\frac{1}{2} \rho R U c^2 \frac{\partial C_{M(cr)}}{\partial \alpha} \Big|_{\alpha=0} \right) C_y \right]$$

$$c_1 = \left[- \left(\frac{1}{2} \rho U^2 c^2 \frac{\partial C_{M(cr)}}{\partial \alpha} \Big|_{\alpha=0} \right) C_y + \left(\frac{1}{2} \rho U c^2 \frac{\partial C_{M(cr)}}{\partial \alpha} \Big|_{\alpha=0} \right) \left(\frac{1}{2} \rho U^2 c \frac{\partial C_L}{\partial \alpha} \Big|_{\alpha=0} \right) + k_y C_\theta + - \left(\frac{1}{2} \rho R U c^2 \frac{\partial C_{M(cr)}}{\partial \alpha} \Big|_{\alpha=0} \right) k_y - \frac{1}{2} \rho U c \left(\frac{\partial C_L}{\partial \alpha} \Big|_{\alpha=0} + C_D \Big|_{\alpha=0} \right) \left(\frac{1}{2} \rho U^2 c^2 \frac{\partial C_{M(cr)}}{\partial \alpha} \Big|_{\alpha=0} \right) \right]$$

$$c_0 = \left[- \left(\frac{1}{2} \rho U^2 c^2 \frac{\partial C_{M(cr)}}{\partial \alpha} \Big|_{\alpha=0} \right) k_y \right]$$

Analysis of the roots of this characteristic equation results in the stability criterion. In other words, for a given configuration of a fairing and riser, it gives the threshold current speed at which unstable behaviour may occur. Unstable motion is diagnosed whenever one of the roots, λ_i , has positive real part.

5.6 Dimensionless Form

Classifying the variables involved in Equation (5-42) and making them dimensionless assists the designer to have a better understanding of the true physical parameters that influence the stability. In fact, the magnitude of the physical parameters varies from case to case and this makes it difficult for engineers to make a judgment about the critical range of variables. But defining meaningful dimensionless parameters provides them with a valuable toolbox and facilitates the perception of complexities associated with the plurality of engaged parameters.

Prior to stepping into the process of specifying these parameters, it is noteworthy to say that in addition to transverse spring stiffness, the last term on the left hand side of the second equation of motion, e.g. Equation (5-31), can be interpreted as hydrodynamic torsional stiffness (for further discussion, see Section 5.9). Thus, angular velocities and natural frequencies of both motions are calculated as below,

$$\omega_y = 2\pi f_y = \sqrt{\frac{k_y}{m + m_a}} \quad 5-43$$

$$\omega_\theta = 2\pi f_\theta = \sqrt{-\frac{1}{2}\rho U^2 c^2 \frac{\partial C_{M(cr)}}{\partial \alpha} \Big|_{\alpha=0} / (J + J_a)} \quad 5-44$$

The first step in making the Equation (5-42) dimensionless is to identify the dimension of its terms. By referring to Equation (5-38), it is clear that λ is of the dimension of (1/Time), i.e. $\text{Dim}[\lambda] = (\text{Time})^{-1}$. A quick look at the terms of Equation (5-42) indicates that they all have the dimension of $(\text{Mass})^2 \cdot (\text{Length})^2 \cdot (\text{Time})^{-4}$. So, it requires to select appropriate parameters for these dimensions, i.e. mass, length and time, and then to divide this equation by them. Mass of the system and chord length of the fairing, i.e. $(m + m_a)$ and c respectively, are appropriate terms for the dimension of mass and length. As the system has two natural periods for transverse

and torsion vibration, thus selecting a period for time is not reasonable. Instead, the term c/U generates a general equivalent for dimension of time which can be applied to both DOFs.

So, each term of the characteristic Equation (5-42) should ultimately be divided by the term $(m + m_a)^2 \cdot (c)^2 \cdot (U/c)^4$ to make it dimensionless. Afterwards, by rearranging the terms it gives,

$$\sum_{i=1}^4 \tilde{c}_i \tilde{\lambda}^i = \sum_{i=1}^4 \frac{c_i}{(m + m_a)^2 \cdot c^2 \cdot (U/c)^{4-i}} \left(\frac{\lambda}{U/c} \right)^i = 0 \quad 5-45$$

$$\tilde{c}_4 = \left[\left(\frac{J + J_a}{(m + m_a) c^2} \right) - \left(\frac{S_x + S_a}{(m + m_a) c} \right)^2 \right]$$

$$\begin{aligned} \tilde{c}_3 = & \left[\left(\frac{\rho \cdot c^2}{2(m + m_a)} \frac{\partial C_{M(cr)}}{\partial \alpha} \Big|_{\alpha=0} - \frac{\rho \cdot c^2}{2(m + m_a)} \frac{R}{c} \left(\frac{\partial C_L}{\partial \alpha} \Big|_{\alpha=0} + C_D \Big|_{\alpha=0} \right) \right) \right. \\ & \left. \left(\frac{S_x + S_a}{(m + m_a) c} \right) + \left(\frac{2C_y}{2 \cdot (m + m_a) \cdot \omega_y} \frac{\omega_y}{U/c} + \frac{\rho \cdot c^2}{2(m + m_a)} \left(\frac{\partial C_L}{\partial \alpha} \Big|_{\alpha=0} + C_D \Big|_{\alpha=0} \right) \right) \right. \\ & \left. \left(\frac{J + J_a}{(m + m_a) c^2} \right) + \left(\frac{2C_\theta}{2 \cdot (J + J_a) \cdot \omega_\theta} \frac{J + J_a}{(m + m_a) c^2} \frac{\omega_\theta}{U/c} - \frac{\rho \cdot c^2}{2(m + m_a)} \frac{R}{c} \frac{\partial C_{M(cr)}}{\partial \alpha} \Big|_{\alpha=0} \right) \right] \end{aligned}$$

$$\begin{aligned} \tilde{c}_2 = & \left[\frac{k_y}{(m + m_a) \omega_y^2} \frac{J + J_a}{(m + m_a) c^2} \left(\frac{\omega_y}{U/c} \right)^2 - \left(\frac{\rho \cdot c^2}{2(m + m_a)} \frac{\partial C_{M(cr)}}{\partial \alpha} \Big|_{\alpha=0} \right) + \right. \\ & \left. \frac{\rho \cdot c^2}{2(m + m_a)} \left(\frac{\partial C_L}{\partial \alpha} \Big|_{\alpha=0} + C_D \Big|_{\alpha=0} \right) \frac{2C_\theta}{2 \cdot (J + J_a) \cdot \omega_\theta} \frac{J + J_a}{(m + m_a) c^2} \frac{\omega_\theta}{U/c} + \right. \\ & \left. \frac{2C_y}{2 \cdot (m + m_a) \cdot \omega_y} \frac{\omega_y}{U/c} \frac{2C_\theta}{2 \cdot (J + J_a) \cdot \omega_\theta} \frac{J + J_a}{(m + m_a) c^2} \frac{\omega_\theta}{U/c} - \left(\frac{\rho \cdot c^2}{2(m + m_a)} \frac{\partial C_L}{\partial \alpha} \Big|_{\alpha=0} \right) \right. \\ & \left. \left(\frac{S_x + S_a}{(m + m_a) c} \right) - \left(\frac{\rho \cdot c^2}{2(m + m_a)} \frac{R}{c} \frac{\partial C_{M(cr)}}{\partial \alpha} \Big|_{\alpha=0} \right) \frac{2C_y}{2 \cdot (m + m_a) \cdot \omega_y} \frac{\omega_y}{U/c} \right] \end{aligned}$$

$$\begin{aligned} \tilde{c}_1 = & \left[- \left(\frac{\rho \cdot c^2}{2(m+m_a)} \frac{\partial C_{M(cr)}}{\partial \alpha} \Big|_{\alpha=0} \right) \frac{2C_y}{2 \cdot (m+m_a) \cdot \omega_y} \frac{\omega_y}{U/c} + \right. \\ & + \left(\frac{\rho \cdot c^2}{2(m+m_a)} \frac{\partial C_{M(cr)}}{\partial \alpha} \Big|_{\alpha=0} \right) \left(\frac{\rho \cdot c^2}{2(m+m_a)} \frac{\partial C_L}{\partial \alpha} \Big|_{\alpha=0} \right) + \\ & + \frac{k_y}{(m+m_a)\omega_y^2} \left(\frac{\omega_y}{U/c} \right)^2 \frac{2C_\theta}{2 \cdot (J+J_a) \cdot \omega_\theta} \frac{J+J_a}{(m+m_a)c^2} \frac{\omega_\theta}{U/c} - \left(\frac{\rho \cdot c^2}{2(m+m_a)} \frac{R}{c} \frac{\partial C_{M(cr)}}{\partial \alpha} \Big|_{\alpha=0} \right) \\ & \left. \frac{k_y}{(m+m_a)\omega_y^2} \left(\frac{\omega_y}{U/c} \right)^2 - \frac{\rho \cdot c^2}{2(m+m_a)} \left(\frac{\partial C_L}{\partial \alpha} \Big|_{\alpha=0} + C_D \Big|_{\alpha=0} \right) \left(\frac{\rho \cdot c^2}{2(m+m_a)} \frac{\partial C_{M(cr)}}{\partial \alpha} \Big|_{\alpha=0} \right) \right] \\ \tilde{c}_0 = & \left[- \left(\frac{\rho \cdot c^2}{2(m+m_a)} \frac{\partial C_{M(cr)}}{\partial \alpha} \Big|_{\alpha=0} \right) \frac{k_y}{(m+m_a)\omega_y^2} \left(\frac{\omega_y}{U/c} \right)^2 \right] \end{aligned}$$

Generally speaking, models discussing the VIV of a cylinder typically suggest that the appropriate dimensionless parameters that are useful in describing the vortex-induced response of continuous structures are (1) structural damping factor, (2) reduced velocity, (3) mass ratio, (4) ratio of stationary cylinder shedding frequency to natural frequency, (5) aspect ratio and (6) Reynolds number (Blevins, 2001). Reduced velocity is a good tool to measure to what extent the body is likely to interact with vortex shedding in its own wake. Mass ratio “is often used to measure the susceptibility of lightweight structures to flow-induced vibration. As the ratio of fluid mass to structural mass increases, so does the propensity for flow-induced vibration”. These suggestions give guidelines as to how to select the dimensionless parameters.

With this in mind, a detailed look into the coefficients of the above equation inspires more clues about how to define the meaningful dimensionless parameters in this specific case. Taking the above into consideration, it reaches the conclusion of defining the following dimensionless parameters,

$$\tilde{\lambda} = \frac{\lambda}{U/c} \tag{5-46}$$

$$\gamma^2 = \frac{J+J_a}{(m+m_a) \cdot c^2} \tag{5-47}$$

$$S_r = \frac{S_x + S_a}{(m + m_a) \cdot c} \quad 5-48$$

$$A = \frac{\rho \cdot c^2}{2(m + m_a)} \quad 5-49$$

$$\xi_y = \frac{C_y}{2 \cdot (m + m_a) \cdot \omega_y} \quad 5-50$$

$$\xi_\theta = \frac{C_\theta}{2 \cdot (J + J_a) \cdot \omega_\theta} \quad 5-51$$

$$U_{ry} = \frac{U}{\omega_y \cdot c} \quad 5-52$$

$$U_{r\theta} = \frac{U}{\omega_\theta \cdot c} = \sqrt{\frac{\gamma^2}{A \left. \frac{-\partial C_{M(cr)}}{\partial \alpha} \right|_{\alpha=0}}} \quad 5-53$$

$$R_r = \frac{R}{c} \quad 5-54$$

where the imaginary part of $\tilde{\lambda}$ shows the ratio of the time that takes a flow particle to pass the chord length to the period of oscillation; γ is the radius of gyration about pivot point; S_r is the dimensionless distance of centre of gravity from pivot point; A is the inverse of mass ratio; ζ_y and ζ_θ are the damping ratio of transverse and torsional motions in water respectively; U_{ry} and $U_{r\theta}$ are the reduced velocities; and R_r is the dimensionless distance of reference point.

By substituting the above parameters in Equation (5-45), the dimensionless form of characteristic equation will appear as the below,

$$\sum_{i=1}^4 \tilde{c}_i \tilde{\lambda}^i = 0 \quad 5-55$$

$$\tilde{c}_4 = [\gamma^2 - S_r^2]$$

$$\tilde{c}_3 = \left[A(S_r - R_r) \left. \frac{\partial C_{M(cr)}}{\partial \alpha} \right|_{\alpha=0} + A(\gamma^2 - R_r S_r) \left(\left. \frac{\partial C_L}{\partial \alpha} \right|_{\alpha=0} + C_D \Big|_{\alpha=0} \right) + 2\gamma^2 \left(\frac{\xi_y}{U_{ry}} + \frac{\xi_\theta}{U_{r\theta}} \right) \right]$$

$$\begin{aligned}\tilde{c}_2 &= \left[\frac{\gamma^2}{U_{ry}^2} - A \left(1 + 2R_r \frac{\xi_y}{U_{ry}} \right) \frac{\partial C_{M(cr)}}{\partial \alpha} \Big|_{\alpha=0} + 2A\gamma^2 \frac{\xi_\theta}{U_{r\theta}} \left(\frac{\partial C_L}{\partial \alpha} \Big|_{\alpha=0} + C_D \Big|_{\alpha=0} \right) + 4\gamma^2 \frac{\xi_y}{U_{ry}} \frac{\xi_\theta}{U_{r\theta}} + \right. \\ &\quad \left. - AS_r \frac{\partial C_L}{\partial \alpha} \Big|_{\alpha=0} \right] \\ \tilde{c}_1 &= \left[-A \left(2 \frac{\xi_y}{U_{ry}} + \frac{R_r}{U_{ry}^2} \right) \frac{\partial C_{M(cr)}}{\partial \alpha} \Big|_{\alpha=0} + 2 \frac{\gamma^2}{U_{ry}^2} \frac{\xi_\theta}{U_{r\theta}} - A^2 \frac{\partial C_{M(cr)}}{\partial \alpha} \Big|_{\alpha=0} C_D \Big|_{\alpha=0} \right] \\ \tilde{c}_0 &= \left[-A \frac{1}{U_{ry}^2} \frac{\partial C_{M(cr)}}{\partial \alpha} \Big|_{\alpha=0} \right]\end{aligned}$$

This equation should be then solved for $\tilde{\lambda}$ to see if the second condition, i.e. $\text{Real}(\tilde{\lambda}) < 0$, is met and any disturbance from equilibrium position dies out. If not, the system is in an unstable status.

The characteristic Equation (5-55) is of the fourth degree and an analytical approach leads to a very complicated solution and does not have a lot of benefit in specifying when one of the roots becomes unstable. Likewise, if it is also attempted to assess the roots of this quartic equation with the aid of Routh-Hurwitz stability criterion (Wiggins, 1990), it will end up with a complex solution which does not make any useful points. Thus, this equation remains to be solved numerically for a given system of the riser and fairing to find the current velocity at which systems becomes unstable.

To this end, Equation (5-55) is solved for a small velocity and the stability of roots is checked by assessing the sign of their real part. If all roots are stable, then the equation is solved again for an increment in velocity and roots are investigated accordingly. This loop is continued and the trend of roots variation against velocity increase is tracked down until either the real part of one of the roots becomes positive and system goes unstable or the magnitude of velocity exceeds the possible current limit in reality.

In the next step, this procedure will be followed for a tank test to verify the robustness of the model.

5.7 Verification

A series of cylinder tests was carried out by ExxonMobil at the David Taylor Model Basin (Slocum et al., 2004). One of the tests was on a rigid cylinder with the fairing shown in Figure 5-3.

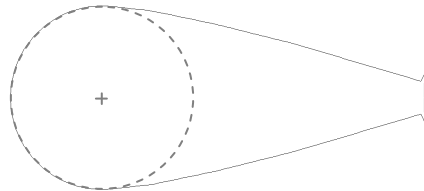


Figure 5-3 ExxonMobil Fairing on a Rigid Cylinder.

In part of these tests, a submerged horizontal spring mounted cylinder was towed through still water while transverse motion was measured. A rigid test cylinder with a diameter of 22cm and a length of 3.9m was fitted with six independent fairing segments, each with a span of 61.2cm, a chord length of 52.6cm, and a maximum thickness of 23.2cm. This system can be modelled with a fairing and a transverse spring as explained in this chapter.

Based on the measured specifications of the test, the dimensionless parameters are evaluated as below:

$$A = 0.8435$$

$$\gamma^2 = 0.0792$$

$$S_r = 0.2016$$

R_r is a reference length for average effect of angular velocity on the angle of attack (see Section 6.1). For an airfoil which rotates about its elastic axis, R_r is chosen to give the AoA at a point three-quarters of the way back from the leading edge (Blevins, 2001). Since CR is at the centre of circular nose of fairing, R_r should be less than half of chord length. Thus, R_r is selected here as 0.40.

$$R_r = 0.40$$

With respect to damping, some experimental tests report high level of in-water damping ratio for riser fitted with fairing, e.g. 0.10 to 0.18 (Lee et al., 2004b). But since the riser is rigid in this test and does not experience any tangible deformation, its contribution to the transverse damping of the system is smaller. Thus, half of the reported value in technical literature was deployed for ξ_y in calculation. Moreover, as the tests emphasise on the rotational freedom of fairing, the positive role of torsional friction damping is ignored in favour of being on the safe and conservative margin.

$$\xi_y = 5 \%$$

$$\xi_\theta = 0 \%$$

The last required data is the hydrodynamic coefficients of the fairing. A CFD analysis was performed as part of this study on a selection of fairing profiles including this section (see Chapter 7). The analysis was done at Reynolds number of 5×10^4 at different angles of attack. On the contrary, the tank test was carried out at much higher Reynolds number of about 5×10^6 . Since the hydrodynamic coefficients are sensitive to Reynolds number, the lift-curve slope and mean drag at aerodynamic centre were selected according to reported data (Slocum et al., 2004). These coefficients are scaled to the chord length of the fairing based on Equations (5-18) and (5-19).

$$\partial C_L / \partial \alpha \Big|_0 = 1.146 \text{ (1/rad)}$$

$$C_D \Big|_0 = 0.176$$

Lift-curve slope, measured at the aerodynamic centre, was shifted to centre of rotation (CR) to compute the moment-curve slope,

$$\partial C_{M(\text{cr})} / \partial \alpha \Big|_0 = -0.0344 \text{ (1/rad)}$$

The critical reduced velocity, U_{cr} , at which the real part of a solution to characteristic Equation (5-55) becomes positive, is obtained numerically by increasing the reduced velocity and solving this equation at each step. For this case study, the analytical model shows the system becomes unstable at $U_{\text{cr}} = U_{\text{ry(critical)}} = 0.51$, which is located in the range of test results (0.42-0.56) (Slocum et al., 2004). This demonstrates the good agreement of theoretical model with previous experiment.

The trace of eigenvalues is illustrated in Figure 5-4. The red circles in this figure show the eigenvalues corresponding to the highest velocity at which a pair of them crosses the imaginary axis and their real part becomes positive. According to Equations (5-46) and (5-52), the imaginary and real parts of roots are multiplied by U_{ry} to remove the effect of non-dimensionalisation. Hence, the horizontal and vertical axes in this figure are $\text{Real}(\lambda/\omega_y)$ and $\text{Imag}(\lambda/\omega_y)$ respectively. The imaginary part of eigenvalue, $\text{Imag}(\lambda)$, represents the frequency of vibration while the real part shows the trend of amplitude variation.

As the governing equations are coupled, the relevant eigenvector or mode shape of each eigenvalue is coupled in the sense it has elements in both DOFs. Thus, it is not possible to attribute the modes into pure transverse or torsion motion.

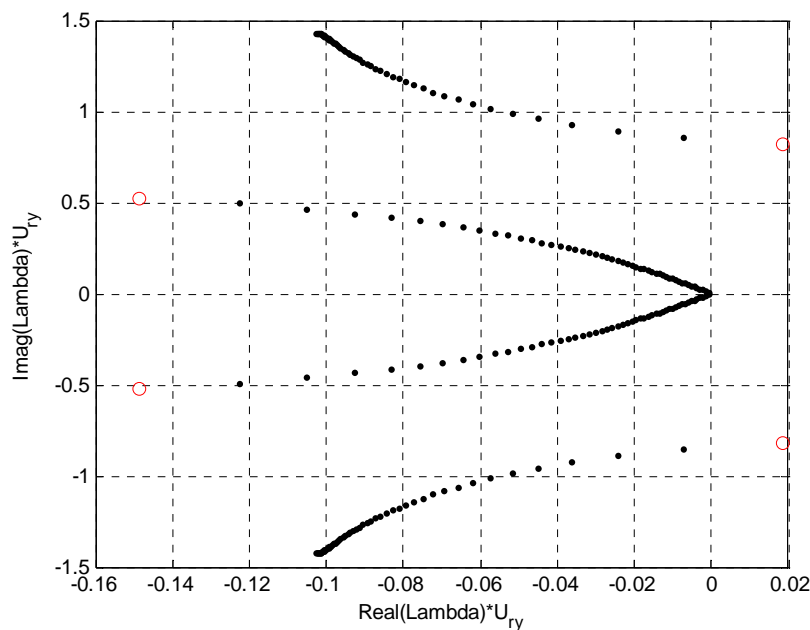


Figure 5-4 Trend of Eigenvalues by Velocity Increment.

5.8 Torsional Friction Damping

Damping in general has remarkable effects on stability analysis of a system as it can affect the system and change its behaviour. When a dynamically stable system goes unstable, the balance of energy exchange is reversed. This means the system is equipped to absorb energy from outside more than it scatters. Thus, any infinitesimal disturbance from rest can trigger the mechanism of putting energy into the system

and raise the amplitude of vibration. Consequently, any mechanism capable of dissipating energy and altering the rate of energy exchange in favour of stability is of interest to designer. Damping in any form has this feature and therefore must be taken into consideration in stability appraisal.

Regarding a system consisting of a riser and fairing, various phenomena are engaged in damping the energy of self-induced vibration. Imagine this system in still water. There is no torsional stiffness and hence any torsional displacement will remain stationary. In other words, any torsional position is in neutral equilibrium and thus no motion and energy damping mechanism exist. However, in the case of transverse distortion, structural stiffness of the riser tries to bring the riser back to the initial condition and the motion created in the fluid is allied with a damping motion. This damping induced by the riser's structural damping in fluid was demonstrated in equations of motion by the term of $C_y \dot{y}$.

Then, when the fluid flow comes into play, some other terms appear too. As was mentioned in Section 5.6 and will be further explained thoroughly later on in Section 5.9, fluid current produces a hydrodynamic torsional stiffness which attempts to align the fairing to the current direction. Therefore, this rotation in fluid is associated with a torsional hydrodynamic damping. Moreover, drag and lift force of the fairing in the presence of a current put some thrust in transverse damping. This hydrodynamic damping emerged in equations of motion through the expansion of hydrodynamic forces.

The third type of damping in the system of a riser and fairing originates from friction generated as a result of the fairing's motion against riser's circumference.

As illustrated in Figure 3-9 to Figure 3-14, a fairing is in contact with the riser at collars located at the two ends and possibly through some pads in between. Thus, upon any rotation these surfaces rub on each other and generate friction which is technically called dry friction, a friction force between objects in the absence of any lubricant. In this case, the frictional forces are practically independent of the magnitude of the velocity of motion and they act in opposite direction to this velocity (Magnus, 1965). If the two sliding surfaces are separated with a thin film of

lubricant, then the viscosity force in lubricant comes into play and forms part of the friction mechanism. So, the characteristics of combined dry and viscous friction damping change.

Models and Characteristics

Several models have been proposed to describe and formulate the friction damping. They are used individually or in combination to represent the friction in a system. The most famous models include Coulomb damping, viscous damping and hysteretic damping.

Charles-Augustine de Coulomb suggested the earliest model for dry friction and because of that, dry friction is sometimes known as Coulomb friction. In his simple model, the friction force is proportional to the normal force exerted between surfaces. The friction force is related to the normal force through the coefficient of friction, μ , which is a function of surface properties like roughness. This friction force resists the motion and therefore is in the opposite direction of motion, \dot{y} .

$$F_{\text{Friction}} = F_{\text{Normal}} \times \mu \times \text{sign}(\dot{y}) \quad 5-56$$

This resisting force which is independent of the velocity reduces the amplitude of vibration in a linear way. The amplitude loss per cycle is equal to $4F_{\text{Friction}}/K$, where K shows the stiffness of the dynamic system (Beards, 1996). Coulomb damping does not alter the natural frequency of vibration.

Many other dry friction formulations have been derived based on the classical (discontinuous) Coulomb model (Duan, 2004, Duan and Singh, 2006), for example stick-slip friction law in which the friction force or torque is defined as a function of the relative velocity or a modified micro-slip model in terms of an elasto-plastic shear layer. In-depth description of these models is out of the scope of this study and the reader is referred to the cited references.

Viscous damping model is also deployed to describe the friction energy loss. In this model, the resisting force is proportional to velocity through damping coefficient, C_y .

$$F_{\text{Friction}} = C_y \times \dot{y} \quad 5-57$$

Contrary to Coulomb friction model, viscose damping changes the natural frequency of system and is characterised by an exponential decay of oscillation (Beards, 1996).

Hysteretic model is the other well-known damping model which is sometimes used to explain the friction effect. Hysteretic damping or complex stiffness mostly emerges in describing the internal friction of solid materials in which there is a phase angle between stress and stress induced strain. While viscose damping is frequency dependent, hysteretic damping is independent of the frequency of vibration, ω (Beards, 1996).

$$F_{\text{Friction}} = C_{\text{Hyst}} \times |y| \times \text{sign}(\dot{y}) \quad 5-58$$

These models are used individually or in a combination form to describe the physics of different systems. Mathematically, the term representing viscose damping model is much easier to deal with and therefore it is very common to define an equivalent viscose damping coefficient for other models, i.e. Coulomb and hysteretic. The equivalent viscose damping coefficient is defined in a way that the energy dissipated in a cycle is equal in both viscose and Coulomb/hysteretic system. If Y_A shows the amplitude of vibration, the equivalent viscose damping coefficient for Coulomb damping is (Beards, 1996, Blevins, 2001),

$$C_y^{\text{eq}} = \frac{4 \cdot F_{\text{Normal}} \cdot \mu}{\pi \cdot \omega \cdot Y_A} \quad 5-59$$

where ω again is the frequency of vibration. Likewise, the equivalent viscose damping coefficient for hysteretic damping is calculated as,

$$C_y^{\text{eq}} = \frac{2 \cdot C_{\text{Hyst}}}{\pi \cdot \omega} \quad 5-60$$

Friction in Fairing

As explained earlier in this section, the fairing and riser are in contact and any twist of the fairing produces friction forces whose resultant is a torque resisting the rotation of the fairing. For the simple model of Coulomb damping, the normal force which presses the two surfaces to each other mainly comes from the resultant of fluid force on the fairing, i.e. drag and lift. At an angle of attack, say α , since the fairings

section is chunky and not designed like thin airfoils to generate small drag and large lift, the drag force is much bigger than lift. Thus, the role of drag in normal force is predominant. Consequently, the helpful effect of lift force on increasing the normal force and associated friction can be ignored in favour of being on the conservative side. There could exist also a small component originating from clamping the fairing to the riser but it should be very tiny as the fairing is clamped loosely to enable it weathervane freely.

So, the normal force at an angle of attack say α , is,

$$N = (\text{Drag})\Big|_{\alpha} = \frac{1}{2} \rho U_{\text{rel}}^2 c C_D \Big|_{\alpha}$$

Through the process of linearization as explained in Section 5.4, the normal force will be simplified to,

$$N = \frac{1}{2} \rho U^2 c \left(C_D \Big|_{\alpha=0} + \alpha \frac{\partial C_D}{\partial \alpha} \Big|_{\alpha=0} \right)$$

If r_s and μ shows the outer radius of a steel riser and the coefficient of friction respectively, using Equation (5-56) with above normal force gives the friction torque,

$$T_{\text{Friction}} = \left(\frac{1}{2} \rho U^2 c \right) \left(C_D \Big|_{\alpha=0} + \alpha \frac{\partial C_D}{\partial \alpha} \Big|_{\alpha=0} \right) \times \mu \times \text{sign}(\dot{\theta}) \times r_s$$

This expression consists of two terms. The first term is Coulomb friction. By comparison with Equation (5-58), the second term resembles the hysteretic friction model. Thus, the equivalent viscose damping coefficient for each term is obtained through Equations (5-59) and (5-60).

$$C_{\theta 1}^{\text{eq}} = \frac{4 \cdot F_{\text{Normal}} \cdot \mu}{\pi \cdot \omega \cdot Y_A} = \frac{4\mu \cdot \left(\frac{1}{2} \rho U^2 c \right) (C_D \Big|_{\alpha=0}) \cdot r_s}{\pi \cdot \Omega_0 \cdot \Theta_A} \quad 5-61$$

$$C_{\theta 2}^{\text{eq}} = \frac{2 \cdot C_{\text{Hyst}}}{\pi \cdot \omega} = \frac{2\mu \cdot \left(\frac{1}{2} \rho U^2 c \right) (\partial C_D / \partial \alpha \Big|_{\alpha=0}) \cdot r_s}{\pi \cdot \Omega_0} \quad 5-62$$

where Θ_A and Ω_0 indicate the amplitude and frequency of torsional vibration respectively. It should be noted that Ω_0 is the frequency of vibration not the natural

frequency of torsional vibration, ω_0 . In stability analysis, therefore, it is equal to the imaginary part of λ , i.e. $\text{Imag}(\lambda) = \Omega_0$.

These equivalent viscose damping terms should be added to the torsional viscose damping (C_θ) in the second governing equation of system, i.e. Equation (5-31). Eventually, all torsional viscose damping terms in characteristic Equation (5-42) are to be substituted by the expression of $(C_\theta + C_{\theta 1}^{\text{eq}} + C_{\theta 2}^{\text{eq}})$. Accordingly, making this term dimensionless with reference to Equation (5-51) gives,

$$\begin{aligned} \xi_{\theta 1}^{\text{eq}} &= \frac{C_{\theta 1}^{\text{eq}}}{2 \cdot (J + J_a) \cdot \omega_\theta} = \frac{4\mu(C_D|_{\alpha=0})}{2\pi\Theta_A} \frac{\frac{1}{2}\rho c^2}{(m + m_a)} \frac{(m + m_a)c^2}{(J + J_a)} \frac{r_s}{c} \frac{U/c}{\text{Imag}(\lambda)} \frac{U/c}{\omega_\theta} \\ &= \frac{2\mu(C_D|_{\alpha=0})A \cdot r_{sr} \cdot U_{r\theta}}{\pi\Theta_A \gamma^2 \text{Imag}(\tilde{\lambda})} \\ \xi_{\theta 2}^{\text{eq}} &= \frac{C_{\theta 2}^{\text{eq}}}{2 \cdot (J + J_a) \cdot \omega_\theta} = \frac{2\mu(\partial C_D / \partial \alpha|_{\alpha=0})}{2\pi\Theta_A} \frac{\frac{1}{2}\rho c^2}{(m + m_a)} \frac{(m + m_a)c^2}{(J + J_a)} \frac{r_s}{c} \frac{U/c}{\text{Imag}(\lambda)} \frac{U/c}{\omega_\theta} \\ &= \frac{\mu(\partial C_D / \partial \alpha|_{\alpha=0})A \cdot r_{sr} \cdot U_{r\theta}}{\pi\gamma^2 \text{Imag}(\tilde{\lambda})} \end{aligned}$$

where r_{sr} is the dimensionless form of the riser's outer radius.

Adding these terms makes the solution of characteristic equation more complicated because now two variables Θ_A and $\text{Imag}(\tilde{\lambda})$ are unknown. Thus, it should be solved in a trial and error loop as explained below.

For a specific U_{ry} (e.g. $(U_{ry})_i$) inside the loop of increasing U_{ry} ,

- Ignore the friction effect and calculate $\tilde{\lambda}_0$. It gives $\Omega_{\theta 0} = \text{Imag}(\tilde{\lambda}_0)$.
- Take the friction into account and for an initial value of Θ_A (e.g. $\frac{\pi}{2}$) calculate $\tilde{\lambda}$. It gives $\text{Imag}(\tilde{\lambda})$ and $\text{Real}(\tilde{\lambda})$.
- Reduce Θ_A and calculate $\tilde{\lambda}$ until $\text{Real}(\tilde{\lambda}) < 0$. Then $\Omega_{\theta j} = \text{Imag}(\tilde{\lambda})$.
- To monitor the convergence, check the condition $\left| (\Omega_{\theta j} - \Omega_{\theta_{j-1}}) / \Omega_{\theta_{j-1}} \right| < \varepsilon$.

If it is satisfied, then $((U_{ry})_i, \Theta_A)$ gives the next point and exit the loop. If not, go one step back and reduce Θ_A .

This algorithm gives a curve of Θ_A versus U_{ry} . Such a curve shows the maximum value of Θ_A beyond which the system is unstable for a specific U_{ry} (Figure 5-5). This means that for a specific U_{ry} , if the torsional disturbance is less than $(\Theta_A)_{max}$ then it will diminish and finally die out. As a consequence the system is stable, however beyond that, the system is unstable and the amplitude of vibration may grow.

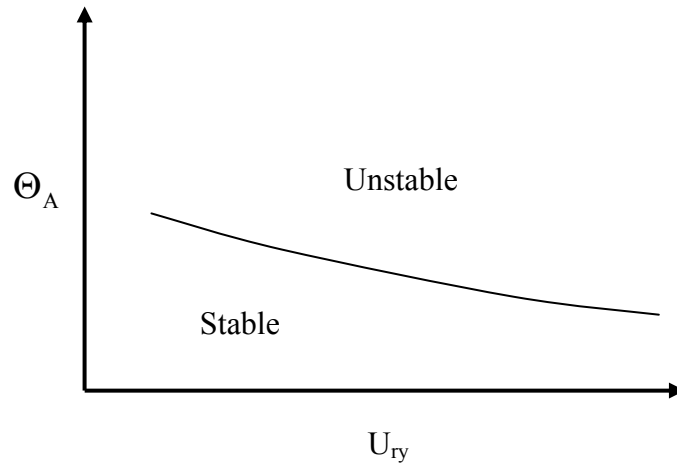


Figure 5-5 Effect of Considering Friction Damping.

Effects and Conclusion

To analyse the effect of adding Coulomb and hysteretic terms of friction damping, the above algorithm will be applied to the case studied in Section 5.7 for verification of the model. With respect to the point that the fairing should be free to weathervane, the sliding friction coefficient is relatively small. For rubbing smooth steel surfaces, the friction coefficient varies between 0.1 to 0.5. The average value is selected as 0.30. The test report did not mention anything about the slope of the drag coefficient. Thus, by considering the growth of projected area due to small rotation of the fairing, the parameter $\partial C_D / \partial \alpha$ can be estimated. In fact for this fairing with 23.2 cm diameter and 52.6 cm chord, the rotating arm behind the pivot point is $52.6 - 23.2/2 = 41$ cm. A small rotation (α) of this arm will increase the projected area (PA) of the unit span to as large as $41 \times \alpha$.

$$PA_{new} = PA_o + 0.41 \times \alpha = 0.232 + 0.41 \times \alpha$$

$$\text{New Drag} = \frac{1}{2} \rho U^2 \cdot PA_{new} \cdot C_{Do} = \frac{1}{2} \rho U^2 \cdot PA_o \cdot C_{Do} \frac{PA_{New}}{PA_o}$$

Thus, the equivalent drag coefficient can be defined as,

$$(C_D)_{EQ} = C_{D_0} \frac{PA_{New}}{PA_0}$$

Consequently, the slope of the drag coefficient can be estimated as below,

$$\partial C_D / \partial \alpha = \frac{(C_D)_{EQ} - C_{D_0}}{\alpha} = \frac{C_{D_0} (PA_{New} - PA_0) / PA_0}{\alpha} = \frac{0.176 \times 0.41 \alpha / 0.232}{\alpha} = 0.311$$

It should be noted that the parameter $\partial C_D / \partial \alpha$ appears as a hysteretic term only. The above algorithm produces Figure 5-6 for considering only the Coulomb term of friction damping. This figure says that when U_{ry} declines, the maximum amplitude of disturbance has a vertical asymptote of about $U_{cr} = 0.51$ which is identical to the previous result when the effect of friction damping was ignored. Accordingly, as U_{ry} increases this maximum limit reduces. In other words, this figure clarifies if $U_{ry} < U_{cr}$, then the system is stable for any small amplitude of torsional distortion and it will eventually die out. But when $U_{ry} > U_{cr}$, for the system to be stable, the amplitude of distortion should be less than a specific value. Otherwise, the system goes unstable.

Taking both Coulomb and hysteretic terms into account demonstrates more interesting results in Figure 5-7. This figure shows that adding the effect of hysteretic term pushes the curve upwards and to the right. It means that the hysteretic term improves the stability and the system goes unstable at a higher velocity and larger disturbance. For $\partial C_D / \partial \alpha$, larger than what was estimated, the curve is moved upwards and further to the right, boosting the stability.

This behaviour of term $C_{\theta 1}^{eq} + C_{\theta 2}^{eq}$ may be justified through the torsional damping term in the second governing equation of system, i.e. Equation (5-31). This term is,

$$\left(C_{\theta 1}^{eq} + C_{\theta 2}^{eq} + C_{\theta} - \frac{1}{2} \rho R U c^2 \left. \frac{\partial C_{M(cr)}}{\partial \alpha} \right|_{\alpha=0} \right) \dot{\theta}$$

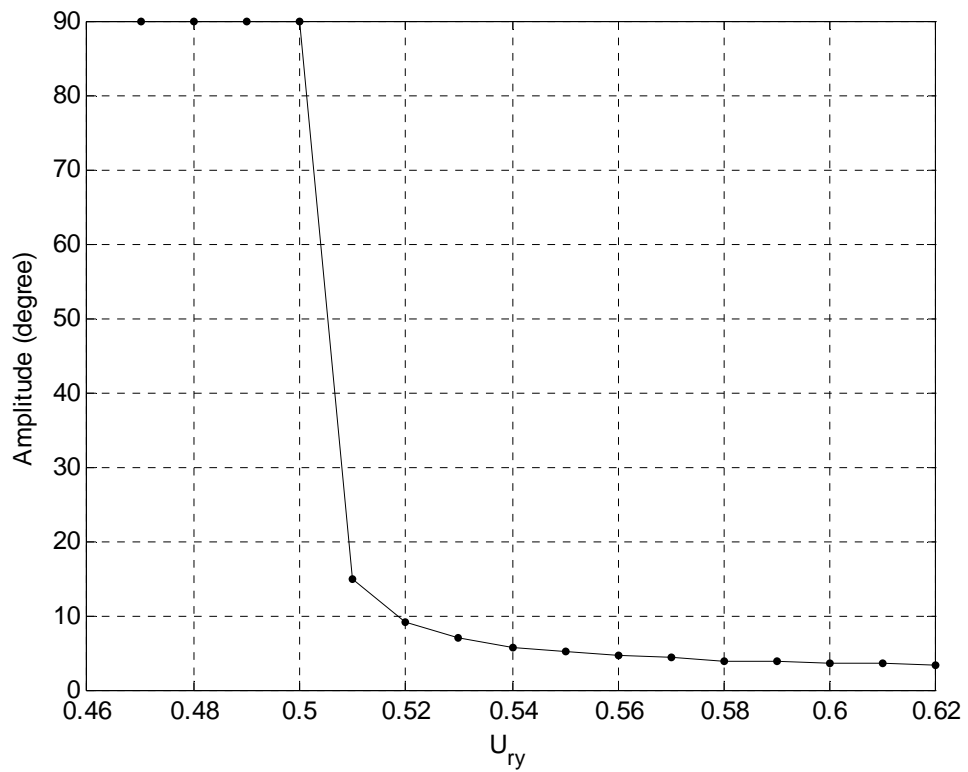


Figure 5-6 Effect of Considering Friction, Coulomb Term.

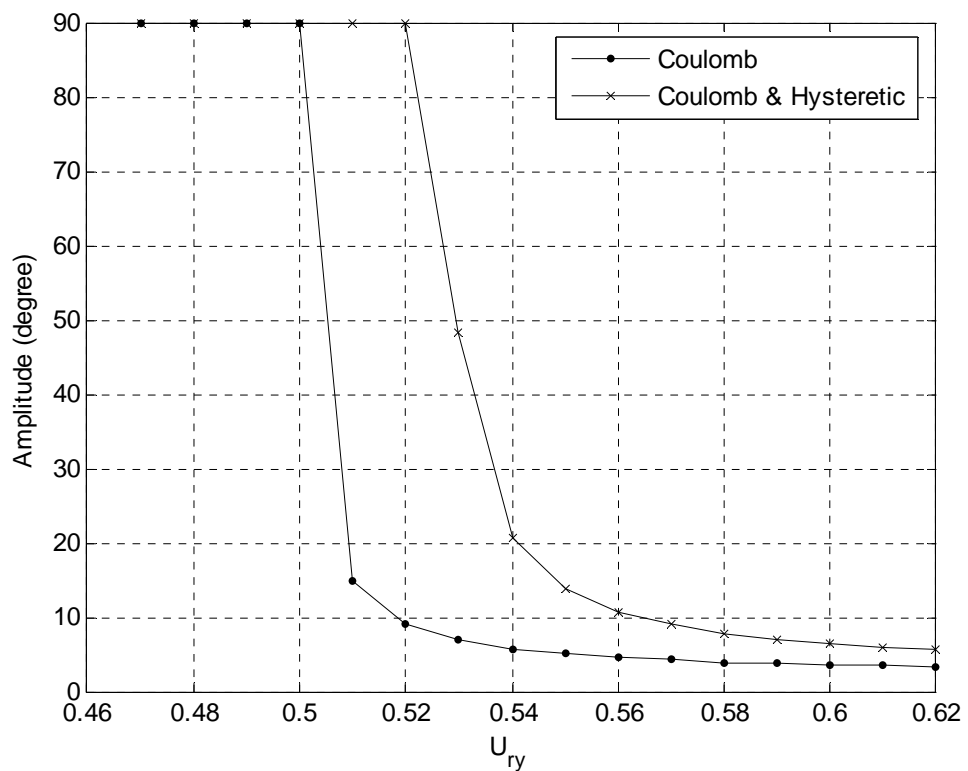


Figure 5-7 Effect of Considering Friction, Coulomb and Hysteretic Terms.

In this term, C_{01}^{eq} and C_{02}^{eq} are proportional to the squared of velocity (Equations (5-61) and (5-62)). At small current velocity, the hydrodynamic torsional damping $-\frac{1}{2}\rho R U c^2 (\partial C_{M(cr)} / \partial \alpha|_{\alpha=0})$ is large enough to keep system stable. This is the case for velocities less than U_{cr} , however, for higher U_{ry} , $C_{01}^{eq} + C_{02}^{eq}$ comes into play which has a reciprocal dependence with amplitude.

Therefore, one may conclude that friction has conservative effect on the amplitude of disturbance and, to be on the safe side, can be ignored or equalised to a viscose damping. The latter is also convenient mathematically and will be deployed in this study.

5.9 Discussion

In this chapter, since the three-dimensional physics of a riser fitted with fairings was complicated, it was simplified to a two-dimensional problem for a fairing on a rigid riser. Two degrees of freedom was identified, i.e. cross-flow translation of the riser and fairing as well as angular twist of the fairing. The equations of motion for these DOFs were derived with the aid of using Lagrange's equation. Hydrodynamic forces including drag, lift and moment emerged as a part of governing equations. These forces were dependent on instantaneous AoA and therefore, the effect of motion, both transverse and torsional, on the real AoA was considered. Based on the purpose of this study, i.e. the assessment of instability onset conditions, an infinitesimal disturbance from the equilibrium position was assumed to track the tendency of amplitude; whether it decreases and dies out or increases and leads to instability. Within this small interval from equilibrium position, the variation of hydrodynamic coefficients was reasonably postulated to be linear. Thus, by using Taylor's series, the hydrodynamic coefficients were expanded and non-linear terms were removed. This resulted in Equations (5-30) and (5-31) which will be discussed further below. Finally, an eigenvalue analysis was carried out to clarify when the real part of one of the roots/eigenvalues becomes positive and the system goes unstable. The characteristic equation was made dimensionless to meaningfully present the significance of physical parameters in the instability criterion. At the end, the effect of torsional friction damping was further investigated.

Now, there are a number of points which need additional attention.

Coupling in Governing Equation of Motions

First of all, it should be noted that the governing Equations (5-30) and (5-31) are coupled in two ways.

These equations are coupled inertially through the term $(S_x + S_a)$, the first mass moment of area. This demonstrates how the acceleration in one DOF affects the inertia of the other DOF.

They are also interrelated hydro-dynamically through the angle of attack. It is due to the fact that hydrodynamic coefficients, which exist in both equations, were written in a linear form of AoA. In addition, AoA is influenced by the distortion angle as well as both transverse and torsion velocities, \dot{y} and $\dot{\theta}$. Thus, these terms as a part of AoA emerge in these equations and inter-relate them thoroughly together.

Hydrodynamic Damping

Secondly, through the process of expanding hydrodynamic coefficients at a small AoA, a number of hydrodynamic terms contributing to stiffness and damping appeared in the governing Equations (5-30) and (5-31). These terms expounds how the hydrodynamic characteristics of a fairing can change the behaviour of the system.

For example, it is obvious that if the system absorbs energy instead of dissipating that through damping, the amplitude of vibration rises continuously and systems goes unstable. In other words, if one of the damping coefficients becomes negative, it means part of the system is gaining energy and, depending on its extent, it can provide the ground for potential instability. Therefore, negative damping can be interpreted as an alert for the risk of instability. Back to these equations, the two terms of $\frac{1}{2}\rho R U c \left(\frac{\partial C_L}{\partial \alpha} \Big|_{\alpha=0} + C_D \Big|_{\alpha=0} \right) \dot{\theta}$ and $\left(-\frac{1}{2}\rho U c^2 \frac{\partial C_{M(cr)}}{\partial \alpha} \Big|_{\alpha=0} \right) \dot{y}$ in Equations (5-30) and (5-31) respectively are parts of the hydrodynamic contribution of the fairing to damping. Thus, according to the above explanation, they should be positive otherwise they obtain energy instead of scattering it. Consequently, one can say that

having a positive coefficient in these terms is a necessary condition for stability of the system, whereas having no roots with a positive real part for the characteristic Equation (5-55) is the sufficient condition. All in all, it can be said that to avoid the instability in the system of the riser and fairing, the necessary and sufficient conditions below should be satisfied,

$$\text{Necessary condition:} \quad 0 < -\left. \frac{\partial C_{M(cr)}}{\partial \alpha} \right|_{\alpha=0} \quad \text{and} \quad 0 < \left(\left. \frac{\partial C_L}{\partial \alpha} \right|_{\alpha=0} + C_D \Big|_{\alpha=0} \right)$$

$$\text{Sufficient condition:} \quad U_{ry} < U_{cr}$$

Hydrodynamic Stiffness

The third point relates to yet another contribution of the hydrodynamic coefficients and it should be noted that the coefficient of the last term in the left hand side of Equation (5-31), $-\left(\frac{1}{2}\rho U^2 c^2 \left. \frac{\partial C_{M(cr)}}{\partial \alpha} \right|_{\alpha=0}\right)\theta$, can be interpreted as the only torsional stiffness which is generated by moment coefficient of the fairing. Thus, if this stiffness is positive, which in fact is identical to satisfying one of the necessary conditions above, the generated moment by fluid force on the fairing, twists it back and helps the fairing with self-alignment to the current. However, in case of negative torsional stiffness, i.e. $-(\partial C_{M(cr)} / \partial \alpha|_{\alpha=0}) < 0$, any infinitesimal rotation from the rest will develop further. In this case, the zero AoA will not be the equilibrium position any more. The equilibrium position as shown in Figure 5-8 will be at an angle like α_2 at which the moment coefficient is zero and the slope of moment curve is negative.

Since the fairing is a symmetric section, therefore its lift and moment coefficients are counter-symmetric. Thus, instead of one single point of equilibrium at zero AoA, there exist two identical equilibrium positions at AoA of α_2 and $-\alpha_2$. In this case, at any infinitesimal twist, say 0^+ , the slope of moment curve is positive and consequently the rotation develops in the positive direction of AoA up to angle α_1 . At this point, the moment is still positive and hence twists the fairing in the positive direction further while the magnitude of moment reduces. This continues up to the point α_2 . At this point, there is no moment to rotate the fairing and, moreover, the slope of the curve is negative and any disturbance will be restored by generation of

appropriate counter-moment. It means α_2 and likewise its counterpart $-\alpha_2$ are the equilibrium positions. In the case of any disturbance, the fairing may switch between these two equilibrium positions depending on the strength of counter-moment. This shift and transition between equilibrium positions resemble the fishtailing as several studies reported that (see sections 3.5 and 3.6). Thus, if any modification to the fairing's section, e.g. adding fins, can resolve the issue of moment coefficient, then the problem of misalignment, and one of the likely causes for fishtailing, will be sorted out. Therefore, it can be concluded that these issues are quite separate and independent of instability and can occur while the fairing is statically stable at its equilibrium positions rather than zero AoA. In other words, misalignment and perhaps fishtailing in one hand and instability in the other hand are two different mechanisms with different governing parameter; one by the moment coefficient and the other by the characteristic equation.

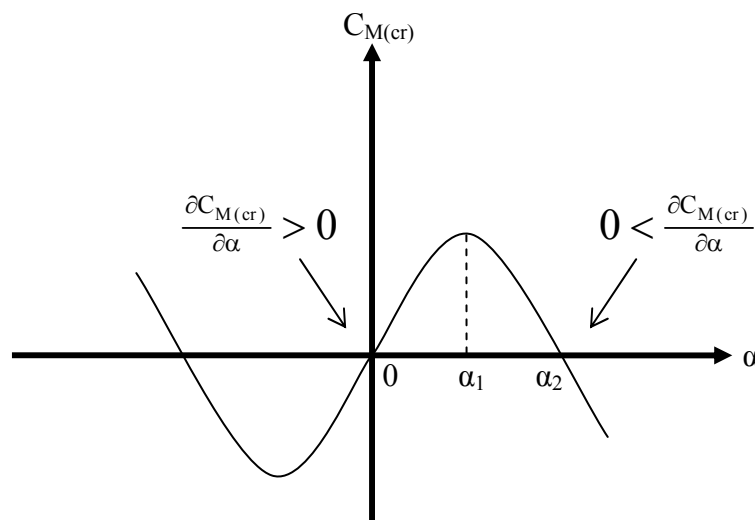


Figure 5-8 Equilibrium AoA.

Identifying hydrodynamic stiffness has another interesting outcome. More scrutiny of the last term in the left hand side of Equation (5-31) reveals that torsional stiffness is proportional to the square of current velocity. It means that as a result of any rise in velocity, the system becomes stiffer torsionally and it is therefore expected that the

frequency of torsional vibration increases too. On the other hand, it should be noted that the imaginary part of the eigenvalue, $\text{Imag}(\lambda)$, represented the frequency of vibration. This feature is illustrated in Figure 5-4 where the imaginary part of two conjugate eigenvalues on the left branches is shown to be increasing. In fact, as the current speed increases, the associated frequency of these eigenvalues rises too. More interesting is that through the process of increasing current velocity and solving the characteristic equations to draw Figure 5-4, as the current speed starts from nearly zero, the only torsional stiffness which is due to hydrodynamic force and proportional to the square of current velocity is therefore very small and almost zero at the beginning. Thus, since there is no torsional stiffness, the frequency of vibration should be zero as well. Another look to Figure 5-4 confirms that the left branches commence from the origin point where the frequency and amplitude are zero.

Now, after development and verification of the theoretical model and also perception of the physical meaning of governing equations, it is necessary to assess the role and influence of key variables identified in Section 5.6. The next Chapter has been dedicated to this issue.

Key Parameters

This chapter presents more details of the key parameters identified through the development of the theoretical model in the previous chapter. The physical meaning of these variables is explored and a method is presented to calculate them for a given system. Finally, a parametric study is carried out to assess the role of each parameter and its influences on the instability onset.

6.1 Introduction

In developing the theoretical model in the previous chapter, it was uncovered that there are three categories of parameters involved in triggering the instability of the riser fairings (see characteristic Equation (5-42)). They include hydrodynamic characteristics of the fairing, structural properties of the system as well as current velocity.

Hydrodynamic characteristics of the fairing appeared in the form of hydrodynamic coefficients and their derivatives, i.e. C_D , $\frac{\partial C_L}{\partial \alpha}$ and $\frac{\partial C_{M(cr)}}{\partial \alpha}$ at zero AoA. The other two groups, i.e. structural properties and current velocity, formed the dimensionless parameters as below (see Equations (5-46) to (5-54)).

$$\tilde{\lambda} = \frac{\lambda}{U/c}$$

$$\gamma^2 = \frac{J + J_a}{(m + m_a) \cdot c^2}$$

$$S_r = \frac{S_x + S_a}{(m + m_a) \cdot c}$$

$$A = \frac{\rho \cdot c^2}{2(m + m_a)}$$

$$\xi_y = \frac{C_y}{2 \cdot (m + m_a) \cdot \omega_y}$$

$$\xi_\theta = \frac{C_\theta}{2 \cdot (J + J_a) \cdot \omega_\theta}$$

$$U_{ry} = \frac{U}{\omega_y \cdot c}$$

$$U_{r\theta} = \frac{U}{\omega_\theta \cdot c} = \sqrt{\frac{\gamma^2}{A \left. \frac{-\partial C_{M(\alpha)}}{\partial \alpha} \right|_{\alpha=0}}}$$

$$R_r = \frac{R}{c}$$

The perception of their physical meaning can help later on in the parametric study to gain a better understanding of what is changing in the system in reality and what influences it entails.

Of the first parameter, λ comes from the Equation (5-38), $\underline{X} = \underline{a}e^{\lambda t}$, and therefore its imaginary part means the frequency of likely oscillation. The term of c/U is the time taking a flow particle to pass a distance as long as the chord. Thus, $\tilde{\lambda}$ relates this time to the period of oscillation.

The next parameter, γ , is also physically meaningful. The fraction of $(J + J_a)/(m + m_a)$ is by definition the square of the radius of gyration about the pivot axis, including the added mass effect. Thus, γ is the dimensionless form of this radius with respect to chord length.

S_r is a geometrical parameter. The fraction of $(S_x + S_a)/(m + m_a)$ implies the distance of the gravity centre of all rotating masses including added mass effect from y axis. Hence, S_r is a dimensionless description of this distance with respect to chord length.

The last geometrical characteristic, A , is related to a well-known concept in hydrodynamics, namely Mass Ratio. Mass ratio is defined as the model mass, which includes structural mass and added mass, to the mass of fluid it displaces (Blevins, 2001). Mass ratio can be a measure of susceptibility of light-weight structures to flow-induced vibration. Generally speaking, as the ratio of fluid mass to structural mass increases, so does the inclination toward flow-induced vibration. With this in mind, A in this case is equal to the inverse of mass ratio of a square section with a side as long as the chord.

There are two sources for structural damping, a vibrating riser which produces transverse damping and torsional friction between the riser and fairing which generates torsional damping. Considering the added mass effect, ξ_y can be illustrated as the in-water structural damping ratio of transverse motion while ξ_θ is the damping ratio for the viscose equivalent of torsional friction damping.

The impact of current in stability emerges in the form of free stream velocity, U . To make it dimensionless, it is divided by a parameter of length dimension, i.e. chord length, and also a parameter of frequency dimension, i.e. frequency of vibration (f_y or f_θ). As the fairing vibrates in the flow, transversely or torsionally, it traces out a wave path. The wave length of the path for one cycle is $U/f_{(y \text{ or } \theta)}$. Thus, reduced velocities, U_{ry} and $U_{r\theta}$, are proportional to the ratio of this wave length to chord length. The point here is as the frequency of vibration is influenced by the square root of the system stiffness and the torsional stiffness of the fairing and riser system is generated by hydrodynamic forces which itself is related to the square of current velocity, therefore the torsional reduced velocity, in contrary to transverse reduced velocity, is a constant parameter and does not change with current velocity increment.

Apart from hydrodynamic coefficients of the fairing which originates directly from its hydrodynamic properties, there exists another parameter relating to hydrodynamic characteristics of the fairing. It is due to the fact that when the fairing moves transversely without rotation, all the points on the contour of the fairing have the same vector of velocity and therefore, the change in AoA induced by vibration is identical for all points. Thus, the situation at which hydrodynamic coefficients are measured is fulfilled and the conventional definition of hydrodynamic coefficients

holds here. The dilemma arises when the fairing starts to rotate about the riser. In torsional vibration, AoA changes with angular position, θ , plus angular velocity, $d\theta/dt$. However, the point is that the magnitude and direction of velocity, and accordingly its X and Y components, vary over the section. To put it more simply, angular velocity generates a vertical component of velocity vector which varies over the section by the horizontal distance from the pivot point. Naturally as illustrated in Section 5.3, the variation of vertical component of the fairing's velocity induces a variable change in AoA at each point along the section. Thus, the definition of measurable hydrodynamic coefficients at which the whole section stands at a specific AoA is violated here. To adapt this variation of AoA to conventional definition, an approximation simulating the effect of angular velocity on the flow field is required. By considering that the fairing is a symmetric section, a reference point on the chord at a radius R with respect to the centre of rotation is chosen. This is used for evaluation of the change in AoA induced by torsional velocity, $d\theta/dt$. Eventually, R_r is the dimensionless description of this distance with respect to chord length.

6.2 Calculation of Properties

The previous section gave some in-depth interpretation of dimensionless parameters. Prior to investigation of their effect in stability of the fairing, it is helpful to provide a tool to calculate these values for a typical section, though the exact calculation of them requires further attention to the details of each particular section. These parameters are classified in three groups of sectional properties, damping and hydrodynamic effects.

(A) Sectional Properties

A fairing's typical section is illustrated in Figure 6-1. It consists of a riser conveying fluid or drill, buoyancy module embracing riser and the fairing shell. The fairing shell contains the riser and buoyancy module in nose and the rest is filled with sea water. As mentioned in Section 4.5, entrapped water is assumed to move with the fairing shell and is treated as a rigid body.

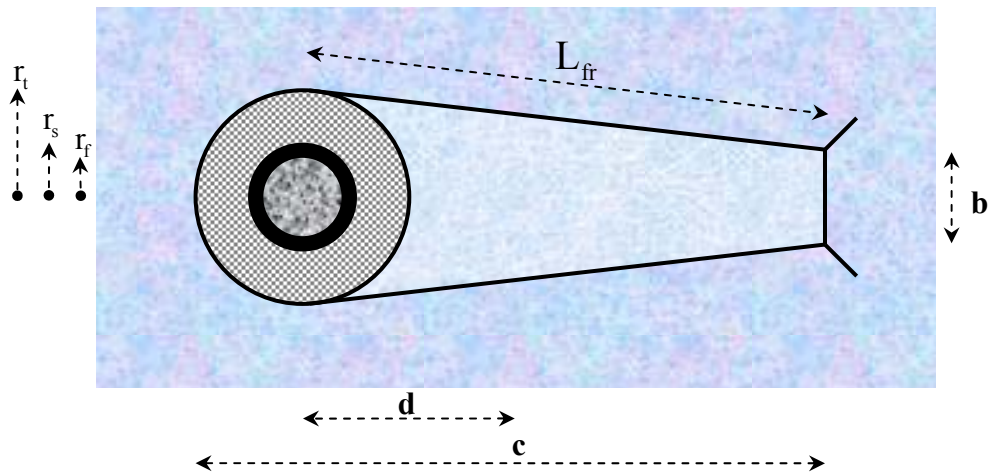


Figure 6-1 Geometry of Typical Fairing.

Through the process of calculation, a number of physical parameters are required which are defined below.

ρ_b, A_b : Density and area of buoyancy module

ρ_s, A_s : Density and area of steel riser

ρ_f, A_f : Density and area of riser internal fluid

ρ_{fr}, A_{fr} : Density and area of fairing

ρ, A_w : Density and area of entrapped water

t_{fr} : Thickness of fairing plate

r_s : Outer radius of steel riser

r_f : Inner radius of steel riser

r_b : Outer radius of buoyancy module

r_t : Outer radius of total/fairing thickness $= r_b + t_{fr} = \frac{1}{2} t$

b : The width of blunt end

d : Distance from middle of fairing to centre of rotation

L_{fr} : Length of fairing leeward side

Thin shell of the fairing can be approximated by a semi-circular plate at the nose, two straight plates on the leeside and a flat plate at the tail. With reference to Figure 6-1, the area occupied by water, riser etc can be evaluated as,

$$A_b = \pi(r_b^2 - r_s^2)$$

$$A_s = \pi(r_s^2 - r_f^2)$$

$$A_f = \pi r_f^2$$

$$A_{fr} = \left[\frac{1}{2} \pi (r_t + r_b) + 2L_{fr} + b \right] t_{fr}$$

$$A_w = \frac{1}{2} \left[(b - 2t_{fr}) + 2r_b \right] \left[(c - 2t_{fr}) - r_b \right] - \frac{1}{2} \pi r_b^2$$

Following that, structural mass is easily calculated as below,

$$m: \text{Structural mass per unit length} = \rho_f A_f + \rho_s A_s + \rho_b A_b + \rho_{fr} A_{fr}$$

The entrapped water is equal to,

$$(m_a)_{in}: \text{Interior added mass} = \rho A_w$$

The fairing is not a simple geometrical section like a circle and therefore there is no closed-form equation for its exterior added mass. Thus, using an approximation is required. Newman (1999) recommended simulating hydrofoil by an ellipse rather than a plate. Consequently, if the major and minor diameters of an ellipse with major diameter along the x axis are denoted by $2a_{ell}$ and $2b_{ell}$ respectively, the added mass coefficients of this ellipse spinning about its centre are easily calculated by using the mapping method, (Brennen, 1982, Newman, 1999),

$$(m_{a-ellipse})_{yy} = \rho \cdot \pi \cdot a_{ell}^2$$

$$(m_{a-ellipse})_{y0} = (m_{a-ellipse})_{0y} = 0$$

$$(m_{a-ellipse})_{00} = \frac{1}{8} \rho \pi \cdot (a_{ell}^2 - b_{ell}^2)^2$$

Where $(m_a)_{ij}$ is the added mass in i direction due to acceleration in j DOF.

From this there are two issues with respect to the fairing. The first point is which ellipse shall be used when estimating the fairing's added mass. The second difference

is that the fairing is rotating about the centre of the riser which is not located in the middle of the chord length. This will be addressed later on in the calculation of the torsional added mass.

There are various options in selecting the equivalent ellipse, for example, equality of chord and thickness of the fairing and ellipse, equality of chord and area and also equality of thickness and area. A common and simple method is to use the equality of chord length and thickness. Thus, the exterior added mass of fairing for transverse motion can be estimated by

$$(m_a)_{Ex} : \text{Exterior added mass} = \frac{1}{4} \rho \pi c^2$$

Eventually, the sum of these two values gives the total added mass of the fairing.

$$m_a = (m_a)_{In} + (m_a)_{Ex}$$

As the tension varies along the riser because of weight, sometimes it is necessary to have the in-water/wet weight to calculate the tension difference at the riser's two ends, $(T_t - T_b)$. The in-water weight is lighter because of the buoyancy force.

$$\text{Buoyancy force per unit length} = (A_f + A_s + A_b + A_{fr}) \rho g$$

$$\text{Weight (flooded system) in air per unit length} = (\rho_f A_f + \rho_s A_s + \rho_b A_b + \rho_{fr} A_{fr}) g$$

$$\text{Weight in water} = \text{weight in air} - \text{buoyancy force} = (T_t - T_b) / L$$

The polar mass moment of inertia is the next parameter to be evaluated. According to Equation (5-7), this variable should be integrated over the rotating part. As the riser and buoyancy module are fixed, the rotating parts consist of thin shell of fairing plus the entrapped water. The latter is considered as interior added polar mass moment of inertia. The polar mass moment of inertia for each plate of the fairing is calculated about its own local coordinates and then is shifted to the centre of rotation. Each bracket in the following equation corresponds to these plates, i.e. semi-circle nose, endplate and two flat plates of leaside respectively.

$$J = \rho_{fr} \left\{ \frac{1}{2} \frac{\pi}{2} \left[\frac{1}{2} (r_t + r_b) \right]^4 + \left[\frac{1}{12} (b t_{fr}^3 + b^3 t_{fr}) + b t_{fr} (c - r_t - \frac{1}{2} t_{fr})^2 \right] + \right. \\ \left. + 2 \left[\frac{1}{12} (L_{fr} t_{fr}^3 + L_{fr}^3 t_{fr}) + L_{fr} t_{fr} \left(\frac{1}{4} (b + (r_t - \frac{1}{2} b))^2 + \frac{1}{4} (c - r_t)^2 \right) \right] \right\} L$$

As mentioned earlier, the contribution of entrapped water is in the form of interior added mass. Again, it is treated as a rigid body. To facilitate the calculation, it is divided into a trapezoid minus a semi-circle of the riser and buoyancy module. The trapezoid is also broken down into a rectangle and two triangles. The polar mass moment of inertia is calculated about the local coordinates for each of these and is then shifted to the centre of rotation.

$$(J_a)_{In} = \frac{1}{12} \rho \left(b^3 (c - r_t) + 4b(c - r_t)^3 \right) + 2\rho \left\{ \frac{1}{12} \left[\left(r_t - \frac{1}{2}b \right) (c - r_t)^3 + \left(r_t - \frac{1}{2}b \right)^3 (c - r_t) \right] + \frac{1}{2} \left(r_t - \frac{1}{2}b \right) (c - r_t) \left(\frac{1}{2}b \right)^2 \right\} - \frac{1}{4} \rho \pi r_b^4$$

It was explained above that there is no explicit equation to calculate the exterior added mass of a fairing and therefore it is approximated by an equivalent ellipse with the same diameters. For a rotating ellipse about its centroid with major diameter of $2a_{ell}$, the added polar mass moment of inertia is as below (Bishop and Price, 1979, Brennen, 1982, Newman, 1999). On the other hand, the added first mass moment of area, $(m_{a-ellipse})_{\theta y}$ and $(m_{a-ellipse})_{y\theta}$, shows the effect of added mass in torsional DOF when the body in a fluid moves transversely and vice versa. For an elliptic section rotating about its centroid, the added first mass moment of area is zero due to symmetry about both major and minor diameters. In other words, no torsional torque is induced when the body accelerates in the transverse direction or no transverse force is generated by rotation about the centroid.

$$(m_{a-ellipse})_{\theta\theta} = \frac{1}{8} \rho \pi \cdot (a_{ell}^2 - b_{ell}^2)^2$$

$$(m_{a-ellipse})_{y\theta} = (m_{a-ellipse})_{\theta y} = 0$$

But, the important issue is that fairing spins about the centre of the riser, at a distance from mid-chord and this effect should be considered. Let's imagine an ellipse rotating by $\ddot{\theta}$ about a pivot point at a distance, say d , from its centroid on chord while the pivot point moves transversely by \ddot{y} (Figure 6-2). When the origin of coordinate system is transferred to the new pivot point, added masses should be transferred to the new coordinate system as well. It is done through the well-known equations below.

$$((m_a)_{\theta\theta})_{New} = (m_a)_{\theta\theta} + (m_a)_{yy} \times d^2$$

$$((m_a)_{y\theta})_{New} = (m_a)_{y\theta} + (m_a)_{yy} \times d$$

Consequently, substituting relevant values in above equations gives

$$((m_{a-ellipse})_{\theta\theta})_{New} = \frac{1}{8} \rho \pi (a^2 - b^2)^2 + \rho \pi a^2 d^2$$

$$((m_{a-ellipse})_{y\theta})_{New} = ((m_{a-ellipse})_{\theta y})_{New} = \rho \pi a^2 d$$

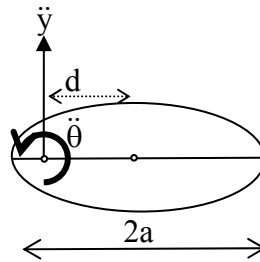


Figure 6-2 Added Polar Mass Moment of Inertia for an Ellipse.

This formulation is in conformity with that of a plate rotating about one edge (Brennen, 1982). Eventually, the exterior added polar mass moment of inertia for a fairing can be estimated by,

$$(J_a)_{Ex} = \rho \left[\frac{1}{8} \pi \left(\frac{1}{4} c^2 - r_t^2 \right)^2 + \pi \left(\frac{1}{4} c^2 \right) d^2 \right]$$

For a fairing the distance d, from mid-chord to pivot point i.e. centre of riser, is,

$$d = \frac{1}{2} c - r_t$$

The sum of these two added polar mass moments of inertia, i.e. interior and exterior, gives the total value,

$$J_a = (J_a)_{In} + (J_a)_{Ex}$$

The first mass moment of area is the next parameter to be evaluated. Similar to previous parameter, this variable is only integrated over the rotating parts (refer to Equation (5-7)). For the thin shell of the fairing, this parameter is calculated for each

plate and is shifted to the centre of riser. The first moment of area for the semi-circle plate of nose is easily obtained by,

$$S_{\text{semi-ring}} = \int_0^\pi r \sin \theta (t_{\text{fr}} r d\theta) = 2t_{\text{fr}} r^2$$

The sum of this parameter over all the fairing's plates gives,

$$S_x = \rho_{\text{fr}} \left[-2t_{\text{fr}} \times \left(\frac{1}{2}(r_b + r_t) \right)^2 + b t_{\text{fr}} (c - r_t) + 2L_{\text{fr}} t_{\text{fr}} \times \frac{1}{2}(c - r_t) \right]$$

Similarly, the entrapped water is modelled as a rigid body and divided into a trapezoid minus a semi-circle.

$$(S_a)_{\text{In}} = \rho \left\{ \frac{1}{2} b (c - r_t)^2 + 2 \left[\frac{1}{6} (r_t - \frac{1}{2} b) (c - r_t)^2 \right] - \frac{2}{3} r_b^3 \right\}$$

If the fairing is approximated by an equivalent ellipse, the added first mass moment of area, $(S_a)_{\text{Ex}}$ corresponds to the parameter of $(m_{\text{a-ellipse}})_{\theta y} = (m_{\text{a-ellipse}})_{y\theta}$ of ellipse as calculated above.

$$(S_a)_{\text{Ex}} = \rho \pi \left(\frac{1}{4} c^2 \right) d$$

Thus, the total first mass moment of area is obtained by the sum of these two values,

$$S_a = (S_a)_{\text{In}} + (S_a)_{\text{Ex}}$$

With the aid of these calculations, the dimensionless properties of section, γ , S_r and A , can now be easily computed.

$$\gamma^2 = \frac{J + J_a}{(m + m_a).c^2}$$

$$S_r = \frac{S_x + S_a}{(m + m_a).c}$$

$$A = \frac{\rho.c^2}{2(m + m_a)}$$

Area moment of inertia is mainly generated by the riser as the buoyancy module is ductile and the fairings are also made in segments.

$$I = I_{\text{riser}} = \frac{1}{4} \pi (r_s^4 - r_f^4)$$

Considering the riser as a tensioned bending beam, the natural period of the fundamental transverse mode vibration in water can be written,

$$\omega_y = \sqrt{\frac{EI\pi^4 + T_a\pi^2}{L^4 + \frac{T_a L^2}{m + m_a}}}$$

Where E is the Young's Modulus of the riser, T_a is the average tension and L is the riser's length.

Consequently, when $U_{cr} = U_{ry(\text{critical})}$ is obtained by solving the characteristic equation, then the critical current velocity (m/s) is $U_{\text{critical}} = U_{cr} \cdot (\omega_y \cdot c)$.

(B) Damping

It was clarified in Chapter 5 that apart from hydrodynamic damping which emerges from the expansion of hydrodynamic coefficients, there are two other damping elements, structural/transverse damping of the system as well as torsional friction damping.

Structural damping of cylindrical bodies in still water has been widely investigated by many researchers. Nevertheless, to the author's knowledge very limited data is available on the damping of cylinders outfitted with fairings with the only known study of its kind being published by Lee et al in 2004. This study showed that deploying the fairings on the riser generates large in-water damping in the range of 0.10 to 0.18 (Lee et al., 2004b). For comparison purpose, the in-water damping for a bare cylinder without fairing is below 5% based on similar tests.

Moreover, the fairing is in contact with the riser at collars located at the ends and possibly through some pads in between. The friction coefficient depends on the substance of these rubbing pads and their surface roughness. These pads could be made-up of Teflon, brass and copper (Denison et al., 2000a). Thus, the friction coefficient will be in the range of 0.04 to 0.74.

(C) Hydrodynamic Properties

The theoretical model developed in Chapter 5 indicated two sets of hydrodynamic properties are needed. The first group comprises of hydrodynamic coefficients of the fairing section or their derivatives, in particular C_D , $\partial C_L / \partial \alpha$ and $\partial C_{M(cr)} / \partial \alpha$. At a specific Reynolds number and surface roughness, they depend on the geometry of section and its details like tail, sharp end or blunt end, with fin or without fin. This produces a broad variety of sections which each of them needs separate and thorough investigation. Hence, Chapter 7 has been dedicated to the assessment of a few common sections. These parameters will be discussed there in detail.

The second set of hydrodynamic properties includes the parameter of R_r . It was explained in the introduction that R_r is a reference length for the average effect of the angular velocity on the AoA. Using vortex-strip theory, Fung (2002) calculated the lift and moment force of a thin foil in rotation and translation. He demonstrated that the lift coefficient of such a foil can be written in the form of $C_L = \partial C_L / \partial \alpha \times [**]$ where,

$$[**] = \theta - \frac{\dot{y}}{U} + \left(\frac{3}{4}c - x_0\right) \frac{\dot{\theta}}{U}$$

The parameter x_0 is the distance of where y is evaluated, i.e. centre of rotation, to the leading edge. Thus, lift coefficient of an oscillating thin foil is measured based on the angle of attack at a reference point located at $\frac{3}{4}$ -chord. In other words, for a thin foil, R_r is chosen to give the AoA at a point three-quarters of the way back from the leading edge (Blevins, 2001). With respect to the equation $R = x_R - x_0$ where x_R is the distance of the reference point from leading edge, if $R > 0$, the reference point is aft of the pivot and if $R < 0$, it is forward of the pivot. For thin foil, $x_R = \frac{3}{4}c$.

As there is no such data available for thick foils like a fairing, it is again necessary to estimate the range of this parameter. Fung in his mathematical method deploys the thin plate model for thin foils. His calculation results in $x_R = \frac{3}{4}c$. Now, consider a rotating circle about its centroid in the same inviscid flow as Fung assumed. Because of symmetry, no AoA is generated and thus $R = 0$ or $x_R = x_0 = \frac{1}{2}c$. It means the

reference point for circle is its centroid. Thus, from a circular section to a flat plate section, the reference point moves from the midway point to the point three-quarters of the way back from the leading edge, i.e. $\frac{1}{2}c < x_R < \frac{3}{4}c$. If it is assumed that the riser is located in the foremost part of the fairing with approximately circular nose, then the pivot point is at least as long as $\frac{1}{2}t$ back from leading edge, $\frac{1}{2}t < x_0$, where t is the thickness of the fairing. However, since the fairing always has a trailing edge, the pivot point will never exceed the mid-chord point, $x_0 < \frac{1}{2}c$. Hence, the reference length of R for a fairing is in the range of,

$$\frac{1}{2}c - \frac{1}{2}t < (R = x_R - x_0) < \frac{3}{4}c - \frac{1}{2}t$$

Consequently, the dimensionless form of R_r varies within the range below,

$$0 < R_r < \frac{3}{4} - \frac{1}{2} t/c$$

For example, the reference length in a fairing with thickness to chord ratio of 60%, i.e. $t/c = 0.6$, is in the range of $0 < R_r < 0.45$. The further pivot point moves away from leading edge, the smaller R_r becomes. Moreover, as the fairing grows in thickness, the reference point comes forward toward leading edge and R_r becomes much smaller.

6.3 Example

Grant and Patterson (1977) performed a series of wind-tunnel tests on two fairing sections for a drilling project off the coast of Brazil. The length to thickness ratio of the selected fairing was fixed at 2. As illustrated in Figure 6-3, this fairing with the total thickness of 1.016 m (40") embraced a riser of 0.609 m (24") diameter plus the choke and kill lines. No buoyancy module was used and sea water filled the gap between the riser and fairing's shell. The fairing was fabricated from 0.0034 m (10 gauge) steel. The riser carries drilling mud with the density of 1795.97 kg/m³ (18 lb/gallon). The effects of the choke and kill lines are ignored in this example.

The first group of parameters to calculate is the sectional properties. To this end, it is necessary to evaluate the physical variables as listed in Section 6.2(A). Since no buoyancy module was used in this case and the gap between the riser and fairing's shell was filled with seawater, the density of buoyancy module is equal to that of

seawater, $\rho_b = \rho = 1025 \text{ kg/m}^3$. The steel riser had the density of $\rho_s = 7850 \text{ kg/m}^3$. It was filled with drilling mud with the density of 1795.97 kg/m^3 .

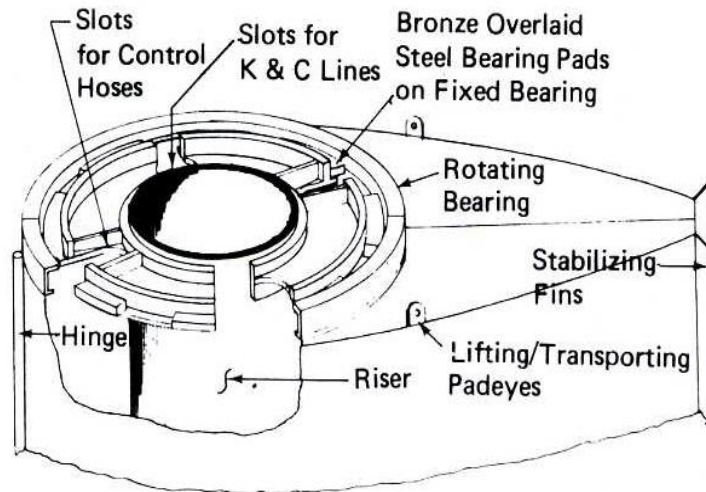


Figure 6-3 Riser Fairing for SEDCO 702 (Grant and Patterson, 1977).

As mentioned above the fairing was fabricated from 0.0034 m (10 gauge) steel and the density of fairing was $\rho_{fr} = 7850 \text{ kg/m}^3$. Since nothing was mentioned in the paper about the wall thickness of 0.609 m (24") steel riser, it is assumed to be in the typical range of 0.04 m, therefore, the outer radius of the riser and fluid flow conveyer can be easily calculated as $r_s = 0.3048 \text{ m}$ and $r_f = r_s - \text{riser's thickness} = 0.2648 \text{ m}$. The total thickness of the fairing was reported 1.016 m (40"). Thus, the outer radius of the fairing and the gap between the riser and fairing are $r_t = 0.508 \text{ m}$ and $r_b = r_t - \text{fairing's thickness} = 0.5046 \text{ m}$. By considering the length to thickness ratio of 2, the chord length will be $c = 2.032 \text{ m}$. The variable d , the distance from middle of the fairing to centre of rotation, as mentioned earlier is calculated as $d = \frac{1}{2}c - r_t = 0.5080 \text{ m}$. Finally, as the end edge of the fairing is sharp, $b = 0 \text{ m}$, and the length of the fairing's leeside is calculated as $L_{fr}^2 = (c - r_t)^2 + (r_t - \frac{1}{2}b)^2$ or $L_{fr} = 1.6066 \text{ m}$. All the required variables to calculate dimensionless parameters are summarised below.

6. Key Parameters

$$\rho = 1025 \text{ kg/m}^3$$

$$\rho_b = 1025 \text{ kg/m}^3$$

$$\rho_s = 7850 \text{ kg/m}^3$$

$$\rho_{fr} = 7850 \text{ kg/m}^3$$

$$\rho_f = 1795.97 \text{ kg/m}^3$$

$$t_{fr} = 0.0034 \text{ m}$$

$$r_s = 0.3048 \text{ m}$$

$$r_f = 0.2648 \text{ m}$$

$$r_t = 0.5080 \text{ m}$$

$$r_b = 0.5046 \text{ m}$$

$$b = 0 \text{ m}$$

$$c = 2.032 \text{ m}$$

$$d = 0.5080 \text{ m}$$

$$L_{fr} = 1.6066 \text{ m}$$

By using the equations derived in Section 6.2(A), the areas occupied by water, riser etc are evaluated.

$$A_b = 0.5080 \text{ m}^2$$

$$A_s = 0.0716 \text{ m}^2$$

$$A_f = 0.2203 \text{ m}^2$$

$$A_{fr} = 0.0164 \text{ m}^2$$

$$A_w = 0.3615 \text{ m}^2$$

All masses involved are calculated then.

$$m = 1606.8 \text{ kg/m}$$

$$(m_a)_{In} = 370.5 \text{ kg/m}$$

$$(m_a)_{Ex} = 3324.0 \text{ kg/m}$$

$$m_a = 3664.5 \text{ kg/m}$$

Polar mass moment of inertia is the next parameter to be evaluated.

$$J = 479.0 \text{ kg.m}$$

$$(J_a)_{\text{In}} = 288.4 \text{ kg.m}$$

$$(J_a)_{\text{Ex}} = 1099.1 \text{ kg.m}$$

$$J_a = 1387.5 \text{ kg.m}$$

First mass moment of area is calculated next.

$$S_x = 51.8 \text{ kg}$$

$$(S_a)_{\text{In}} = 314.6 \text{ kg}$$

$$(S_a)_{\text{Ex}} = 1688.6 \text{ kg}$$

$$S_a = 2003.2 \text{ kg}$$

Eventually, with reference to the definition of dimensionless parameters at the beginning of this chapter, three of them can be obtained now.

$$\gamma^2 = \frac{J + J_a}{(m + m_a).c^2} = 0.0853$$

$$S_r = \frac{S_x + S_a}{(m + m_a).c} = 0.1908$$

$$A = \frac{\rho.c^2}{2(m + m_a)} = 0.3992$$

No data was reported in Grant and Patterson's research about the damping properties of the system. Hence, with reference to the discussion presented in Section 6.2(B), damping coefficients are selected in the lower bound which results in the smallest critical current velocity.

$$\xi_y = 0.05$$

$$\xi_0 = 0.01$$

Following the wind-tunnel test, Grant and Patterson (1977) presented a curve for each hydrodynamic coefficient at various AoA (Figure 6-4). In this figure, C_a , C_t and C_m represent the axial force, total force and moment coefficients respectively. Accordingly, the required hydrodynamic coefficients are obtained as below.

6. Key Parameters

$$C_{D|_0} = 0.09$$

$$\partial C_L / \partial \alpha|_0 = 3.05 \quad (1/\text{rad})$$

$$\partial C_{M(\text{cr})} / \partial \alpha|_0 = -0.24 \quad (1/\text{rad})$$

The last hydrodynamic property to obtain is the reference length of R_r . It was estimated in Section 6.2(B) that R_r is in the following range.

$$0 < R_r < \frac{3}{4} - \frac{1}{2} t/c$$

In this example, the ratio of c/t is equal to 2.0 and therefore, R_r is at most 0.50 for a flat plate. As explained earlier, it reduces for a fairing and is estimated as 0.40.

$$R_r = 0.40$$

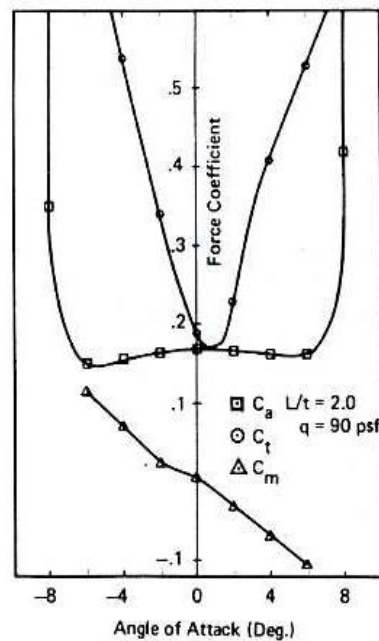


Figure 6-4 Force Coefficients of Fairing Model (Grant and Patterson, 1977).

Now, all the necessary parameters to analyse the stability of a two-dimensional system are available.

$$\gamma^2 = 0.0853$$

$$S_r = 0.1908$$

$$A = 0.3992$$

$$\xi_y = 0.05$$

6. Key Parameters

$$\xi_0 = 0.01$$

$$C_D|_0 = 0.09$$

$$\frac{\partial C_L}{\partial \alpha}|_0 = 3.05$$

$$\frac{\partial C_{M(cr)}}{\partial \alpha}|_0 = -0.24$$

$$R_r = 0.40$$

The characteristic Equation (5-55) is used again here. Starting from zero, the reduced velocity of U_{ry} increases gradually and for each increment this equation is solved numerically until the real part of an eigenvalue becomes positive. In this example, the analytical model shows the system goes unstable at $U_{cr} = 0.43$. The trajectory of real and imaginary parts of eigenvalues, as U_{ry} rises, is demonstrated in Figure 6-5. Red circles correspond to critical U_{ry} where the real part of solution has crossed over the imaginary axis.

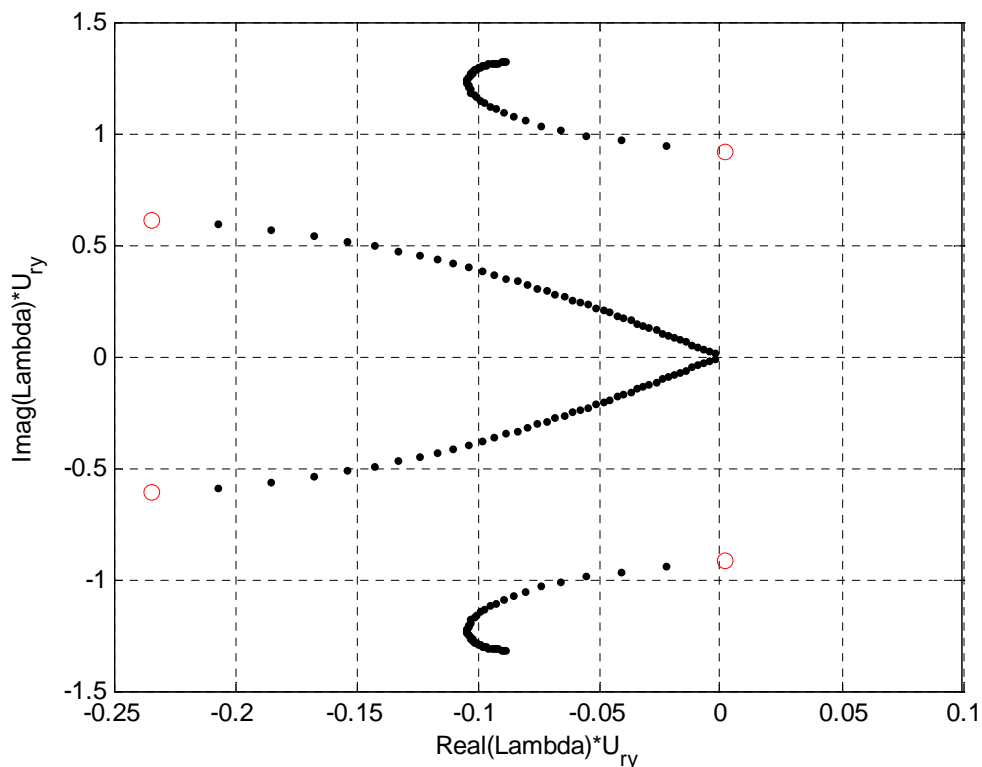


Figure 6-5 Trend of Eigenvalues by Velocity Increment.

6.4 Results of Parametric Investigation

The above example demonstrated a method to estimate the parameters required in the model. In this section, a parametric study is carried out to identify how the variation in each of these parameters influences the threshold of instability.

For this study, the set of parameters corresponding to the above example is selected. Each parameter varies in the range of half to five times of the present value unless otherwise is stated. The red circle in following figures shows the base case.

(A) Effect of Drag, C_d

Figure 6-6 shows that the instability onset is not particularly sensitive to the drag coefficient. The drag coefficient came into play through the process of finding instantaneous AoA and emerged in hydrodynamic damping terms. The undesirable effect of drag on U_{cr} is negligible perhaps because it is the sum of drag and lift slope which forms a term in hydrodynamic damping. Moreover, the value of drag in this example is much less than the lift slope and therefore its impact is not tangible.

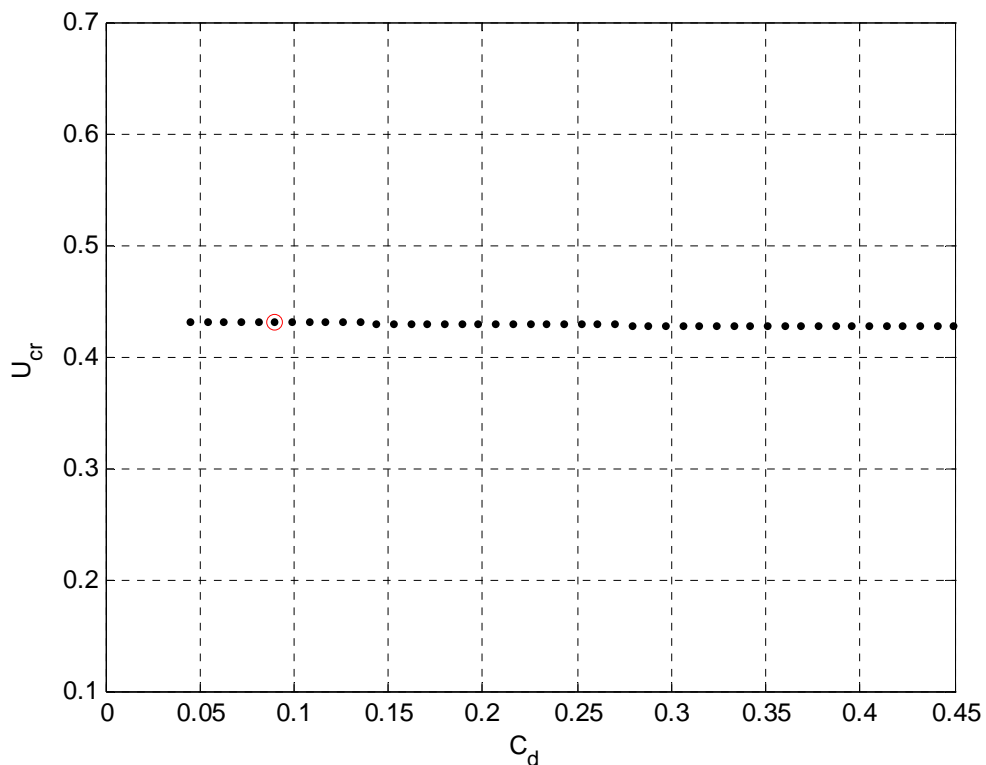


Figure 6-6 U_{cr} vs. Drag Coefficient.

(B) Effect of Lift, $\partial C_L/\partial\alpha$

Lift force as observed in Figure 6-7 has an adverse effect on stability of the system. In fact, the threshold of stability reduces as the slope of the lift coefficient increases. In other words, as the fairing diverges from its design philosophy, which is streamlining the flow and becomes similar to foils generating high lift force, it loses its suitability for use on a riser.

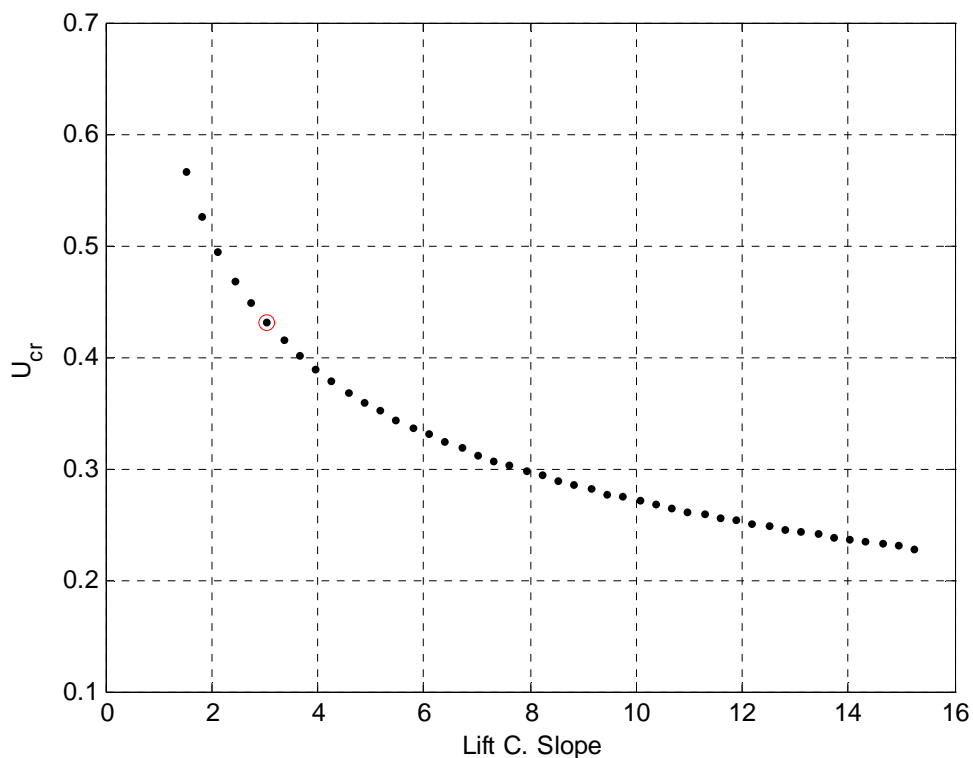


Figure 6-7 U_{cr} vs. Lift Coefficient.

(C) Effect of Moment, $\partial C_M/\partial\alpha$

The moment coefficient displays both a positive and negative role in instability. In Figure 6-8, as the absolute value of $\partial C_M/\partial\alpha$ rises, the critical reduced velocity can increase or decline based on where the initial value is.

As was discussed in Section 5.9, that $\partial C_M/\partial\alpha < 0$ is a necessary condition for stability and when it is violated, the system is unstable. Further investigation confirms this issue in this example and shows that the real part of one of the solutions is positive for a very small current speed if $\partial C_M/\partial\alpha > 0$.

6. Key Parameters

In addition, it was revealed that if $|\partial C_M/\partial \alpha|$ becomes large enough, it makes the system stable for a normal range of U_{cr} . In this example, for large $|\partial C_M/\partial \alpha|$ the system was still stable while U_{cr} increased up to 6. For instance when $\partial C_M/\partial \alpha = -1.2$, the trend of eigenvalues for U_{cr} up to 6 has been shown in Figure 6-9.

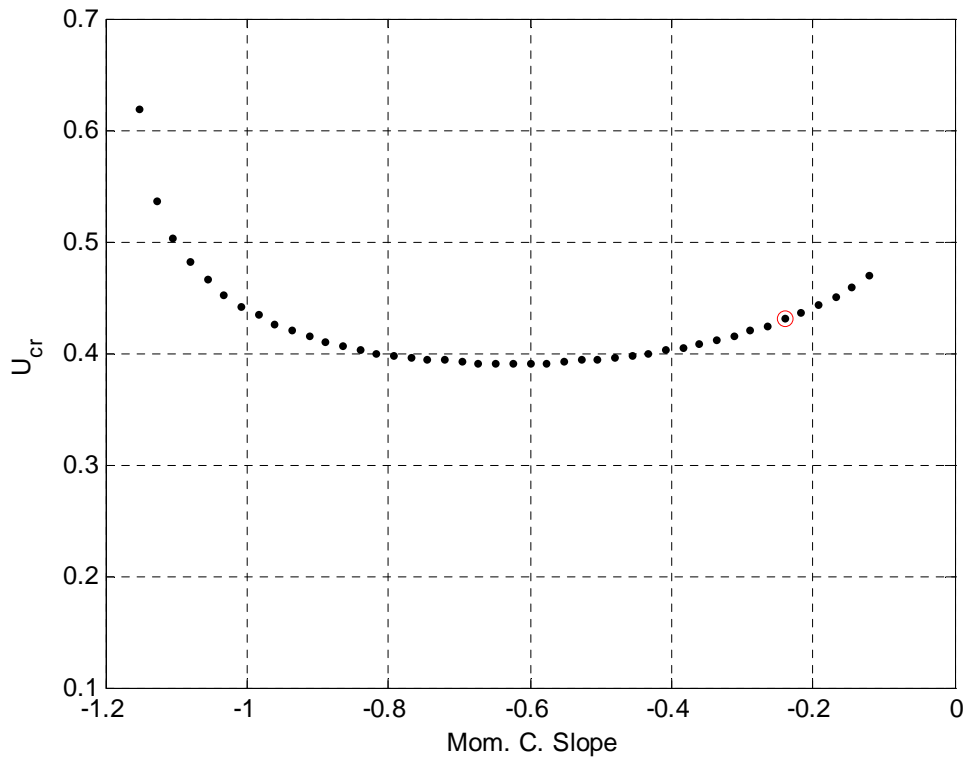


Figure 6-8 U_{cr} vs. Moment Coefficient.

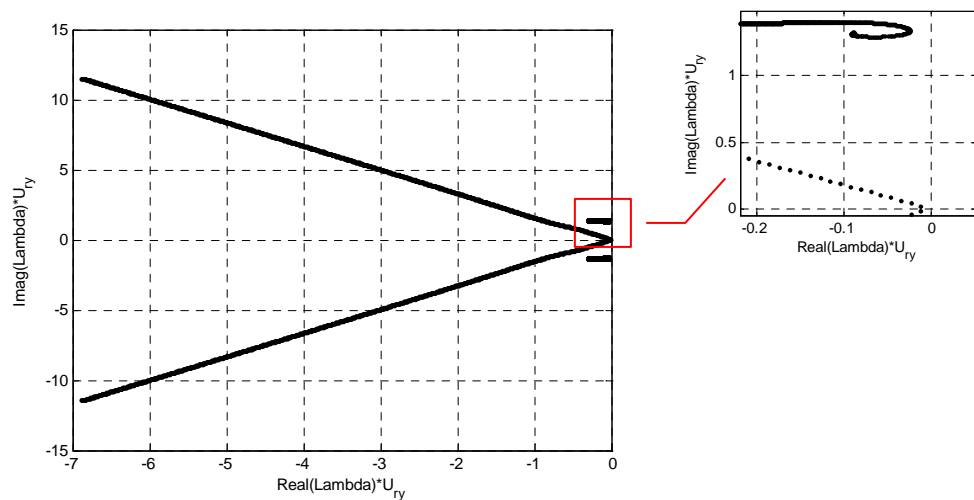


Figure 6-9 Trend of Eigenvalues at High Moment Coefficient.

(D) Effect of Transverse Damping

According to Figure 6-10, and as was expected, transverse damping delays the instability to a higher current velocity and improves the stability span.

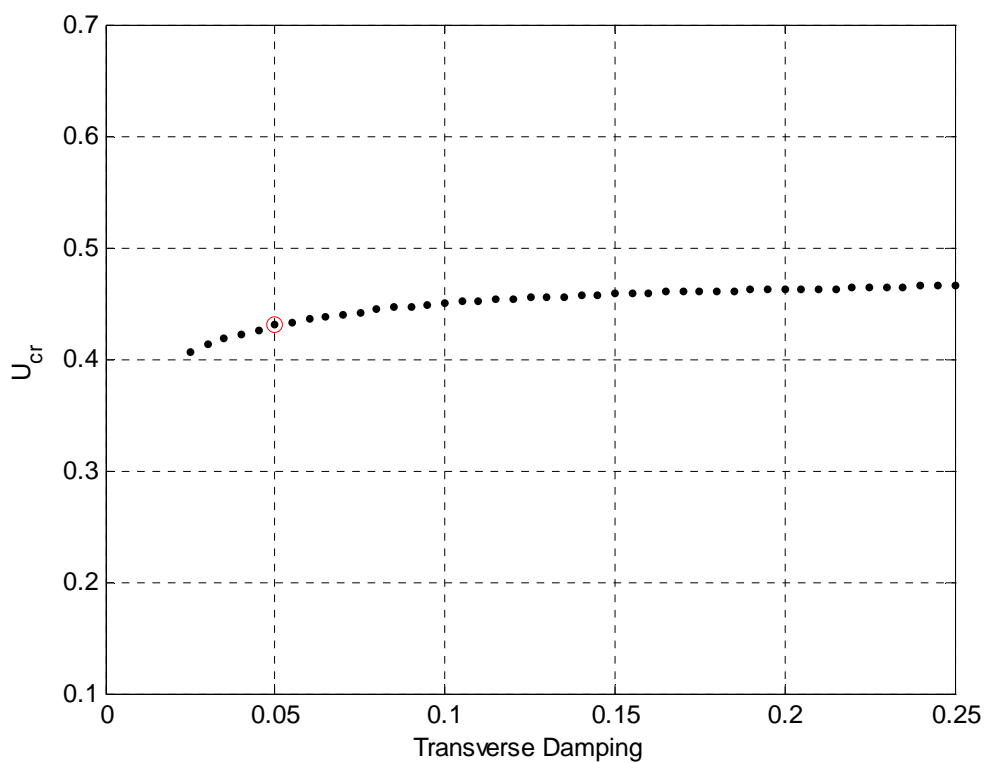


Figure 6-10 U_{cr} vs. Transverse Damping.

(E) Effect of Torsional Damping

Likewise, torsional damping improves the stability (Figure 6-11). In this figure damping ratio varies between 0.5 to 10 times of the base value as this value was very small.

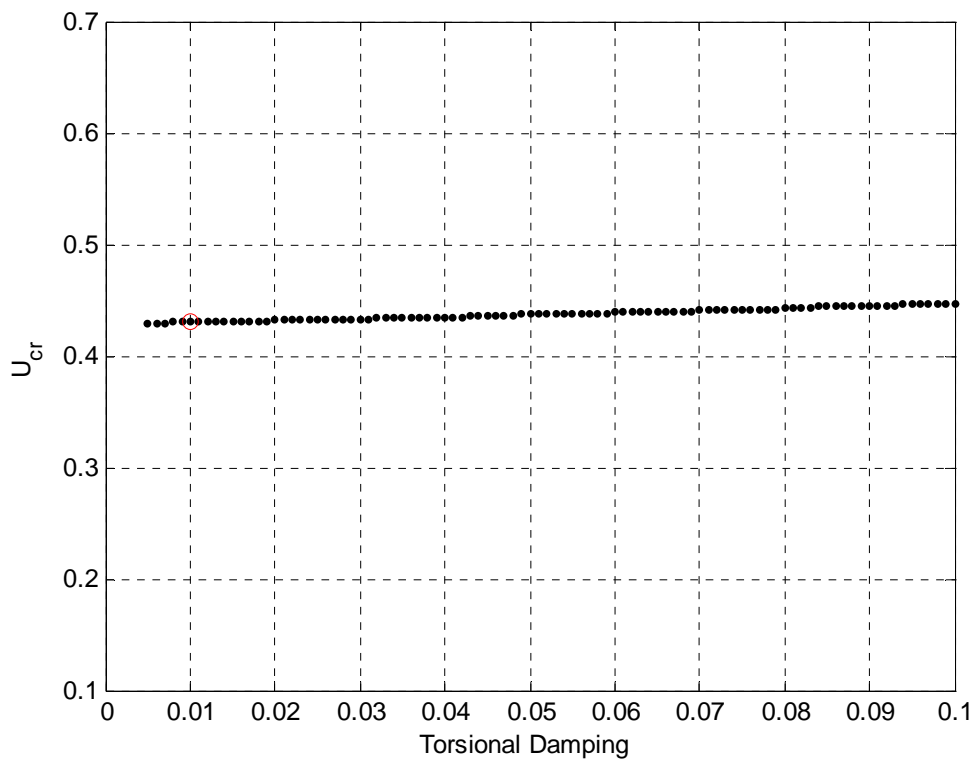


Figure 6-11 U_{cr} vs. Torsional Damping.

(F) Effect of Structural Properties, A

Earlier in the introduction to this chapter, it was explained that parameter A is equal to the inverse of mass ratio of a square section with a side as long as the chord. Therefore, it is proportional to the ratio of fluid mass to structural mass. Moreover, it was also mentioned that, in general, as the ratio of fluid mass to structural mass increases so does the inclination toward flow-induced vibration. Here in this example, Figure 6-12 is in conformity with this principle and confirms the above point. It also demonstrates that as A rises, the critical reduced velocity declines.

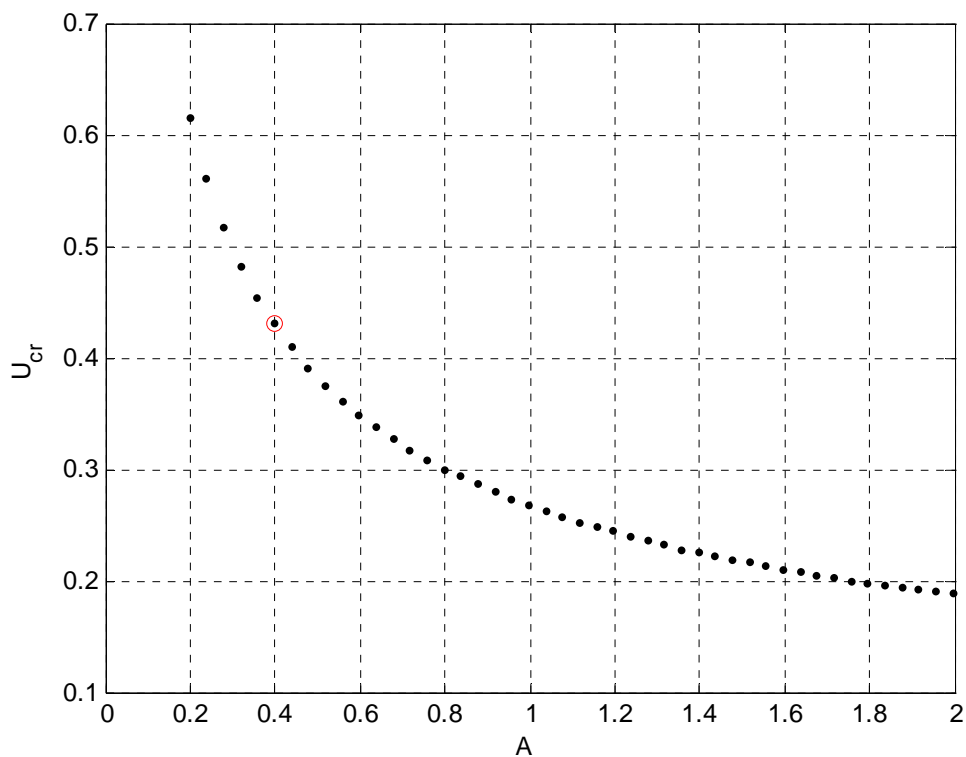


Figure 6-12 U_{cr} vs. A .

(G) Effect of Structural Properties, γ^2

According to Figure 6-13, parameter γ which is a dimensionless symbol of the radius of gyration about the pivot axis has a positive influence on U_{cr} . This shows that as the distribution of mass increases its distance from the pivot point, the system becomes unstable when a higher velocity is reached. One simple conclusion may be that adding mass to the tail of the fairing, like bumps and fins, improves the stability.

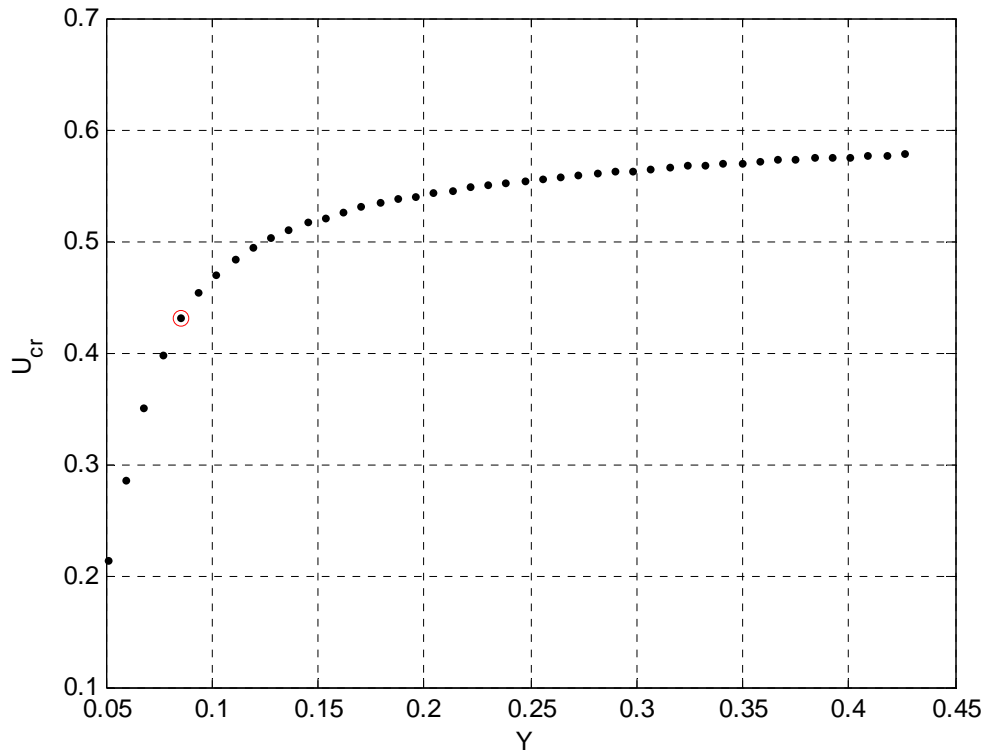


Figure 6-13 U_{cr} vs. γ^2 .

(H) Effect of Structural Properties, S_r

Parameter S_r , as explained in Section 5.9, shows how two DOFs are coupled inertially. Figure 6-14 says that as the level of coupling decreases and DOFs become inertially independent, critical reduced velocity is shifted to higher values.

This study showed that beyond a certain amount of S_r , for instance 0.292 in this example, the system is unstable for any small current velocity. Thus, in Figure 6-14 S_r varies within 10% to 150% of base value.

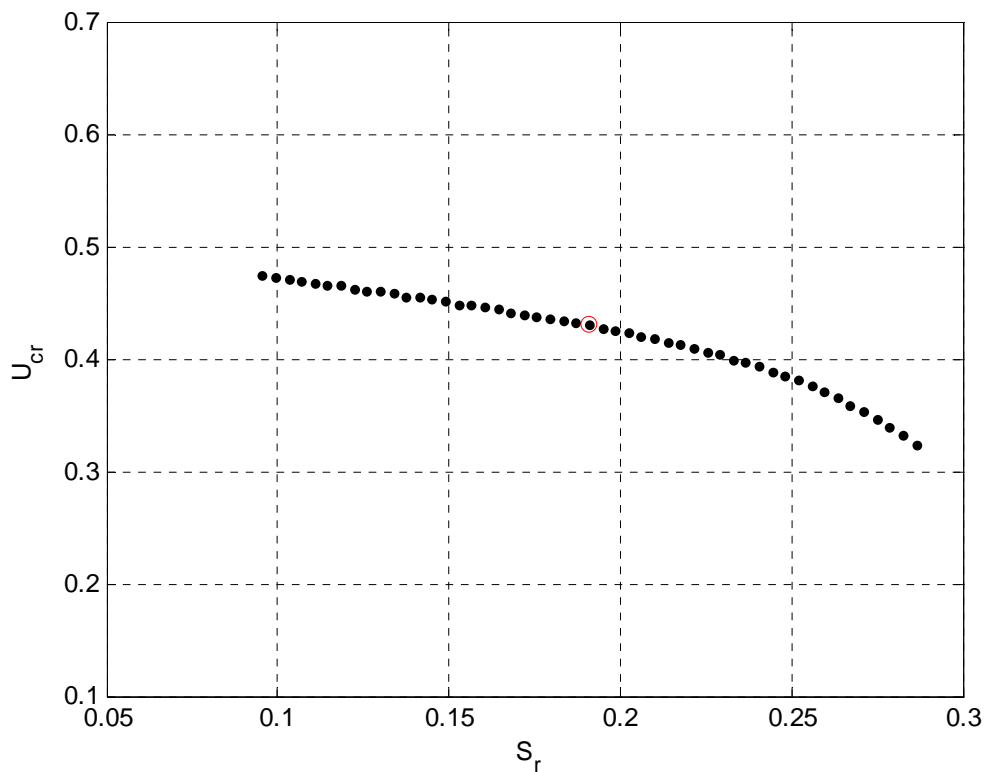


Figure 6-14 U_{cr} vs. S_r .

(I) Effect of Hydrodynamic Property, R_r

It was discussed in the calculation of parameters (Section 6.2(C)) that the parameter R_r will be in the range of $0 < R_r < \frac{3}{4} - \frac{1}{2} t/c$. In this example with the length to chord ratio of 2, R_r cannot exceed 0.5. Therefore, in the parametric study shown in Figure 6-15, R_r varies between 0.5 to 1.5 times the base value ($R_r = 0.40$). The upper limit is selected beyond physical limit merely to investigate the effect of this parameter more clearly.

Figure 6-15 indicates that the critical reduced velocity increases and then decreases as the length of R_r extends.

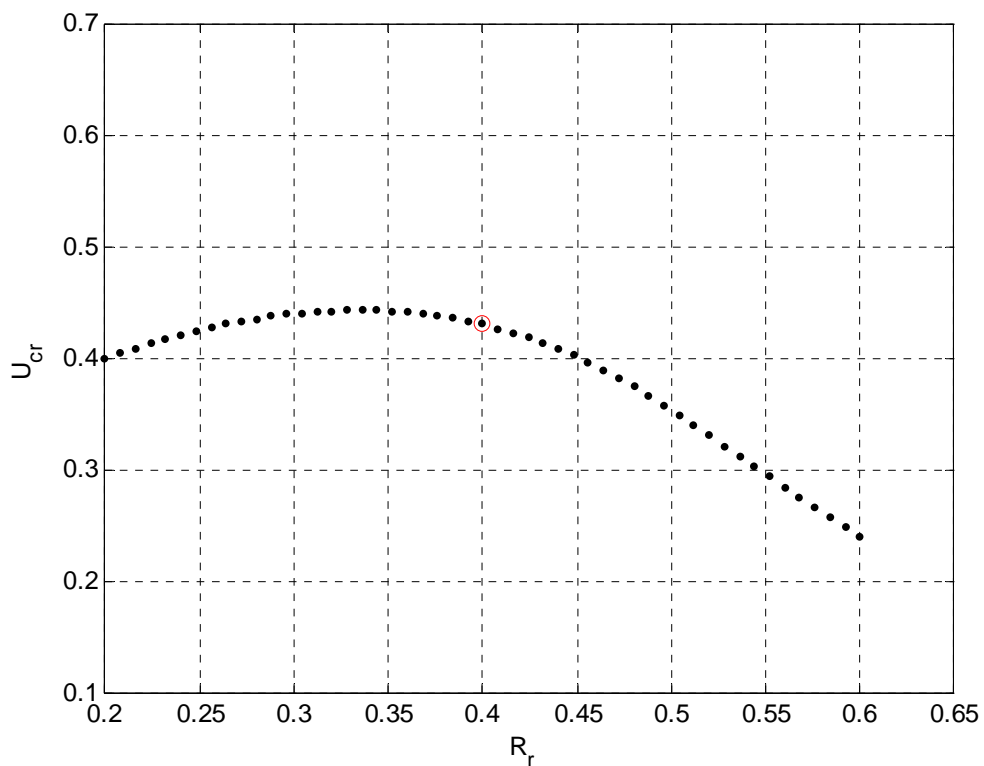


Figure 6-15 U_{cr} vs. R_r .

6.5 Summary

With respect to the theoretical model developed in the previous chapter, this chapter focused upon the analysis of the identified key parameters. At the beginning, the physical meaning of dimensionless parameters was discussed. It was followed by providing a method to calculate the required variables. Then, as an example this method was applied to a riser fairing used on SEDCO 702, off the coast of Brazil. Finally, based on this example, a parametric study was carried out to examine the role of each variable.

Hydrodynamic coefficients had a significant role in the stability of the system. The lift coefficient had an adverse effect while the moment coefficient, depending on its value, could have positive or negative influences.

As expected, damping either transverse or torsional enhanced the stability.

The behaviour of parameter A confirms the principle that an increase of the structural mass of a body in the flow enriches the stability. More interestingly, growth in radius of gyration, γ , resulted in higher critical velocity. This showed the benefit of mass distribution in stability. It can be concluded that adding mass to the tail of the fairing improves the stability. Thus, adding fins or bumps to the trailing edge, as reported in the literature, has another stabilising effect apart from improving the hydrodynamic coefficients.

Parameter S_r was an indicator of how two DOFs are coupled inertially. Its investigation made clear that as these modes become more independent, the stability is strengthened. In other words, this instability is made from a combination of the torsional and transverse modes with phase and amplitude that gain energy from the flow and when either mode acts alone, the system is stable. Blevins (2001) explained this through the natural frequency. What he showed was that at the onset of instability, there is a tendency for natural frequencies of both transverse and torsional modes to unite to form a single frequency-coupled mode that does not exist without flow. Based on present studies, one way to hinder the instability of the fairing is to reduce S_r and coupling by moving the mass centre towards the pivot point. This idea

is called “mass balancing” in aerodynamics. Additionally, this study showed that if S_r exceeds a limit, the system will be unstable at any small flow.

The trend of U_{cr} versus R_r was very important. R_r exposed two distinct behaviours. Depending on the range of variation, increase of R_r can boost or weaken the stability.

In summary, the parametric study confirms the significance of two parameters which were already neglected by Slocum et al (2004) in a simpler model. They include damping and the effect of body’s motion in AoA. In light of this study, it was uncovered that many elements are involved in determining the instability threshold. Among these, hydrodynamic coefficients possess a vital role. Hence, the next chapter will discuss these coefficients for a set of fairing sections.

Section Hydrodynamic Coefficients

This chapter centres on the computation of hydrodynamic coefficients of a two dimensional fairing section. In this chapter, the available methods for obtaining information about hydrodynamics of a thick foil will be assessed. Then, the appropriate method is chosen and accordingly the selected sections will be investigated. The impact of some important details like adding fins will be evaluated and finally, the results will be presented in way to render useful guidelines for the design of new fairing sections.

7.1 Introduction

The analytical model developed by the author showed that the threshold of instability to a large extent depends on the section hydrodynamic properties of the fairing. Thus, this chapter was planned to investigate the hydrodynamic characteristics of a few profiles which have been already used or are suggested to be utilised in industry. They include NACA0070, Shell's Short Fairing, Guide Vane and Exxon-Mobil's fairing with various size fins. In short, this study aims to:

- Identify the hydrodynamics coefficients of sections.
- Measure the suppression capability of each profile.
- Clarify the effect of adding fins to the trailing edge of a fairing.

At the beginning, the fairing profiles are shown in scale. A short discussion probes the controversial aspects of this study such as mesh convergence. Then the summary

results are illustrated which explain the discrepancies between behaviour of sections and assist the designer with comparing the characteristics of different sections. In Appendix A, the reader can find the detailed results of each individual section. The offset tables of all profiles are also given in Appendix A for further research.

7.2 Thick Foil and Available Methods

Riser fairings look like a foil and therefore hydrodynamic characteristics of a typical fairing profile may initially be assumed to be like those of foils. Foils have been investigated extensively in aerodynamics and hydrodynamics. A number of theoretical methods have been established to predict the dynamics of foils. As explained earlier in Chapter 4, these theories are on the basis of inviscid flow which is not applicable in dynamics of fairing in seawater. Moreover, they assume foils to be thin, quite different from fairings with the thickness to chord ratio of several times larger. High thickness is a great challenge for analytical methods and due to rare usage of a thick foil and by the advent of numerical methods; no other purely theoretical approach was developed for the analysis of these foils in a viscous fluid. In consequence, the available theories are not an appropriate tool for assessing the hydrodynamic behaviour of the fairing.

Beside the development of theoretical models, huge amount of experimental works has been carried out on various foil sections in different conditions. The purpose of these studies was mainly related to application of foils in aviation. Accordingly, the majority of selected profiles were asymmetric and among the minority which had symmetric section, the thickness was occasionally high. For example, Bullivant, Eastman et al, and Raghunathan et al reported the test data for three thick foils of NACA0021, NACA0025 and NACA0035 with thickness to chord ratio of 0.21, 0.25 and 0.35 respectively (Bullivant, 1941, Eastman, 1932, Eastman et al., 1933, Raghunathan et al., 1988). These comprised the data of the thickest foils at the disposal of author. Nevertheless, the thickness to chord ratio of 35 percent was still below the minimum value for a fairing. In addition, a fairing may benefit from some subtle details like fins which these studies had not considered. Thus, there is not

sufficient data to make a rational judgment about the hydrodynamic behaviour of a fairing.

For these reasons, there is no other choice than doing some specific studies on a fairing's section. In order to analyse a new profile, there exists two methods; physical modelling in the lab and computational modelling. The purpose of this portion of research is to assess a few sections and identify the generic behaviour of a fairing. While complex physical modelling may give more accurate results, this research, as mentioned above, only requires a generic outlook of the behaviour of a fairing and therefore it was decided that a computational method would match the objectives of this research the best.

It should be noted that numerical solutions, e.g. CFD (computational fluid dynamics), are not absolutely exact and accurate solutions and have their own limitations and dependencies. Like physical modelling, CFD modelling has delicate features too, e.g. selection of parameters and discretization of domain, and therefore needs to be deployed with extreme care. The result depends on many parameters including Reynolds number. Despite these restrictions, due to the lack of test data, CFD analysis is a good tool to distinguish the behavioural differences of these profiles. In other words, if this CFD study cannot give the exact value of required parameters for a real case at least it will bring to light their trend. This study has benefited from the FLUENT software package (Version 6.2).

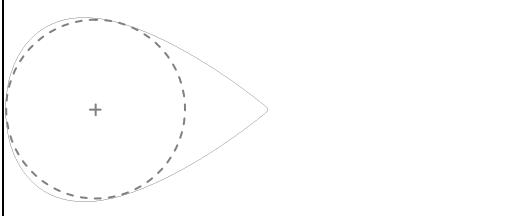
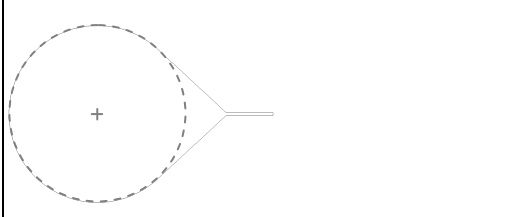
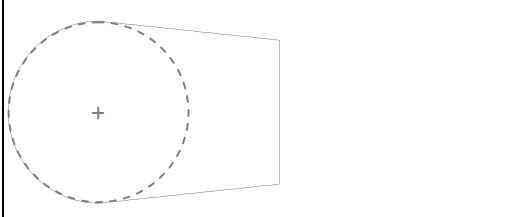
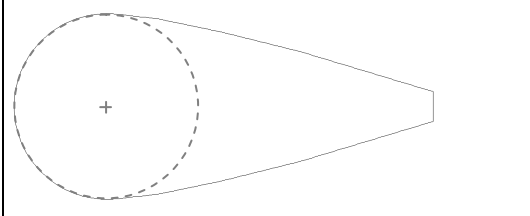
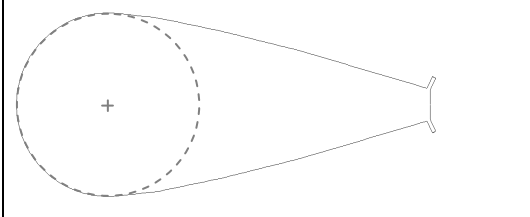
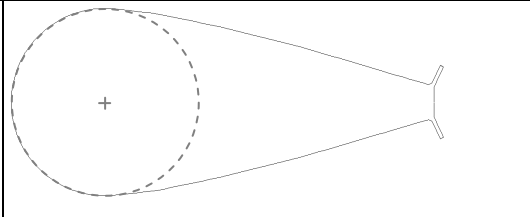
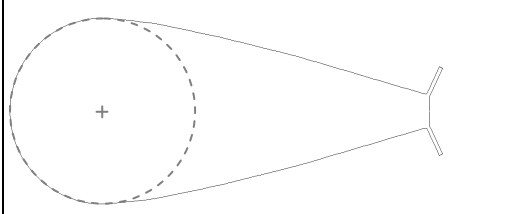
7.3 Fairing Profiles

Four sections were selected for CFD analysis. The first profile is NACA0070, a simple symmetric airfoil from aviation with adequate thickness to chord ratio of 70 percent to accommodate a riser. The second profile is called the "Short Fairing". It involves a new concept which was introduced by Shell Global Solution (Allen and Henning, 1995b). The next profile is a guide vane with a blunt end. This closed section has been reported to have good streamlining capacity (Rogers, 1983). The last profile is the section ExxonMobil used in the tank test (Slocum et al., 2004). To investigate the influences of adding fins to the trailing edge of the fairing, the latter section will be assessed for four sizes of fins, i.e. without fin section and sections

with fin length of 3, 5 and 7 percent of chord length. These seven profiles are shown in Table 7-1. This table also gives the thickness to chord ratio of each section. The location of the centre of rotation (CR) on the chord line is also presented in the form of a fraction of the chord length. It is measured from the leading edge. The offset tables of all used profiles are also given in Appendix A for further research.

Each of these profiles will be assessed at four angles of attack (AoA), 0° , 5° , 10° and 15° .

Table 7-1 Selected Fairing Profiles for CFD Analysis.

	Shape	c/t	t/c (%)	CR (%c)
NACA0070		1.43	70	35.03
Short Fairing		1.49	67	33.50
Guide Vane		1.49	67	33.50
Exxon's Fairing 0%		2.27	44.1	22.05
Exxon's Fairing 3%		2.27	44.1	22.05
Exxon's Fairing 5%		2.27	44.1	22.05
Exxon's Fairing 7%		2.27	44.1	22.05

7.4 Definitions

Prior to establishing the computational model in FLUENT software package, it is necessary to define the coordinate system and some variables which will be used later.

Coordinate System

The coordinate system is defined as shown in Figure 7-1. For all sections in this study, the origin is at the nose of section or in other words, at the front point on the chord line. The reference point of the moment is the centre of rotation (CR), located at the centre of embedded circle (riser) and measured from the front point in percentage of the chord length. Similar to the previous convention in Chapter 5, the angle of attack (AoA) and moment are both positive in the clock-wise direction. Lift is positive upwards. Drag is positive in the flow direction, i.e. positive in the x-axis direction.

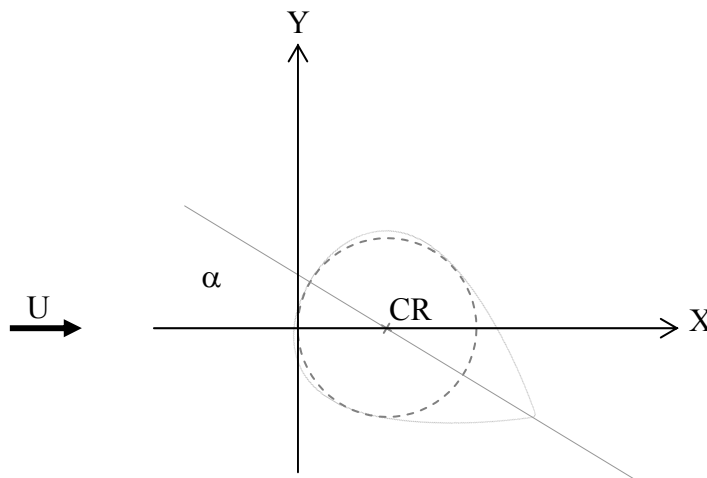


Figure 7-1 Coordinate System in CFD Analysis.

Non-dimensional Coefficients

In this chapter, the free stream velocity U and its associated pressure p_o , as well as the thickness and chord length of the foil, t and c respectively, are used for most non-

dimensional results. More specifically, the mean drag, lift and moment coefficients are defined as follows.

$$C_d = \frac{\text{Mean_ Drag}}{\frac{1}{2}\rho U^2 c}$$

$$C_L = \frac{\text{Mean_ Lift}}{\frac{1}{2}\rho U^2 c}$$

$$C_M = \frac{\text{Mean_ Moment}}{\frac{1}{2}\rho U^2 c^2}$$

where ρ is the fluid density.

The foil may be also subject to unsteady hydrodynamic forces. These unsteady components are periodic and they are measured by the force fluctuation amplitude from its mean level, i.e.

$$\text{Amp}(C_d) = \frac{\text{Drag_ Amplitude}}{\frac{1}{2}\rho U^2 c}$$

$$\text{Amp}(C_L) = \frac{\text{Lift_ Amplitude}}{\frac{1}{2}\rho U^2 c}$$

$$\text{Amp}(C_M) = \frac{\text{Moment_ Amplitude}}{\frac{1}{2}\rho U^2 c^2}$$

The mean pressure p , i.e. dynamic pressure averaged over the time, along the upper and lower surfaces of the foil is also given. The pressure coefficient is defined as,

$$C_p = \frac{p - p_0}{\frac{1}{2}\rho U^2}$$

According to Equation (3-5), Strouhal number is defined as,

$$S = \frac{f_s \cdot t}{U}$$

where f_s is the force fluctuation frequency in Hertz.

Reynolds number is defined here based on the chord length as

$$Re_c = \frac{U \cdot c}{\nu}$$

where ν is kinematic fluid viscosity.

Wall Y-plus Y^+ is a variable used in discretizing domain near the walls and is defined as,

$$Y^+ = \frac{\rho u_\tau y_p}{\mu_{\text{Fluid}}}$$

where u_τ is the friction velocity, y_p is the distance from point P to the wall, and μ_{Fluid} is the fluid viscosity at point P.

7.5 Discretization, Mesh Convergence and Reynolds Number

Prior to investigation about the impact of the fairing's section on its behaviour, it is necessary to address couple of issues that influence the accuracy and validity of results. They include discretization and mesh generation plus Reynolds number.

Discretization

The size of the domain is the first parameter to be determined. In this study it is a rectangle of $25c$ long and $10c$ wide where c is the chord length. The head of the fairing is located $5c$ back from the front edge of domain (Figure 7-2). A structured grid was used to generate the mesh inside the domain. According to the guideline of FLUENT package, the first cell next to the fairing's wall should be small enough to be located inside boundary layer and the parameter Y-plus be less than unit. An interface boundary (Figure 7-3) was also employed at a distance far enough from the fairing. In this study it consists of a circle of $2.5c$ diameter of which the centre is located at mid-chord of the fairing. This technique facilitated the rotation of the fairing with no need to re-generation of mesh.

The chord length of the fairing was set to 1 m. The number of elements for each model was in the range of 105000 to 150000 quadrilateral cells. The period of vortex

shedding behind a circular cylinder of the same diameter was calculated and time step was selected as a fraction of 1/20 to 1/50 of this period. The total run time was about 40 times this period. This run time was sufficient during the run to reach to stable situation.

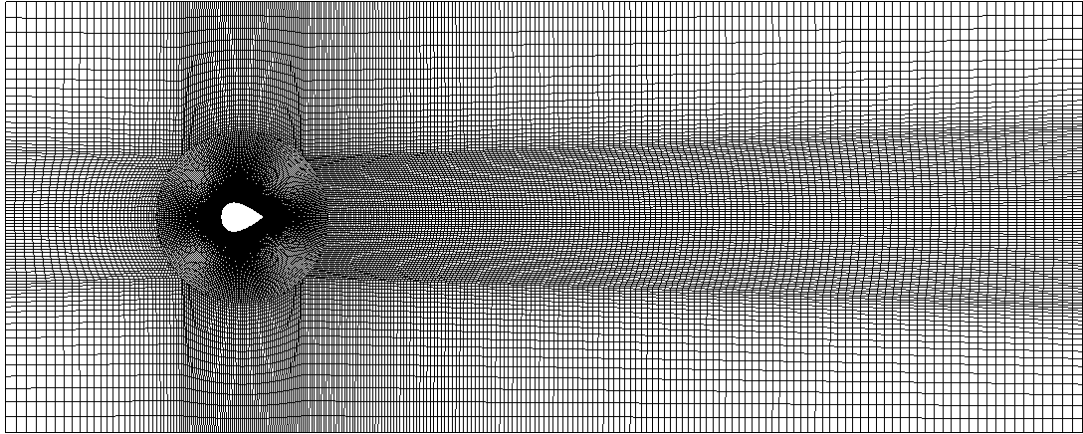


Figure 7-2 Computational Domain and Mesh, NACA0070.

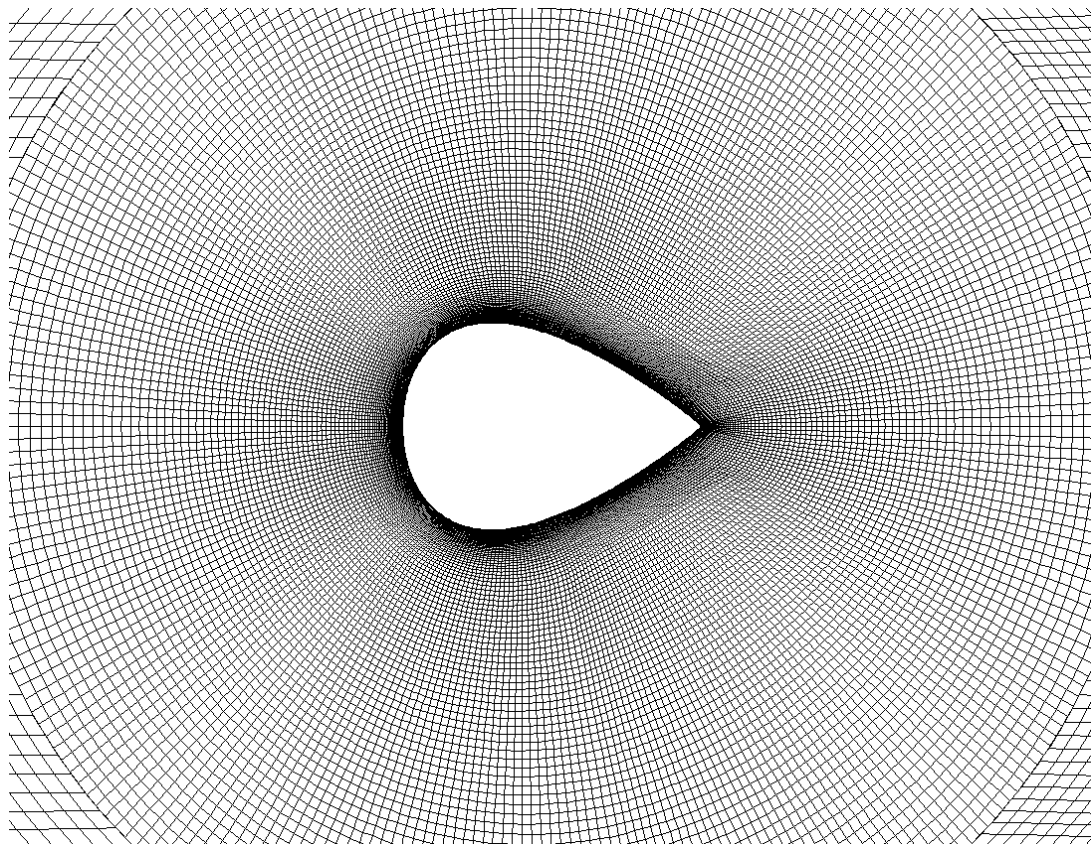


Figure 7-3 Mesh Close to The Fairing, NACA0070.

Mesh Convergence

Generally, numerical solutions including CFD are approximate methods to approach to the exact solution when it is not achievable analytically. Therefore, all numerical solutions have an error to some extent and this inaccuracy is dependent on many parameters including mesh or discretization of geometry in terms of its pattern and number of cells. In theory, accuracy of numerical analysis of a simple problem is proportional to the density of mesh and by increasing the number of cells for a specific case, the solution will converge toward the exact analytical solution.

However, this is not so straightforward for complicated problems. In this case, this is the task of the researcher to validate the results and identify what mesh density is suitable for a given problem. Moreover, the researcher should decide about the mesh pattern and layout in terms of the type of element and relative local density of mesh. The researcher then specifies which part of grid needs finer mesh and by how much.

In the present study dealing with turbulent flow, there is another parameter to be considered. In turbulent flow, in addition to what mentioned above, the first cell next to the wall should be small enough to be located in narrow boundary layer. It is measured in CFD analysis by a variable called Y^+ which should be less than one to fulfil this condition. To keep Y^+ under one, it requires fine mesh in vicinity of object or more generally walls. This question may arise again as to how much fineness is necessary to achieve an accurate result. Consequently, the mesh fineness and associated value of Y^+ is another significant issue in mesh convergence.

To assess the effect of these parameters on the present study, a few analyses were carried out on NACA0070 with different meshes at a fixed Reynolds number. The results are shown in Table 7-2. These results are corresponding to NACA0070 profile at incident angle of 15° using the realisable $k-\epsilon$ turbulence model in FLUENT package.

All meshes are in conformity with the pattern illustrated in Figure 7-2 and Figure 7-3. Meshes 1, 4 and 5 comprise of 103k cells and the only difference is in the distribution of cell density in imaginary circle surrounding the object. Mesh 2 with

7. Section Hydrodynamic Coefficients

202k cells is now as twice as fine than mesh 1 and, by contrast, mesh 3 with 66k is now as twice as coarse. Test 1 is identical to the data presented in Appendix A. Tests 2 to 5 are for the same conditions as test 1 except the mesh. In particular, in tests 4 and 5, the cells in vicinity of object have been shifted inward in order to reduce Y^+ .

Table 7-2 Effect of Mesh Convergence on Hydrodynamic Coefficients of NACA0070 at 15°.

Test	Re_c	Mesh	Cells	Y^+	C_d	Amp(C_d)	C_L	Amp(C_L)	C_M	Amp(C_M)
1	5×10^4	1	103k	0.860	0.510	0.008	-0.492	0.103	0.023	0.014
2	5×10^4	2	202k	0.868	0.499	0.006	-0.505	0.100	0.023	0.014
3	5×10^4	3	66k	0.859	0.520	0.008	-0.470	0.110	0.022	0.014
4	5×10^4	4	103k	0.200	0.458	0.008	-0.593	0.098	0.023	0.013
5	5×10^4	5	103k	0.038	0.425	0.009	-0.662	0.093	0.024	0.012

With regard to the effect of mesh convergence, it can be easily deduced from the comparison of first three tests that the increase in population of cells along with keeping key parameter Y^+ fixed, will reduce the drag coefficient by two percent and will raise the absolute value of lift coefficient by the same percentage. The moment coefficient plus the amplitudes of hydrodynamic coefficients are relatively insensitive to mesh population.

Comparison of Tests 1, 4 and 5 reveals the influence of cell density in vicinity of object on drag, lift and moment coefficients and their associated amplitudes. In this specific case, moment coefficient plus the amplitudes of all hydrodynamic coefficients are relatively constant against the reduction of Y^+ , however, the decline in Y^+ from 0.86 to 0.20 results in to 10% decrease of drag coefficient and 20% increase of lift coefficient. Therefore, hydrodynamic coefficients are sensitive to the size of cell next to the wall and cell density in this area. It is noticeable that for a specific case, say a given profile and Re_c , the value of Y^+ does not change dramatically for different incidences and it is quite constant during the run for each incidence. Table 7-3 conveys the magnitude of Y^+ at different incidences for Test 1.

Table 7-3 Variation of Y^+ Due to Different Incidences, NACA0070.

AoA	0°	5°	10°	15°
Y^+	0.826	0.830	0.844	0.860

Effect of Reynolds Number

The next important issue to be specified is Reynolds number (Re). It is clear that as Re changes, so do the hydrodynamic coefficients; it also influences the CFD model. As the current velocity increases and the flow falls into the critical or supercritical group, CFD modelling needs very sensitive caution. Thus, for the main part of this study which seeks the behaviour of hydrodynamic parameters, Re_c was selected to be in subcritical domain; almost about 5×10^4 (see Appendix A for each case). In addition, the general effect of Reynolds number has been probed in the following.

The point here is about the effects of the Reynolds number on the fairing hydrodynamic coefficients. It has been observed that the Reynolds number has a considerable influence on hydrodynamic coefficients. For instance, a Reynolds number increase in subcritical flow leads to drag coefficient decrease but in CFD analysis, it should be clarified to what extent this issue is tackled.

To this end, a few runs for different Reynolds number were carried out on the profile of NACA0070 at the incidence of 15 degree, using the realisable k- ϵ turbulence model in FLUENT package. About 126k cells were utilised to discretize the domain and the mesh pattern was the same as what was illustrated in Figure 7-2 and Figure 7-3. The only difference was the distance of the first cell from the wall due to shifting the cells in the vicinity of object toward the walls to keep the parameter of Y^+ almost constant and around 0.5 and to eliminate its influences. The results are shown in Table 7-4 and Figure 7-4 to Figure 7-6. The results are consistent with a set of experimental data (Hoerner, 1992).

It is deduced from Figure 7-4 that by increasing Reynolds number, hydrodynamic coefficients vary relatively sharply up to Re_c of 6×10^5 and then, the rate of response

to variation of Re_c drops down. As it is expected from experimental test data, this figure indicates that regardless of the sign, absolute value of the drag coefficient reduces by moving toward a higher Re_c while the absolute value of lift and moment coefficients rises. This variation in hydrodynamic coefficients can reach up to two times for a jump in the Reynolds number from 5×10^4 to 1.6×10^6 .

Figure 7-5 along with the Table 7-4 indicates that for this range of variation in the Reynolds number, the amplitude of the drag coefficient which is a symbol of in-flow vibration can triple whereas the amplitude of the lift coefficient decreases by 11% at Re_c of 6×10^5 and then increases again. The amplitude of the moment coefficient changes by about 15%. The remarkable point here is that for all values of Reynolds number, the cross-flow vibration is dominant (Figure 7-6).

Table 7-4 Effects of Reynolds Number on Hydrodynamic Coefficients of NACA0070 at 15°.

Test	Re_c	Y^+	C_d	Amp(C_d)	C_L	Amp(C_L)	C_m	Amp(C_m)
1	5×10^4	0.492	0.475	0.005	-0.550	0.091	0.024	0.013
2	1×10^5	0.490	0.427	0.006	-0.673	0.087	0.025	0.013
3	2×10^5	0.566	0.383	0.007	-0.800	0.081	0.029	0.012
4	4×10^5	0.521	0.339	0.011	-0.940	0.081	0.038	0.012
5	6×10^5	0.483	0.316	0.013	-1.002	0.080	0.045	0.011
6	8×10^5	0.480	0.307	0.013	-1.034	0.085	0.049	0.011
7	1×10^6	0.465	0.295	0.014	-1.053	0.086	0.051	0.011
8	1.2×10^6	0.481	0.289	0.015	-1.062	0.084	0.053	0.011
9	1.4×10^6	0.474	0.284	0.015	-1.073	0.086	0.055	0.011
10	1.6×10^6	0.441	0.279	0.015	-1.077	0.087	0.058	0.011

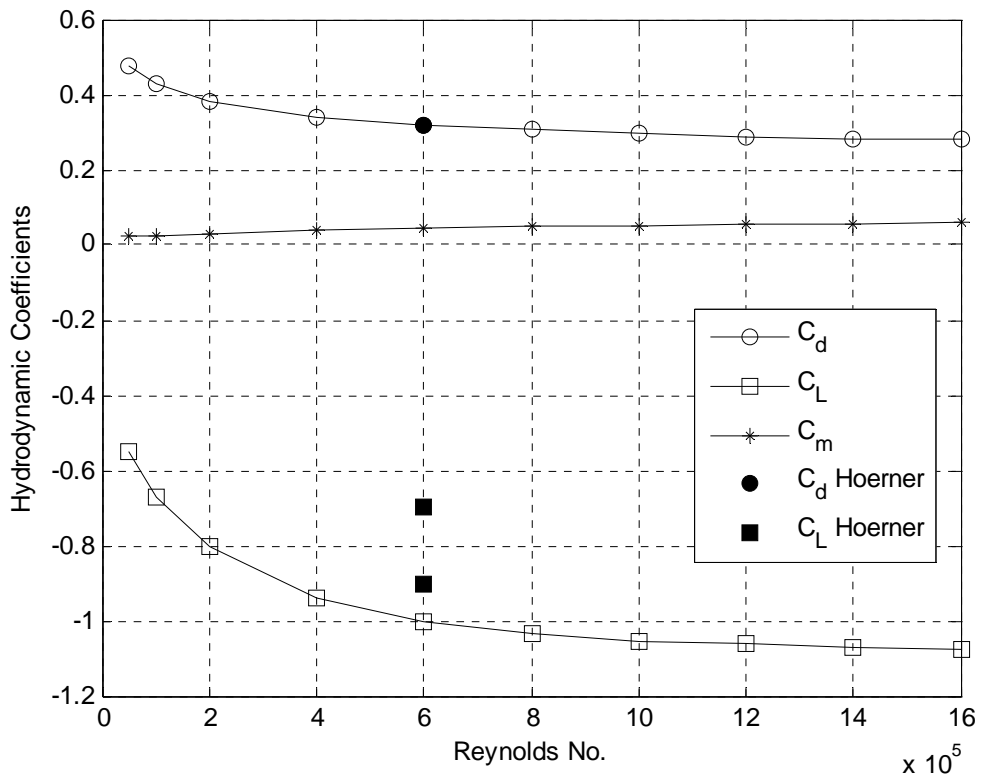


Figure 7-4 Hydrodynamic Coefficients vs. Re_c , NACA0070 at 15° .

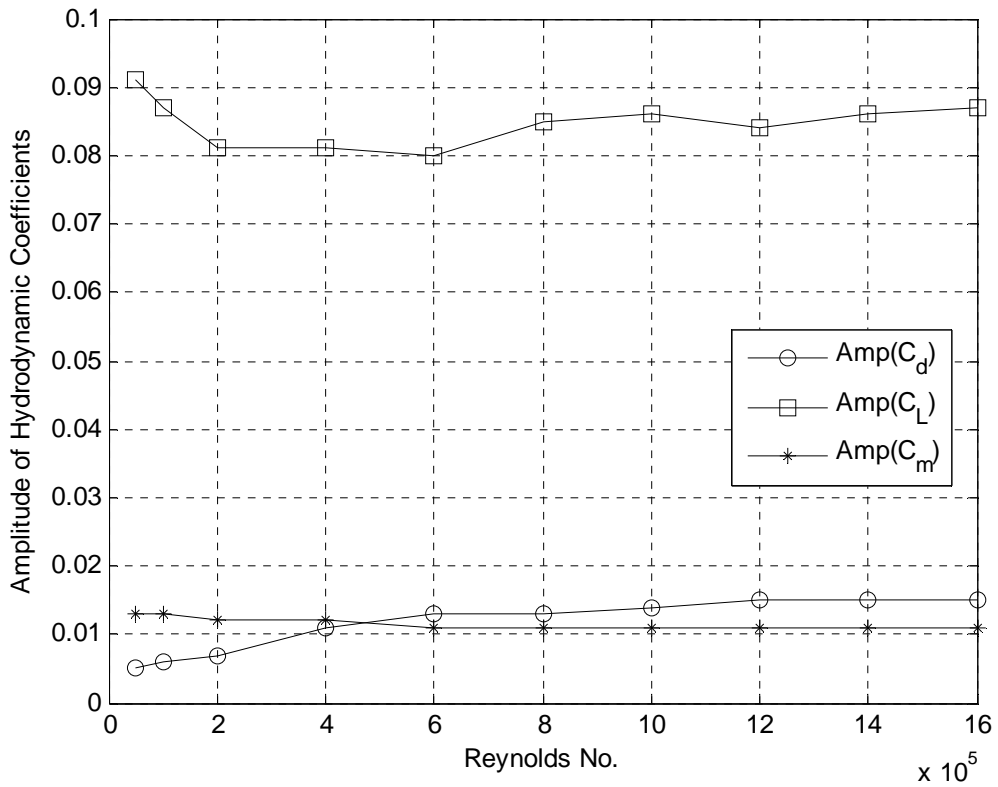


Figure 7-5 Amplitude of Hydrodynamic Coefficients vs. Re_c , NACA0070 at 15° .

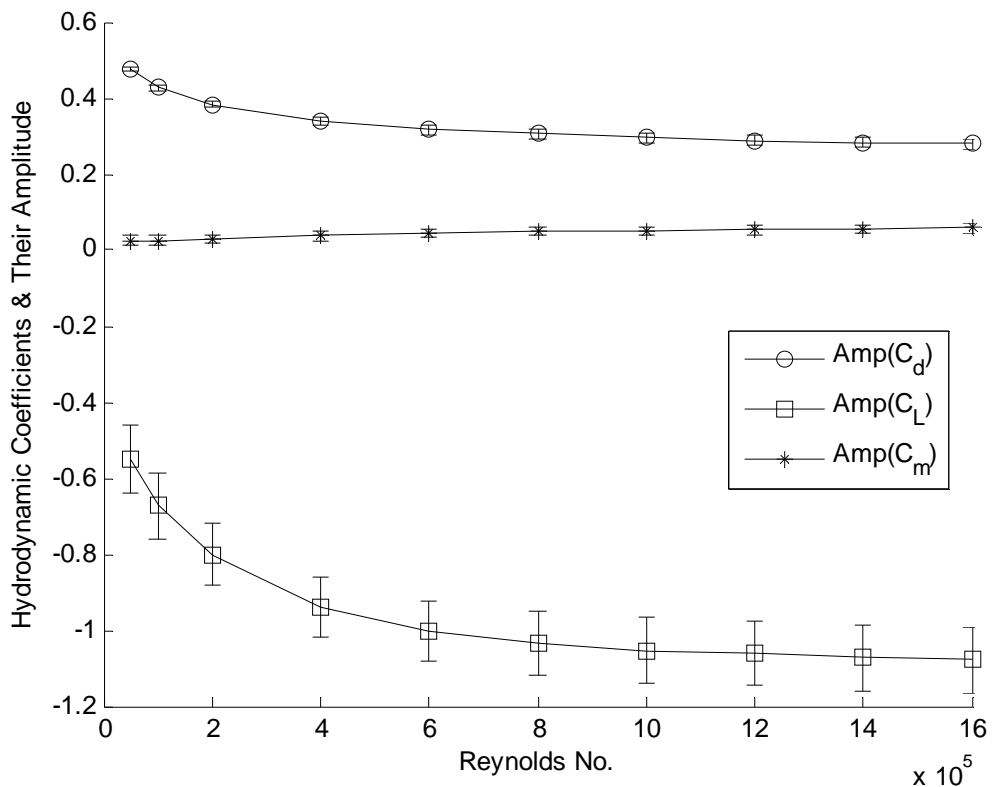


Figure 7-6 Hydrodynamic Coefficients & Their Amplitudes vs. Re_c , NACA0070 at 15° .

7.6 Summary Results

In order to make sure the software is used correctly, the outcome of CFD analysis for NACA0070 was verified against test data (see Figure 7-4). Then, each section was assessed at four AoA. For each case, the time history of drag, lift and moment coefficients was obtained. Figure 7-7 shows a sample result for the lift coefficient of NACA0070 at zero AoA. After the full development of flow when the results reached a stable status, the mean and fluctuating components of hydrodynamic coefficients were extracted from such figure. The summary of these results are presented in the following. Full details of results are available in Appendix A.

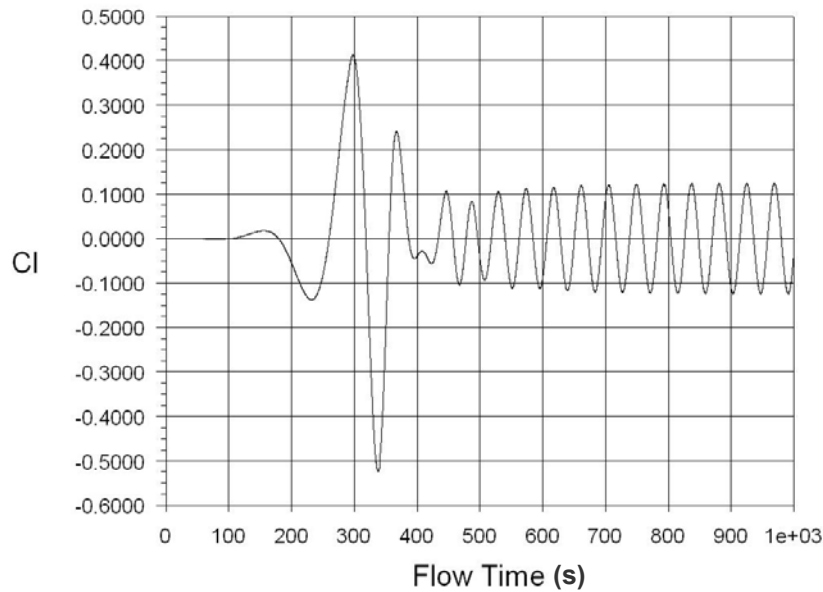


Figure 7-7 Sample Result, Time History of Lift Coefficient, NACA0070 at 0°.

Drag Coefficient

Figure 7-8 to Figure 7-10 show the drag coefficient and its amplitude. Figure 7-8 indicates that C_d of the vane increases with AoA while it reduces for NACA0070. It is almost constant for the Short Fairing.

In Figure 7-9, the amplitude of drag oscillation is negligible when the sections are in line with the current. But as AoA increases, so does the drag oscillation. Nevertheless, Figure 7-10 states that the amplitude of the drag coefficient relative to its mean value is almost minute.

According to Figure 7-8 and Figure 7-9, by increasing the fin length, the mean drag coefficient declines slightly at the zero incidence angle while the drag coefficient amplitude is relatively constant and therefore, in this case, the fins are of benefit to drag at normal position (0° AoA). At a higher incidence angle, the longer fin raises both mean drag and its oscillatory component. For example, the 5% fin increases mean drag around 30% from 0.209 to 0.273 at angle of 5°. The remarkable point is that for sections without the fin and 3% fin, C_d slightly declines at the beginning (from 0° to 5°) and then rises again.

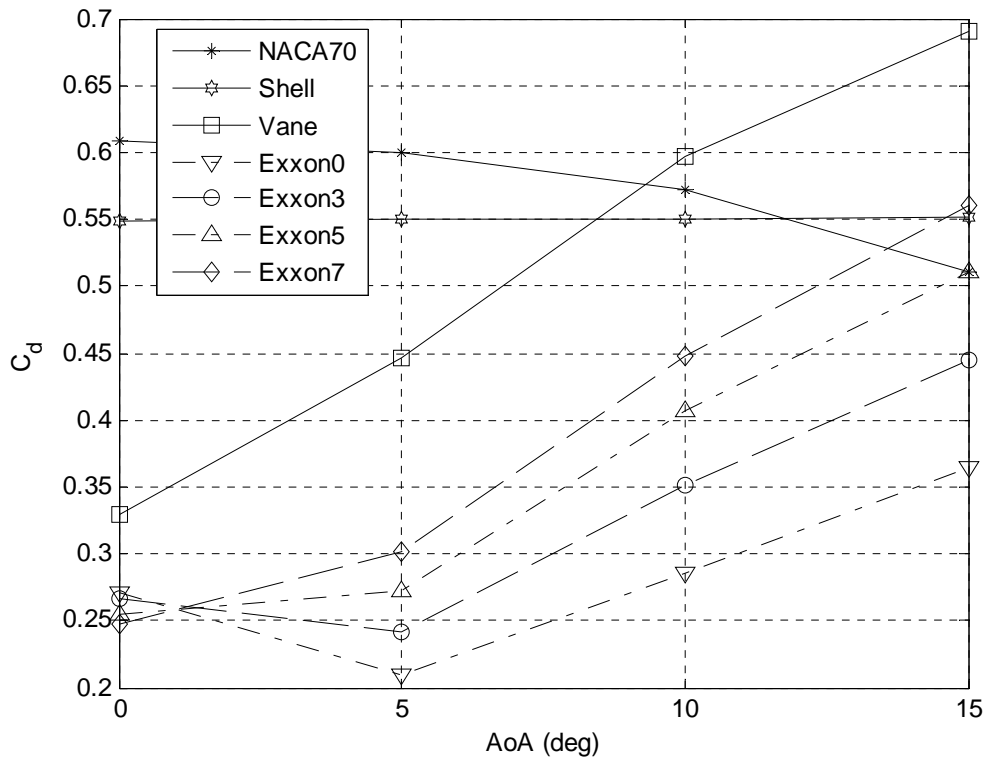


Figure 7-8 Drag Coefficients of Different Sections.

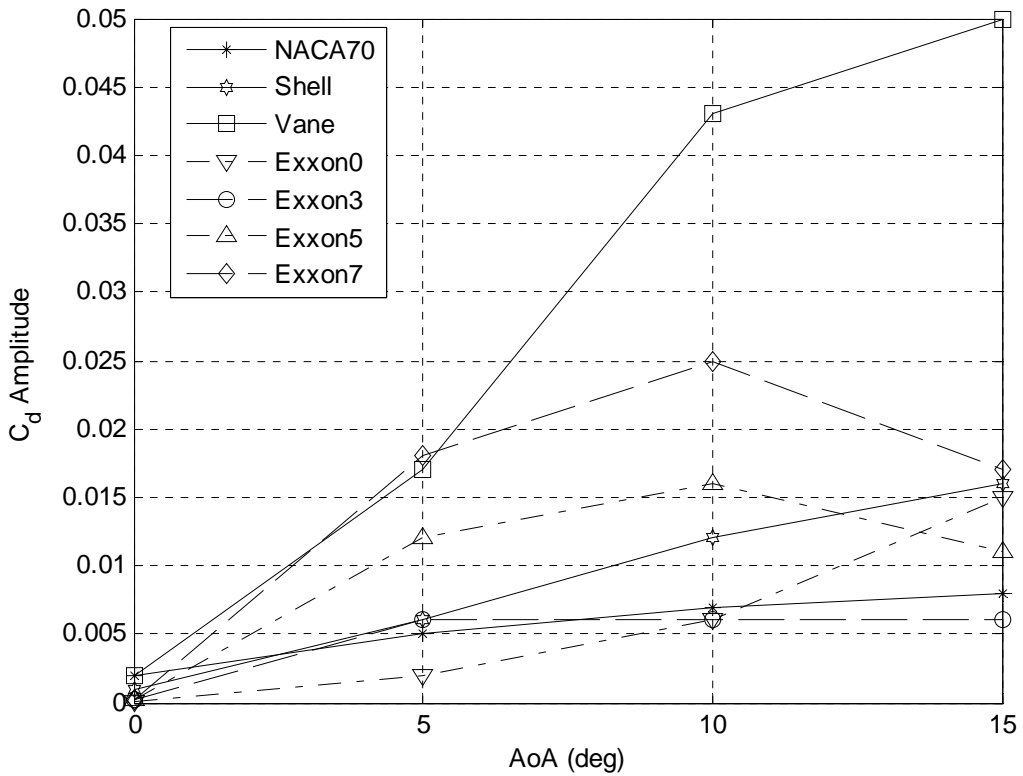


Figure 7-9 Drag Coefficient Amplitudes of Different Sections.

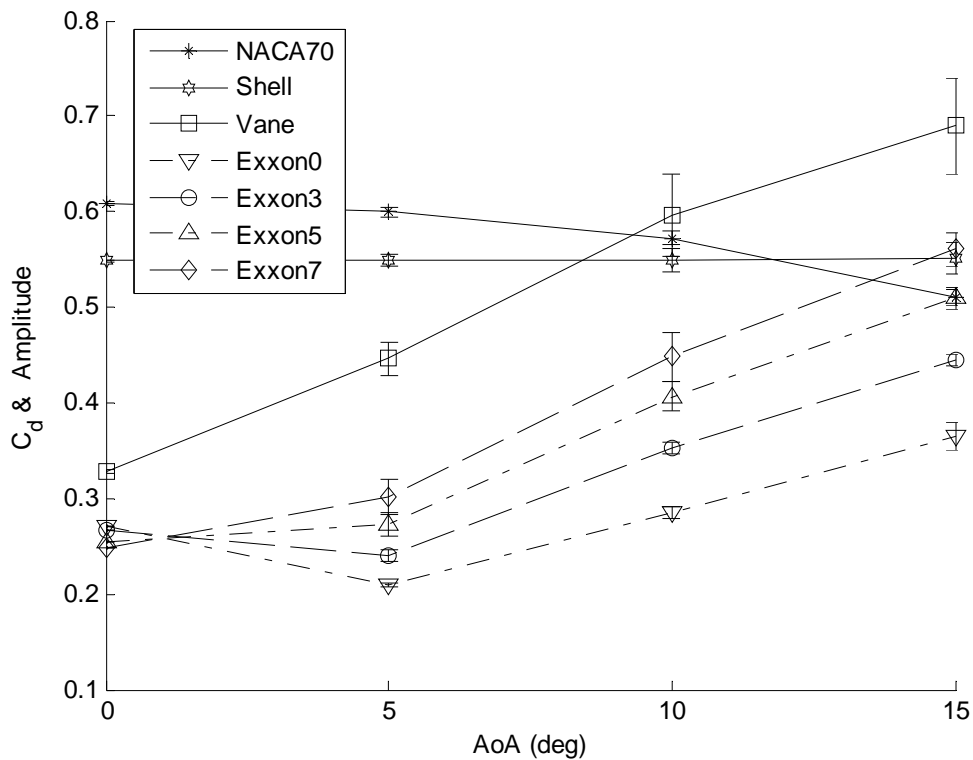


Figure 7-10 Drag Coefficients & Their Amplitudes of Different Sections.

Lift Coefficient

The mean lift coefficient is shown in Figure 7-11. As expected for the fairing section, which is a symmetric profile around chord, the mean lift coefficient is zero when the fairing is aligned to the current, i.e. zero AoA. What really matters here however is the lift coefficient slope which plays a significant role in stability of the fairing. It is observed in this figure that the slope of the lift coefficient at zero AoA is negative for five sections except the guide vane and Exxon's fairing with long fins. Experiments had already confirmed the negative lift coefficient up to 20 degrees for NACA0070 (Hoerner, 1992). It was attributed to the separation of the flow at the leeside (Ericsson and Reding, 1980). To some extent, the Short Fairing with a high angle of leeside demonstrates similar behaviour. By contrast in the guide vane, a low angle of leeside, minimises flow separation and tries to keep it attached to the surface. Hence, experiment confirms that C_L of this section grows with the AoA (Grimminger, 1945).

The amplitude of the lift oscillation is plotted in Figure 7-12. These curves are a good scale to measure the severity of shed vortices and associated cross flow (CF) forces. At zero AoA, the NACA0070 and Short Fairing experience the highest CF forces. The guide vane is in the third place. Large C_L amplitude of some sections means they still experience vortex shedding and may have the chance of undergoing VIV. In case of instability, CF forces can trigger extensive vibrations. Contrary to drag, oscillatory component of lift coefficient is noticeable in comparison with mean value (Figure 7-13).

With regard to the effect of adding fins, Figure 7-11 illustrates how using longer fins shifts $(\partial C_L / \partial \alpha)_0$ from negative values to positive ones. Thus, adding fins helps the stability of the fairing. On the other hand, Figure 7-12 indicates that at the normal position (0° AoA), the lift coefficient amplitude which is a sign of CF forces is reduced by fitting and prolonging fins. So, fins improve the VIV suppression capability of the fairing. The key point here is that by lengthening the fins, the improvement rate of suppression capability falls down. It means the 2% jump in fins' length from 3% to 5% has a larger impact than the 2% jump from 5% to 7% in fins length. All in all, this study shows fins improve both stability and VIV suppression capability of the fairing profiles.

This is consistent with experimental tests which were carried out by Grant and Patterson. Their observations proved that the medium sized fins stabilised the fairing at zero AoA without increasing drag. The small fins did not stabilise the fairing, and the large fins added to the drag while increasing the stability over that for the medium fins (Grant and Patterson, 1977).

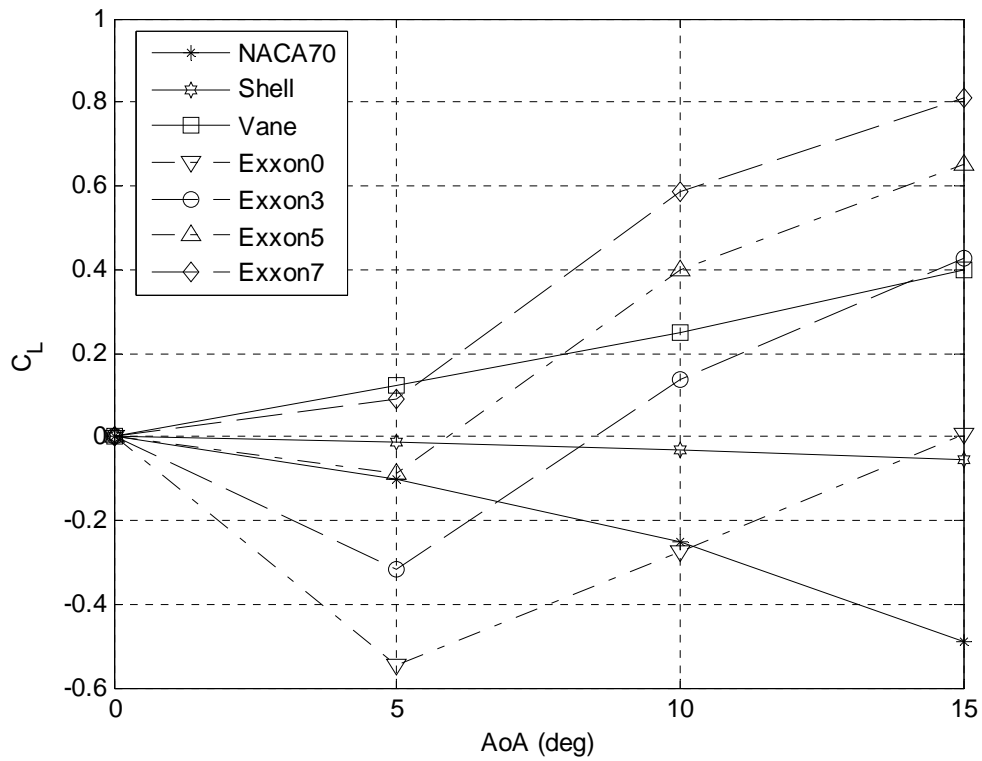


Figure 7-11 Lift Coefficients of Different Sections.

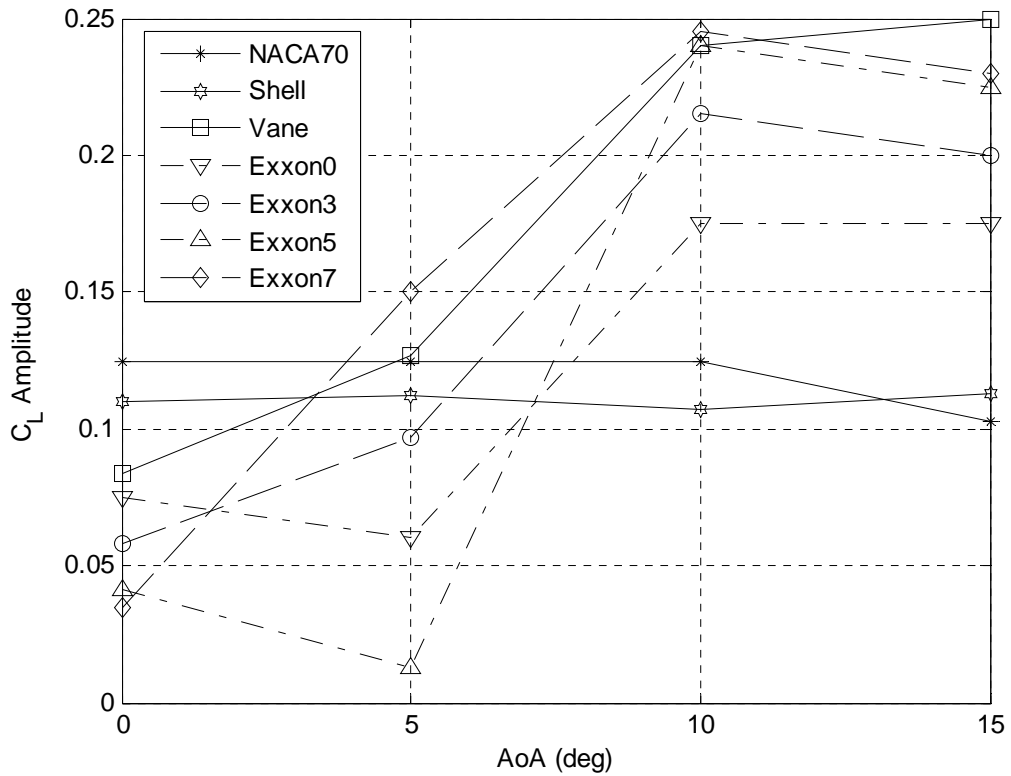


Figure 7-12 Lift Coefficient Amplitudes of Different Sections.

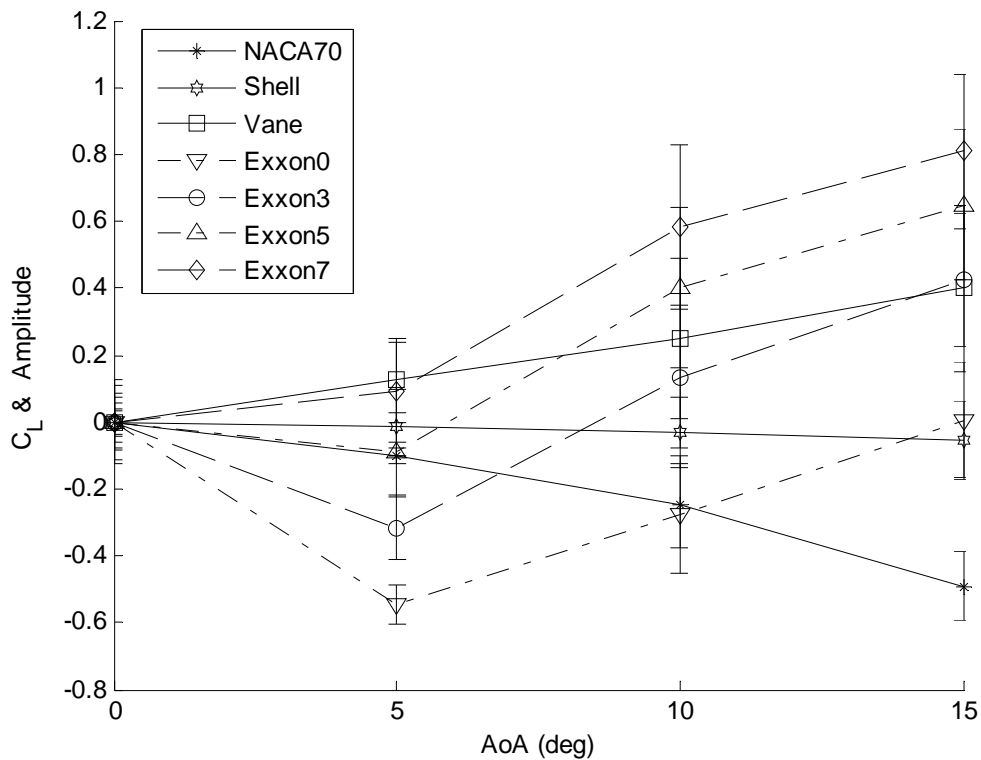


Figure 7-13 Lift Coefficients & Their Amplitudes of Different Sections.

Moment Coefficient

The moment coefficient measured at the centre of rotation is illustrated in Figure 7-14. Again for symmetric profiles of the fairing, the mean value of this coefficient is zero when the fairing is in line with the flow. This figure states that at this Reynolds number, one of the necessary conditions for stability, i.e. $(\partial C_{M(CR)} / \partial \alpha)_0 < 0$, is satisfied for the guide vane and Exxon's fairing with the two longest fins. It should be noted that this parameter was also identified as a sign for misalignment and propensity to potential fishtailing (see Section 5.9). For example for Exxon's fairing with the fin length of $0.03c$, comparison of this curve with Figure 5-8 reveals that the equilibrium position for this profile is at an angle about 6 degrees rather than normal zero AoA. Similar to lift coefficient figure, NACA0070 and Short Fairing has an analogous trend at a different level. This is the case in Figure 7-15 too. This figure presents the amplitude of oscillations for moment coefficient. At zero AoA, the Exxon7 has the best performance in the sense it produces minimum amplitude for

rotational moment. The NACA0070 and Short Fairing are in the next place. According to Figure 7-16, most profiles generate small moment amplitude at zero AoA.

The small amplitude of the moment oscillation may be because of two separate reasons. The first reason is that the given profile streamlines flow well and therefore sheds weak vortices or no vortices at all. This results in a small amplitude for both lift and moment forces. The second reason is that in the given profile, the pivot point is located near the centre of pressure and consequently, hydrodynamic forces have a small arm for an overturning force and therefore produce a small moment about this pivot point. By considering the large lift amplitude and small mean moment of these sections, NACA0070 and Short Fairing, the small moment amplitude seems to be due to the latter reason.

With regard to the impact of adding fins, it is observed in Figure 7-14 that fins changes the moment coefficient slope from positive to negative and satisfies the second necessary condition of stability. Moreover, negative moment coefficient slope makes the fairing align itself correctly. Thus, fins eliminate the misalignment and the status of dual equilibrium position which may be a latent cause for fishtailing. On the other hand, fishtailing can be excited by the oscillatory component of the moment force. Figure 7-15 shows that adding fin reduces the moment coefficient amplitude and accordingly mitigates the fishtailing problem. It should be mentioned again that by lengthening the fins, the improvement rate of fishtailing falls down, similar to improvement rate of cross flow vibrations.

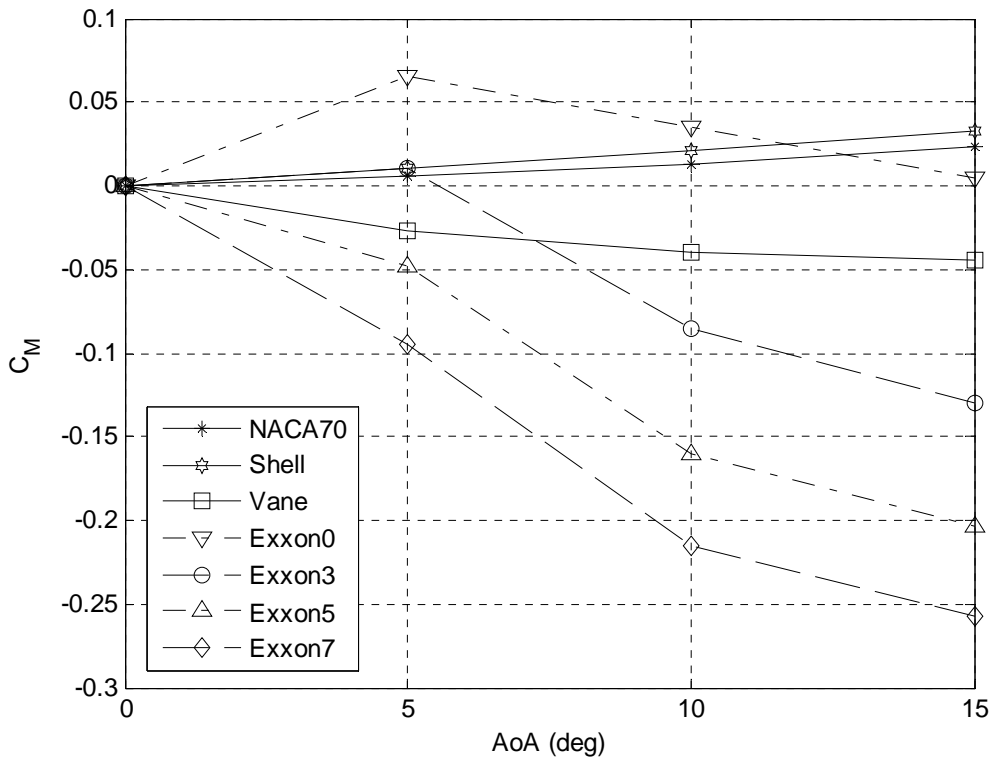


Figure 7-14 Moment Coefficients of Different Sections.

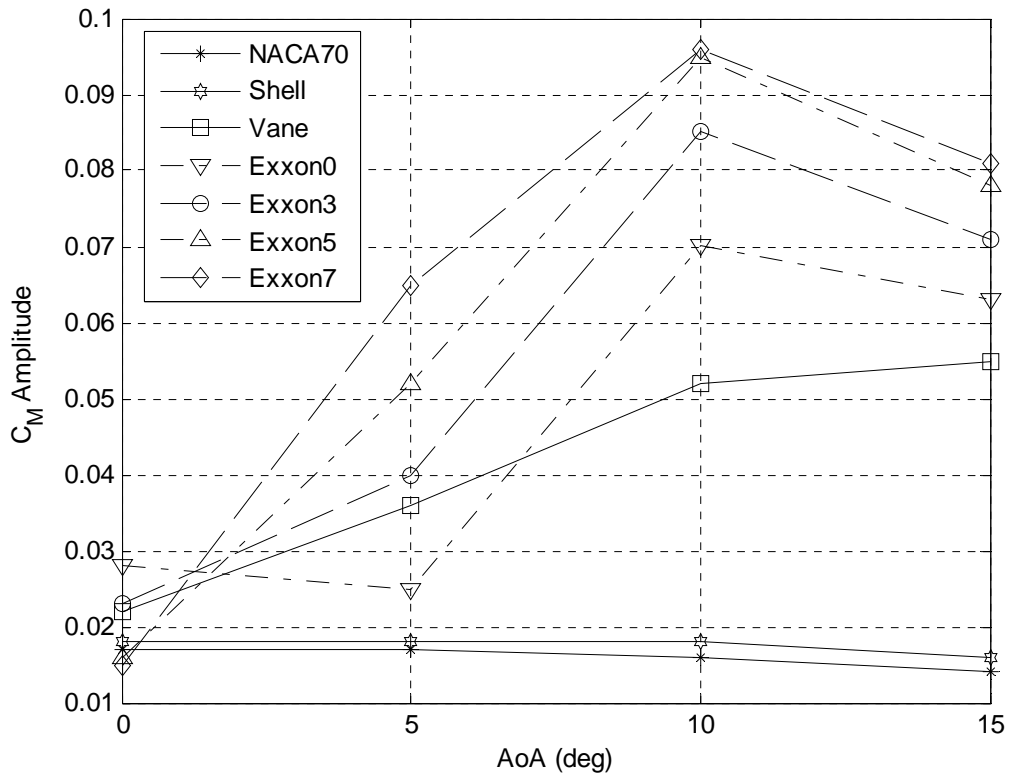


Figure 7-15 Moment Coefficient Amplitudes of Different Sections.

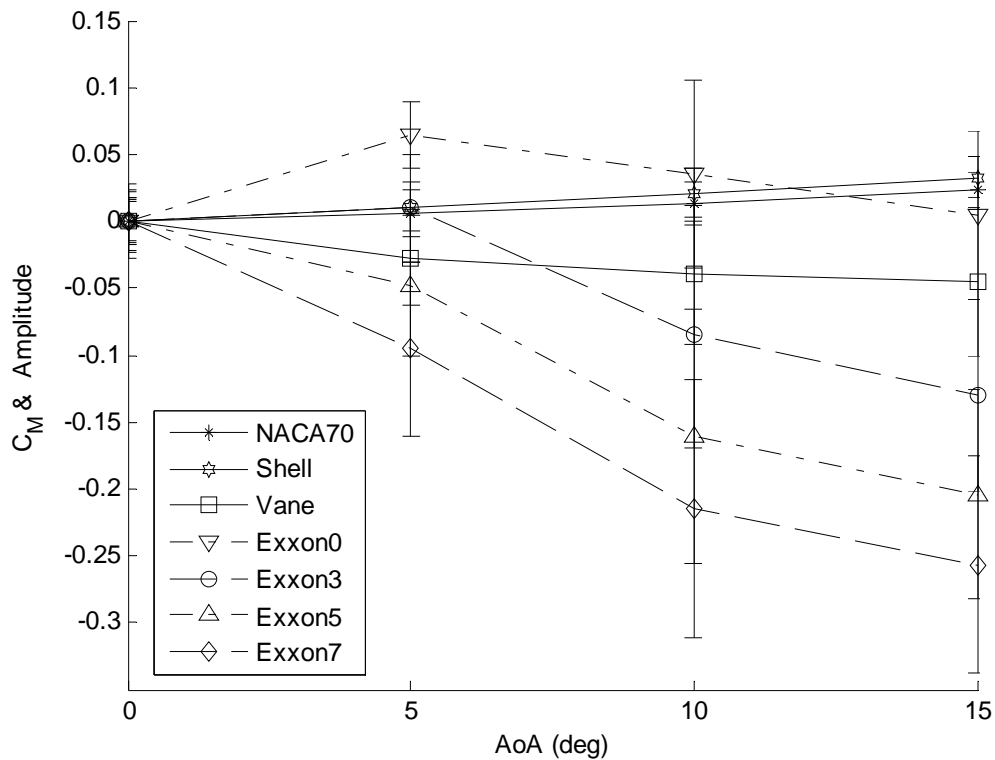


Figure 7-16 Moment Coefficients & Their Amplitudes of Different Sections.

Strouhal Number

For each case, i.e. a specific profile at a given angle, the frequency of oscillation for lift/moment coefficient was measured. It is drawn in dimensionless form of Strouhal number in Figure 7-17. This figure says that moving from Exxon fairings to NACA0070, Short Fairing and then the guide vane brings along higher frequency of force oscillation. This feature may be of interest to designers to reduce the risk of resonance and associated destructive vibration.

According to Figure 7-17, adding fins has a small effect on frequency of vortex shedding at no incidence angle.

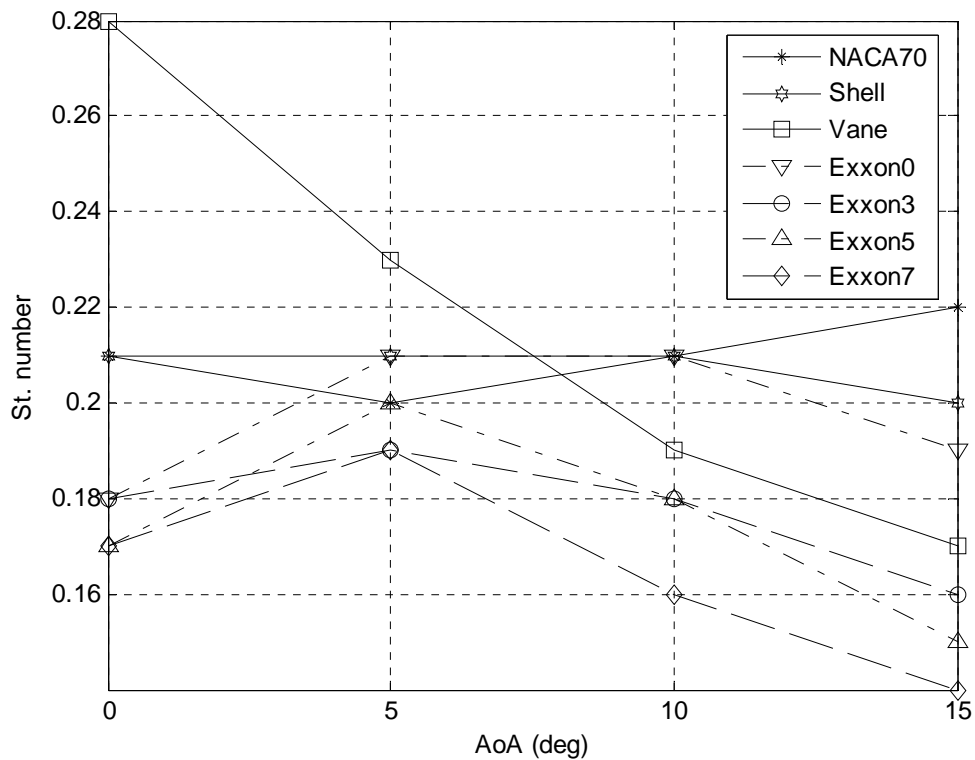


Figure 7-17 Strouhal Number of Different Sections.

Pressure Distribution Over Foils With Fin

The effect of adding fins on pressure distribution over the Exxon section was also scrutinised. Figure 7-18 and Figure 7-19 shows the mean pressure coefficient on upper and lower surfaces at two AoA, 0° and 5° respectively. When the Exxon fairing with or without fin is in line with current, there exists symmetry on both the upper and lower surfaces and therefore corresponding curves for each profile overlap each other. Figure 7-18 says that at zero AoA for the Exxon fairings with different fin-lengths, the mean pressure coefficient is almost the same except at the vicinity of trailing edge. In other words, at zero AoA adding fins will, in general, change the pressure coefficient near the tail of the fairing.

However, this is not the case at higher angles. For example at the angle of 5° as shown in Figure 7-19, longer fins reduce the pressure coefficient on the upper surface and increase it on the lower surface. Moreover, on the leeside of the fairing

they bring the crossing point of these two curves forward. This has two impacts on the hydrodynamic coefficient. It counter-balances the pressure on two surfaces and results in a smaller negative lift or even positive lift. Furthermore, near the trailing edge it produces larger counter-moment which tries to return the fairing back to a zero angle of attack. This corrects the moment coefficient from positive for the fairing without a fin to negative for the fairing with the longest fin.

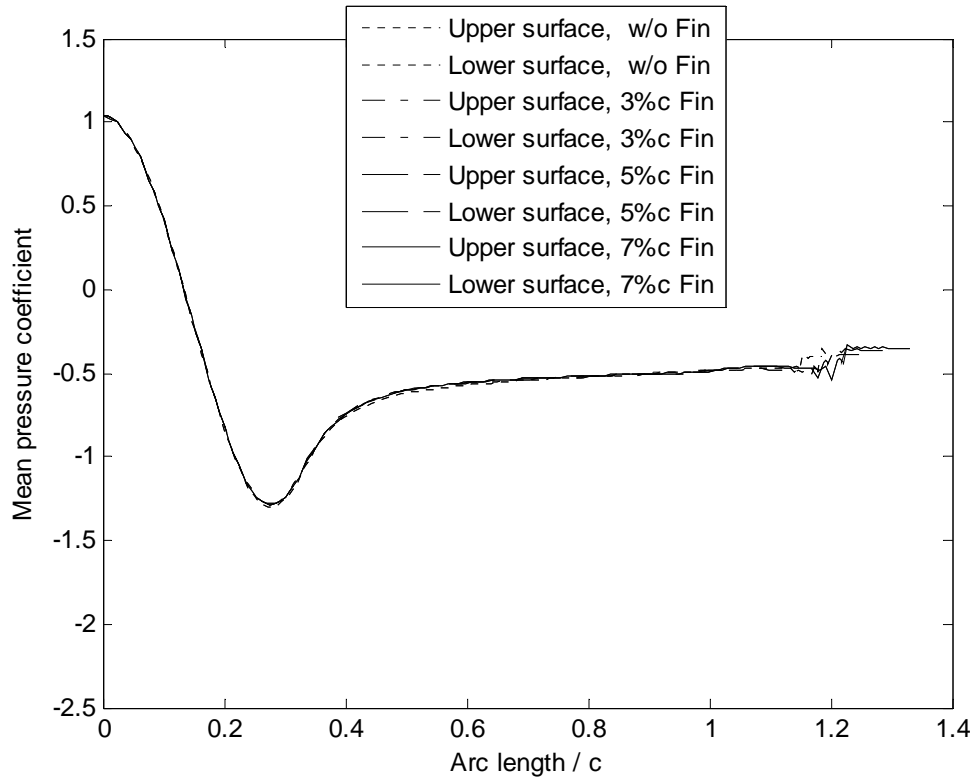


Figure 7-18 Effect of Adding Fin on Mean Pressure Coefficient At 0° .

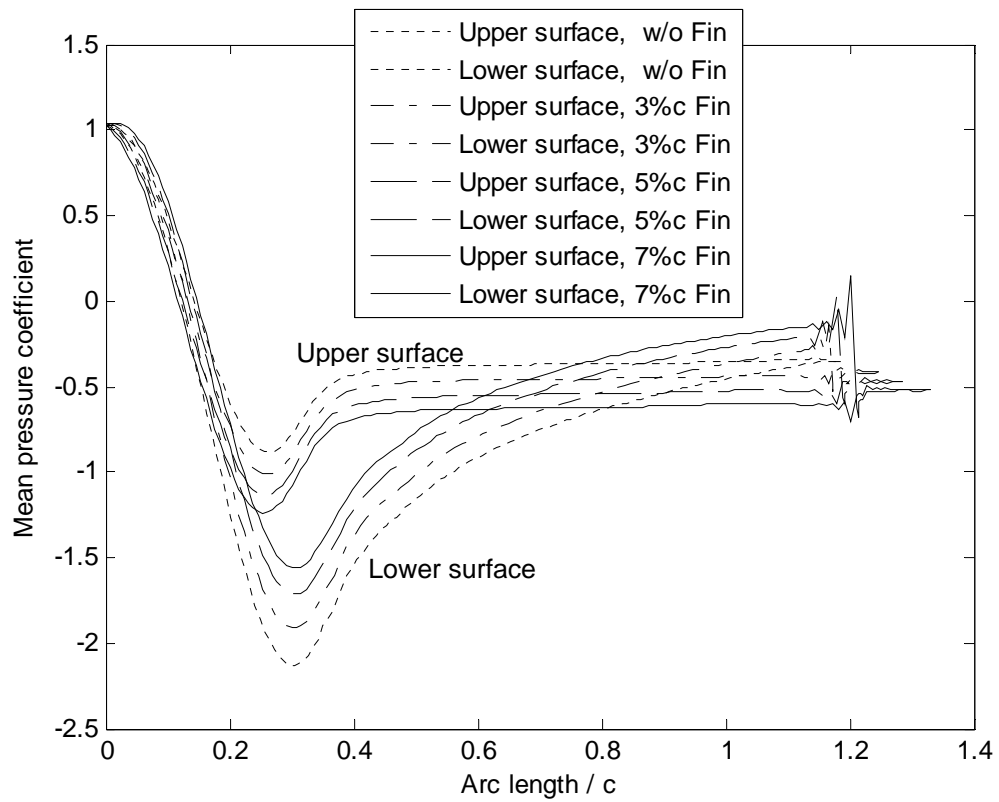


Figure 7-19 Effect of Adding Fin on Mean Pressure Coefficient At 5° .

Stability and Capability of VIV Suppression

In summary, the drag coefficient plus the necessary conditions of stability are presented in Figure 7-20. In this figure from left to right, the drag coefficient, which was defined based on chord length, declines. Among three sections of the NACA0070, Short Fairing and the guide vane with relatively similar thickness to chord ratio, the guide vane generates the smallest drag force. On the other hand, this figure says that at this Reynolds number only two sections of the guide vane and Exxon7 satisfy the necessary conditions of stability. Nevertheless, the Short Fairing slightly violates the condition related to torsion. In practice, this might be compensated by other damping, e.g. friction, and the system becomes stable. The effect of adding fins on stability is more obvious in this figure. It should be noted that with respect to stability, adding fins only helps to satisfy the necessary conditions of stability but does not guarantee the stability of the system which requires the investigation of the characteristic equation.

Considering the oscillation amplitude of hydrodynamic coefficients as a criterion for the severity of fluctuating force, Figure 7-21 shows the capability of suppressing VIV for each profile. Lower amplitude of the lift coefficient means the fairing is more capable of mitigating the vortex shedding. As was mentioned earlier, a small amplitude of moment coefficient could be because of another reason and therefore is not an appropriate tool to measure the capacity of alleviating VIV. Among the first three sections on the left hand side, i.e. the NACA0070, Short Fairing and the guide vane, the latter demonstrates the best performance. This superior behaviour may be due to a low angle of leeside which impedes the flow separation from surface and consequent vortex formation. This figure also embodies the positive impact of adding fin on VIV suppression capability of the fairing.

7. Section Hydrodynamic Coefficients

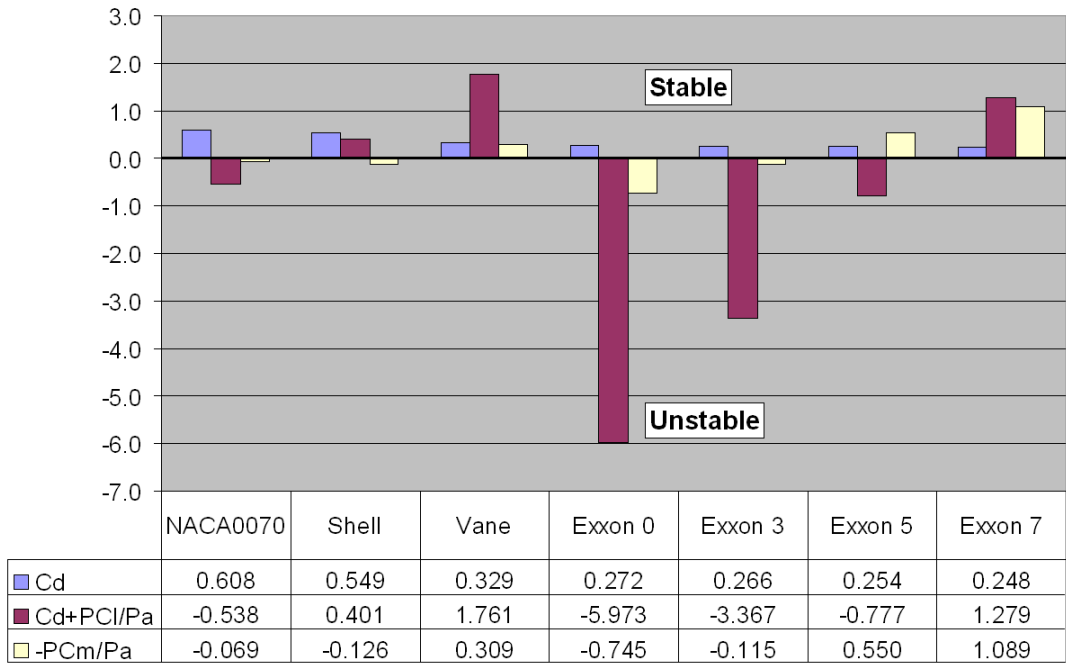


Figure 7-20 Necessary Conditions of Stability.

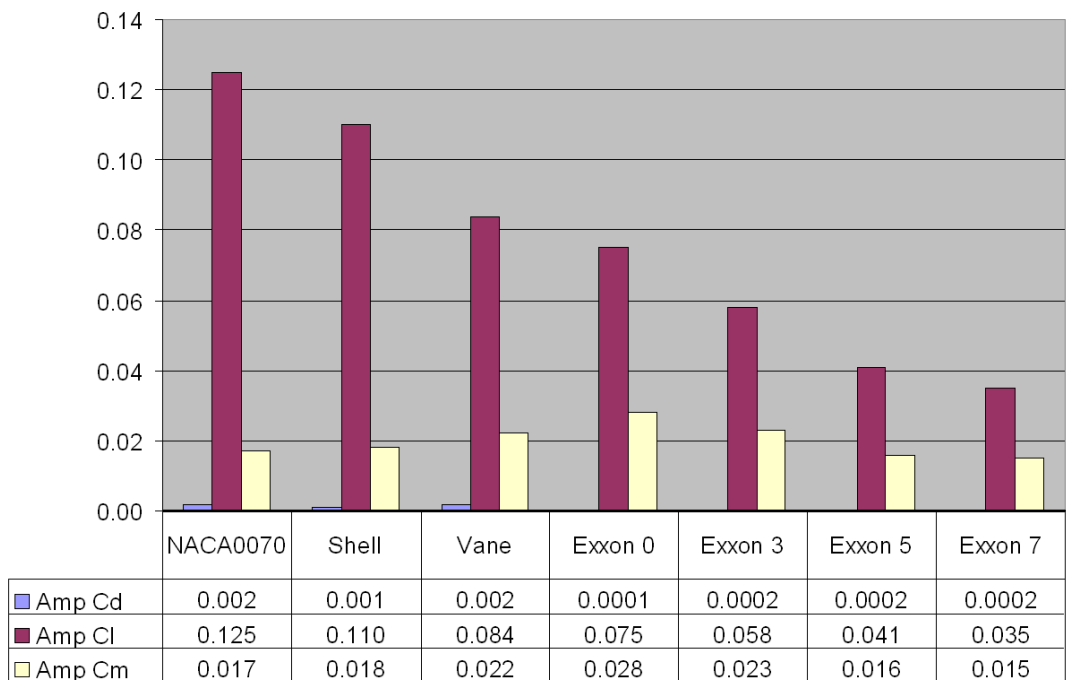


Figure 7-21 Capability of Suppressing VIV at 0°.

7.7 Fairing Length vs. Operational Constraints

The design philosophy of a fairing is to prevent vortex formation by streamlining the flow and avoiding flow separation. Blevins believes that to be effective, streamlining the downstream side of a profile requires an angle of taper less than 8 to 10 degrees (Blevins, 2001). Otherwise, flow separation may happen which is followed by vortices and associated vibration. Moreover, flow separation can change the positive lift slope into negative.

When some fairing profiles demonstrated vibrations, some researchers tried to explain this through early separation of the boundary layer (Calkins, 1984, Ericsson and Reding, 1980, Ikeda et al., 2003). Accordingly, it was recommended to reduce the angle of the leeside of the fairing, to avoid vortices and negative lift slope (Ericsson and Reding, 1980, Grimminger, 1945).

For example, Grimminger tested several open-end sections as guide vanes for the purpose of reducing drag and vibration. He reported that drag became less when the width of the opening at the rear of the guide vanes was increased and therefore the angle of leeside decreased. His observations showed that this width can be almost as much as the diameter of the cylinder itself and the guide vanes will still prevent vibrations of the cylinder. He concluded the performance of the system in terms of reducing drag and vibration can be made considerably better than the performance of the cylinder alone, provided the distance between edges of the vane is large, i.e. downstream side angle is small, and also provided the leading edges start well forward of the 90-degree point around the cylinder. Meyer et al. stated the latter in a different way (Meyer et al., 1995). He reported that for some profiles with circular nose, the flow separates shortly after reaching the fairing. In order to stop this and keep the flow attached to the surface, the fairing profile should be contoured so that the flow continues to slip over the foil (Figure 7-22). This leads to a thicker fairing and to keep the angle of leeside constant it needs a longer chord.

In this study, comparison of three sections of the NACA0070, Short Fairing and the guide vane confirms the effect of leeside as well. These profiles have relatively similar thickness to chord ratio. The NACA0070 and Short Fairing with steep

downstream side generate higher lift amplitude and have negative lift slope whereas the guide vane with low angle of leeside streamlines the flow more effectively and has positive lift slope.

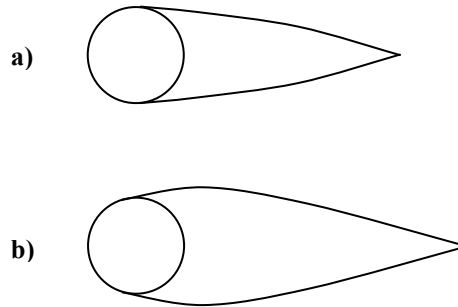


Figure 7-22 Modification in Circular Head of Fairing, a) Original b) Modified.

In brief, the key issue in design of a fairing is to prevent flow separation for anticipated current speed. The angle of leeside plays a significant role in keeping flow attached to the surface and generally speaking, longer fairings suppress the VIV more effectively and are more likely to have positive lift slope.

On the other hand, operational constraints do not allow for the use of lengthy profiles. One solution to fulfil both requirements is to clip the trailing edge of the fairing. In other words, the blunt-end is the result of constraining the fairing profile to the same cross-sectional envelope as the original section when the leeside angle is reduced and the trailing-edge is prolonged to improve the behaviour.

But this question certainly arises as to what consequences this technique entails. In response, Ericsson and Reding says that drag force is extremely sensitive to the blunt-end length, whereas data indicates that trimming the trailing edge does not significantly manipulate the slope of lift curve based on the actual chord length (Ericsson and Reding, 1980). Grimminger (1945) also reported good performance of several guide vanes with the blunt and open ends. They behaved very well in reducing drag and mitigating VIV.

This fact was observed in this study as well. The guide vane with the closed end presented very good performance characteristics in comparison with the NACA0070 and Short Fairing.

Consequently, it may be concluded that reducing the steepness of leeside is the top priority and clipping the trailing edge in favour of having lower angle of downstream side is quite reasonable, although it may alter drag.

7.8 Concluding Remarks

In previous chapters an analytical model had been established for instability of a riser fairing and it was observed through the parametric study that the hydrodynamic coefficients have a significant impact in this mechanism. Thus, this chapter was designed to assess the hydrodynamic behaviour of few profiles.

Due to the lack of data in literature about the hydrodynamics of thick foils, the CFD analysis method was selected as it was more appropriate for the purpose of this study in comparison with physical modelling like wind tunnel tests. Four main sections were chosen and three sizes of flat fin were installed on one of the profiles as well. Each section was assessed for four incidence angles and the hydrodynamic coefficients along with their oscillation amplitude were measured. The influences of adding fins were probed and an explanation of how they change the behaviour of the fairing was given. In brief, adding fins enhances the stability of the riser fairing by modifying the slope of lift and moment coefficients. It boosts the VIV suppression capability and improves the self-alignment characteristic of the fairing as well. Moreover, this study explored the effect of reducing the angle of leeside and clipping the tail of the fairing.

These techniques are usually used to create a better and more operable fairing. In the eyes of a riser designer, the best fairing has several hydrodynamic features.

- It streamlines the flow efficiently with no flow separation and therefore causes minimum VIV.
- It produces small drag.
- It experiences no instability.

- It will be able to align itself to current.
- It will be free of fishtailing.

In such a fairing, the maximum thickness is located as close to leading edge as possible to keep the centre of rotation forward of the hydrodynamic centre for weathervane stability.

Operationally, in a good fairing profile the thickness to chord length ratio is selected relatively high in order to reduce the required operational space for the fairing.

Generally speaking, it is very difficult to reconcile all the above virtues in a single fairing profile. Thus, it is necessary to compromise with some features.

Preliminary study of this chapter implies that the guide vane not only is adequately short for operational ease but also presents acceptable performance in VIV suppression and stability and therefore should be added to the list of desirable fairing profiles.

So far two-dimensional (2D) model has provided the basis to understand the mechanism of instability in a riser fairing and to identify and scrutinise key parameters. Now, it is time to expand this model to the real case of three dimensions and take the effect of length into consideration. The next chapter is dedicated to this issue.

3D Theoretical Model

In this chapter the analytical model will be expanded to a three-dimensional case. At first, the model will be developed for a general case in which tension and current speed varies along a riser partially covered with fairings. Then, the complicated general model will be simplified for the uniform case in which all parameters are constant along the riser length. Finally, the general model will be validated against an experimental case.

8.1 Introduction

Chapter 5 explored a two-dimensional model for instability of a riser fairing. The effect of third dimension along the riser was modelled by a spring. The necessary assumptions were explained and the limitations and the scope of validity of this model were clarified.

With the same assumptions and limitations in mind, this model is expanded to a top tensioned riser. It is also assumed that the riser cross-section is uniform along the length at all depths and therefore, its properties like flexural stiffness are constant.

Likewise, fairing is assumed to have a uniform profile wherever it is installed. Therefore, its structural properties and hydrodynamic behaviour are constant. As mentioned before, the entire riser length is not necessarily covered by fairings.

In addition to the coverage, there are other variables varying along the riser. Current profile may be non-uniform, for example a sheared flow. Tension may also decrease from the top end to the bottom of the riser if the weight of the system is not carried by other means.

All these variation along the riser length (Figure 8-1) distinguish a general 3D problem from uniform 2D case and therefore a separate model is required.

In reality, the riser fairings are in segments with finite length (Figure 8-1). Many of these individual segments are installed to cover part of a riser. They behave independently and are not continuous. The important point is that in practice the ratio of a fairing's span to a riser's length is so small that one may assume the fairings are continuous. For instance, if a riser of 700m length is fitted with fairings of 7m span (Grant and Patterson, 1977) which is one of the longest reported segments, this ratio equals to 0.01, small enough to assume continuity of the fairing. This ratio will be much less for shorter span length of the fairing.

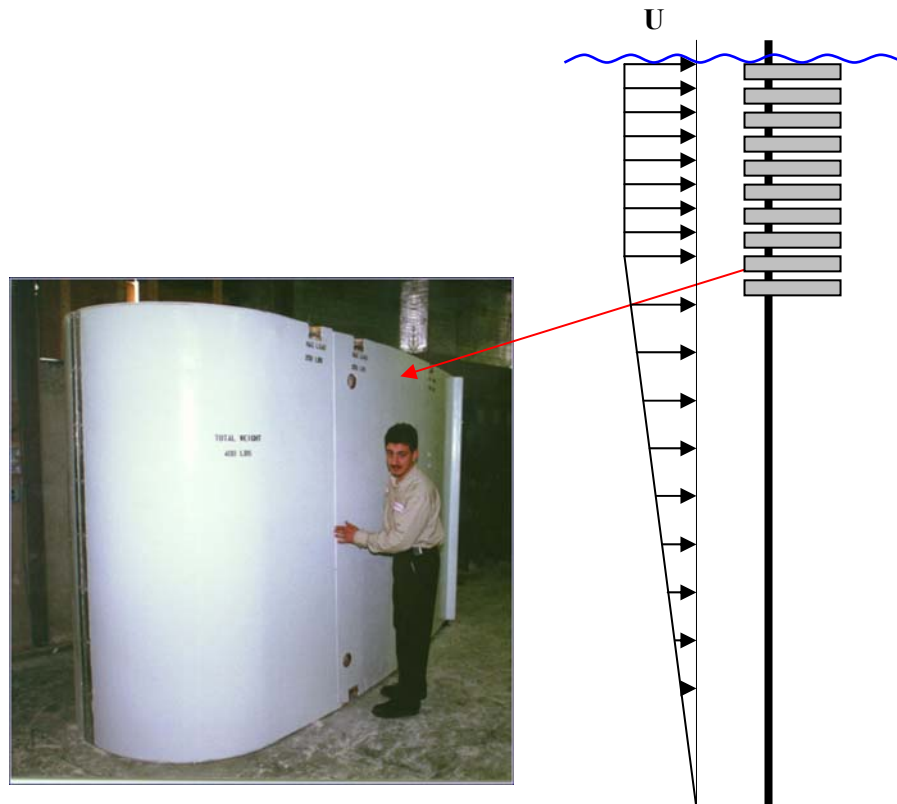


Figure 8-1 Three-Dimensionality of Riser with Fairings.

8.2 General Case

Governing Equations

In this case, the riser is outfitted partially with fairings in the area that the vortex shedding is severe. Therefore, it can be assumed that in the area remaining, fluid current has no exciting role and only behaves as a damper. Moreover, tension reduces from top end to the bottom end due to the weight. The riser is also exposed to a non-uniform current.

To differentiate the two parts of the riser, i.e. the bare riser and the portion fitted with the fairing, it is necessary to define a parameter $s(z)$ that specifies the spanwise extent of the area fitted with fairings,

$$s(z) = \begin{cases} 1, & \text{Fitted with fairing} \\ 0, & \text{Bare riser} \end{cases} \quad 8-1$$

The entire riser can move in cross-flow direction which comprises the first degree of freedom, $y(z,t)$. A fairing, wherever installed along the riser length ($s=1$), moves transversely with the riser, $y(z,t)$, but it is also permitted to weathervane which introduces the second degree of freedom, $\theta(z,t)$.

Consequently, the degrees of freedom (DOFs) in 3D model, as shown in Figure 8-2, consist of,

$$y = y(z, t) \quad 8-2$$

$$\theta = \theta(z, t) \quad 8-3$$

The origin of the coordinate system is located at the bottom end of the riser. Axis x is in line with the current direction and positive z is upward. For an observer looking at the system from the riser's top end, the definitions of positive AoA and cross-flow displacement are identical to those in 2D case, i.e. positive AoA in clockwise direction and positive y normal to the plane and inward.

The riser and fairing interact and exert forces on each other in both DOFs. The interaction forces can be written as,

$$F_{\text{int}}^y = F_{\text{int}}^y(z, t) \quad 8-4$$

$$F_{int}^\theta = F_{int}^\theta(z, t) \quad 8-5$$

The riser, where not fitted with fairings, is subject to current and therefore its cross-flow motion induces hydrodynamic damping (Blevins, 2001, Barltrop and Adams, 1991). By keeping the linear term, this damping which depends on current velocity and drag coefficient can be simplified as:

$$\text{CF damping effect of bare riser} = -\frac{1}{2}\rho U c C_{Dr} \dot{y}(z, t) (1-s(z)) \quad 8-6$$

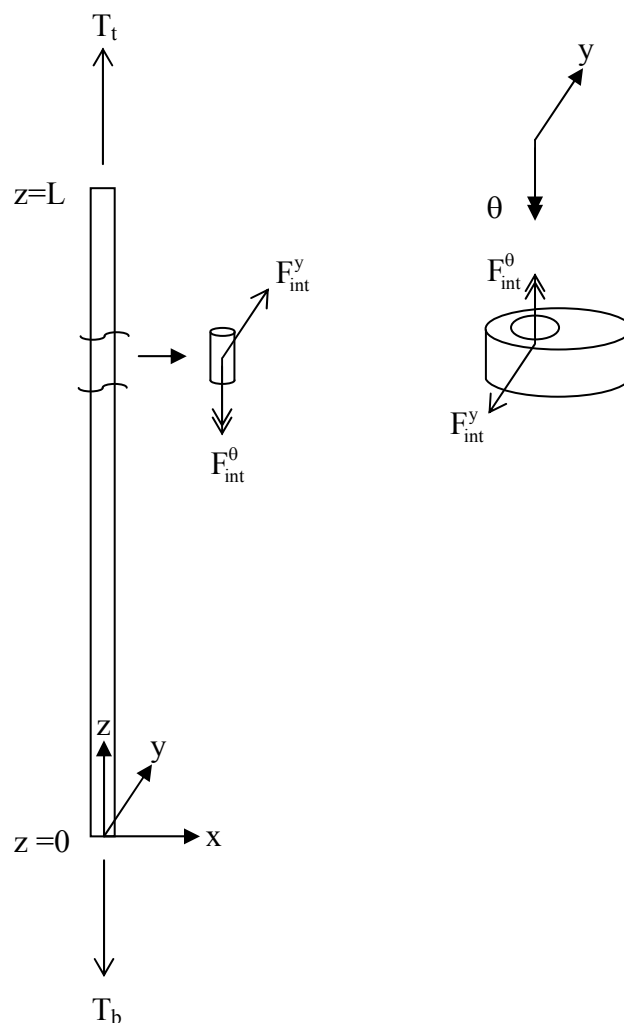


Figure 8-2 Free Body Diagram, 3D Model.

For simplicity in presentation, the riser's equation of motion is restricted to the case of planar, small angle, linear strain analysis of an initially straight riser. Then, it is

qualified to be modelled as a tensioned beam (API, 1998, Patel and Witz, 1991). The static equilibrium equation for lateral displacement of a tensioned beam is,

$$\frac{d^2}{dz^2} \left[EI(z) \frac{d^2 y}{dz^2} \right] - \frac{d}{dz} \left[T_e(z) \frac{dy}{dz} \right] = F^y(z) \quad 8-7$$

where E is the Young's modulus; I is the moment of inertia, EI denotes the bending stiffness of the cross section and T_e is the effective riser tension. F^y is the applied lateral load, not including the applied hydrostatic and pressures.

The beam's resistance to deformation consists of flexural stiffness and more importantly, geometric stiffness originating from axial tension. The tension to be taken into account in analysing an immersed, fluid-filled tube-like riser is known as effective tension, T_e . Effective tension at a cross section can be formulated clearly as,

$$T_e = T_n + (-P_i \times A_i) - (-P_o \times A_o) \quad 8-8$$

where T_n is axial tension in the structural element (pipe wall); $P_i A_i$ is axial tension in the internal fluid column (A_i = internal sectional area, P_i = internal pressure); $P_o A_o$ is axial tension in the displaced fluid column (A_o = external or displaced cross-sectional area, P_o = external pressure).

For a uniform riser's section, bending stiffness (EI) is constant along the riser's length but the tension force varies along the z axis because of the riser's weight. The variable tension, $T_e(z)$, is equal to,

$$T_e(z) = T_t - (L - z) \cdot w_r = T_b + z \cdot w_r \quad 8-9$$

where T_t and T_b are the top and bottom tensions respectively and w_r indicates the in-water weight of the riser per unit length,

$$w_r = (m_r + m_{fr} s(z)) \cdot g - \text{Buoyancy Force}(z) \quad 8-10$$

Consequently, by substituting Equation (8-9) and with the assumption of constant EI for uniform cross section, the static equilibrium Equation (8-7) can be expanded as,

$$EI \cdot y^{(IV)}(z) - T_e(z) \cdot y''(z) - w_r \cdot y'(z) = F^y(z) \quad 8-11$$

where prime is the symbol of the derivative with respect to the z axis.

The dynamic governing equation can be obtained from Equation (8-11) by incorporating inertia forces and a mechanism for energy loss. This model is adequate for many riser analyses and moreover, the description of this model can be used to introduce most of the fundamental concepts (API, 1998). Assuming viscose damping, the appropriate term for energy loss will be $C_y \cdot \dot{y}$ (Clough and Penzien, 1993), where the superscript dot indicates the derivative with respect to time.

The inertia force of a bare riser contains the effect of a riser's structural mass (m_r) and added mass (m_{ar}). For this part of the riser, the applied load consists of hydrodynamic damping as stated in Equation (8-6). Hence, the equation of lateral motion for this part can be written as,

$$\left[EI \cdot y^{(IV)} - T_e \cdot y'' - w_r \cdot y' + (m_r + m_{ar}) \cdot \ddot{y} + C_y \cdot \dot{y} = -\frac{1}{2} \rho U c C_{Dr} \dot{y} \right] (1-s) \quad 8-12$$

For the portion of the riser fitted with a fairing, it does not have contact with water and therefore the inertia force contains the effect of only structural mass. The lateral interaction with the fairing makes the applied load. Thus, the equation of lateral motion for this part is,

$$\left[EI \cdot y^{(IV)} - T_e \cdot y'' - w_r \cdot y' + m_r \cdot \ddot{y} + C_y \cdot \dot{y} = F_{int}^y \right] s \quad 8-13$$

The final equation of the riser's lateral motion is obtained by the summation of Equations (8-12) and (8-13) as follows,

$$EI \cdot y^{(IV)} - T_e \cdot y'' - w_r \cdot y' + (m_r + m_{ar}(1-s)) \cdot \ddot{y} + C_y \cdot \dot{y} = F_{int}^y s - \frac{1}{2} \rho U c C_{Dr} \dot{y} (1-s) \quad 8-14$$

Since the fairing is permitted to spin, the only torsional contribution of the riser is the friction torque, $T_{Friction}$ between the rubbing surfaces of the riser and fairing. The riser is assumed stiff enough not to undergo any torsion.

$$\left[T_{Friction} = F_{int}^\theta \right] s \quad 8-15$$

For simplicity, equivalent viscose damping, as discussed in Section 5.8, can be deployed for the frictional damping, $T_{\text{Friction}} = C_{\theta} \dot{\theta}$. Thus, the torsional interaction force is,

$$\left[C_{\theta} \dot{\theta} = F_{\text{int}}^{\theta} \right] s \quad 8-16$$

It is assumed that the cross-section of the fairing does not change along the riser. Thus, for an element of the fairing with unit height, the governing situation is identical to that of 2D section. Consequently, by using Lagrange's equation as fully explained in Section 5.2, the governing equations of motion for two DOFs of the fairing will be the same as Equations (5-11) and (5-12). They state,

$$\left[(m_{\text{fr}} + m_a) \ddot{y} - (S_x + S_a) \ddot{\theta} = [\text{Hydrodynamic Force}]_y - F_{\text{int}}^y \right] s \quad 8-17$$

$$\left[(J + J_a) \ddot{\theta} - (S_x + S_a) \ddot{y} = [\text{Hydrodynamic Force}]_{\theta} - F_{\text{int}}^{\theta} \right] s \quad 8-18$$

In summary, with the aid of considering the interaction forces, the governing equations of the riser and fairing were derived individually. To remove the terms of interaction, they are substituted from Equations (8-14) and (8-16) in Equations (8-17) and (8-18). By re-arranging the result, it gives,

$$\begin{aligned} EI \cdot y^{(IV)} - T_e \cdot y'' - w_r \cdot y' + (m_r + (m_{\text{fr}} + m_a)s + m_{\text{ar}}(1-s)) \cdot \ddot{y} + \\ + (C_y + \frac{1}{2} \rho U c C_{\text{Dr}}(1-s)) \cdot \dot{y} - (S_x + S_a) \ddot{\theta} s = [\text{Hydrodynamic Force}]_y s \end{aligned} \quad 8-19$$

$$\left[-(S_x + S_a) \ddot{y} + (J + J_a) \ddot{\theta} + C_{\theta} \dot{\theta} = [\text{Hydrodynamic Force}]_{\theta} \right] s \quad 8-20$$

Hydrodynamic forces were already described in Section 5.3. The final form of these hydrodynamic forces emerged in Equations (5-28) and (5-29). That is,

$$\begin{aligned} [\text{Hydrodynamic Force}]_y = \frac{1}{2} \rho U^2 c \left(\frac{\partial C_L}{\partial \alpha} \Big|_{\alpha=0} \right) \theta \\ - \frac{1}{2} \rho U c \left(\frac{\partial C_L}{\partial \alpha} \Big|_{\alpha=0} + C_D \Big|_{\alpha=0} \right) \dot{y} + \frac{1}{2} \rho R U c \left(\frac{\partial C_L}{\partial \alpha} \Big|_{\alpha=0} + C_D \Big|_{\alpha=0} \right) \dot{\theta} \end{aligned} \quad 8-21$$

$$\begin{aligned} [\text{Hydrodynamic Force}]_{\theta} = \left(\frac{1}{2} \rho U^2 c^2 \frac{\partial C_{M(\alpha)}}{\partial \alpha} \Big|_{\alpha=0} \right) \theta + \\ - \left(\frac{1}{2} \rho U c^2 \frac{\partial C_{M(\alpha)}}{\partial \alpha} \Big|_{\alpha=0} \right) \dot{y} + \left(\frac{1}{2} \rho R U c^2 \frac{\partial C_{M(\alpha)}}{\partial \alpha} \Big|_{\alpha=0} \right) \dot{\theta} \end{aligned} \quad 8-22$$

By replacing these linearised hydrodynamic force terms in Equations (8-19) and (8-20), the governing equation will emerge as below,

$$\begin{aligned}
 EI \cdot y^{(IV)} - T_e \cdot y'' - w_r \cdot y' + (m_r + (m_{fr} + m_a)s + m_{ar}(1-s)) \cdot \ddot{y} + \\
 + \left(C_y + \frac{1}{2} \rho U c \left(\frac{\partial C_L}{\partial \alpha} \Big|_{\alpha=0} + C_D \Big|_{\alpha=0} \right) s + \frac{1}{2} \rho U c C_{Dr} (1-s) \right) \cdot \dot{y} - (S_x + S_a) \ddot{\theta} s \\
 - \frac{1}{2} \rho R U c \left(\frac{\partial C_L}{\partial \alpha} \Big|_{\alpha=0} + C_D \Big|_{\alpha=0} \right) \dot{\theta} s - \frac{1}{2} \rho U^2 c \left(\frac{\partial C_L}{\partial \alpha} \Big|_{\alpha=0} \right) \theta s = 0
 \end{aligned} \tag{8-23}$$

$$\begin{aligned}
 \left[- (S_x + S_a) \ddot{y} - \left(\frac{1}{2} \rho U c^2 \frac{\partial C_{M(cr)}}{\partial \alpha} \Big|_{\alpha=0} \right) \dot{y} + (J + J_a) \ddot{\theta} + \left(C_\theta + \left(\frac{1}{2} \rho R U c^2 \frac{\partial C_{M(cr)}}{\partial \alpha} \Big|_{\alpha=0} \right) \right) \dot{\theta} \right. \\
 \left. + \left(\frac{1}{2} \rho U^2 c^2 \frac{\partial C_{M(cr)}}{\partial \alpha} \Big|_{\alpha=0} \right) \theta = 0 \right] s
 \end{aligned} \tag{8-24}$$

Galerkin's Method

The coupled differential equations are varied in time and space and they are too complicated to be solved in closed form. Thus, it is necessary to introduce a trial solution in series form for variation in space,

$$y(z, t) = \sum_{i=1}^N \phi_i(z) p_i(t) \tag{8-25}$$

$$\theta(z, t) = \sum_{j=1}^N \phi_j(z) q_j(t) \tag{8-26}$$

where $\phi_i(z)$ comprises the basis functions or in other words mode shapes. p_i and q_j are unknown functions of time which are to be determined. For a simply supported flexural beam with constant axial force, the governing equation of transverse displacement is equivalent to a simple Sturm-Liouville differential equation and the basis functions will be in the form of sinusoidal mode shape (Clough and Penzien, 1993). As the boundary conditions at the two ends of the riser are identical to that of a simply supported beam, these basis functions satisfies the boundary conditions for this problem as well and can be deployed in this study for uniform or non-uniform tension. Thus,

$$\phi_i(z) = \sin\left(\frac{i\pi z}{L}\right) \tag{8-27}$$

Consequently, in governing Equations (8-23) and (8-24) the required derivatives with respect to time and space will be as below,

$$y' = \sum_{i=1}^N \left(\frac{i\pi}{L}\right) \cos\left(\frac{i\pi z}{L}\right) p_i = \sum_{i=1}^N \left(\frac{i\pi}{L}\right) \phi_i' p_i$$

$$y'' = -\sum_{i=1}^N \left(\frac{i\pi}{L}\right)^2 \sin\left(\frac{i\pi z}{L}\right) p_i = -\sum_{i=1}^N \left(\frac{i\pi}{L}\right)^2 \phi_i p_i$$

$$y^{(IV)} = \sum_{i=1}^N \left(\frac{i\pi}{L}\right)^4 \sin\left(\frac{i\pi z}{L}\right) p_i = \sum_{i=1}^N \left(\frac{i\pi}{L}\right)^4 \phi_i p_i$$

$$\dot{y} = \sum_{i=1}^N \sin\left(\frac{i\pi z}{L}\right) \dot{p}_i = \sum_{i=1}^N \phi_i \dot{p}_i$$

$$\ddot{y} = \sum_{i=1}^N \sin\left(\frac{i\pi z}{L}\right) \ddot{p}_i = \sum_{i=1}^N \phi_i \ddot{p}_i$$

$$\dot{\theta} = \sum_{j=1}^N \sin\left(\frac{j\pi z}{L}\right) \dot{q}_j = \sum_{j=1}^N \phi_j \dot{q}_j$$

$$\ddot{\theta} = \sum_{j=1}^N \sin\left(\frac{j\pi z}{L}\right) \ddot{q}_j = \sum_{j=1}^N \phi_j \ddot{q}_j$$

Substitution of the trial solution and required derivatives in the governing equations leads to two equations in which p_i and q_j are unknown and should be determined.

In theory in order to find the coefficients of a trial solution to a partial differential equation, it is sufficient to set the weighted residual to zero for infinitive number of weight functions. There are many methods of selecting weight function but one of the most prevalent methods, which is also used in the Finite Element Analysis, is Galerkin's Method. Galerkin suggested using the shape/basis functions as weight functions. It will be very beneficial when the set of basis functions are orthogonal, like this problem.

To implement Galerkin's method here, the trial solution will be replaced in the governing equations and each of the governing equations will be multiplied by shape functions individually and integrated over the domain, i.e. the riser's length. The

obtained integral is set to zero. By using N shape functions, this leads to N individual equations for each governing equation.

For instance, the first governing equation and a shape function, e.g. ϕ_k , gives,

$$\int_0^L \phi_k(z) \cdot [\text{Eq. (8-23)}] dz = 0 \quad 8-28$$

This integral consists of several terms. Substituting the terms of governing Equation (8-23) gives them as below,

$$+\int_0^L EIy^{(IV)} \cdot \phi_k dz = \sum_{i=1}^N EI\left(\frac{i\pi}{L}\right)^4 p_i \int_0^L \phi_k \phi_i dz = EI\left(\frac{k\pi}{L}\right)^4 p_k \frac{1}{2}$$

$$\begin{aligned} -\int_0^L T_e \cdot y'' \cdot \phi_k dz &= \sum_{i=1}^N (T_t - w_r \cdot L) \left(\frac{i\pi}{L}\right)^2 p_i \int_0^L \phi_k \phi_i dz + \sum_{i=1}^N \pi^2 w_r \left(\frac{i}{L}\right)^2 p_i \int_0^L z \phi_k \phi_i dz = \\ &= (T_t - w_r \cdot L) \left(\frac{k\pi}{L}\right)^2 p_k \frac{1}{2} + \sum_{i=1}^N \pi^2 w_r Y_{ki}^1 p_i \end{aligned}$$

$$Y_{ki}^1 = \left(\frac{i}{L}\right)^2 \int_0^L z \phi_k \phi_i dz$$

$$-\int_0^L w_r \cdot y' \cdot \phi_k dz = -\sum_{i=1}^N \pi w_r \left(\frac{i}{L}\right) p_i \int_0^L \phi_k \phi_i' dz = -\sum_{i=1}^N \pi^2 w_r Y_{ki}^2 p_i$$

$$Y_{ki}^2 = \left(\frac{i}{\pi L}\right) \int_0^L \phi_k \phi_i' dz$$

$$+\int_0^L (m_r + (m_{fr} + m_a)s + m_{ar}(1-s)) \ddot{y} \cdot \phi_k dz =$$

$$= \sum_{i=1}^N (m_r + m_{ar}) \ddot{p}_i \int_0^L \phi_k \phi_i dz + \sum_{i=1}^N (m_{fr} + m_a - m_{ar}) \ddot{p}_i \int_0^L s \phi_k \phi_i dz =$$

$$= (m_r + m_{ar}) \ddot{p}_k \frac{1}{2} + \sum_{i=1}^N (m_{fr} + m_a - m_{ar}) Y_{ki}^3 \ddot{p}_i$$

$$Y_{ki}^3 = \int_0^L s \phi_k \phi_i dz$$

$$\begin{aligned}
 & + \int_0^L \left(C_y + \frac{1}{2} \rho U c \left(\frac{\partial C_L}{\partial \alpha} \Big|_{\alpha=0} + C_D \Big|_{\alpha=0} \right) s + \frac{1}{2} \rho U c C_{Dr} (1-s) \right) \dot{y} \cdot \phi_k \, dz = \\
 & = \sum_{i=1}^N C_y \dot{p}_i \int_0^L \phi_k \phi_i \, dz + \sum_{i=1}^N \left(\frac{1}{2} \rho c C_{Dr} \right) \dot{p}_i \int_0^L U \phi_k \phi_i \, dz + \\
 & + \sum_{i=1}^N \frac{1}{2} \rho c \left(\frac{\partial C_L}{\partial \alpha} \Big|_{\alpha=0} + C_D \Big|_{\alpha=0} - C_{Dr} \right) \dot{p}_i \int_0^L U s \phi_k \phi_i \, dz = \\
 & = C_y \dot{p}_k \frac{L}{2} + \sum_{i=1}^N \left(\frac{1}{2} \rho c C_{Dr} \right) \dot{Y}_{ki} \dot{p}_i + \sum_{i=1}^N \frac{1}{2} \rho c \left(\frac{\partial C_L}{\partial \alpha} \Big|_{\alpha=0} + C_D \Big|_{\alpha=0} - C_{Dr} \right) \dot{Y}_{ki} \dot{p}_i \\
 & \dot{Y}_{ki} = \int_0^L U \phi_k \phi_i \, dz \\
 & \dot{Y}_{ki} = \int_0^L U s \phi_k \phi_i \, dz \\
 \\
 & - \int_0^L (S_x + S_a) \ddot{\theta} s \cdot \phi_k \, dz = - \sum_{j=1}^N (S_x + S_a) \ddot{q}_j \int_0^L s \phi_k \phi_j \, dz = - \sum_{j=1}^N (S_x + S_a) \dot{Y}_{kj} \ddot{q}_j \\
 \\
 & - \int_0^L \frac{1}{2} \rho R U c \left(\frac{\partial C_L}{\partial \alpha} \Big|_{\alpha=0} + C_D \Big|_{\alpha=0} \right) \dot{\theta} s \cdot \phi_k \, dz = - \sum_{j=1}^N \frac{1}{2} \rho R c \left(\frac{\partial C_L}{\partial \alpha} \Big|_{\alpha=0} + C_D \Big|_{\alpha=0} \right) \dot{q}_j \int_0^L U s \phi_k \phi_j \, dz = \\
 & = - \sum_{j=1}^N \frac{1}{2} \rho R c \left(\frac{\partial C_L}{\partial \alpha} \Big|_{\alpha=0} + C_D \Big|_{\alpha=0} \right) \dot{Y}_{kj} \dot{q}_j \\
 \\
 & - \int_0^L \frac{1}{2} \rho U^2 c \left(\frac{\partial C_L}{\partial \alpha} \Big|_{\alpha=0} \right) \theta s \cdot \phi_k \, dz = - \sum_{j=1}^N \frac{1}{2} \rho c \left(\frac{\partial C_L}{\partial \alpha} \Big|_{\alpha=0} \right) q_j \int_0^L U^2 s \phi_k \phi_j \, dz = \\
 & = - \sum_{j=1}^N \frac{1}{2} \rho c \left(\frac{\partial C_L}{\partial \alpha} \Big|_{\alpha=0} \right) \dot{Y}_{kj} q_j \\
 & \dot{Y}_{kj} = \int_0^L U^2 s \phi_k \phi_j \, dz \tag{8-29}
 \end{aligned}$$

In short, through the process of expanding Equation (8-28) these variables needed to be calculated.

$$\dot{Y}_{ki}^1 = \left(\frac{i}{L} \right)^2 \int_0^L z \phi_k \phi_i \, dz$$

$$\dot{Y}_{ki}^2 = \left(\frac{i}{\pi L} \right) \int_0^L \phi_k \phi_i' \, dz$$

$$\dot{Y}_{ki}^3 = \int_0^L s \phi_k \phi_i dz$$

$$\dot{Y}_{ki}^4 = \int_0^L U \phi_k \phi_i dz$$

$$\dot{Y}_{ki}^5 = \int_0^L U s \phi_k \phi_i dz$$

$$\dot{Y}_{ki}^6 = \int_0^L U^2 s \phi_k \phi_i dz$$

Similarly, applying this procedure on the second governing equation gives,

$$\int_0^L \phi_h(z) \cdot [\text{Eq. (8-24)}] dz = 0 \quad 8-30$$

By substituting the Equation (8-24) in the above integral, following terms appear.

$$-\int_0^L (S_x + S_a) \ddot{y} s \cdot \phi_h dz = -\sum_{i=1}^N (S_x + S_a) \ddot{p}_i \int_0^L s \phi_h \phi_i dz = -\sum_{i=1}^N (S_x + S_a) \dot{Y}_{hi}^3 \ddot{p}_i$$

$$\begin{aligned} -\int_0^L \left(\frac{1}{2} \rho U c^2 \frac{-\partial C_{M(cr)}}{\partial \alpha} \Big|_{\alpha=0} \right) \dot{y} s \cdot \phi_h dz &= -\sum_{i=1}^N \left(\frac{1}{2} \rho c^2 \frac{-\partial C_{M(cr)}}{\partial \alpha} \Big|_{\alpha=0} \right) \dot{p}_i \int_0^L U s \phi_h \phi_i dz = \\ &= -\sum_{i=1}^N \left(\frac{1}{2} \rho c^2 \frac{-\partial C_{M(cr)}}{\partial \alpha} \Big|_{\alpha=0} \right) \dot{Y}_{hi}^5 \dot{p}_i \end{aligned}$$

$$+\int_0^L (J + J_a) \ddot{\theta} s \cdot \phi_h dz = \sum_{j=1}^N (J + J_a) \ddot{q}_j \int_0^L s \phi_h \phi_j dz = \sum_{j=1}^N (J + J_a) \dot{Y}_{hj}^3 \ddot{q}_j$$

$$\begin{aligned} +\int_0^L \left(C_\theta + \frac{1}{2} \rho R U c^2 \frac{-\partial C_{M(cr)}}{\partial \alpha} \Big|_{\alpha=0} \right) \dot{\theta} s \cdot \phi_h dz &= \\ &= \sum_{j=1}^N C_\theta \dot{q}_j \int_0^L s \phi_h \phi_j dz + \sum_{j=1}^N \left(\frac{1}{2} \rho R c^2 \frac{-\partial C_{M(cr)}}{\partial \alpha} \Big|_{\alpha=0} \right) \dot{q}_j \int_0^L U s \phi_h \phi_j dz = \\ &= \sum_{j=1}^N C_\theta \dot{Y}_{hj}^3 \dot{q}_j + \sum_{j=1}^N \left(\frac{1}{2} \rho R c^2 \frac{-\partial C_{M(cr)}}{\partial \alpha} \Big|_{\alpha=0} \right) \dot{Y}_{hj}^5 \dot{q}_j \end{aligned}$$

$$\begin{aligned}
 & + \int_0^L \left(\frac{1}{2} \rho U^2 c^2 \frac{-\partial C_{M(cr)}}{\partial \alpha} \Big|_{\alpha=0} \right) \theta s \cdot \phi_h dz = \sum_{j=1}^N \left(\frac{1}{2} \rho c^2 \frac{-\partial C_{M(cr)}}{\partial \alpha} \Big|_{\alpha=0} \right) q_j \int_0^L U^2 s \phi_h \phi_j dz = \\
 & = \sum_{j=1}^N \left(\frac{1}{2} \rho c^2 \frac{-\partial C_{M(cr)}}{\partial \alpha} \Big|_{\alpha=0} \right) \Upsilon_{hj} q_j \qquad \qquad \qquad 8-31
 \end{aligned}$$

Consequently, by using trial solution and Galerkin's method, $(2 \times N)$ coupled equations are obtained,

$$\begin{aligned}
 & EI \left(\frac{k\pi}{L} \right)^4 p_k \frac{L}{2} + (T_t - w_r \cdot L) \left(\frac{k\pi}{L} \right)^2 p_k \frac{L}{2} + \sum_{i=1}^N \pi^2 w_r \Upsilon_{ki}^1 p_i - \sum_{i=1}^N \pi^2 w_r \Upsilon_{ki}^2 p_i + \\
 & + (m_r + m_{ar}) \ddot{p}_k \frac{L}{2} + \sum_{i=1}^N (m_{fr} + m_a - m_{ar}) \Upsilon_{ki}^3 \ddot{p}_i \\
 & + C_y \dot{p}_k \frac{L}{2} + \sum_{i=1}^N \left(\frac{1}{2} \rho c C_{Dr} \right) \Upsilon_{ki}^4 \dot{p}_i + \sum_{i=1}^N \frac{1}{2} \rho c \left(\frac{\partial C_L}{\partial \alpha} \Big|_{\alpha=0} + C_D \Big|_{\alpha=0} - C_{Dr} \right) \Upsilon_{ki}^5 \dot{p}_i \\
 & - \sum_{j=1}^N (S_x + S_a) \Upsilon_{kj}^3 \ddot{q}_j - \sum_{j=1}^N \frac{1}{2} \rho R c \left(\frac{\partial C_L}{\partial \alpha} \Big|_{\alpha=0} + C_D \Big|_{\alpha=0} \right) \Upsilon_{kj}^5 \dot{q}_j \\
 & - \sum_{j=1}^N \frac{1}{2} \rho c \left(\frac{\partial C_L}{\partial \alpha} \Big|_{\alpha=0} \right) \Upsilon_{kj}^6 q_j = 0 \qquad \qquad i = 1 \text{ to } N \qquad \qquad \qquad 8-32
 \end{aligned}$$

$$\begin{aligned}
 & - \sum_{i=1}^N (S_x + S_a) \Upsilon_{hi}^3 \ddot{p}_i - \sum_{i=1}^N \left(\frac{1}{2} \rho c^2 \frac{-\partial C_{M(cr)}}{\partial \alpha} \Big|_{\alpha=0} \right) \Upsilon_{hi}^5 \dot{p}_i + \sum_{i=1}^N (J + J_a) \Upsilon_{hj}^3 \ddot{q}_j + \sum_{i=1}^N C_\theta \Upsilon_{hj}^3 \dot{q}_j \\
 & + \sum_{j=1}^N \left(\frac{1}{2} \rho R c^2 \frac{-\partial C_{M(cr)}}{\partial \alpha} \Big|_{\alpha=0} \right) \Upsilon_{hj}^5 \dot{q}_j + \sum_{j=1}^N \left(\frac{1}{2} \rho c^2 \frac{-\partial C_{M(cr)}}{\partial \alpha} \Big|_{\alpha=0} \right) \Upsilon_{hj}^6 q_j = 0 \qquad h = 1 \text{ to } N \qquad 8-33
 \end{aligned}$$

These $(2 \times N)$ equations are only functions of time variables, i.e. $p_i(t)$, $q_i(t)$ and their derivatives. They can be rewritten in matrix form. To this end, vector \underline{X}_{2N} is defined as the vector of unknown variables,

$$\underline{X}_{2N} = \begin{Bmatrix} p_1 \\ \vdots \\ p_N \\ - \\ q_1 \\ \vdots \\ q_N \end{Bmatrix} \qquad \qquad \qquad 8-34$$

With this in mind, writing the above $(2 \times N)$ equations in matrix form leads to the following matrix equation,

$$\underline{\underline{\mathfrak{M}}}\ddot{\underline{\underline{X}}} + \underline{\underline{C}}\dot{\underline{\underline{X}}} + \underline{\underline{K}}\underline{\underline{X}} = \underline{\underline{0}} \quad 8-35$$

where the square matrices $\underline{\underline{\mathfrak{M}}}_{2N \times 2N}$, $\underline{\underline{C}}_{2N \times 2N}$ and $\underline{\underline{K}}_{2N \times 2N}$ are,

$$\underline{\underline{\mathfrak{M}}} = \begin{bmatrix} \dots & \dots & \dots & | & \dots & \dots & \dots \\ \dots & M_{ki} & \dots & | & \dots & -(\mathbf{S}_x + \mathbf{S}_a)^3 \dot{\Upsilon}_{kj} & \dots \\ \dots & \dots & \dots & | & \dots & \dots & \dots \\ \dots & \dots & \dots & | & \dots & \dots & \dots \\ \dots & -(\mathbf{S}_x + \mathbf{S}_a)^3 \dot{\Upsilon}_{hi} & \dots & | & \dots & (\mathbf{J} + \mathbf{J}_a)^3 \dot{\Upsilon}_{hj} & \dots \\ \dots & \dots & \dots & | & \dots & \dots & \dots \end{bmatrix}$$

$$M_{ki} = \begin{cases} (m_{fr} + m_a - m_{ar})^3 \dot{\Upsilon}_{ki} & k \neq i \\ (m_{fr} + m_a - m_{ar})^3 \dot{\Upsilon}_{kk} + (m_r + m_{ar}) \frac{1}{2} & k = i \end{cases} \quad 8-36$$

$$\underline{\underline{C}} = \begin{bmatrix} \dots & \dots & \dots & | & \dots & \dots & \dots \\ \dots & C_{ki} & \dots & | & \dots & -\frac{1}{2} \rho R c \left(\frac{\partial C_L}{\partial \alpha} \Big|_{\alpha=0} + C_D \Big|_{\alpha=0} \right)^5 \dot{\Upsilon}_{kj} & \dots \\ \dots & \dots & \dots & | & \dots & \dots & \dots \\ \dots & \dots & \dots & | & \dots & \dots & \dots \\ \dots & -\left(\frac{1}{2} \rho c^2 \frac{\partial C_{M(cr)}}{\partial \alpha} \Big|_{\alpha=0} \right)^5 \dot{\Upsilon}_{hi} & \dots & | & \dots & C_\theta^3 \dot{\Upsilon}_{hj} + \left(\frac{1}{2} \rho R c^2 \frac{\partial C_{M(cr)}}{\partial \alpha} \Big|_{\alpha=0} \right)^5 \dot{\Upsilon}_{hj} & \dots \\ \dots & \dots & \dots & | & \dots & \dots & \dots \end{bmatrix}$$

$$C_{ki} = \begin{cases} \left(\frac{1}{2} \rho c C_{Dr} \right)^4 \dot{\Upsilon}_{ki} + \frac{1}{2} \rho c \left(\frac{\partial C_L}{\partial \alpha} \Big|_{\alpha=0} + C_D \Big|_{\alpha=0} - C_{Dr} \right)^5 \dot{\Upsilon}_{ki} & k \neq i \\ \left(\frac{1}{2} \rho c C_{Dr} \right)^4 \dot{\Upsilon}_{kk} + \frac{1}{2} \rho c \left(\frac{\partial C_L}{\partial \alpha} \Big|_{\alpha=0} + C_D \Big|_{\alpha=0} - C_{Dr} \right)^5 \dot{\Upsilon}_{kk} + C_y \frac{1}{2} & k = i \end{cases} \quad 8-37$$

$$\underline{\underline{\mathbf{K}}} = \left[\begin{array}{ccc|ccc} \dots & \dots & \dots & \dots & \dots & \dots \\ \dots & \mathbf{K}_{ki} & \dots & \dots & -\frac{1}{2} \rho c \left(\frac{\partial C_L}{\partial \alpha} \Big|_{\alpha=0} \right)^6 \Upsilon_{kj} & \dots \\ \dots & \dots & \dots & \dots & \dots & \dots \\ - & - & - & - & - & - \\ & & & \dots & \dots & \dots \\ & 0 & & \dots & \left(\frac{1}{2} \rho c^2 \frac{\partial C_{M(er)}}{\partial \alpha} \Big|_{\alpha=0} \right)^6 \Upsilon_{hj} & \dots \\ & & & \dots & \dots & \dots \end{array} \right]$$

$$\mathbf{K}_{ki} = \begin{cases} \pi^2 w_r^1 \Upsilon_{ki}^1 - \pi^2 w_r^2 \Upsilon_{ki}^2 & k \neq i \\ \pi^2 w_r^1 \Upsilon_{kk}^1 - \pi^2 w_r^2 \Upsilon_{kk}^2 + EI \left(\frac{k\pi}{L} \right)^4 \frac{L}{2} + (T_t - w_r \cdot L) \left(\frac{k\pi}{L} \right)^2 \frac{L}{2} & k = i \end{cases} \quad 8-38$$

Eigenvalue Analysis

Similar to the 2D case in Chapter 5, the purpose of this step is to assess the trend of the vibration amplitude variation through the time when a small disturbance from equilibrium position occurs. This analysis reveals at what conditions this amplitude may not diminish and leads to instability of the system.

A general solution in exponential form is assumed,

$$\underline{\underline{\mathbf{Z}}} = \underline{\underline{\mathbf{a}}} e^{\lambda t} \rightarrow \dot{\underline{\underline{\mathbf{Z}}}} = \underline{\underline{\mathbf{a}}} \lambda e^{\lambda t} \quad 8-39$$

where $\underline{\underline{\mathbf{a}}}$ is a vector of constants. This solution is substituted in Equation (8-35).

$$\left[\underline{\underline{\mathfrak{M}}} \lambda^2 + \underline{\underline{\mathbf{C}}} \lambda + \underline{\underline{\mathbf{K}}} \right] \underline{\underline{\mathbf{a}}} e^{\lambda t} = \underline{\underline{\mathbf{0}}} \quad 8-40$$

Similar to the 2D case, this matrix equation needs to have non-trivial solution to illustrate the response of system to a disturbance. More significantly, this response should be stable.

This linear homogenous equation has non-trivial solutions only if the coefficient matrix is singular which requires the matrix determinant to be zero. Moreover, the stability of the system dictates that the amplitude of response should decline through

the time. This means the real part of power in assumed exponential solution should be negative. Consequently, to satisfy the above conditions, it necessitates having,

$$(1) \left[\underline{\underline{\mathfrak{M}}}\lambda^2 + \underline{\underline{C}}\lambda + \underline{\underline{K}} \right] = \text{singular} \quad \rightarrow \quad \det \left[\underline{\underline{\mathfrak{M}}}\lambda^2 + \underline{\underline{C}}\lambda + \underline{\underline{K}} \right] = 0$$

$$(2) \text{Real}(\lambda) < 0$$

Setting the determinant to zero renders a characteristic equation in λ which is of $2 \times 2N$ degree. Analysis of the roots of this characteristic equation results in a stability criterion which clarifies whether an unstable behaviour may occur. Unstable motion is probable whenever a root λ_i has positive real part.

Dimensionless Form

As explained in Section 5.6, classifying the variables helps to have a better understanding of true physical parameters that influence the stability.

The first step in making the characteristic equation dimensionless is to identify the dimension of its terms. Equation (8-39) reveals that λ is of the dimension of $(1/\text{Time})$, i.e. $\text{Dim}[\lambda] = (\text{Time})^{-1}$.

With reference to Equations (8-36), (8-37) and (8-38), each of three matrices $\underline{\underline{\mathfrak{M}}}_{2N \times 2N}$, $\underline{\underline{C}}_{2N \times 2N}$ and $\underline{\underline{K}}_{2N \times 2N}$ consists of four square sub-matrices of size N . A quick look to the elements of these sub-matrices indicates they have different dimensions. It has been shown below,

$$\text{Dim}[\underline{\underline{\mathfrak{M}}}_{2N \times 2N}] = \left[\begin{array}{c|c} \text{(Mass)} & \text{(Mass) \cdot (Length)} \\ \hline \text{(Mass) \cdot (Length)} & \text{(Mass) \cdot (Length)}^2 \end{array} \right]$$

$$\text{Dim}[\underline{\underline{C}}_{2N \times 2N}] = \left[\begin{array}{c|c} \text{(Mass) \cdot (Time)}^{-1} & \text{(Mass) \cdot (Length) \cdot (Time)}^{-1} \\ \hline \text{(Mass) \cdot (Length) \cdot (Time)}^{-1} & \text{(Mass) \cdot (Length)}^2 \cdot \text{(Time)}^{-1} \end{array} \right]$$

$$\text{Dim}[\underline{\underline{K}}_{2N \times 2N}] = \left[\begin{array}{c|c} \frac{(\text{Mass}) \cdot (\text{Time})^2}{(\text{Mass}) \cdot (\text{Length}) \cdot (\text{Time})^2} & \frac{(\text{Mass}) \cdot (\text{Length}) \cdot (\text{Time})^2}{(\text{Mass}) \cdot (\text{Length})^2 \cdot (\text{Time})^2} \\ \hline & \hline \end{array} \right]$$

Now, this needs to select appropriate parameters for these dimensions, i.e. mass, length and time. Chord length of the fairing is an appropriate term for the dimension of length. Mass of the system if entirely fitted with fairings, i.e. $(m + m_a) \cdot L$ where $(m = m_r + m_{fr})$, suits the dimension of mass. Similar to the 2D case, the term c/U generates a general form for the dimension of time but the point here is that U varies over the riser length. So, a constant velocity U_o needs to be selected, for example the velocity at the water surface and the current velocity profile is defined as function of U_o .

$$U = U(U_o, z) \tag{8-41}$$

With reference to the dimension of expression $\underline{\underline{R}} = \underline{\underline{\mathfrak{M}}}\lambda^2 + \underline{\underline{C}}\lambda + \underline{\underline{K}}$, each row and column of $\underline{\underline{R}}_{2N \times 2N}$ should be divided by appropriate dimensions as shown below,

$$\begin{array}{c} (c)^{-1} \\ \times \\ \left((m + m_a) \cdot L \right)^{-1} \cdot (c/U_o)^2 \quad \times \quad \left| \begin{array}{c|c} \underline{\underline{R}}_{11} & \underline{\underline{R}}_{12} \\ \hline \underline{\underline{R}}_{21} & \underline{\underline{R}}_{22} \end{array} \right| = 0 \end{array} \tag{8-42}$$

Applying this procedure results in the dimensionless form of $\underline{\underline{R}}_{2N \times 2N}$,

$$\underline{\underline{\tilde{R}}} = \underline{\underline{\tilde{\mathfrak{M}}}}\tilde{\lambda}^2 + \underline{\underline{\tilde{C}}}\tilde{\lambda} + \underline{\underline{\tilde{K}}}$$

where similar to 2D case, $\tilde{\lambda} = \frac{\lambda}{U_o/c}$. Dimensionless matrices $\underline{\underline{\tilde{\mathfrak{M}}}}$, $\underline{\underline{\tilde{C}}}$ and $\underline{\underline{\tilde{K}}}$ are,

$$\underline{\underline{\tilde{\mathfrak{M}}}} = \left[\begin{array}{ccc|ccc} \dots & \dots & \dots & \dots & \dots & \dots \\ \dots & \tilde{M}_{ki} & \dots & \dots & -\frac{(S_x + S_a)^3}{(m + m_a)c} \frac{\dot{\gamma}_{kj}}{L} & \dots \\ \dots & \dots & \dots & \dots & \dots & \dots \\ \dots & \dots & \dots & \dots & \dots & \dots \\ \dots & -\frac{(S_x + S_a)^3}{(m + m_a)c} \frac{\dot{\gamma}_{hi}}{L} & \dots & \dots & \frac{(J + J_a)^3}{(m + m_a)c^2} \frac{\dot{\gamma}_{hj}}{L} & \dots \\ \dots & \dots & \dots & \dots & \dots & \dots \end{array} \right]$$

$$\tilde{M}_{ki} = \begin{cases} \frac{(m_{fr} + m_a - m_{ar})}{(m + m_a)} \frac{\dot{\gamma}_{ki}^3}{L} & k \neq i \\ \frac{(m_{fr} + m_a - m_{ar})}{(m + m_a)} \frac{\dot{\gamma}_{kk}^3}{L} + \frac{1}{2} \frac{(m_r + m_{ar})}{(m + m_a)} & k = i \end{cases} \quad 8-43$$

$$\underline{\underline{\tilde{C}}} = \left[\begin{array}{ccc|ccc} \dots & \dots & \dots & \dots & \dots & \dots \\ \dots & \tilde{C}_{ki}^{11} & \dots & \dots & \tilde{C}_{kj}^{12} & \dots \\ \dots & \dots & \dots & \dots & \dots & \dots \\ \dots & \dots & \dots & \dots & \dots & \dots \\ \dots & \dots & \dots & \dots & \dots & \dots \\ \dots & \tilde{C}_{hi}^{21} & \dots & \dots & \tilde{C}_{hj}^{22} & \dots \\ \dots & \dots & \dots & \dots & \dots & \dots \end{array} \right]$$

$$\tilde{C}_{ki}^{11} = \begin{cases} \frac{\frac{1}{2} \rho c^2}{(m + m_a)} C_{Dr} \frac{\dot{\gamma}_{ki}^4}{U_o L} + \frac{\frac{1}{2} \rho c^2}{(m + m_a)} \left(\frac{\partial C_L}{\partial \alpha} \Big|_{\alpha=0} + C_D \Big|_{\alpha=0} - C_{Dr} \right) \frac{\dot{\gamma}_{ki}^5}{U_o L} & k \neq i \\ \frac{\frac{1}{2} \rho c^2}{(m + m_a)} C_{Dr} \frac{\dot{\gamma}_{kk}^4}{U_o L} + \frac{\frac{1}{2} \rho c^2}{(m + m_a)} \left(\frac{\partial C_L}{\partial \alpha} \Big|_{\alpha=0} + C_D \Big|_{\alpha=0} - C_{Dr} \right) \frac{\dot{\gamma}_{kk}^5}{U_o L} + \frac{C_y}{2(m + m_a)\omega_y} \frac{\omega_y c}{U_o} & k = i \end{cases}$$

$$\begin{aligned}\tilde{C}_{kj}^{12} &= -\frac{\frac{1}{2}\rho c^2}{(m+m_a)} \frac{R}{c} \left(\left. \frac{\partial C_L}{\partial \alpha} \right|_{\alpha=0} + C_D \Big|_{\alpha=0} \right) \frac{\dot{Y}_{kj}^5}{U_o L} \\ \tilde{C}_{hi}^{21} &= -\frac{\frac{1}{2}\rho c^2}{(m+m_a)} \left. \frac{-\partial C_{M(cr)}}{\partial \alpha} \right|_{\alpha=0} \frac{\dot{Y}_{hi}^5}{U_o \cdot L} \\ \tilde{C}_{hj}^{22} &= 2 \frac{C_\theta}{2 \cdot (J+J_a) \cdot \omega_\theta} \frac{(J+J_a)}{(m+m_a)c^2} \frac{\omega_\theta c}{U_o} \frac{\dot{Y}_{hj}^3}{L} + \frac{\frac{1}{2}\rho c^2}{(m+m_a)} \frac{R}{c} \left. \frac{-\partial C_{M(cr)}}{\partial \alpha} \right|_{\alpha=0} \frac{\dot{Y}_{hj}^5}{U_o L}\end{aligned}\quad 8-44$$

$$\tilde{\underline{\underline{K}}} = \left[\begin{array}{ccc|ccc} \dots & \dots & \dots & \dots & \dots & \dots \\ \dots & \tilde{K}_{ki} & \dots & \dots & -\frac{\frac{1}{2}\rho c^2}{(m+m_a)} \left(\left. \frac{\partial C_L}{\partial \alpha} \right|_{\alpha=0} \right) \frac{\dot{Y}_{kj}^6}{U_o^2 L} & \dots \\ \dots & \dots & \dots & \dots & \dots & \dots \\ - & - & - & - & - & - \\ \dots & \dots & \dots & \dots & \dots & \dots \\ \dots & 0 & \dots & \dots & \frac{\frac{1}{2}\rho c^2}{(m+m_a)} \left. \frac{-\partial C_{M(cr)}}{\partial \alpha} \right|_{\alpha=0} \frac{\dot{Y}_{hj}^6}{U_o^2 L} & \dots \\ \dots & \dots & \dots & \dots & \dots & \dots \end{array} \right]$$

$$\tilde{K}_{ki} = \begin{cases} \frac{\pi^2 \cdot w_r \cdot L}{(m+m_a)L^2} \frac{c^2}{U_o^2} \dot{Y}_{ki}^1 - \frac{\pi^2 \cdot w_r \cdot L}{(m+m_a)L^2} \frac{c^2}{U_o^2} \dot{Y}_{ki}^2 & k \neq i \\ \frac{\pi^2 \cdot w_r \cdot L}{(m+m_a)L^2} \frac{c^2}{U_o^2} \dot{Y}_{kk}^1 - \frac{\pi^2 \cdot w_r \cdot L}{(m+m_a)L^2} \frac{c^2}{U_o^2} \dot{Y}_{kk}^2 + \\ + \frac{\pi^4 EI}{(m+m_a)L^4} \frac{c^2}{U_o^2} \frac{k^4}{2} + \frac{\pi^2 (T_t - w_r \cdot L)}{(m+m_a)L^2} \frac{c^2}{U_o^2} \frac{k^2}{2} & k = i \end{cases}\quad 8-45$$

It should be noted that the first natural frequency of a taut string is $\sqrt{\pi^2 T / mL^2}$ where T is the tension, m is mass per unit length and L is the total length of string. Moreover, the first natural frequency of a simply supported uniform beam is $\sqrt{\pi^4 EI / mL^4}$ where EI is flexural stiffness. With this in mind, all terms in expression

(8-45) are meaningful. For example, $w_r \cdot L$ is the total wet weight of the riser and therefore the term $[\pi^2 w_r \cdot L / (m + m_a) L^2]$ is the squared of natural frequency of this riser in water when it acts as a cable under a uniform tension equal to its weight. Likewise, the term $[\pi^2 T_t / (m + m_a) L^2]$ means the squared of natural frequency of such cable under the uniform tension of T_t . Similarly, the term $[\pi^4 EI / (m + m_a) L^4]$ is the squared of natural frequency of this riser in water when it acts as a simply supported beam. In this study, $[\pi^2 T_t / (m + m_a) L^2]$ is used as the main transverse natural frequency and the other two are defined as a fraction of that.

$$\omega_y = \sqrt{\frac{\pi^2 T_t}{(m + m_a) L^2}} \quad 8-46$$

To this end, two parameters FF and TTF are defined as Flexural Factor and Top Tension Factor respectively. FF shows the ratio of flexural stiffness to the stiffness induced by tension. TTF is the ratio of top tension to the riser's wet weight.

$$FF = \frac{\pi^2 EI}{T_t \cdot L^2} \quad 8-47$$

$$TTF = \frac{T_t}{w_r \cdot L} \quad 8-48$$

With reference to last term on the left hand side of Equation (8-24) and with the help of definition for torsional frequency in 2D case (see Equation (5-44)), the torsional natural frequency for 3D case is defined as,

$$\omega_\theta = \sqrt{-\frac{1}{2} \rho U_o^2 c^2 \frac{\partial C_{M(cr)}}{\partial \alpha} \Big|_{\alpha=0} / (J + J_a)}$$

Taking the dimensionless parameters for the 2D case in mind, a more precise look to Equations (8-43) to (8-45) suggests the following dimensionless parameters for the 3D case as well.

$$\gamma^2 = \frac{J + J_a}{(m + m_a) \cdot c^2} \quad 8-49$$

$$S_r = \frac{S_x + S_a}{(m + m_a) \cdot c} \quad 8-50$$

$$A = \frac{\rho \cdot c^2}{2(m + m_a)} \quad 8-51$$

$$\xi_y = \frac{C_y}{2 \cdot (m + m_a) \cdot \omega_y} \quad 8-52$$

$$\xi_\theta = \frac{C_\theta}{2 \cdot (J + J_a) \cdot \omega_\theta} \quad 8-53$$

$$U_{ry} = \frac{U_o}{\omega_y \cdot c} \quad 8-54$$

$$U_{r\theta} = \frac{U_o}{\omega_\theta \cdot c} = \sqrt{A \frac{\gamma^2}{-\frac{\partial C_{M(\alpha)}}{\partial \alpha} \Big|_{\alpha=0}}} \quad 8-55$$

$$R_r = \frac{R}{c} \quad 8-56$$

They are identical to what has been already defined in the 2D case, however, since part of the riser may not be fitted with a fairing and consequently the possibility of having the mass change over the length, a Mass Factor (MF) is required. The MF will show the ratio of total mass (added-mass inclusive) of a bare part to the total mass of a riser segment covered with the fairing.

$$MF = \frac{m_r + m_{ar}}{m + m_a} \quad 8-57$$

With reference to the above equation and definition of m , i.e. structural mass of the riser and fairing ($m_r + m_{fr}$), it is clear that $(m_{fr} + m_a - m_{ar}) / (m + m_a) = 1 - MF$.

The dimensionless form of integrals $\overset{1}{Y}_{ki}$ to $\overset{6}{Y}_{ki}$ will be,

$$\overset{1}{Y}_{ki} = \overset{1}{Y}_{ki} = \left(\frac{i}{L}\right)^2 \int_0^L z \phi_k \phi_i dz \quad 8-58$$

$$\overset{2}{Y}_{ki} = \overset{2}{Y}_{ki} = \left(\frac{i}{\pi L}\right) \int_0^L \phi_k \phi_i' dz \quad 8-59$$

$$\overset{3}{Y}_{ki} = \overset{3}{Y}_{ki} = \frac{1}{L} \int_0^L s \phi_k \phi_i dz \quad 8-60$$

$$\overset{4}{Y}_{ki} = \frac{1}{U_o \cdot L} \overset{4}{Y}_{ki} = \frac{1}{U_o \cdot L} \int_0^L U \phi_k \phi_i dz \quad 8-61$$

$$\overset{5}{\tilde{Y}}_{ki} = \frac{1}{U_o \cdot L} \overset{5}{Y}_{ki} = \frac{1}{U_o \cdot L} \int_0^L U s \phi_k \phi_i dz \quad 8-62$$

$$\overset{6}{\tilde{Y}}_{ki} = \frac{1}{U_o^2 \cdot L} \overset{6}{Y}_{ki} = \frac{1}{U_o^2 \cdot L} \int_0^L U^2 s \phi_k \phi_i dz \quad 8-63$$

Finally, by replacing the above dimensionless parameters in Equations (8-43) to (8-45), matrices $\underline{\underline{\tilde{M}}}$, $\underline{\underline{\tilde{C}}}$ and $\underline{\underline{\tilde{K}}}$ are given as,

$$\underline{\underline{\tilde{M}}} = \left[\begin{array}{ccc|ccc} \dots & \dots & \dots & \dots & \dots & \dots \\ \dots & \tilde{M}_{ki} & \dots & \dots & -S_r \overset{3}{\tilde{Y}}_{kj} & \dots \\ \dots & \dots & \dots & \dots & \dots & \dots \\ \dots & \dots & \dots & \dots & \dots & \dots \\ \dots & \dots & \dots & \dots & \dots & \dots \\ \dots & -S_r \overset{3}{\tilde{Y}}_{hi} & \dots & \dots & \gamma^2 \overset{3}{\tilde{Y}}_{hj} & \dots \\ \dots & \dots & \dots & \dots & \dots & \dots \end{array} \right]$$

$$\tilde{M}_{ki} = \begin{cases} (1-MF) \overset{3}{\tilde{Y}}_{ki} & k \neq i \\ (1-MF) \overset{3}{\tilde{Y}}_{kk} + \frac{1}{2} MF & k = i \end{cases} \quad 8-64$$

$$\underline{\underline{\tilde{C}}} = \left[\begin{array}{ccc|ccc} \dots & \dots & \dots & \dots & \dots & \dots \\ \dots & \tilde{C}_{ki}^{11} & \dots & \dots & \tilde{C}_{kj}^{12} & \dots \\ \dots & \dots & \dots & \dots & \dots & \dots \\ \dots & \dots & \dots & \dots & \dots & \dots \\ \dots & \dots & \dots & \dots & \dots & \dots \\ \dots & \tilde{C}_{hi}^{21} & \dots & \dots & \tilde{C}_{hj}^{22} & \dots \\ \dots & \dots & \dots & \dots & \dots & \dots \end{array} \right]$$

$$\tilde{C}_{ki}^{11} = \begin{cases} A \overset{4}{\tilde{Y}}_{ki} C_{Dr} + A \overset{5}{\tilde{Y}}_{ki} \left(\left. \frac{\partial C_L}{\partial \alpha} \right|_{\alpha=0} + C_D|_{\alpha=0} - C_{Dr} \right) & k \neq i \\ A \overset{4}{\tilde{Y}}_{kk} C_{Dr} + A \overset{5}{\tilde{Y}}_{kk} \left(\left. \frac{\partial C_L}{\partial \alpha} \right|_{\alpha=0} + C_D|_{\alpha=0} - C_{Dr} \right) + \frac{\xi_y}{U_{ry}} & k = i \end{cases}$$

$$\tilde{C}_{kj}^{12} = -AR_r \overset{5}{\tilde{Y}}_{kj} \left(\left. \frac{\partial C_L}{\partial \alpha} \right|_{\alpha=0} + C_D|_{\alpha=0} \right)$$

$$\begin{aligned}\tilde{C}_{hi}^{21} &= -A \tilde{Y}_{hi}^5 \frac{-\partial C_{M(cr)}}{\partial \alpha} \Big|_{\alpha=0} \\ \tilde{C}_{hj}^{22} &= 2\gamma^2 \tilde{Y}_{hj}^3 \frac{\xi_{\theta}}{U_{r0}} + AR_r \tilde{Y}_{hj}^5 \frac{-\partial C_{M(cr)}}{\partial \alpha} \Big|_{\alpha=0}\end{aligned}\quad 8-65$$

$$\begin{aligned}\underline{\tilde{K}} &= \begin{bmatrix} \dots & \dots & \dots & | & \dots & \dots & \dots \\ \dots & \tilde{K}_{ki} & \dots & | & \dots & -A \tilde{Y}_{kj}^6 \left(\frac{\partial C_L}{\partial \alpha} \Big|_{\alpha=0} \right) & \dots \\ \dots & \dots & \dots & | & \dots & \dots & \dots \\ - & - & - & | & - & - & - \\ \dots & \dots & \dots & | & \dots & \dots & \dots \\ \dots & 0 & \dots & | & \dots & A \tilde{Y}_{hj}^6 \frac{-\partial C_{M(cr)}}{\partial \alpha} \Big|_{\alpha=0} & \dots \\ \dots & \dots & \dots & | & \dots & \dots & \dots \end{bmatrix} \\ \tilde{K}_{ki} &= \begin{cases} \frac{(\tilde{Y}_{ki}^1 - \tilde{Y}_{ki}^2)}{TTF \cdot U_{ry}^2} & k \neq i \\ \frac{(\tilde{Y}_{ki}^1 - \tilde{Y}_{ki}^2)}{TTF \cdot U_{ry}^2} + \frac{k^4 \cdot FF + k^2}{2U_{ry}^2} - \frac{k^2}{2TTF \cdot U_{ry}^2} & k = i \end{cases}\end{aligned}\quad 8-66$$

In the end, these matrices are substituted in characteristic equation below,

$$\det \left[\underline{\tilde{M}} \tilde{\lambda}^2 + \underline{\tilde{C}} \tilde{\lambda} + \underline{\tilde{K}} \right] = 0 \quad 8-67$$

This equation is of $2 \times 2N$ degree for $\tilde{\lambda}$. All roots of this characteristic equation should have negative real part in order to have a stable system.

In summary, the following steps will be taken in order to analyse the stability of a given riser and fairing in the 3D model. The current profile varying in depth is specified as a function of a specific speed, U_0 . A set of shape/mode functions is selected and integrals \tilde{Y}_{ki}^1 to \tilde{Y}_{ki}^6 are calculated from Equations (8-58) to (8-63) for all mode functions. Three factors of FF, TF and MF are obtained and dimensionless parameters are calculated from Equations (8-49) to (8-56). Afterwards, three

matrices $\underline{\underline{\tilde{M}}}$, $\underline{\underline{\tilde{C}}}$ and $\underline{\underline{\tilde{K}}}$ will be assembled through Equations (8-64) to (8-66). Finally, Equation (8-67) is solved for $\tilde{\lambda}$. To find the threshold of instability, U_o and accordingly U_{Ty} are increased and for a velocity increment the above procedure is repeated until the real part of one of the roots of Equation (8-67) becomes positive.

These equations will be less complicated for special cases like uniform configuration. This case will be explored in the following.

8.3 Uniform Case

In this case, all conditions are uniform along the riser. More precisely, the entire riser is fitted with a fairing. The system is exposed to a uniform current and tension is constant at all levels.

Entire coverage with the fairing means Mass Factor in Equation (8-57) and $s(z)$ in Equation (8-1) are equal to one.

$$MF = 1$$

$$s(z) = 1$$

Uniform current profile says that in Equation (8-41),

$$U = U(U_o, z) = U_o$$

Constant tension throughout the riser means the riser's weight is either negligible compared with tension or is compensated by other equipments like buoyancy modules. All in all, having constant tension in Equation (8-9) mathematically results in,

$$T_t = T_b$$

$$w_r = 0$$

Thus, the inverse of Top Tension Factor in Equation (8-48) is zero.

$$\frac{1}{TTF} = 0$$

As discussed earlier, sinusoidal shape functions of Equation (8-27) fit to this case as well. These functions are orthogonal and therefore integrals $\overset{3}{\tilde{Y}}_{ki}$ to $\overset{6}{\tilde{Y}}_{ki}$ are zero unless the indices i and k are equal.

$$\overset{3}{\tilde{Y}}_{ki} = \frac{s}{L} \int_0^L \phi_k \phi_i dz = \begin{cases} 0 & k \neq i \\ \frac{1}{2} & k = i \end{cases}$$

$$\overset{4}{\tilde{Y}}_{ki} = \frac{U}{U_0 \cdot L} \int_0^L \phi_k \phi_i dz = \begin{cases} 0 & k \neq i \\ \frac{1}{2} & k = i \end{cases}$$

$$\overset{5}{\tilde{Y}}_{ki} = \frac{U_s}{U_0 \cdot L} \int_0^L \phi_k \phi_i dz = \begin{cases} 0 & k \neq i \\ \frac{1}{2} & k = i \end{cases}$$

$$\overset{6}{\tilde{Y}}_{ki} = \frac{U^2_s}{U_0^2 \cdot L} \int_0^L \phi_k \phi_i dz U_s = \begin{cases} 0 & k \neq i \\ \frac{1}{2} & k = i \end{cases}$$

With respect to integrals $\overset{1}{\tilde{Y}}_{ki}$ and $\overset{2}{\tilde{Y}}_{ki}$ which are used in Equation (8-66), since the inverse of TTF in this equation is zero, there is no need to calculate these integrals.

Three dimensionless matrices $\underline{\underline{\tilde{\mathfrak{M}}}}$, $\underline{\underline{\tilde{C}}}$ and $\underline{\underline{\tilde{K}}}$ are to be calculated next. By substituting above magnitudes in Equation (8-64), $\underline{\underline{\tilde{\mathfrak{M}}}}$ emerges in the form of a matrix with four diagonal sub-matrices.

$$\underline{\underline{\tilde{\mathfrak{M}}}} = \begin{bmatrix} \tilde{\mathfrak{M}}_{11} I_{N \times N} & \tilde{\mathfrak{M}}_{12} I_{N \times N} \\ \tilde{\mathfrak{M}}_{21} I_{N \times N} & \tilde{\mathfrak{M}}_{22} I_{N \times N} \end{bmatrix}$$

$$\tilde{\mathfrak{M}}_{11} = \frac{1}{2}$$

$$\tilde{\mathfrak{M}}_{12} = -\frac{1}{2} S_r$$

$$\tilde{\mathfrak{M}}_{21} = -\frac{1}{2} S_r$$

$$\tilde{\mathfrak{M}}_{22} = \frac{1}{2} \gamma^2$$

where $I_{N \times N}$ is the identity matrix of size N . Replacing the variables in Equation (8-65) shows that similar to $\underline{\underline{\tilde{\mathfrak{M}}}}$, $\underline{\underline{\tilde{C}}}$ is also a matrix with four diagonal sub-matrices.

$$\underline{\underline{\tilde{C}}} = \begin{bmatrix} \tilde{C}_{11} I_{N \times N} & \tilde{C}_{12} I_{N \times N} \\ \tilde{C}_{21} I_{N \times N} & \tilde{C}_{22} I_{N \times N} \end{bmatrix}$$

$$\begin{aligned}\tilde{C}_{11} &= \frac{1}{2} A \left(\left. \frac{\partial C_L}{\partial \alpha} \right|_{\alpha=0} + C_D \Big|_{\alpha=0} \right) + \frac{\xi_y}{U_{ry}} & \tilde{C}_{12} &= -\frac{1}{2} AR_r \left(\left. \frac{\partial C_L}{\partial \alpha} \right|_{\alpha=0} + C_D \Big|_{\alpha=0} \right) \\ \tilde{C}_{21} &= -\frac{1}{2} A \left. \frac{-\partial C_{M(er)}}{\partial \alpha} \right|_{\alpha=0} & \tilde{C}_{22} &= \gamma^2 \frac{\xi_0}{U_{r0}} + \frac{1}{2} AR_r \left. \frac{-\partial C_{M(er)}}{\partial \alpha} \right|_{\alpha=0}\end{aligned}$$

Equation (8-66) reveals that in the uniform case, $\tilde{\underline{\underline{K}}}$ is also a matrix with diagonal sub-matrices.

$$\tilde{\underline{\underline{K}}} = \begin{bmatrix} \tilde{\underline{\underline{K}}}_{11} & \tilde{\underline{\underline{K}}}_{12} I_{N \times N} \\ 0 & \tilde{\underline{\underline{K}}}_{22} I_{N \times N} \end{bmatrix}$$

$$\tilde{\underline{\underline{K}}}_{11} = \begin{bmatrix} \ddots & 0 & 0 & 0 & 0 \\ 0 & \frac{(i-1)^4 \cdot FF + (i-1)^2}{2U_{ry}^2} & 0 & 0 & 0 \\ 0 & 0 & \frac{i^4 \cdot FF + i^2}{2U_{ry}^2} & 0 & 0 \\ 0 & 0 & 0 & \frac{(i+1)^4 \cdot FF + (i+1)^2}{2U_{ry}^2} & 0 \\ 0 & 0 & 0 & 0 & \ddots \end{bmatrix}_{N \times N}$$

$$\tilde{\underline{\underline{K}}}_{12} = -\frac{1}{2} A \left. \frac{\partial C_L}{\partial \alpha} \right|_{\alpha=0}$$

$$\tilde{\underline{\underline{K}}}_{22} = \frac{1}{2} A \left. \frac{-\partial C_{M(er)}}{\partial \alpha} \right|_{\alpha=0}$$

If these three matrices are substituted in characteristic Equation (8-67), it gives,

$$\begin{aligned}\det \left[\tilde{\underline{\underline{\mathfrak{M}}}} \tilde{\lambda}^2 + \tilde{\underline{\underline{C}}} \tilde{\lambda} + \tilde{\underline{\underline{K}}} \right] &= \det \begin{bmatrix} \left(\tilde{\mathfrak{M}}_{11} \tilde{\lambda}^2 + \tilde{C}_{11} \tilde{\lambda} \right) I_{N \times N} + \tilde{\underline{\underline{K}}}_{11} & \left(\tilde{\mathfrak{M}}_{12} \tilde{\lambda}^2 + \tilde{C}_{12} \tilde{\lambda} + \tilde{\underline{\underline{K}}}_{12} \right) I_{N \times N} \\ \left(\tilde{\mathfrak{M}}_{21} \tilde{\lambda}^2 + \tilde{C}_{21} \tilde{\lambda} \right) I_{N \times N} & \left(\tilde{\mathfrak{M}}_{22} \tilde{\lambda}^2 + \tilde{C}_{22} \tilde{\lambda} + \tilde{\underline{\underline{K}}}_{22} \right) I_{N \times N} \end{bmatrix} = \\ &= \det \left[\left(\left(\tilde{\mathfrak{M}}_{11} \tilde{\lambda}^2 + \tilde{C}_{11} \tilde{\lambda} \right) I_{N \times N} + \tilde{\underline{\underline{K}}}_{11} \right) \cdot \left(\tilde{\mathfrak{M}}_{22} \tilde{\lambda}^2 + \tilde{C}_{22} \tilde{\lambda} + \tilde{\underline{\underline{K}}}_{22} \right) I_{N \times N} - \right. \\ &\quad \left. \left(\tilde{\mathfrak{M}}_{12} \tilde{\lambda}^2 + \tilde{C}_{12} \tilde{\lambda} + \tilde{\underline{\underline{K}}}_{12} \right) I_{N \times N} \cdot \left(\tilde{\mathfrak{M}}_{21} \tilde{\lambda}^2 + \tilde{C}_{21} \tilde{\lambda} \right) I_{N \times N} \right] = \\ &= \det \left[\left(\tilde{\mathfrak{M}}_{11} \tilde{\lambda}^2 + \tilde{C}_{11} \tilde{\lambda} \right) \cdot \left(\tilde{\mathfrak{M}}_{22} \tilde{\lambda}^2 + \tilde{C}_{22} \tilde{\lambda} + \tilde{\underline{\underline{K}}}_{22} \right) I_{N \times N} + \right. \\ &\quad \left(\tilde{\mathfrak{M}}_{22} \tilde{\lambda}^2 + \tilde{C}_{22} \tilde{\lambda} + \tilde{\underline{\underline{K}}}_{22} \right) \tilde{\underline{\underline{K}}}_{11} - \\ &\quad \left. \left(\tilde{\mathfrak{M}}_{12} \tilde{\lambda}^2 + \tilde{C}_{12} \tilde{\lambda} + \tilde{\underline{\underline{K}}}_{12} \right) \cdot \left(\tilde{\mathfrak{M}}_{21} \tilde{\lambda}^2 + \tilde{C}_{21} \tilde{\lambda} \right) I_{N \times N} \right] = 0\end{aligned}$$

Since $I_{N \times N}$ and \tilde{K}_{11} are both diagonal matrices, the last expression is the determinant of a diagonal matrix which that equals to the product of diagonal elements. This means to find $\tilde{\lambda}$, each of diagonal terms should be set to zero. This results in N fourth degree equations of $\tilde{\lambda}$. For instance, for i^{th} diagonal element it states,

$$\begin{aligned} & (\tilde{\mathfrak{M}}_{11}\tilde{\lambda}^2 + \tilde{C}_{11}\tilde{\lambda}) \cdot (\tilde{\mathfrak{M}}_{22}\tilde{\lambda}^2 + \tilde{C}_{22}\tilde{\lambda} + \tilde{K}_{22}) + (\tilde{\mathfrak{M}}_{22}\tilde{\lambda}^2 + \tilde{C}_{22}\tilde{\lambda} + \tilde{K}_{22})\tilde{k}_{ii} + \\ & (\tilde{\mathfrak{M}}_{12}\tilde{\lambda}^2 + \tilde{C}_{12}\tilde{\lambda} + \tilde{K}_{12}) \cdot (\tilde{\mathfrak{M}}_{21}\tilde{\lambda}^2 + \tilde{C}_{21}\tilde{\lambda}) = 0 \end{aligned}$$

Substituting scalar parameters in above equation and re-arranging the result leads to a quartic characteristic equation,

$$\sum_{i=1}^4 \tilde{c}_i \tilde{\lambda}^i = 0 \quad 8-68$$

$$\tilde{c}_4 = [\gamma^2 - S_r^2]$$

$$\tilde{c}_3 = \left[A(S_r - R_r) \frac{\partial C_{M(cr)}}{\partial \alpha} \Big|_{\alpha=0} + A(\gamma^2 - R_r S_r) \left(\frac{\partial C_L}{\partial \alpha} \Big|_{\alpha=0} + C_D \Big|_{\alpha=0} \right) + 2\gamma^2 \left(\frac{\xi_y}{U_{ry}} + \frac{\xi_\theta}{U_{r\theta}} \right) \right]$$

$$\begin{aligned} \tilde{c}_2 = & \left[\frac{\gamma^2 G}{U_{ry}^2} - A \left(1 + 2R_r \frac{\xi_y}{U_{ry}} \right) \frac{\partial C_{M(cr)}}{\partial \alpha} \Big|_{\alpha=0} + 2A\gamma^2 \frac{\xi_\theta}{U_{r\theta}} \left(\frac{\partial C_L}{\partial \alpha} \Big|_{\alpha=0} + C_D \Big|_{\alpha=0} \right) + 4\gamma^2 \frac{\xi_y}{U_{ry}} \frac{\xi_\theta}{U_{r\theta}} + \right. \\ & \left. - AS_r \frac{\partial C_L}{\partial \alpha} \Big|_{\alpha=0} \right] \end{aligned}$$

$$\tilde{c}_1 = \left[-A \left(2 \frac{\xi_y}{U_{ry}} + \frac{R_r G}{U_{ry}^2} \right) \frac{\partial C_{M(cr)}}{\partial \alpha} \Big|_{\alpha=0} + 2 \frac{\gamma^2 G}{U_{ry}^2} \frac{\xi_\theta}{U_{r\theta}} - A^2 \frac{\partial C_{M(cr)}}{\partial \alpha} \Big|_{\alpha=0} C_D \Big|_{\alpha=0} \right]$$

$$\tilde{c}_0 = \left[-A \frac{G}{U_{ry}^2} \frac{\partial C_{M(cr)}}{\partial \alpha} \Big|_{\alpha=0} \right]$$

where G is related to the ratio of flexural and tensile stiffness for i^{th} mode, i.e. when only $\phi_i(z)$ is used in approximating $y(z, t)$ and $\theta(z, t)$,

$$G = i^4 \cdot FF + i^2$$

Apart from the appearance of parameter G, these coefficients are very similar to those of a 2D case. More precisely, in the case tension is predominant in the riser's stiffness and the effect of flexural stiffness is negligible, i.e. $FF = 0$, then the 2D

analysis is identical to the 3D analysis of a uniform problem for the first mode where $G = 1$.

8.4 Verification

As part of the VIV research activities NDP (Norwegian Deepwater Programme), a series of cylinder tests was carried out at MARINTEK to investigate the effectiveness of fairings (Braaton et al., 2008). This work was partly a follow up activity to the work reported by Slocum et al (2004).

A top tensioned flexible riser was tested with two different fairing designs in uniform current profile at different towing speeds. The riser model was made of a fibreglass reinforced pipe with the length of 9.324 m, the outer diameter of 20 mm and the wall thickness of 1.5 mm.

In part of this study, the riser model was fully covered with Fairing II. This fairing was similar to the one used in Slocum et al (2004) in terms of section profile and it was smaller in scale by a factor of about 6.4 (see Figure 5-3 and Figure 8-3). They had a span length of 88.2 mm, a chord length of 84 mm and maximum nose thickness of 36 mm. The given specifications of the test set-up are presented in Table 8-1 and Table 8-2. The ratio of fairing's span to riser's length is 0.009 and therefore using the continuous model is valid.

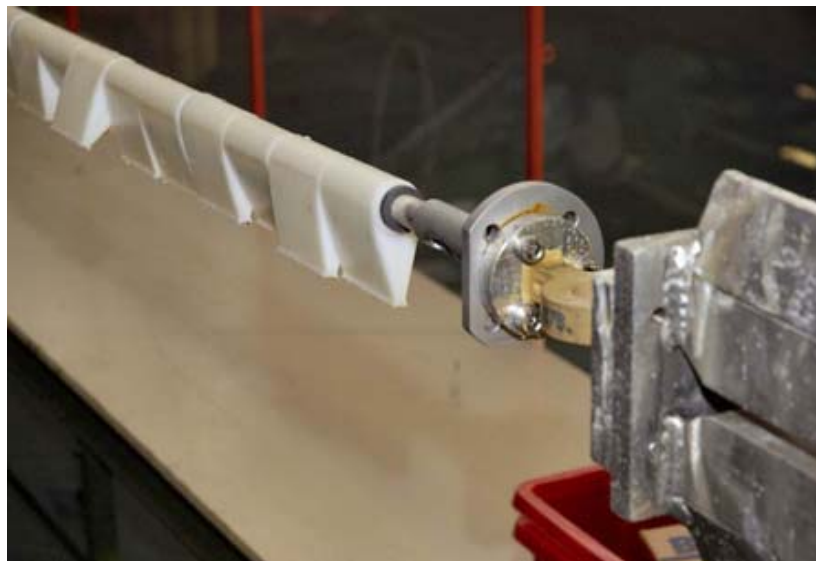


Figure 8-3 Fairing II on The Flexible Riser Model (Braaton et al., 2008).

Table 8-1 Riser Model Data.

Parameter	Dimension
Total length between pinned ends	9.324 m
Outer diameter	20 mm
Wall thickness of pipe	1.5 mm
Bending stiffness, EI	90.1 Nm ²
Young modulus for pipe, E	2.4 10 ¹⁰ N/m ²
Axial stiffness, EA	2.09 10 ⁶ N
Mass of riser (flooded)	0.518 kg/m
Axial tension (top/bottom)	670/640 kN

Table 8-2 Faring II Data.

Parameter	Dimension
Chord length	84 mm
Maximum thickness	36 mm
Span-wise length of section	88.2 mm
Number of sections	96
Chord length to thickness ratio	2.33
Mass in air	1.170 kg/m
Weight in water	0.000 N/m
Mass of riser (flooded) with fairings	1.579 kg/m
Pre-tension (top/bottom)	625/603 N
Reynolds number range	3200-95000

Detailed specifications of the fairing and clamping system are not given in the paper. Thus, it is necessary to approximate the required dimensionless parameters based on equations derived in Section 6.2(A). To check the estimation with real data, masses of the flooded riser alone and with fairing on are used as the benchmark.

Calculation of the flooded riser mass shows that the density of pipe is 3350 kg/m³. The fairing in this test is not thin shell and hollow section. To match the equations with this case, the density of the fairing and entrapped water are assumed equal and an imaginary thickness of 1 mm is considered for the fairing plate. Calculation of the flooded riser mass fitted with fairing indicates that the average density of the fairing material including the clamping system is 750 kg/m³. All the required variables to calculate dimensionless parameters are summarised below.

8. 3D Theoretical Model

$$\rho = 1000 \text{ kg/m}^3$$

$$\rho_b = 750 \text{ kg/m}^3$$

$$\rho_s = 3350 \text{ kg/m}^3$$

$$\rho_{fr} = 750 \text{ kg/m}^3$$

$$\rho_f = 1000 \text{ kg/m}^3$$

$$t_{fr} = 0.001 \text{ m}$$

$$r_s = 0.010 \text{ m}$$

$$r_f = 0.0085 \text{ m}$$

$$r_t = 0.018 \text{ m}$$

$$r_b = 0.017 \text{ m}$$

$$b = 0.0047 \text{ m}$$

$$c = 0.084 \text{ m}$$

$$d = 0.0239 \text{ m}$$

$$L_{fr} = 0.0677 \text{ m}$$

By using the above estimated variables, the calculated masses compare well to the real values in Table 8-3.

Table 8-3 Accuracy of Calculated Mass vs. Measured Values.

Parameter	Measured (kg/m)	Calculated (kg/m)
Mass of flooded riser	0.518	0.519
Mass of flooded riser with fairing	1.579	1.662
Mass of fairing in air	1.170	1.144

The above estimated values give the structural dimensionless parameters as below.

$$A = 0.4894$$

$$\gamma^2 = 0.1006$$

$$S_r = 0.2613$$

With regard to Mass Factor, the added mass coefficient of a bare cylinder in theory is

1. Accordingly, Mass Factor will be worked out as,

$$MF = \frac{m_r + m_{ar}}{m + m_a} = 0.116$$

The Young modulus of the pipe along with the top end and bottom end tensions are given. Thus, wet weight of the system, natural transverse frequency and parameters FF and TTF can be easily calculated.

$$w_r = (T_t - T_b)/L = 2.197 \text{ N}$$

$$\omega_y = 3.142 \text{ (rad/s)}$$

$$FF = 0.0164$$

$$TTF = 28.410$$

No hydrodynamic characteristic was measured in the test; however, the fairing section is similar to Slocum et al (2004). Thus, regardless of the Reynolds number effect in the subcritical range, hydrodynamic properties of this fairing are assumed to be identical to previous one. That is,

$$R_r = 0.40$$

$$C_{D|_0} = 0.176$$

$$\partial C_L / \partial \alpha|_0 = 1.146 \quad (1/\text{rad})$$

$$\partial C_{M(cr)} / \partial \alpha|_0 = -0.0344 \quad (1/\text{rad})$$

The typical drag coefficient for a bare cylinder when calculated based on diameter is about 1.2. In the present formulation, it needs to be scaled to the fairing chord length.

$$C_{Dr} = 1.2 \times (20\text{mm}/84\text{mm}) = 0.286$$

With respect to damping, contrary to rigid cylinder tests, a flexible riser experiences noticeable deformation and therefore contributes in the transverse damping of the system. Thus, to be on the safe margin the lower limit of reported in-water damping for a riser fitted with a fairing, i.e. 0.10 to 0.18 (Lee et al., 2004b), is selected.

In the research it is emphasised that the fairing is free to rotate, therefore the positive role of torsional frictional damping is ignored.

$$\xi_y = 10 \%$$

$$\xi_\theta = 0 \%$$

The entire riser was outfitted with fairings and exposed to uniform current profile.

$$U = U_o$$

For the above parameters and by considering the first five modes, the 3D analytical model developed in this chapter predicts that the system goes unstable at $U_{cr} = 0.72$. Figure 8-4 shows that in this example U_{cr} is not sensitive to the number of considered first few modes. With reference to definition of U_{ry} , this critical reduced velocity is equal to towing speed of 0.19 m/s.

$$U_o = U_{ry} \cdot \omega_y \cdot c = 0.72 \times 3.142 \times 0.84 = 0.19 \text{ m/s}$$

Test results (Figure 8-5) show that the amplitude of vibration for Fairing II has two peaks. The onset of increasing amplitude for the first peak occurs at towing speed of about 0.20 m/s and for the second peak about 0.60 m/s. Despite some approximation in parameters, the theoretical model anticipated the range of velocity of the first peak accurately. Nevertheless, the important question is that whether this large amplitude vibration happens due to VIV or instability of the system.

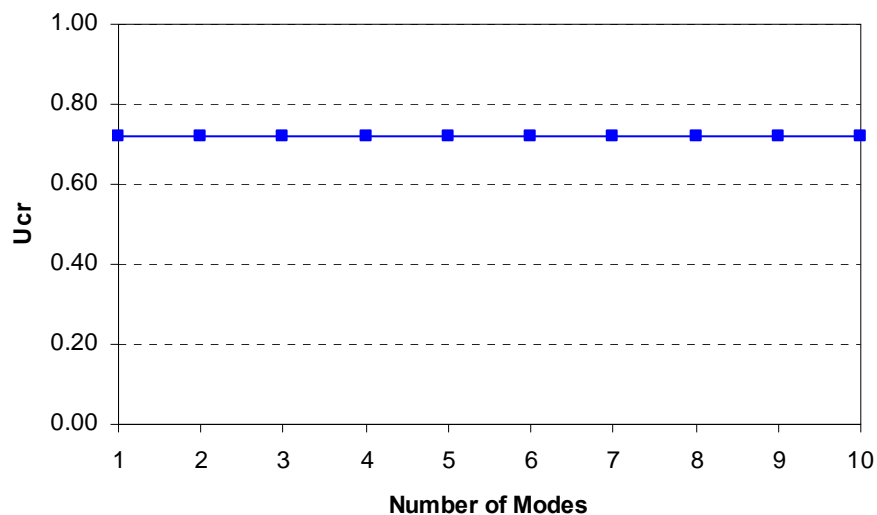


Figure 8-4 Effect of Considering Limited Number of Modes.

The frequency of predominant vibration was also measured in the test. Figure 8-6 shows this frequency along with the predicted vortex-shedding frequency for Fairing II (fs_2). In this figure, the measured frequency of vibration for the bare riser is very close to the predicted frequency of VIV (fs_1) and confirms that oscillation of the bare riser was due to VIV. On the contrary, the frequency of vibration for Fairing II at two amplitude peaks is less than fs_2 and it can be concluded that they indicate the instability of the system and not VIV.

Although the predicted instability coincides with the velocity range of large amplitude vibration in the above test, it is still difficult to make a judgment on the validity of the model for other cases due to external factors. For example, lack of repeated test data raises the question about reliability and approximating mass, added mass, natural frequency and hydrodynamic coefficients have left some uncertainties both in the model test and also in the assumed parameters. In addition, the ability of the model in more complex conditions, like sheared flow profile and partly coverage of the riser with fairing, remains to be verified against further model tests.

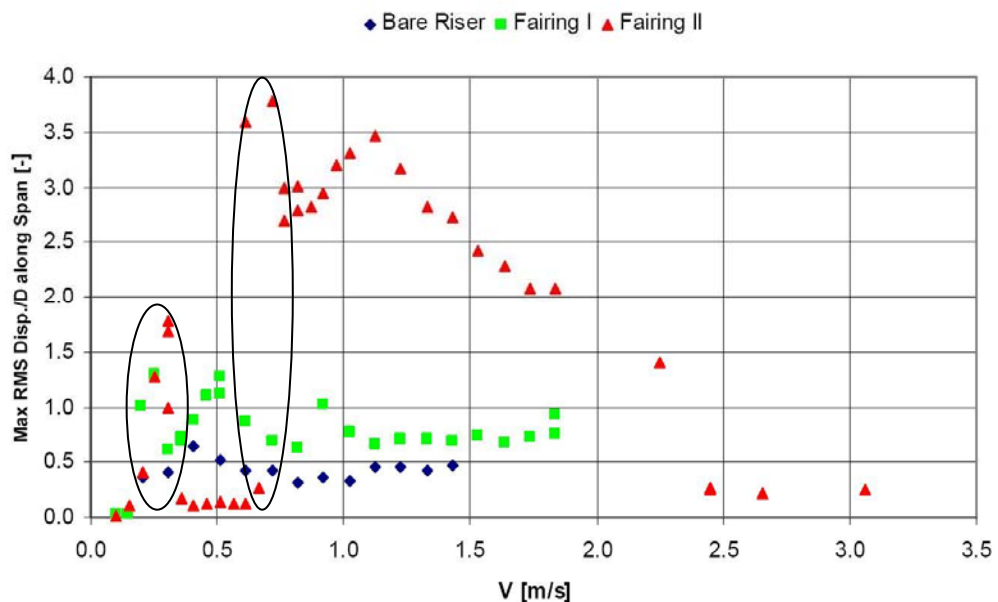


Figure 8-5 Threshold of Instability Onset, Test Results (Braaton et al., 2008).

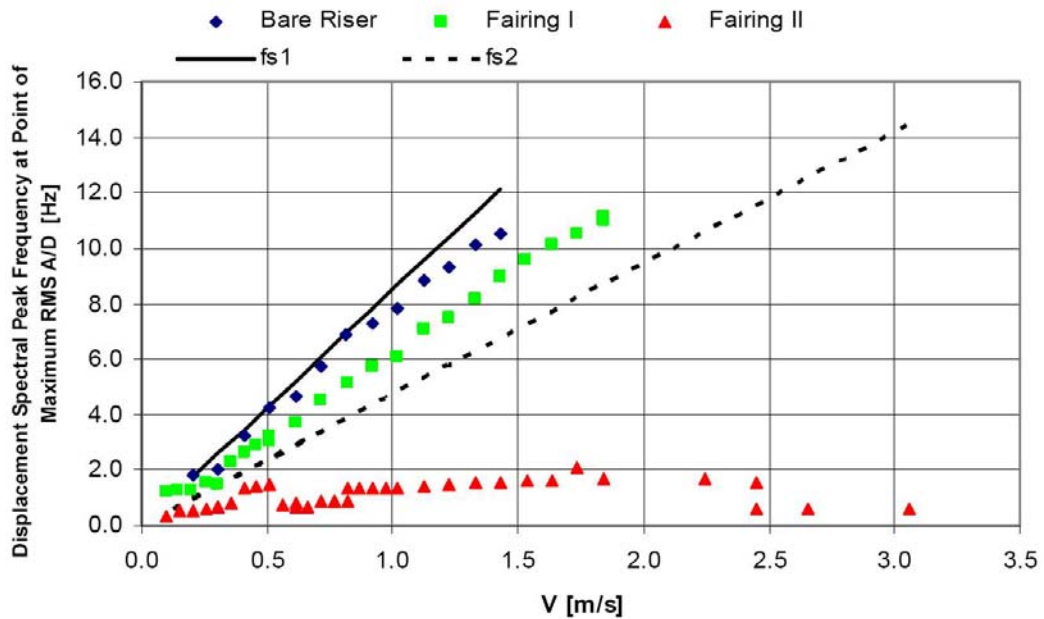


Figure 8-6 Frequency of Predominant Vibration, Test Results (Braaton et al., 2008).

8.5 Comments

In this chapter, an analytical model was developed for a top tensioned riser in general form. This model was applied to a tank test and predicted the threshold of instability reasonably well.

In the general case, the selected shape functions in Galerkin's method are orthogonal, but since some variables like tension and current velocity varies over the length, the resultant equations are coupled and the final vibration mode (eigenvector) is a combination of mode shapes. Thus, it is not possible to distinguish the unstable mode and say which mode goes unstable first. In other words, in the general case what can be determined is merely the critical reduced velocity, U_{cr} .

The other important issue is the convergence of the result versus number of considered modes. The rate of convergence may vary from case to case but it should be noted that lower modes must be always considered while the number of modes is being increased for the sake of convergence. Otherwise, it is very likely to miss the

lowest current velocity which entails instability of the system. For instance, Figure 8-7 shows the lowest U_{cr} versus different set of five modes for the example used in this chapter for verification.

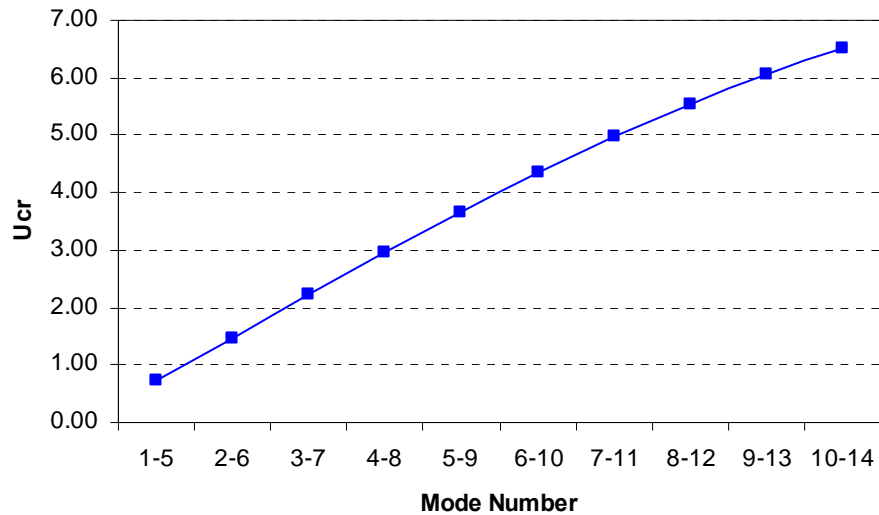


Figure 8-7 Effect of Missing Lower Modes in U_{cr} .

The complicated model of the general case was simplified for the uniform case. In this specific case, the characteristic equation turned into independent equations for each mode. This equation was identical to the characteristic equation in the 2D case except the emergence of a new term which stated the influence of using different modes.

To track the effect of this parameter in the critical velocity of a uniform case, an example is considered in which all parameters along the riser are equal to the corresponding value at the top end of the riser used in this chapter. Figure 8-8 demonstrates the trend of U_{cr} versus the mode number in uniform conditions. This figure shows that by increasing the mode number, U_{cr} rises too and after the first few modes, the critical reduced velocity is so high that there may exist no sea current velocity to excite the instability of higher modes. This figure also clarifies how taking the flexural stiffness into account influences U_{cr} in each mode. In general, the

effect of flexural stiffness in raising U_{cr} becomes more noticeable as the mode number increases.

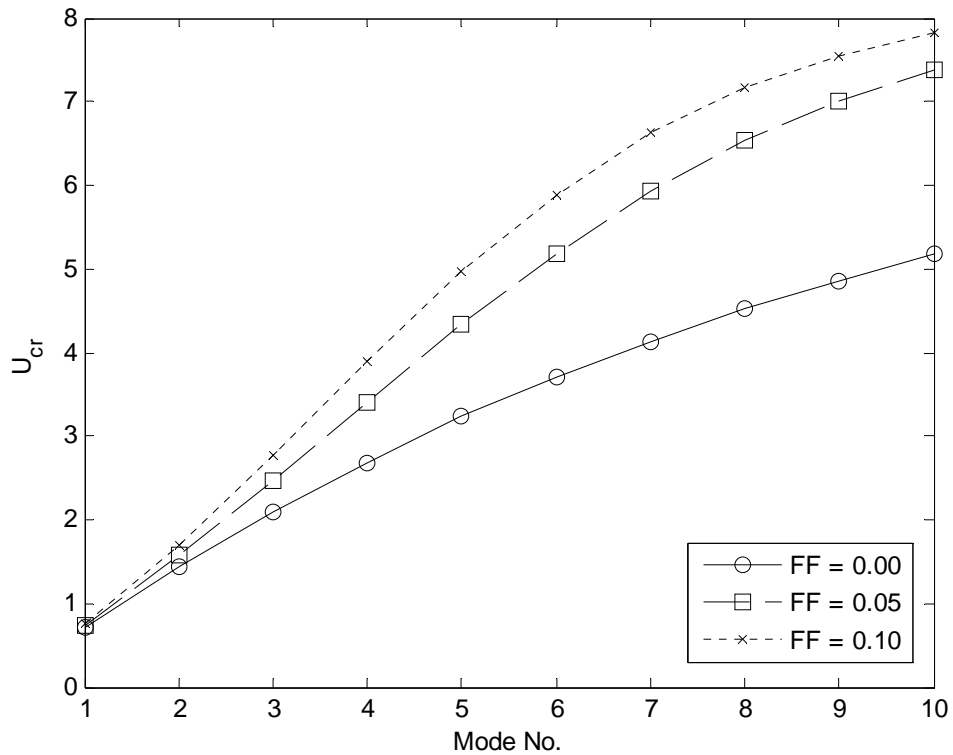


Figure 8-8 U_{cr} vs. Mode Number, Uniform Case.

This chapter centred on developing the 3D analytical model for fairing instability. The effects of some parameters like fairing hydrodynamic characteristics on critical velocity were already investigated for 2D model in Chapter 6. The next chapter will check if these effects are the same in the 3D model and will also discuss the influences of new parameters which emerged in this chapter such as current profile and coverage length.

3D Example and Parametric Study

Numerical examples are discussed in this chapter. At first, the general conditions will be considered and the critical current velocity will be calculated. Then, the effect of dimensionless parameters will be assessed in order to evaluate the consistency of the 2D study with this case. Finally, the influences of new parameters emerging from considering the third dimension will be investigated too.

9.1 Introduction

The preceding chapter explored the governing equations of the riser and fairing system in real conditions, i.e. three-dimensional form. An analytical model was developed for stability of this system in general conditions. This model led to such complicated characteristic equations that predicting the effect of different parameters in improving or deteriorating the stability of the system was not straightforward.

Further investigation indicated that in the case of considering uniform conditions for all variables along the riser length, this complex characteristic equation will be simplified to that of a 2D problem but with the emergence of a new parameter. Therefore, the parametric study carried out in the 2D case holds here as well and there is no need to repeat it again. The only difference refers to the new parameter, G . It was already demonstrated that in uniform conditions higher mode results in higher critical velocity. This is the case for higher values of the Flexural Factor too. In summary, it can be concluded that as parameter G increases, so does the critical velocity.

Now, it is time to apply the 3D analytical model to a real general case and assess how each parameter impacts the stability.

9.2 An Example of the General Case

Specifications of a real drilling riser working off the coast of Brazil were presented in Section 6.3. Grant and Patterson states in their paper that this riser was deployed in water of 500 feet (152.4 m) depth without installation of buoyancy modules (Grant and Patterson, 1977). In this example, this riser will be considered in a water of double depth, i.e. 300 m. Thus, in order to keep the tension in the same range, it is necessary to implement the buoyancy module as well.

Buoyancy materials are in various forms. For instance, in water depths no more than 600 m they vary from typical materials weighing about 771 kg/m^3 to ultra-light materials (353 kg/m^3) and super ultra-light materials (320 kg/m^3) (Wang and Watkins, 2004). In this example, “Standard Density” material 24 lb/ft^3 (384 kg/m^3) from Cuming corporation brochure is selected.

Tension at the top end of the riser (T_t) is 1471 kN. The bottom end tension will be calculated later based on the wet weight of the system.

The CFD analysis of a few fairing sections in Chapter 7 indicated that the guide vane is one of the profiles that satisfy the necessary conditions for stability. Moreover, it benefits from the relatively short chord length which facilitates the operational conditions. Hence, this fairing is chosen for this example. If the impact of Reynolds number on hydrodynamic coefficients is ignored, the use of this profile means,

$$\text{Angle of leeward} = 6^\circ$$

$$t/c = 0.67$$

$$R_r = 0.40$$

$$C_D|_0 = 0.329$$

$$\partial C_L / \partial \alpha|_0 = 1.432 \quad (1/\text{rad})$$

$$\partial C_{M(\text{cr})} / \partial \alpha|_0 = -0.309 \quad (1/\text{rad})$$

Fairing shell of 10 mm thickness is fabricated from reinforced fibreglass (1500 kg/m³). Based on what is mentioned above, all design parameters are summarised below (For definition of parameters, reader is referred to Section 6.2(A)).

$$\rho = 1025 \text{ kg/m}^3$$

$$\rho_b = 384 \text{ kg/m}^3$$

$$\rho_s = 7850 \text{ kg/m}^3$$

$$\rho_{fr} = 1500 \text{ kg/m}^3$$

$$\rho_f = 1795.97 \text{ kg/m}^3$$

$$t_{fr} = 0.010 \text{ m}$$

$$r_s = 0.3048 \text{ m}$$

$$r_f = 0.2648 \text{ m}$$

$$r_t = 0.5080 \text{ m}$$

$$r_b = 0.4980 \text{ m}$$

$$b = 0.804 \text{ m}$$

$$c = 1.516 \text{ m}$$

$$d = 0.250 \text{ m}$$

$$L_{fr} = 1.014 \text{ m}$$

By using the equations derived in Section 6.2(A), structural dimensionless parameters are obtained.

$$\gamma^2 = 0.0699$$

$$S_r = 0.1577$$

$$A = 0.3298$$

With reference to the discussion presented in Section 6.2(B), damping ratios are selected in the midrange.

$$\xi_y = 0.10$$

$$\xi_\theta = 0.05$$

The riser length is 300 m and the wet weight of flooded system is calculated as 3.6 kN per unit length. Young's modulus for steel riser is 212×10^9 N/m². Accordingly, bottom tension and three dimensionless factors of TTF, FF and MF are easily calculated,

$$\text{TTF} = 1.362$$

$$\text{FF} = 0.0461$$

$$\text{MF} = 0.5438$$

$$T_b = 39.85 \text{ tons}$$

Natural frequency of transverse vibration in water is obtained from Equation (8-46),

$$\omega_y = 0.2125 \text{ (rad/s)}$$

Finally, if the drag coefficient of a circular cylinder, i.e. bare riser with buoyancy module of 0.5046m radius, is assumed as 1.2, the scaled drag coefficient with respect to the fairing chord length is,

$$C_{Dr} = 1.2 \times (2 \times 0.5046\text{m} / 1.516\text{m}) = 0.799$$

This riser system is exposed to a sheared current in which the current velocity at the bottom end of the riser is equal to 20% of that at the top end. If U_o is measured at the top end of the riser, the current profile for a riser of unit length will be,

$$U = U_o \times (0.8 \times Z + 0.2)$$

To produce a general problem, it is assumed that the upper half of the riser is fitted with fairings.

All parameters required in the model are now available. By considering the first three modes, the analytical model anticipates that this system goes unstable when the reduced velocity (U_{ry}) exceeds 1.98. Figure 9-1 shows that in this example the first three modes are the minimum required number of modes to achieve the convergence in result and obtain U_{cr} accurately. The solutions to characteristic equation of stability are plotted in Figure 9-2 for each velocity increment.

With reference to the definition of reduced velocity and by substitution of natural frequency and fairing chord length in Equation (8-54), this model predicts that the

system is prone to instability when the current velocity at the top end, where U_o is measured, is about 0.64 m/s.

$$U_o = U_{ry} \cdot \omega_y \cdot c = 1.98 \times 0.2125 \times 1.516 = 0.64 \text{ m/s}$$

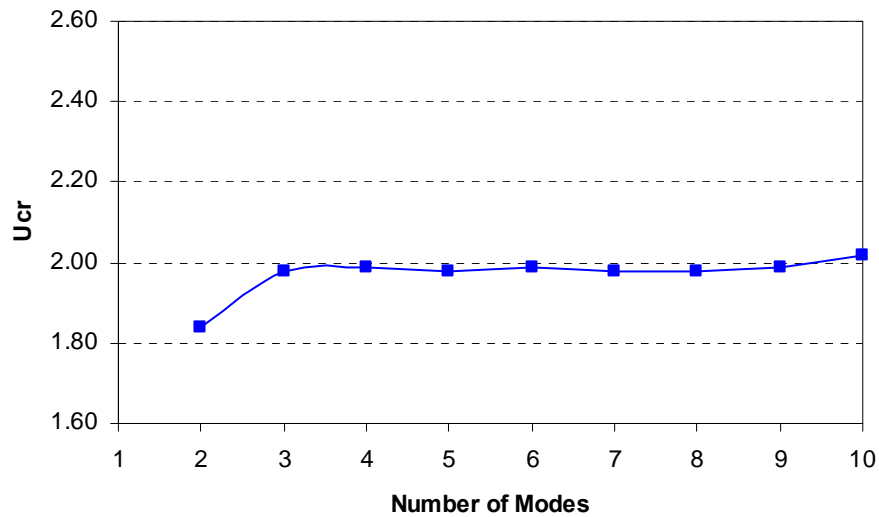


Figure 9-1 Effect of Considering Limited Number of Modes.

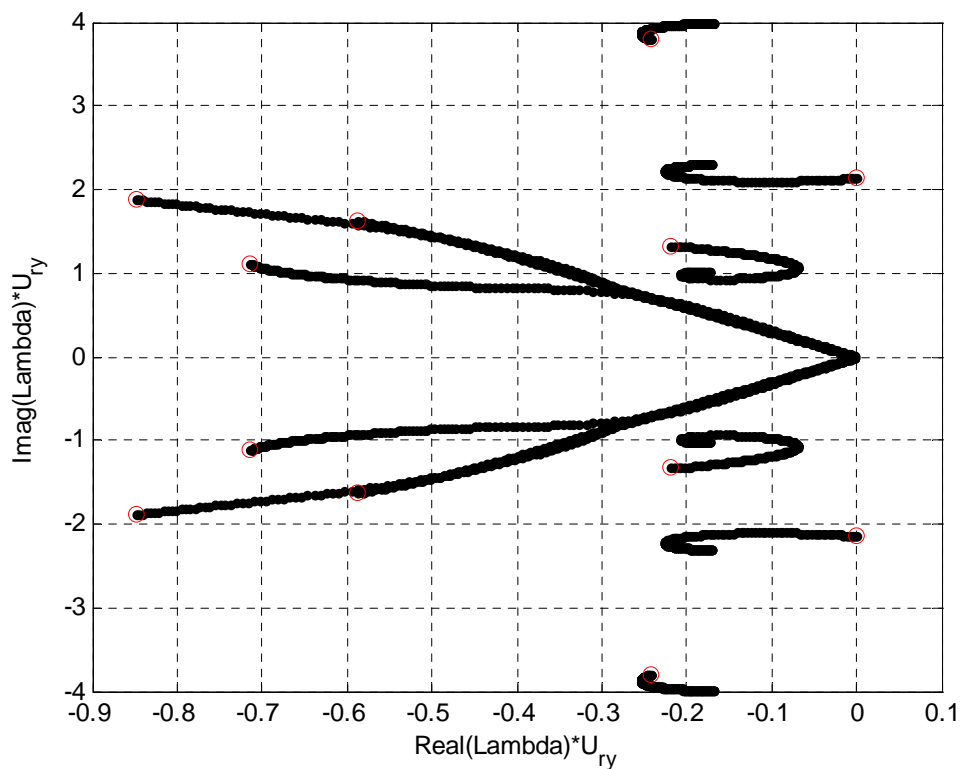


Figure 9-2 Trajectory of Eigenvalues, General Case, First 3 Modes.

9.3 Parametric Study

A parametric study on the 2D model was carried out in Chapter 6. As emphasised earlier, the 2D model is very similar to the 3D model in the uniform case and therefore the results of that parametric study is valid here and there is no need to repeat them.

However, as the 3D problem moves toward general conditions, it is necessary to investigate to ascertain whether those results are still applicable to 3D conditions or not. To this end, this section will first explore the effect of common parameters and compare the trend of variations in the general case with that in the 2D model. Then the impact of new parameters emerging in the 3D model will be probed as well.

The general example explained earlier in this chapter is used for this parametric study. Similarly the first three modes are selected and each parameter varies in the range of 50% to 150% of the present values unless otherwise stated. The red circle in the following figures shows the base case.

(A) Common Parameters

There are many dimensionless parameters in the 3D model which were already defined in the 2D model too. Their physical meaning was illustrated in Chapter 6. In the following, the trend of stability versus variation of these parameters in the 3D model is compared with that in the 2D model.

Effect of Drag, C_d

The variation of critical reduced velocity (U_{cr}) versus drag coefficient is plotted in Figure 9-3. This graph does not show a remarkable adverse impact of drag in the stability of the system. Comparison of this plot with Figure 6-6 reveals that it was the case for the 2D model as well. It was explained there, that it might be due to the fact that the sum of drag and lift slope forms the hydrodynamic damping terms and as the drag is small relative to lift slope, its impact is not tangible.

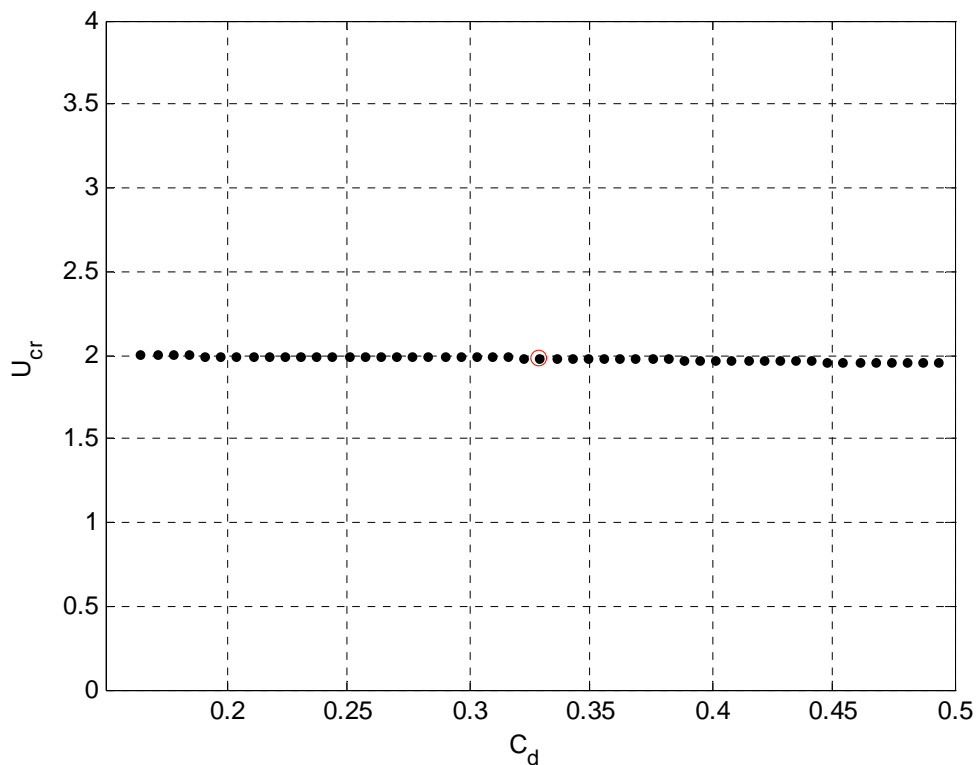


Figure 9-3 U_{cr} vs. Drag Coefficient, 3D Model.

Effect of Lift, $\partial C_L/\partial \alpha$

The 2D parametric study indicated that an increase in the slope of the lift coefficient curve makes the system more vulnerable and results in lower U_{cr} (see Figure 6-7) (Khorasanchi and Huang, 2009). Figure 9-4 confirms this fact in the 3D case where a decreasing non-linear relationship with evidence of a discrete drop is observed when $\partial C_L/\partial \alpha$ changes from 82% of its value in base case to 84% of that. Further investigation showed that this is due to the change of the instable mode as shown in Figure 9-5. In this figure, the eigenvalue which first crosses the imaginary axis is highlighted by an ellipse. Therefore, an increase of the lift coefficient entails the mode change and in each mode causes U_{cr} to decline.

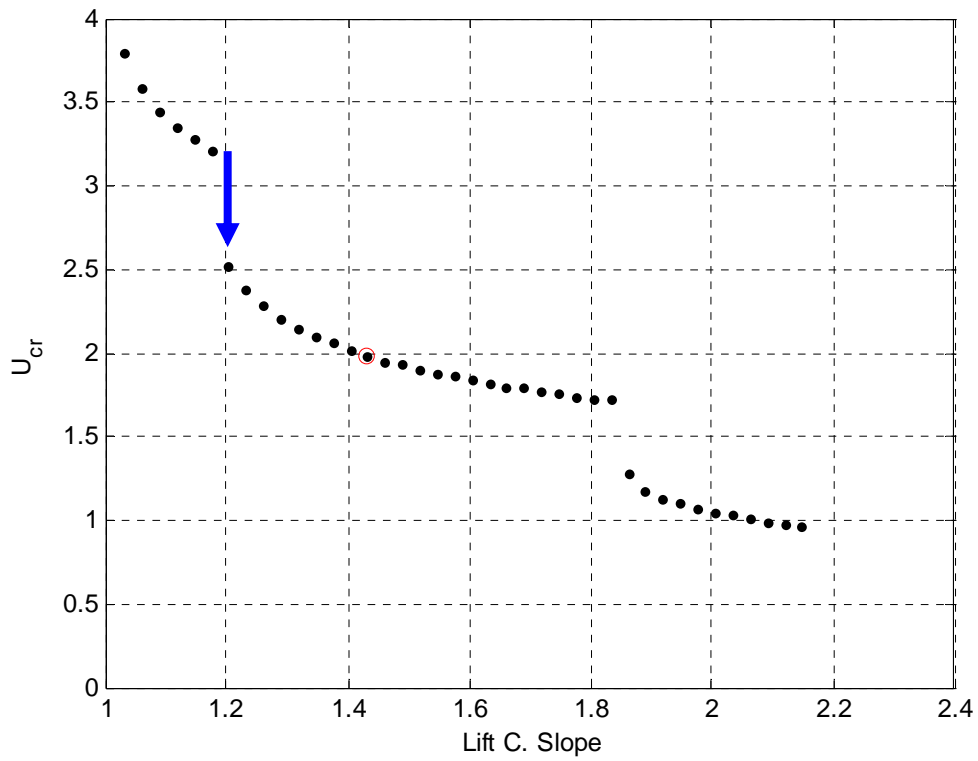


Figure 9-4 U_{cr} vs. Lift Coefficient, 3D Model.

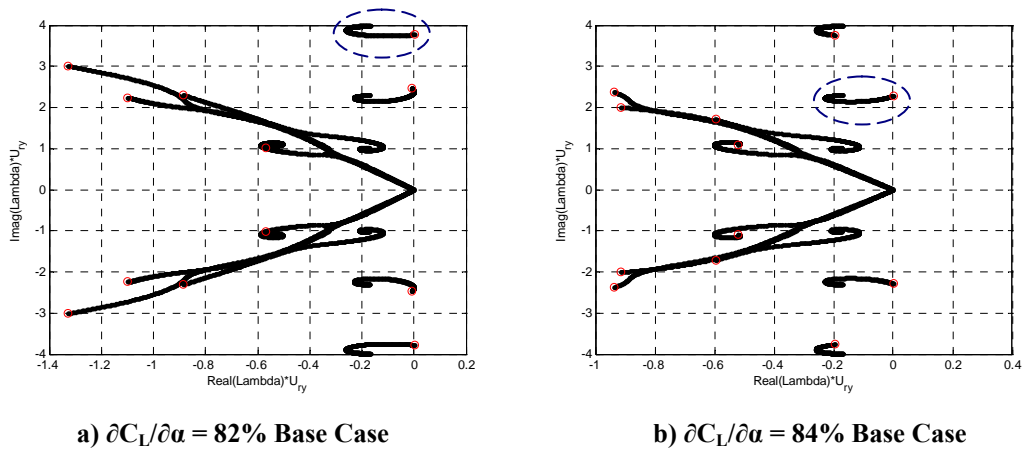


Figure 9-5 Mode Change Due to Increase of Lift Coefficient, 3D Model.

Effect of Moment, $\partial C_M/\partial \alpha$

Figure 6-8 in the 2D study showed that for small moment slope, its increase led to lower U_{cr} but then the trend of variation changed and moment slope improved the

stability. The present 3D example is consistent with the second part of this graph. In Figure 9-6, U_{cr} grows when the absolute value of the moment coefficient increases. Again there is a discrete movement in the smooth curve which is due to mode change as presented in Figure 9-7.

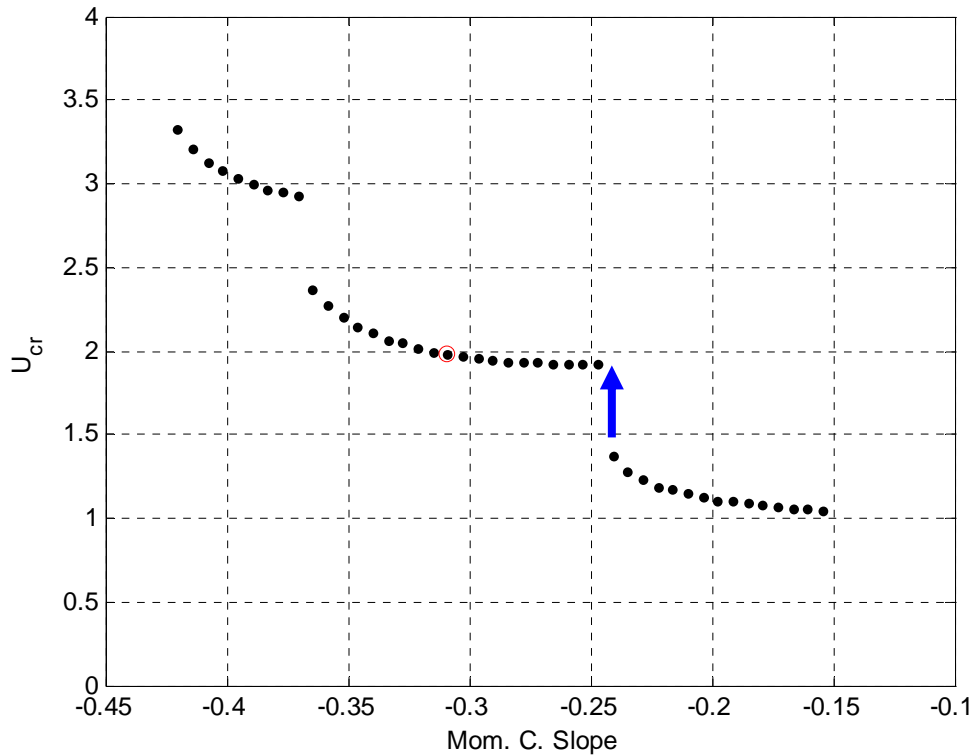
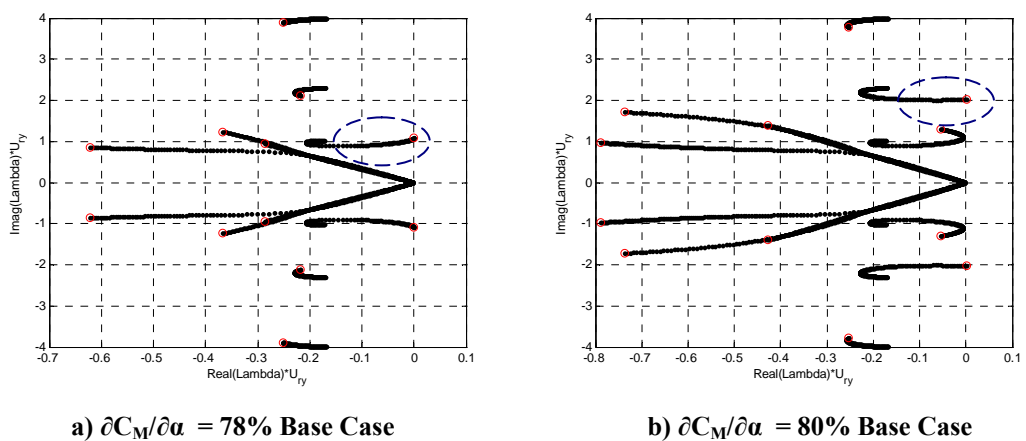


Figure 9-6 U_{cr} vs. Moment Coefficient, 3D Model.



a) $\partial C_M / \partial \alpha = 78\%$ Base Case

b) $\partial C_M / \partial \alpha = 80\%$ Base Case

Figure 9-7 Mode Change Due to Increase of Moment Coefficient, 3D Model.

Effect of Transverse Damping

In conformity with Figure 6-10, transverse damping improves the stability status in the 3D case as well. In Figure 9-8, U_{cr} rises up with higher damping ratios.

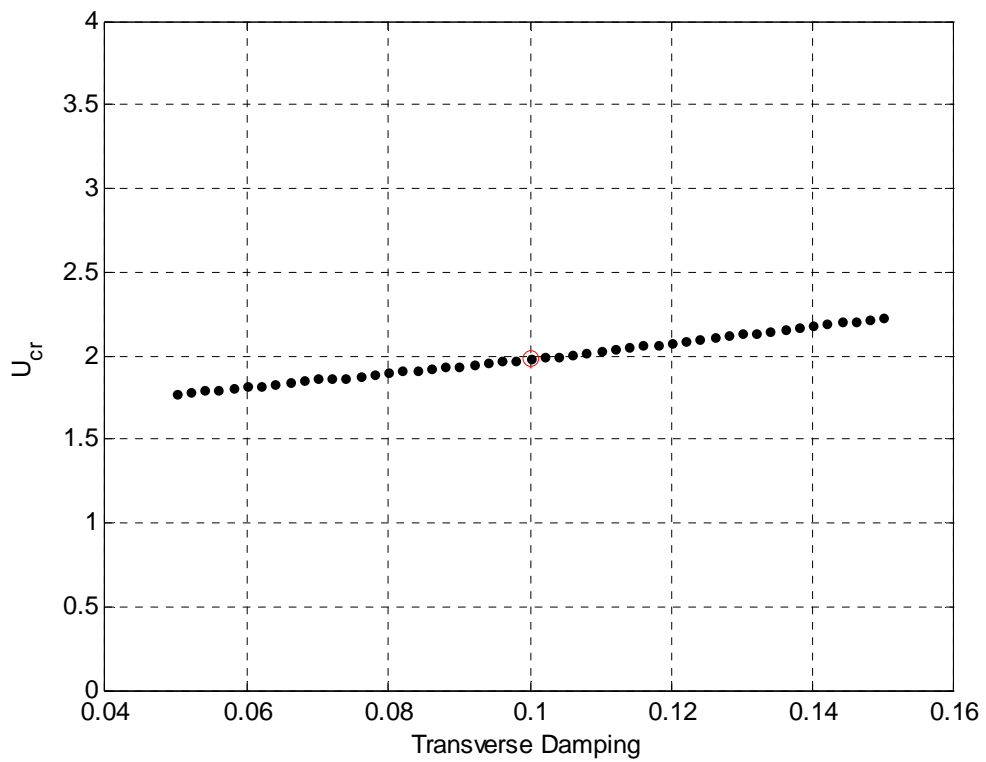


Figure 9-8 U_{cr} vs. Transverse Damping, 3D Model.

Effect of Torsional Damping

Torsional damping plays a positive role in confining the instability. This was already observed for the 2D model in Figure 6-11 and was repeated for the 3D model in Figure 9-9.

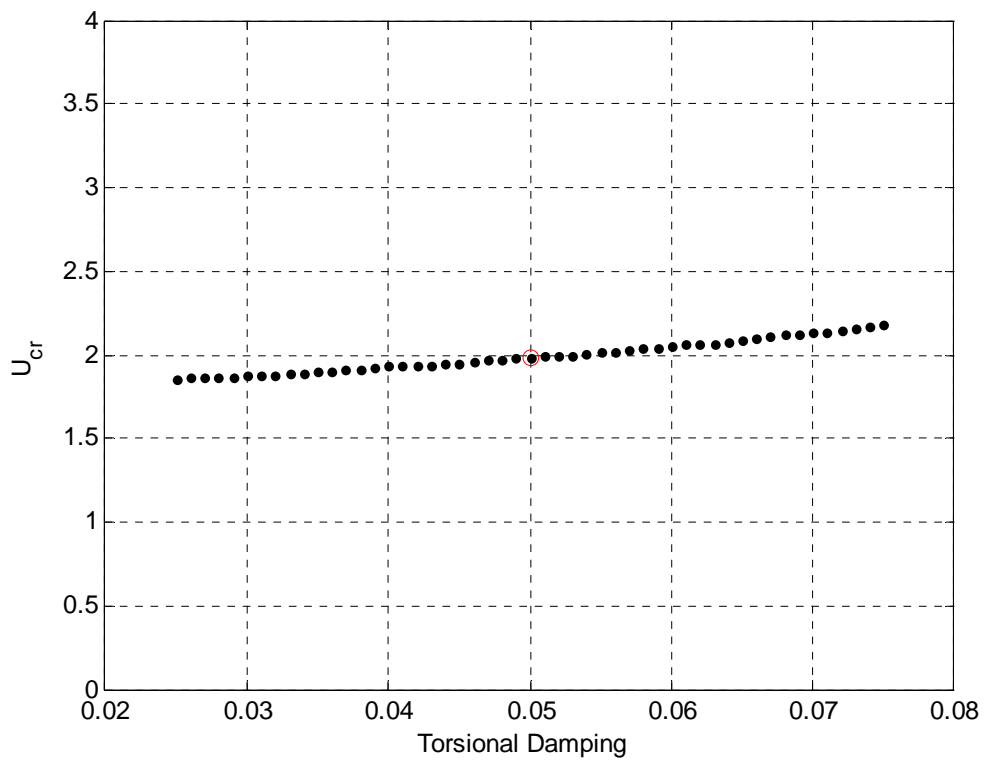


Figure 9-9 U_{cr} vs. Torsional Damping, 3D Model.

Effect of Structural Properties, A

It was well explained in Chapter 6 that parameter A is proportional to a ratio of fluid mass to structural mass and has been shown, in general, as this ratio escalates so does the inclination toward flow-induced vibration. This principle was observed in the 2D model as well (Figure 6-12). It is also spotted in this example in Figure 9-10. This figure shows a good agreement and demonstrates that as A rises, the critical reduced velocity falls down and the system becomes more susceptible to instability.

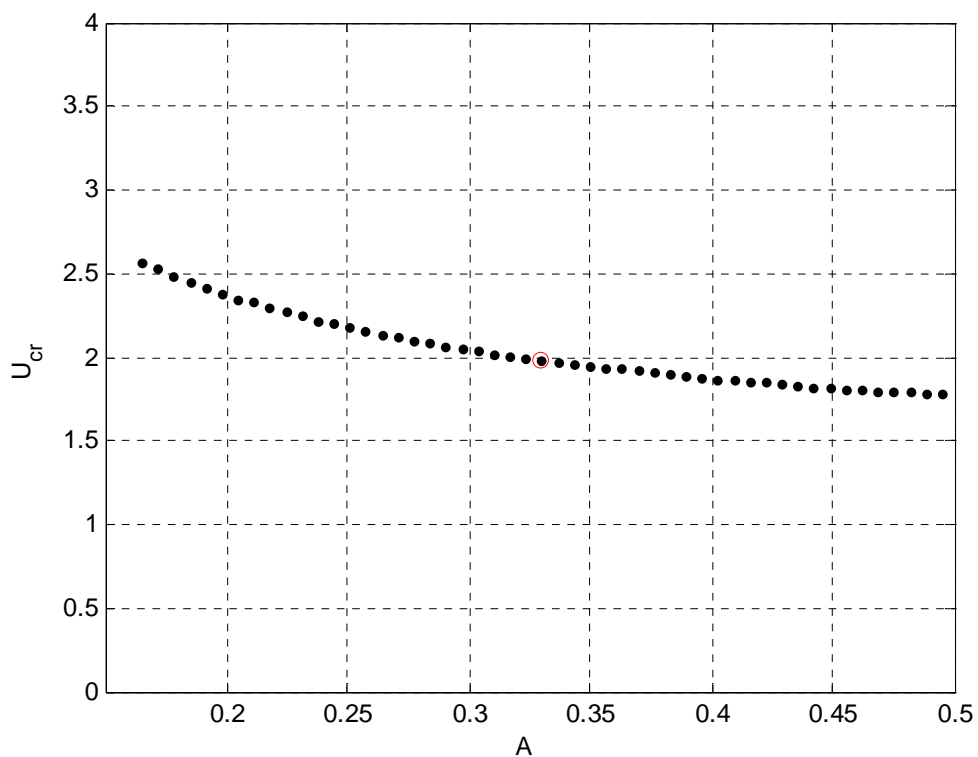


Figure 9-10 U_{cr} vs. A, 3D Model.

Effect of Structural Properties, γ^2

Figure 6-13 in the 2D study revealed that larger magnitudes of parameter γ^2 hinder the instability onset to higher velocity. This is the general trend in Figure 9-11 as well. However, at small values of γ^2 where it is about half of the base case, it shows

different behaviour and increase of γ^2 reduces U_{cr} . This is along with a discrete drop between 66% and 68% of value in the base case. Similar to previous figures, this is due to mode change (Figure 9-12).

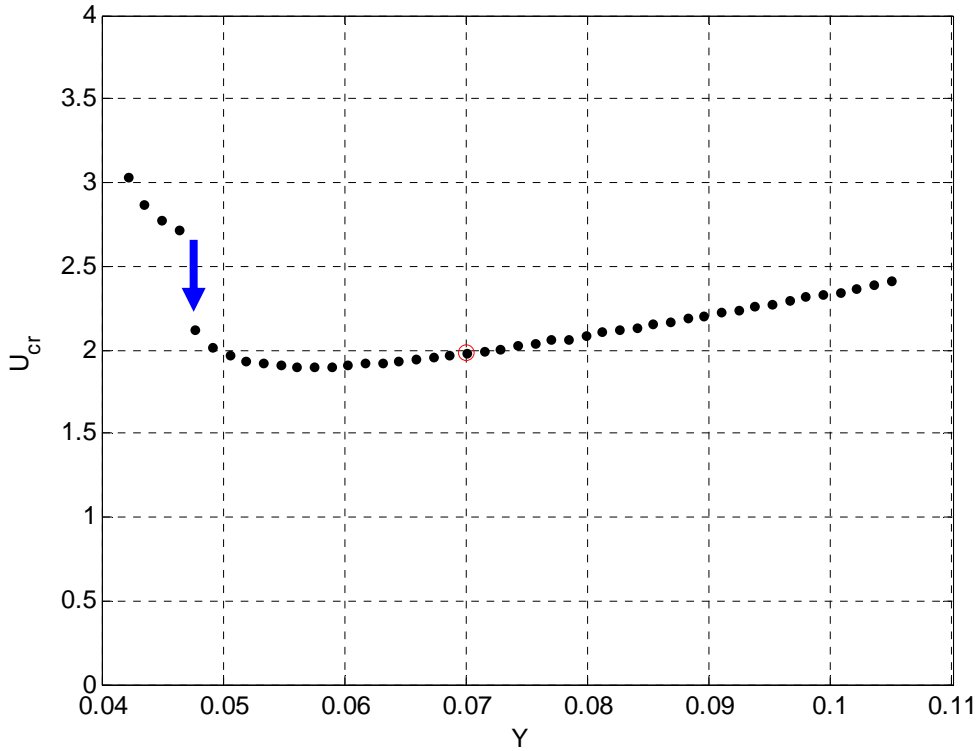


Figure 9-11 U_{cr} vs. γ^2 , 3D Model.

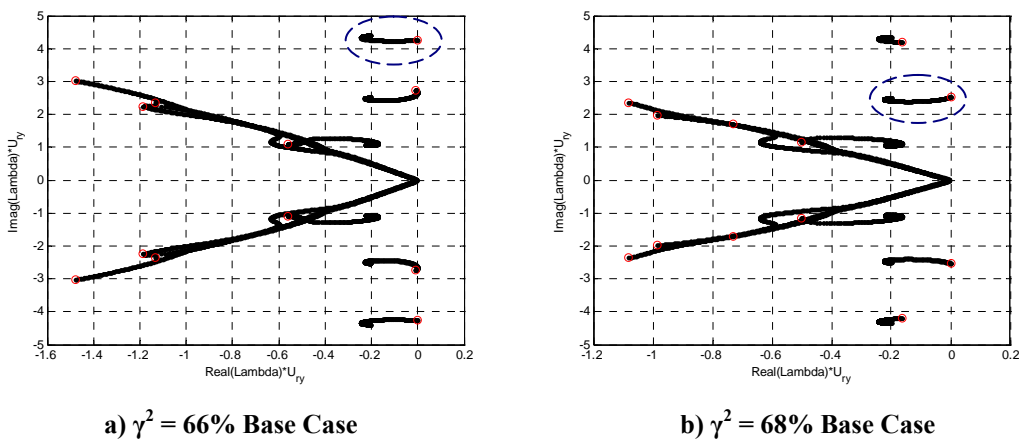


Figure 9-12 Mode Change Due to Increase of γ^2 , 3D Model.

Effect of Structural Properties, S_r

The previous study for the 2D model demonstrates an increase of S_r , endangering the stability of the system which leads to lower values of U_{cr} (Figure 6-14). This is the case for the main part of curve in this example. The discrete drop in Figure 9-13 is due to a mode change between 70% and 72% of initial value (Figure 9-14).

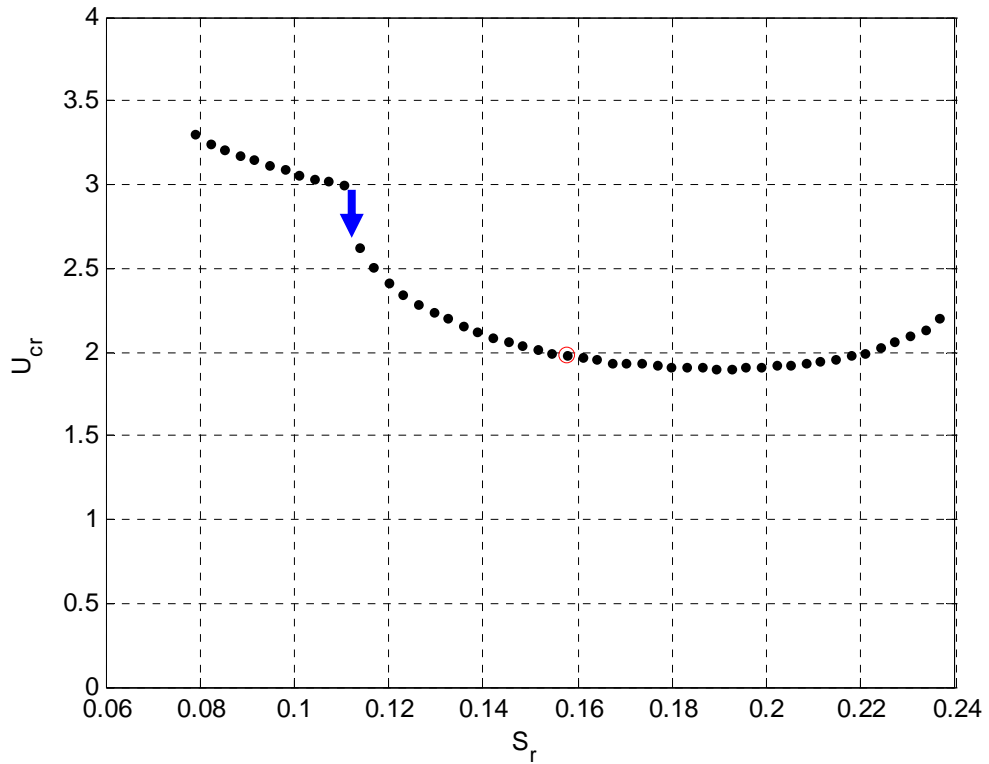


Figure 9-13 U_{cr} vs. S_r , 3D Model.

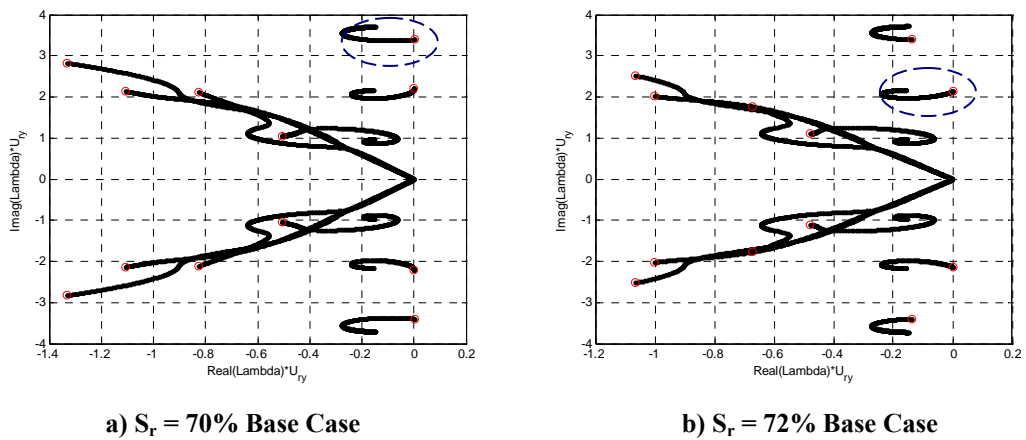


Figure 9-14 Mode Change Due to Increase of S_r , 3D Model.

Effect of Hydrodynamic Property, R_r

The previous study (Figure 6-15) discovered that the growth of R_r at first improves the stability and increases U_{cr} . This continues up to the point where further growth of R_r beyond that has adverse impact on instability and decreases U_{cr} . Figure 9-15 demonstrates this behaviour in the 3D case again.

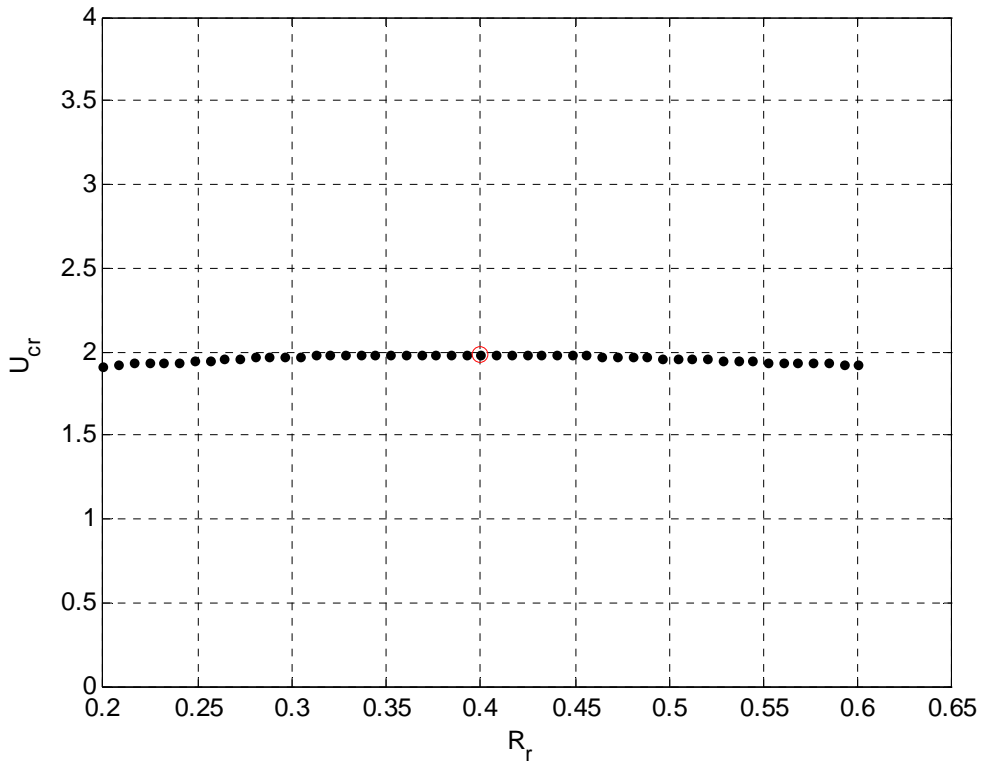


Figure 9-15 U_{cr} vs. R_r , 3D Model.

(B) New Parameters

Taking the third dimension into consideration introduces new parameters. These parameters either demonstrate the impact of the third dimension in stiffness, e.g. riser length (L), wet weight (w_r) and tension at top end (T_t) or show the variation of variables along the riser length such as current profile and length of coverage with fairings. The first group of variables were categorized in two dimensionless parameters, i.e. Top Tension Factor (TTF) and Flexural Factor (FF) while the second group needs to be addressed individually. In the following the influence of these parameters will be investigated.

Effect of Top Tension Factor (TTF)

Based on the definition of TTF in Equation (8-48), this parameter is the ratio of tension at the top end of riser (T_t) to the wet weight of the entire system ($w_r \cdot L$). Thus, for a given system, an increase in TTF will result in a higher stiffness and should improve the stability. Figure 9-16 proves this trend. In this figure since TTF cannot be less than one, TTF varies between 80% to 180% of the base value. This figure shows higher critical velocity for larger values of TTF.

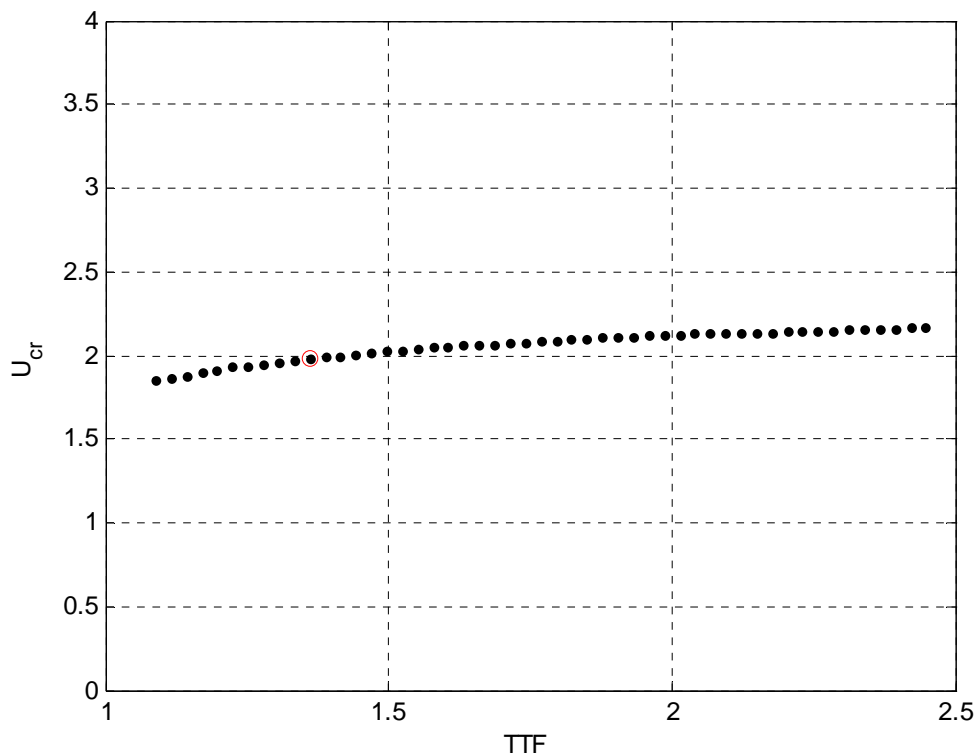


Figure 9-16 U_{cr} vs. TTF, 3D Model.

Effect of Flexural Factor (FF)

Parameter FF was defined in Equation (8-47). This variable presents the ratio of flexural stiffness to the stiffness generated by tension. In theory, higher flexural stiffness helps the stability but as the role of this parameter in total stiffness is very small, in practice, change of this variable does not influence the stability to a large extent (Figure 9-17).

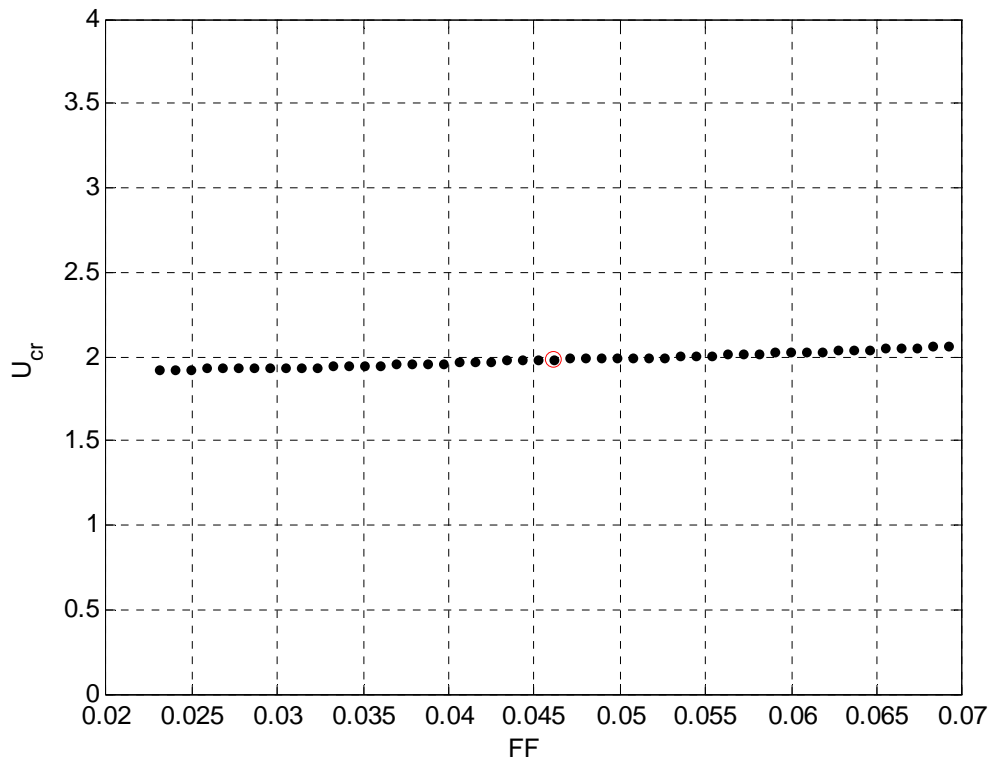


Figure 9-17 U_{cr} vs. Flexural Factor (FF), 3D Model.

Effect of Coverage Length

Figure 9-18 demonstrates the effect of coverage length in stability. The ratio of top portion outfitted with the fairing to the total length of the riser is plotted in the horizontal axis. With the assumption that the part of the riser which is bare does not produce vortices and only contributes to damping the vibration; this figure shows fitting longer segment of the riser with fairings will increase the risk of instability and reduces U_{cr} .

Moreover, longer coverage of the riser can change the mode of instability. This appears in the form of a discrete drop in Figure 9-18. It was investigated in Figure 9-19. Vertical axis in the latter figure is proportional to imaginary part of the eigenvalue and implies the frequency of vibration. It was said that modes are coupled but if one attributes the upper curves with higher frequency to higher mode numbers of vibration, this means that covering the top part of the riser provokes higher modes

(Figure 9-19 (a)) and as the length of coverage increases, lower modes (Figure 9-19 (b)) are excited subsequently.

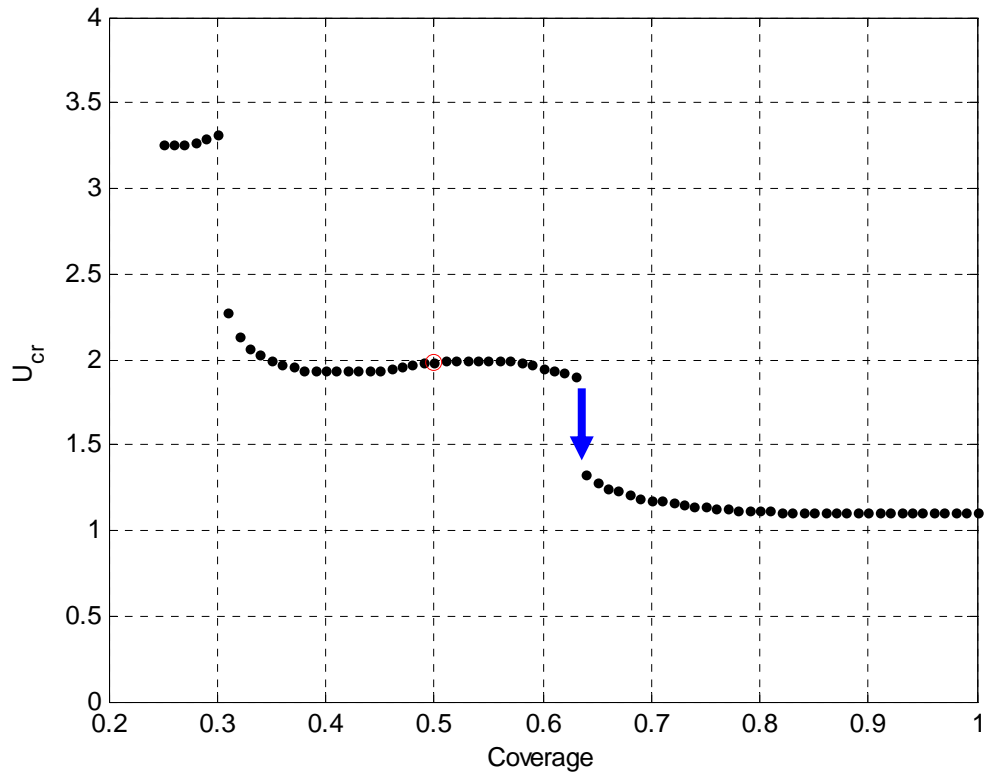
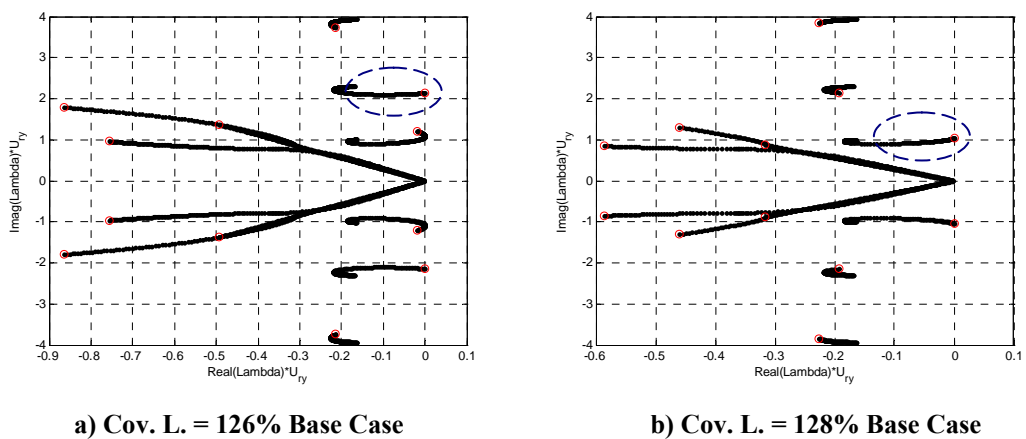


Figure 9-18 U_{cr} vs. Length of Coverage, 3D Model.



a) Cov. L. = 126% Base Case

b) Cov. L. = 128% Base Case

Figure 9-19 Mode Change Due to Increase of Coverage Length, 3D Model.

Effect of Current Profile

In this example sheared current was investigated. Current velocity at the top end was selected as the measure for instability analysis (U_o). It was mentioned earlier in Section 9.2 that if U_o is measured at the top end of the riser (Figure 9-20), the current profile for a riser of unit length will be,

$$U = U_o \times (aa \times Z + bb)$$

The term $(aa \times Z + bb)$ shows the type of variation in current profile. Since this term should be equal to one at the top end ($Z = 1$) where U_o is measured, this means $aa = 1 - bb$. In other words, the current profile is only a function of bb which shows the ratio of current speed at bottom end to that at the top end. For this example in the base case, the current velocity at the bottom end of riser was equal to 20% of that at the top end, i.e. $bb = 0.20$ (see Section 9.2). When $bb = 1$, it presents the uniform current condition.

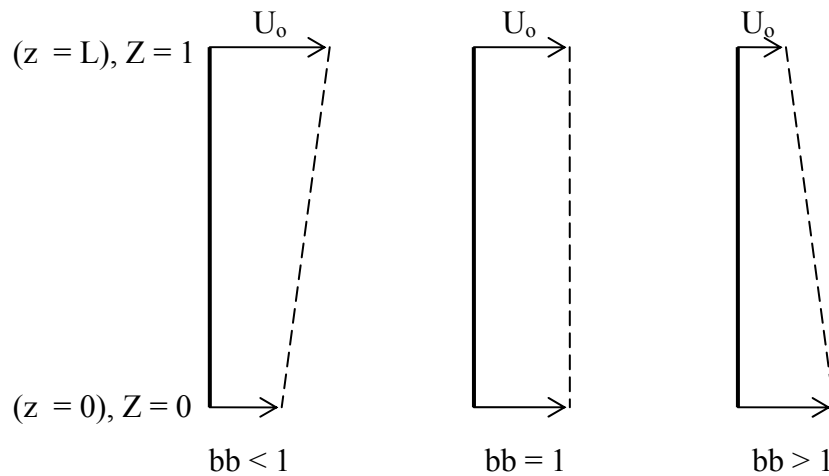


Figure 9-20 Sheared Current Profile.

The process of drawing the trend of critical velocity against the variation of bb is as below. For a specific value of bb , U_o increases from zero until the system goes unstable. Then the corresponding U_{ry} is calculated based on U_o . Figure 9-21 shows

this trend when the bottom to top ratio of current velocity varies within the range of 0 to 2.

For the base profile ($U_0 = 1$), when $bb > 1$ current velocity is higher at the lower end and in general is larger at all points along the riser compared to when $bb < 1$ (Figure 9-20). Naturally, larger profile leads to lower critical velocity. This is observed in Figure 9-21. From left to right, as the parameter bb increases and current profile enlarges critical velocity declines.

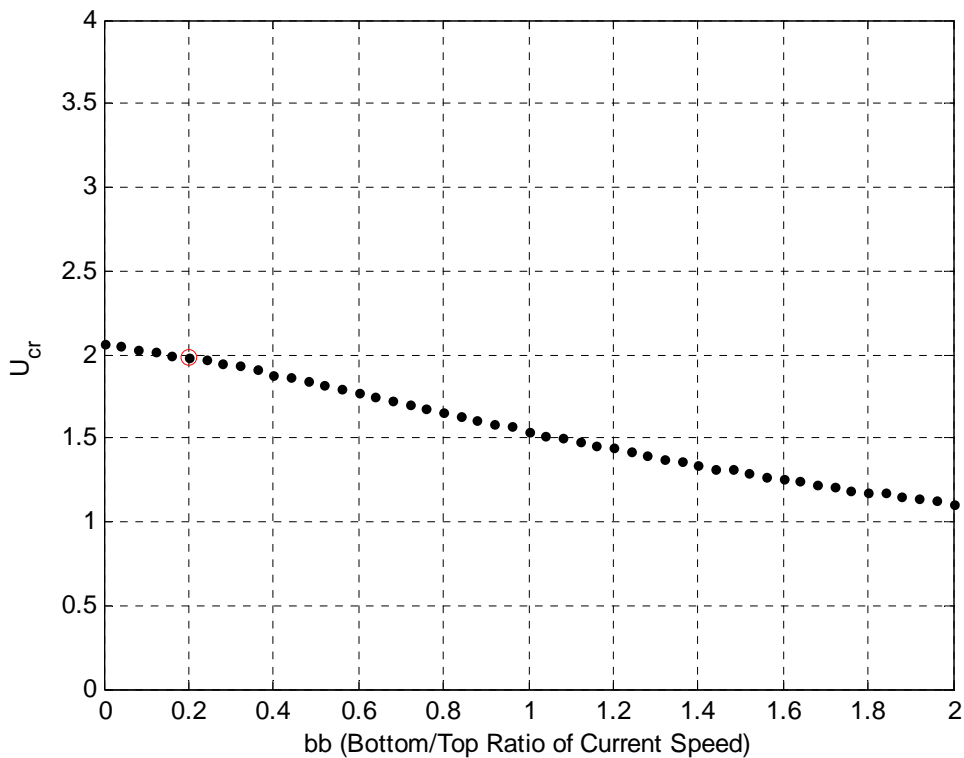


Figure 9-21 U_{cr} vs. Bottom/Top Ratio of Current Speed, 3D Model.

9.4 Summary of Findings

It was explained that the 2D model is identical to the 3D model in the uniform case for mode number one when flexural stiffness in comparison to tension is negligible ($FF = 0$). For other mode numbers or when FF is considerable, the new parameter G comes into play. It will enhance the stability.

Afterwards, a typical riser was selected and the stability of this system fitted with the guide vane as fairing was investigated. Based on this example, a parametric study

was carried out for the 3D general case. First the common parameters between the 2D and 3D models were probed. This investigation disclosed that the general behaviour of these parameters is similar in both models and the discussions presented in Chapter 6 holds here. Although the 2D parametric study was consistent with the study of the 3D case, some new features emerged. In the 3D model, variation of parameters may result in the change of mode and this was accompanied by a discrete movement in continuous curves. Generally speaking, the impact of dimensionless parameters was identical in both studies and within each mode.

This study also looked into the effects of new parameters introduced in the 3D model. The impact of the riser's length, in-water weight and top tension along with flexural stiffness, was summarised in two dimensionless parameters namely Top Tension Factor (TTF) and Flexural Factor (FF). In addition, the variation of some features along the riser such as length of coverage and current profile were also considered.

This part of parametric study indicated the variation of TTF entails tangible influences on critical velocity while small amount of Flexural Factor does not change the stability status notably. Nevertheless, the positive effect of TTF is not highly significant compared with some other parameters like hydrodynamic coefficients. In addition, raising the top tension is a very expensive decision. Therefore, in order to impede the instability, modifying the fairing is more cost effective than increasing the top tension.

Length of coverage plays an important role in the instability onset and the excited mode. This impact is far more severe for shorter length of coverage but as this length exceeds for instance 80% of the riser's total length in this example, it loses its importance and the curve flats.

The last issue to address was the current profile. Sheared flow was investigated and the obtained results clarified that distribution of current speed along the riser is critical to stability condition.

This chapter presents a review of what was done in this study. It will discuss the selected method and enlighten the challenges encountered through the process of solution. It will review the lessons learnt and describe the contributions of this study. Eventually, it will enlarge on areas that need further research and investigation in future.

10.1 A Look Back

It was mentioned that the oil and gas demand has increased dramatically over the past decades and caused producers to look for new reservoirs in ever deeper waters. Such development requires longer tubulars including risers of all types. As the industry deploys lengthy risers, new features appear which can endanger the serviceability life span of these infrastructures. Vortex-induced-vibration (VIV) was one of these new challenges. Several techniques were devised to overcome this difficulty. Fitting a riser with VIV suppression equipment became one of the most common methods. This type of equipment varies in many aspects such as the way they mitigate vibration. Among them, the riser fairing emerged when reduction of drag was also a serious concern for designers in addition to VIV.

This study tried to explore the merits and drawbacks of riser fairings. Some of the reported difficulties were diagnosed for further research like misalignment and more significantly propensity of instable behaviour at high current velocity. The latter was recently observed in some experiments and needed a theoretical assessment to

identify the roots involved and also predict this situation for forthcoming designs. To this end, this study initially explored various types of fluid-induced-vibration and their causes. It was found out that possible instability of a riser fairing is similar to classical wing flutter in some ways and simultaneously different in some features and therefore demands separate investigation.

Theoretical analysis of this phenomenon necessitated setting up the governing equations of the system which consists of a riser, fairing and fluid. The interaction of the fairing with surrounding fluid made the problem so complicated that Navier-Stokes equation could not be solved analytically for the moving fluid around the fairing. One available approach was to use computational methods but this would make the solution very case sensitive and mask the primary aim of providing a tool for prediction of this problem in future projects. Consequently, this purpose along with the complexity of the problem called for some assumptions to simplify the situation and make an analytical solution possible. In return, these assumptions dictated some limitations to the application of the method.

At first, and in the light of the above assumptions, an analytical model was developed for a simpler case of a two-dimensional (2D) problem. By the use of Lagrange's equations, the governing equations were derived. Hydrodynamic forces were calculated and the effect of motion on these forces was taken into consideration. The obtained equations were linearised and an eigenvalue analysis was carried out in order to find the situation at which the real part of one of the solutions becomes positive and system goes unstable. Through defining physically meaningful dimensionless parameters, the characteristic equation was made dimensionless. This model was validated against the results of a lab test and showed a good agreement. Then the effect of torsional friction damping was assessed.

A method was presented to calculate the necessary dimensionless parameters for a given system of a riser and fairing. This method was deployed in a real example and the critical condition was determined. Afterwards, the impact of each dimensionless parameter on instability onset was assessed. This study showed that some parameters, e.g. hydrodynamic coefficients, are more important and influential.

Therefore, a few fairing sections were selected and the behaviour of flow in vicinity of these profiles was evaluated. With the aid of the CFD method, hydrodynamic coefficients of these sections were obtained. This study demonstrated the effect of section's details on hydrodynamic performance of a fairing. Particularly, the impacts of adding fins, blunt end as well as the angle of leeward side of the fairing were seen.

When the influence of parameters involved in the model was fully explored, the limited model of two-dimensional was expanded to three-dimensional (3D). Similar to the previous model, the governing equations were derived and by using the Galerkin's method, continuous partial differential equations along the riser length were converted to several equations with time variable only. An eigenvalue analysis was carried out and the obtained characteristic equation was made dimensionless. The majority of the defined dimensionless parameters were in common with the 2D model while a few new parameters emerged as well. The simpler case of having a uniform condition along the riser was also assessed and it was illustrated how it relates to the 2D model. The 3D model was verified against a lab test and was in conformity with the results.

Eventually, based on the 3D model, a parametric study was devised for two purposes; firstly to assess the validity of the 2D parametric study and to compare the impact of common parameters in the 2D and 3D models, and secondly, to investigate the effect of new parameters. This study corroborated the consistency of the 2D parametric study with that of the 3D model.

It should be noted that this analytical study was based on the assumptions explained in Section 4.5. Using these assumptions imposed some limitations on the scope of this model. One of the key issues was that this model postulates the quasi-steady condition. To be valid, it requires the frequency of periodic components of fluid force to be above the vibration frequency of the structure. This condition is usually met at a high reduced velocity (see Section 4.5). It was also mentioned that the design philosophy of a fairing is to streamline the flow and prevent any vortex formation. Thus, in an ideal case no VIV and cyclic fluid force exists and therefore the above condition holds. This study indicated that some fairing profiles still generate vortices and undergo associated periodic forces. Thus, this necessitates

checking the validity of the quasi-steady condition for each case by comparing the frequency of the structure with the frequency of the fluid force. In general, Blevins believes this condition is satisfied if the reduced velocity is high enough, for example about $U_{ry} = 1.90$ (equivalent to $U/f_y D > 20$ for a fairing with 60% thickness to chord ratio).

The other lesson learnt from this study relates to the linearization. Since the phenomenon of instability with many hydrodynamic and structural parameters involved is not linear in nature, the question may arise that to what extent the linearised model is a reliable approximation of the real case? Fortunately, good agreement of theoretical result with experimental data showed that such assumption can predict the onset conditions for instability fairly accurately. Nevertheless, it cannot anticipate or explain the evolution of motion once the unstable vibration starts. This is not only because of linearization but because other events may come into play like stall, turbulence and vortex shedding.

10.2 Own Contributions

This study opened new windows to the subject of riser fairing and illuminated some relevant outstanding and un-researched issues. This project expanded the knowledge of a riser fairing in different aspects some of which are outlined below.

- A) This study developed a more accurate analytical model to predict the instability onset of a riser fairing system in ocean currents.
- B) This model took the effect of damping, both hydrodynamic and structural, into consideration.
- C) The parametric study prepared a valuable guideline and tool for designers enabling them to decide what change in which direction delays the possible instability.
- D) This research helped to understand the root of another well-known shortcoming of fairing, i.e. misalignment.

- E) The investigation of hydrodynamic behaviour of a few fairing sections disclosed constructive issues like the effect of adding fins and gave some hints to move toward ideal profile.

10.3 Future Research

This study delivered the predefined goal of assessing the instability of a riser fairing but through this journey, this study found other issues and aspects of a riser fairing which were out of the scope of this project and on the other hand deserve a separate and more comprehensive look. They can be summarised as following.

- A) This study only addressed the onset conditions of instability and did not investigate the evolution and development of excessive vibration when the instability was triggered. Moreover, some tests showed that for current velocities much beyond the critical velocity, system obtained its stability again (Braaton et al., 2008). Thus, post-stability-loss behaviour of system is one of the significant issues to be probed further.
- B) This project assessed the effect of partial coverage of a riser with fairing. This study assumed that if a portion of a riser is left bare it means this segment does not experience any VIV and only contributes to the hydrodynamic damping of system. However, in reality there may exist cases that part of a riser undergoes VIV while because of other reasons like cutting the costs, it is left without suppression device. Consequently, vortex shedding from this part may excite the instability of the whole system at velocities lower than what was predicted. Therefore, a separate study should tackle the issue and probe the excitation effect of VIV in the bare part.
- C) Added mass in both forms, interior and exterior, emerged through the process of model developing. The entrapped water was modelled like a solid body as interior added mass. The calculation of exterior added-mass of an arbitrary fairing profile was also a challenge. This was done through an approximation of a fairing with other simple sections. But more realistic modelling of

entrapped water and accurate calculation of exterior added-mass requires a separate study.

- D) Another parameter appeared in the analytical model was R , a reference length to denote the effect of angular velocity on AoA. This parameter was already calculated for thin foils in aviation industry but no data was available for thick foils. Naturally, nothing has been mentioned so far about this parameter in more complicated profiles like fairing. On the other hand, this parameter proved to be very influential in the stability limit. Therefore, the impact of thickness and changing other details of a profile on this parameter needs further research.
- E) Many commercial fairing sections have been introduced. There are other sections in the literature which has this potential but have not been considered yet. Investigation of hydrodynamic behaviour of more fairing profiles will provide a precious database for riser engineers to select from for a specific project. In addition to hydrodynamic coefficients, such database should also keep the effect of various alterations in the fairing profile like fins or blunt end. This information directs toward optimum section.

Conclusion

The first objective of this project was to explore the issue of vortex-induced-vibration (VIV) in general and to assess the associated impacts on marine risers. This research looked at the mechanism of vortex formation and reviewed the available methods of mitigating the generated vibrations. It appraised various methods among which adding a vortex suppression device was one of the popular techniques. This study went through the pros and cons of using a riser fairing. Fairing had many advantages to other suppression devices but suffered from some difficulties as well. The critical review showed that misalignment and instability were the most significant reported drawbacks.

This research targeted the issue of probable instability. As this fact was already tested and observed in experimental programmes, this project addressed the issue in a new way and developed an analytical model for this physical phenomenon. This model was more complete than the previous simple model and disclosed the effect of damping of different types including hydrodynamic and structural. This model indicated that there are two necessary and sufficient conditions for stability of system. To be satisfied, necessary condition requires positive factor for resultant damping in governing equations whereas sufficient condition demands negative real part for the solution of characteristic equation. Through establishing the above model, it was also understood that the other significant shortcoming of fairing, i.e. misalignment, have some roots in common with instability.

The last aim of this research was to identify the key parameters in instability onset of a riser fairing. The above analytical model clarified that there is a combination of three parameter sets which governs the stability of system. They consist of structural properties, hydrodynamic characteristics of fairing and finally current speed. The present study investigated the influence of all factors through conducting a parametric study. This survey showed how mass and its distribution contributed to the stability of the system. Moreover, this probe indicated that covering the riser with a fairing beyond the necessary length dictated by VIV would increase the risk of instability. In addition, this investigation emphasised on the high importance of the hydrodynamic features of the fairing section.

Pursuant to this fact, a separate CFD assessment of these aspects for a few fairing sections revealed that the small slope of fairing contour in the leeward side is very effective in enhancement of fairing performance. It affirmed the worth of this action even at the price of clipping the trailing edge in order to keep the operability of such fairing at the same level. Furthermore, this CFD study illustrated how adding fins manipulates the pressure distribution over the fairing section and modifies hydrodynamic coefficients. The CFD study along with the above theoretical model helped to explain why some tests had already reported that installation of fins increases the stability and also improves the self-alignment capability of fairing and reduces its fishtailing.

Overall, this research project provided the riser designers with a theoretical tool to predict the instability onset in a system of a riser and fairing. Moreover, it presented valuable guidelines which direct and enable the design engineer to hinder this destructive vibration if preliminary plan was diagnosed with the chance of instable behaviour during service life.

References

- ABBOTT, I. H. & VON DOENHOFF, A. E. (1959) *Theory of Wing Sections*, New York, USA, Dover Publications.
- ALLEN, D. W. (2003) Performance Characteristics of Short Fairings. *Offshore Technology Conference (OTC03-15285)*. Houston, U.S.A.
- ALLEN, D. W. & ALLEN, C. W. (2008) Fairing versus Helical Strakes for Suppression of Vortex-Induced-Vibration: Installation, Maintenance and Economic Considerations. *Offshore Technology Conference (OTC08-19374)*. Houston, USA.
- ALLEN, D. W. & HENNING, D. L. (1995a) Flexible Fairings to Reduce Vortex-Induced-Vibrations. IN PATENT, U. S. (Ed.) USA, Shell Oil Company, Houston.
- ALLEN, D. W. & HENNING, D. L. (1995b) Small Fixed Teardrop Fairing for Vortex Induced Vibration Suppression. IN PATENT, U. S. (Ed.) USA, Shell Oil Company, Houston.
- ALLEN, D. W. & HENNING, D. L. (2001a) Spar Fairing. IN PATENT, U. S. (Ed.) USA, Shell Oil Company.
- ALLEN, D. W. & HENNING, D. L. (2001b) Staggered Fairing System for Suppressing Vortex-Induced-Vibration. IN PATENT, U. S. (Ed.) USA, Shell Oil Company, Houston.
- ALLEN, D. W. & HENNING, D. L. (2001c) Ultra-short Fairings for Suppressing Vortex-Induced-Vibration. IN PATENT, U. S. (Ed.) USA, Shell Oil Company, Houston.
- ALLEN, D. W. & HENNING, D. L. (2008) Comparisons of Various Fairing Geometries for Vortex Suppression at High Reynolds Numbers. *Offshore Technology Conference (OTC08-19377)*. Houston, USA.
- ALLEN, D. W., HENNING, D. L. & LEE, L. (2007a) Drilling Riser Fairing Tests at Prototype Reynolds Numbers. *26th International Conference on Offshore Mechanics and Arctic Engineering (OMAE07-29219)*. San Diego, USA, American Society of Mechanical Engineers (ASME).

- ALLEN, D. W., HENNING, D. L. & LEE, L. (2007b) The Effect of Partial Span Coverage for Deepwater Marine Risers and Tendons with Fairings. *Offshore Technology Conference (OTC07-18594)*. Houston, USA.
- ALLEN, D. W. & LEE, L. (2004) Some of the Recent VIV R&D Activities at Shell. Trondheim, Norway.
- ALLEN, D. W., LEE, L. & HENNING, D. L. (2008) Fairing versus Helical Strakes for Suppression of Vortex-Induced-Vibration: Technical Comparisons. *Offshore Technology Conference (OTC08-19373)*. Houston, USA.
- ANDERSON, J. D. (2007) *Fundamentals of Aerodynamics*, New York, USA, McGraw Hill.
- API (1998) *Design of Risers for Floating Production Systems (FPSs) and Tension-Leg Platforms (TLPs)*, Washington, USA, American Petroleum Institute (API).
- ARMSTRONG, S. P. (2004a) Retrofitting VIV Suppression Fairings in Deep Water. World Pipelines.
- ARMSTRONG, S. P. (2004b) VIV Suppression Installation on Existing Horizontal Pipeline Spans. *Offshore Technology Conference (OTC04-16600)*. Houston, USA.
- ARMSTRONG, S. P. (2004c) Vortex Induced Vibration Suppression Device Retrofit Installation Advances. *Subsea South America Conference*. Rio De Janeiro, Brazil.
- ARMSTRONG, S. P. (2006) Planning, Procedures, and Results of a Deepwater Vertical SCR VIV Suppression Retrofit Project. *Offshore Technology Conference (OTC06-18362)*. Houston, USA.
- BAI, Y. & BAI, Q. (2005) *Subsea Pipelines and Risers*, Oxford, UK, Elsevier Ltd.
- BALCH, E. R., KAVANAGH, W. K., GRIFFIN, P. E., CHOUINARD, L. E., COOPER, C. & THOMPSON, H. M. (2003) Running Fairings for Deepwater Drilling in the Gulf of Mexico - A Cost-Benefit Approach to Deciding the Faired Length. *Offshore Technology Conference (OTC03-15286)*. Houston, USA.
- BARLTROP, N. D. P. & ADAMS, A. J. (1991) *Dynamics of Fixed Marine Structures*, Oxford, UK, Butterworth-Heinemann Ltd.
- BEARDS, C. F. (1996) *Structural Vibration, Analysis and Damping*, New York, USA, Halsted Press.
- BERTIN, J. J. & SMITH, M. L. (1998) *Aerodynamics for Engineers*, London, UK, Prentice-Hall.

- BISHOP, R. E. D. & PRICE, W. G. (1979) *Hydroelasticity of Ships*, Cambridge, UK, Cambridge University Press.
- BISPLINGHOFF, R., ASHLEY, H. & HALFMAN, R. L. (1996) *Aeroelasticity*, New York, USA, Dover Publications.
- BLEVINS, R. D. (2001) *Flow-Induced Vibrations*, Florida, USA, Krieger Publishing Company.
- BP (2007) Statistical Review of World Energy. BP.
- BRAATON, H., LIE, H. & SKAUGSET, K. (2008) Higher Order Modal Response of Riser Fairings. *27th International Conference on Offshore Mechanics and Arctic Engineering (OMAE08-57971)*. Estoril, Portugal, American Society of Mechanical Engineers (ASME).
- BRENNEN, C. E. (1982) A Review of Added Mass and Fluid Inertial Forces (CR82.010). Port Hueneme, USA, Naval Civil Engineering Laboratory.
- BRESLIN, J. P. & ANDERSEN, P. (1994) *Hydrodynamics of Ship Propellers*, Cambridge, UK, University of Cambridge.
- BRITANNICA (2008) Encyclopaedia Britannica. Britannica Inc. (www.britannica.com).
- BROWN, A. J. & KING, R. (2008) Tests with a Flexible Quasi-Fairing to Reduce Riser Drag, Suppress VIV and Limit Drilling Down-Time. *Offshore Technology Conference (OTC08-19161)*. Houston, USA.
- BULLIVANT, W. K. (1941) Tests of The NACA 0025 and 0035 Airfoils in The Full-Scale Wind Tunnel. *Report No 708*. National Advisory Committee for Aeronautics (NACA).
- CALKINS, D. E. (1984) Two-Dimensional Hydrodynamic Characteristics of a Bluff Symmetrical Fairing Section. *AIAA Journal*, 22, 1216-1221.
- CHEN, C. H., CHEN, C. R. & MERCIER, R. S. (2006) CFD Simulation of Riser VIV. Texas, USA, Texas A&M University.
- CLOUGH, R. W. & PENZIEN, J. (1993) *Dynamics of structures*, New York, McGraw-Hill.
- CUMING-CORP. Fairings for Marine Risers. *Technical Note 100-8*. Avon, USA, Cuming Corporation.
- DENISON, E. B., MCDANIEL, R. B. & MCMILLAN, D. W. (2000a) Copper Protected Fairings. IN PATENT, U. S. (Ed.) USA, Shell Oil Company, Houston.

- DENISON, E. B., MCMILLAN, D. W. & MCDANIEL, R. B. (2000b) Fairings for Deepwater Drilling Risers. IN PATENT, U. S. (Ed.) USA, Shell Oil Company, Houston.
- DENISON, E. B., MCMILLAN, D. W. & MCDANIEL, R. B. (2000c) Vortex-Induced-Vibration Protection for Deepwater Drilling Risers. IN PATENT, U. S. (Ed.) USA, Shell Oil Company, Houston.
- DOWELL, E. H., CRAWLEY, E. F., CURTISS JR., H. C., PETERS, D. A., SCANLAN, R. H. & SISTO, F. (1995) *A Modern Course in Aeroelasticity*, Dordrecht, Netherlands, Kluwer Academic Publishers.
- DUAN, C. (2004) Dynamic Analysis of Dry Friction Path in A Torsional System. *Department of Mechanical Engineering*. Ohio, USA, Ohio State University.
- DUAN, C. & SINGH, R. (2006) Dynamics of 3dof Torsional System with a Dry Friction Controlled Path. *Journal of Sound and Vibration*, 289, 657-688.
- EASTMAN, N. J. (1932) The aerodynamic characteristics of eight very thick airfoils from tests in the variable density wind tunnel. *Report No 391*. National Advisory Committee for Aeronautics (NACA).
- EASTMAN, N. J., KENNETH, E. W. & PINKERTON, R. M. (1933) The Characteristics of 78 Related Airfoil Sections from Tests in The Variable-Density Wind Tunnel. *Report No 460*. National Advisory Committee for Aeronautics (NACA).
- ERICSSON, L. E. & REDING, J. P. (1980) Potential Hydroelastic Instability of Profiled Underwater Structures. *Journal of Hydronautics*, 14, 97-104.
- FUNG, Y. C. (2002) *Theory of Aeroelasticity*, New York, USA, Dover Publications.
- GARDNER, T. N. & COLE, M. W. (1982) Deepwater Drilling in High Current Environment. *Offshore Technology Conference (OTC82-4316)*. Houston, USA.
- GRANT, R. & PATTERSON, D. (1977) Riser Fairing for Reduced Drag and Vortex Suppression. *Offshore Technology Conference (OTC77-2921)*. Houston, USA.
- GRIMMINGER, G. (1945) The Effect of Rigid Guide Vanes on The Vibration and Drag of a Towed Circular Cylinder. *Report No 504*. Washington, USA, David Taylor Model Basin.
- HARRIS, J. W. & STOCKER, H. (1998) *Handbook of Mathematics and Computational Science*, New York, USA, Springer-Verlag.
- HOERNER (1992) *Fluid-Dynamic Lift: Practical Information on Aerodynamic and Hydrodynamic Lift*, USA, Hoerner Fluid Dynamics.

- HOERNER, S. (1965) *Fluid Dynamic Drag: Practical Information on Aerodynamic Drag and Hydrodynamic Resistance*, USA, Hoerner Fluid Dynamics.
- IKEDA, Y., KATAYAMA, T. & ENOMOTO, T. (2003) Reduction of Inclination and Vortex-Induced-Oscillation of a Spar Buoy in Rapid Current. *13th International Offshore and Polar Engineering Conference*. Honolulu, USA.
- KHORASANCHI, M. & HUANG, S. (2009) Preliminary Instability-Analysis of Deepwater Riser With Fairings. *28th International Conference on Offshore Mechanics and Arctic Engineering (OMAE09-79116)*. Honolulu, USA, American Society of Mechanical Engineers (ASME).
- KUMAR, R. A., SOHN, C. H. & GOWDA, B. H. L. (2008) Passive Control of Vortex-Induced Vibrations: An Overview. *Recent Patents on Mechanical Engineering*. Karachi, Pakistan, Bentham Science Publishers Ltd.
- LEE, L. & ALLEN, D. W. (2004) VIV Modelling of Bare and Suppressed Risers. *Offshore Technology Conference (OTC04-16183)*. Houston, USA.
- LEE, L. & ALLEN, D. W. (2005) The Dynamic Stability of Short Fairings. *Offshore Technology Conference (OTC05-17125)*. Houston, USA.
- LEE, L. & ALLEN, D. W. (2007) An Approach to VIV Design of Marine Risers. *26th International Conference on Offshore Mechanics and Arctic Engineering (OMAE07-29095)*. San Diego, USA, American Society of Mechanical Engineers (ASME).
- LEE, L., ALLEN, D. W. & HENNING, D. L. (2004a) Motion Trajectory of Bare and Suppressed Tubulars Subjected to Vortex Shedding at High Reynolds Numbers. *14th International Offshore and Polar Engineering Conference*. Toulon, France.
- LEE, L., ALLEN, D. W. & HENNING, D. L. (2005) Measured and Predicted VIV Responses of Faired Drilling Riser Models. *Offshore Europe (SPE96290)*. Aberdeen, UK, Society of Petroleum Engineers.
- LEE, L., ALLEN, D. W. & HENNING, D. L. (2006a) VIV Suppression Performance of Tail-Fin Fairings for Drilling Risers. Shell Global Solutions (US) Inc.
- LEE, L., ALLEN, D. W. & HENNING, D. L. (2006b) Vortex-Induced Vibration Tests of Two Faired Cylinders in Tandem at Prototype Reynolds Numbers. *25th International Conference on Offshore Mechanics and Arctic Engineering (OMAE06-92331)*. Hamburg, Germany, American Society of Mechanical Engineers (ASME).
- LEE, L., ALLEN, D. W., HENNING, D. L. & MCMULLEN, D. (2004b) Damping Characteristics of Fairings for Suppressing Vortex-Induced Vibrations. *23rd International Conference on Offshore Mechanics and Arctic Engineering (OMAE04-51209)*. Vancouver, Canada, American Society of Mechanical Engineers (ASME).

- MAGNUS, K. (1965) *Vibrations*, London, UK, Blackie and Sons.
- MASTERS, R. W., MASTERS, R. H. & EDFELDT, M. P. (2002) Snap-on Rotating Reduction Fairing. IN PATENT, U. S. (Ed.) USA, AIMS International Inc, Houston.
- MCMILLAN, D. W. & ALLEN, D. W. (2006) Apparatus and Methods for Providing VIV Suppression to a Riser System Comprising Umbilical Elements. IN PATENT, U. S. (Ed.) USA, Shell Oil Company, Houston.
- MCMILLAN, D. W., DENISON, E. B. & MCDANIEL, R. B. (1999) Fairings for Drilling Riser Control Pod Hoses. IN PATENT, U. S. (Ed.) USA, Shell Oil Company, Houston.
- MEYER, P. A., FORT, J. A., SHEKARRIZ, A. & RUSSELL, D. A. (1995) Hydrodynamic Performance of an Offshore Drilling Riser Fairing. *3rd International Symposium on Performance Enhancement for Marine Applications*. Newport, USA.
- MIYAZAKI, E., OZAKI, M., NISHIOKA, S. & MINAMIURA, J. (2008) Application of Riser Fairings to The D/V "CHIKYU" During Drilling in High Current Area. *OCEANS (OTO08)*. Kobe, Japan, MTS/IEEE.
- NAIR, S. & HEGEMIER, G. (1979) Stability of Faired Underwater Towing Cables. *Journal of Hydronautics*, 13, 20-27.
- NAIR, S. & HUNG, C. Y. (1984) Planar Towing and Hydroelastic Stability of Faired Underwater Cables. *AIAA Journal*, 22, 1786-1790.
- NEWMAN, J. N. (1999) *Marine Hydrodynamics*, Cambridge, USA, MIT Press.
- ORTLOFF, J. E., GREER, M. N. & GARDNER, T. N. (1983) Fairing for Elongated Elements. IN PATENT, U. S. (Ed.) E21B 33/035 ed. USA, Exxon Production Research Co., Houston.
- PANTAZOPOULOS, M. S. (1994) Vortex-Induced Vibration Parameters: Critical Review. *International Conference on Offshore Mechanics and Arctic Engineering (OMAE94)*. Houston, USA, American Society of Mechanical Engineers (ASME).
- PATEL, M. H. (1989) *Dynamics of Offshore Structures*, Somerset, UK, Butterworth & Co. (Publishers) Ltd.
- PATEL, M. H. & WITZ, J. A. (1991) *Compliant Offshore Structures*, Oxford, UK, Butterworth-Heinemann Ltd.
- PONTAZA, J. P. & MENON, R. G. (2008) Numerical Simulations of Flow Past an Aspirated Fairing with Three Degree-of-Freedom Motion. *27th International Conference on Offshore Mechanics and Arctic Engineering (OMAE08-*

- 57552). Estoril, Portugal, American Society of Mechanical Engineers (ASME).
- RAGHUNATHAN, S., HARRISON, J. R. & HAWKINST, B. D. (1988) Thick Airfoil at Low Reynolds Number and High Incidence. *Journal of Aircraft*, 25, 669-671.
- RICHARDSON, G. E., NIXON, L. D., BOHANNON, C. M., KAZANIS, E. G., MONTGOMERY, T. M. & GRAVOIS, M. P. (2008) Deepwater Gulf of Mexico 2008: America's Offshore Energy Future. New Orleans, USA, U.S. Department of Interior Minerals Management Services (MMS).
- ROGERS, A. C. (1983) An Assessment of Vortex Suppression Devices for Production Risers and Towed Deep Ocean Pipe Strings. *Offshore Technology Conference (OTC83-4594)*. Houston, USA.
- SAUNDERS, H. E. (1956) *Hydrodynamics in Ship Design*, New York, USA, The Society of Naval Architects & Marine Engineers.
- SLOCUM, S. T., DING, Z. J., FRANK, W. R. & COX, M. R. (2004) Flutter Instability in Riser Fairings. *Offshore Technology Conference (OTC04-16342)*. Houston, USA.
- SPENCER, D., LEVERETTE, S., MASTERS, R. H., QUINN, R. & SCHAUDT, K. J. (2007) Enabling Enhancements of Riser VIV Design Techniques Through Detailed Interpretation of Test Results for VIV Suppression Devices. *Offshore Technology Conference (OTC07-18973)*. Houston, USA.
- SWEETMAN, J. A. (1998) Fairing for Marine Risers. IN PATENT, U. S. (Ed.) USA, Mobil Oil Corporation, Fairfax.
- SWORN, A. (2004) BP's VIV Activities. *NTNU VIV Workshop*.
- THEODORSEN, T. (1933) Theory of Wing Sections of Arbitrary Shape. *Report No 411*. National Advisory Committee for Aeronautics (NACA).
- THEODORSEN, T. (1935) General Theory of Aerodynamic Instability and the Mechanism of Flutter. *Report No 496*. National Advisory Committee for Aeronautics (NACA).
- THEODORSEN, T. & GARRICK, I. E. (1934) General Potential Theory of Arbitrary Wing Sections. *Report No 452*. National Advisory Committee for Aeronautics (NACA).
- THEODORSEN, T. & GARRICK, I. E. (1940) Mechanism of Flutter. a Theoretical and Experimental Investigation of the Flutter Problem. *Report No 685*. National Advisory Committee for Aeronautics (NACA).

- THEODORSEN, T. & GARRICK, I. E. (1942) Flutter Calculations in Three Degrees of Freedom. *Report No 741*. National Advisory Committee for Aeronautics (NACA).
- VANDIVER, J. K. & MAZEL, C. H. (1976) A Field Study of Vortex-Excited Vibrations of Marine Cables. *Offshore Technology Conference (OTC76-2491)*. Houston, USA.
- WANG, W. & WATKINS, L. (2004) Use of Composite Materials in Protecting and Maintaining Subsea Equipments. *23rd International Conference on Offshore Mechanics and Arctic Engineering (OMAE04-51278)*. Vancouver, Canada, American Society of Mechanical Engineers (ASME).
- WEST, C., ARMSTRONG, S. P., MCMILLAN, D. W. & ALLEN, D. W. (2007) S-Lay Installation of Riser Fairings for the Independence Hub. *26th International Conference on Offshore Mechanics and Arctic Engineering (OMAE07-29416)*. San Diego, USA, American Society of Mechanical Engineers (ASME).
- WIGGINS, S. (1990) *Introduction to Applied Nonlinear Dynamical Systems and Chaos*, New York, USA, Springer-Verlag.
- WINGHAM, P. J. (1983) Comparative Steady State Deep Towing Performance of Bare and Faired Cable Systems. *Ocean Engineering*, 10, 1-32.
- WINGHAM, P. J. & KESHAVAN, N. R. (1978) Predicting the Equilibrium Depth of a Body Towed by a Faired Cable. *Ocean Engineering*, 5, 15-35.
- ZDRAVKOVICH, M. M. (1981) Review and classification of various aerodynamic and hydrodynamic means for suppressing vortex shedding. *Journal of Wind Engineering and Industrial Aerodynamics*, 7, 145.

Appendix A: CFD Results

NACA0070

$$U = 0.08 \text{ (m/s)}$$

$$Re_c = 5 \times 10^4$$

$$Y^+ = 0.826$$

Turbulence model: Realisable $k - \varepsilon$

Size of computational domain (L (upstream-downstream) x W): 25c (5c-19c) x 10c

Number of cells: 103158

Results

AoA	C_d	Amp(C_d)	C_L	Amp(C_L)	C_m	Amp(C_m)	St. No.	Run(s)
0°	0.608	0.002	0	0.125	0	0.017	0.21	1000
5°	0.600	0.005	-0.100	0.125	0.006	0.017	0.20	1000
10°	0.572	0.007	-0.250	0.125	0.013	0.016	0.21	1000
15°	0.510	0.008	-0.492	0.103	0.023	0.014	0.22	1000

$$\left. \frac{\partial C_L}{\partial \alpha} \right|_{\alpha=0} = -1.146$$

$$\left. \frac{\partial C_{M(CR)}}{\partial \alpha} \right|_{\alpha=0} = 0.069$$

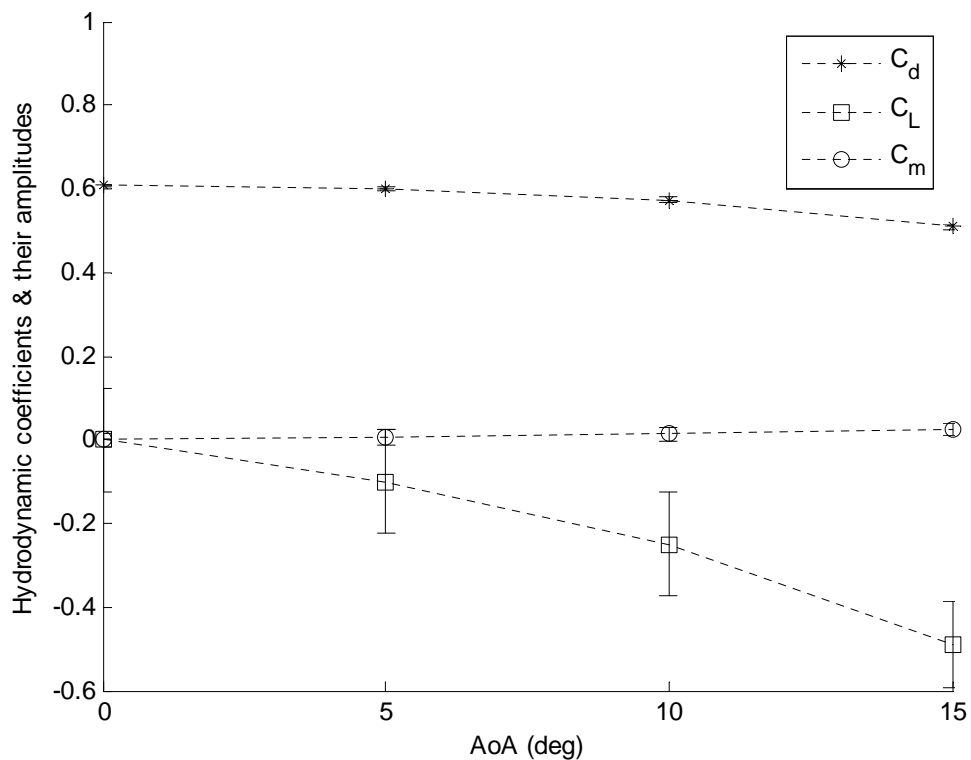


Figure A-1 Hydrodynamic Coefficients & Their Amplitudes.

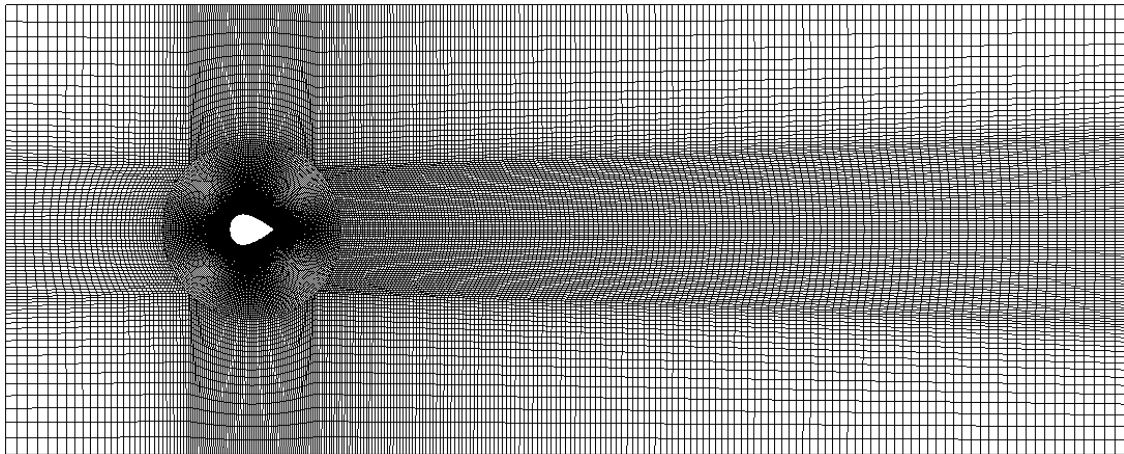


Figure A-2 Computational Domain And Mesh.

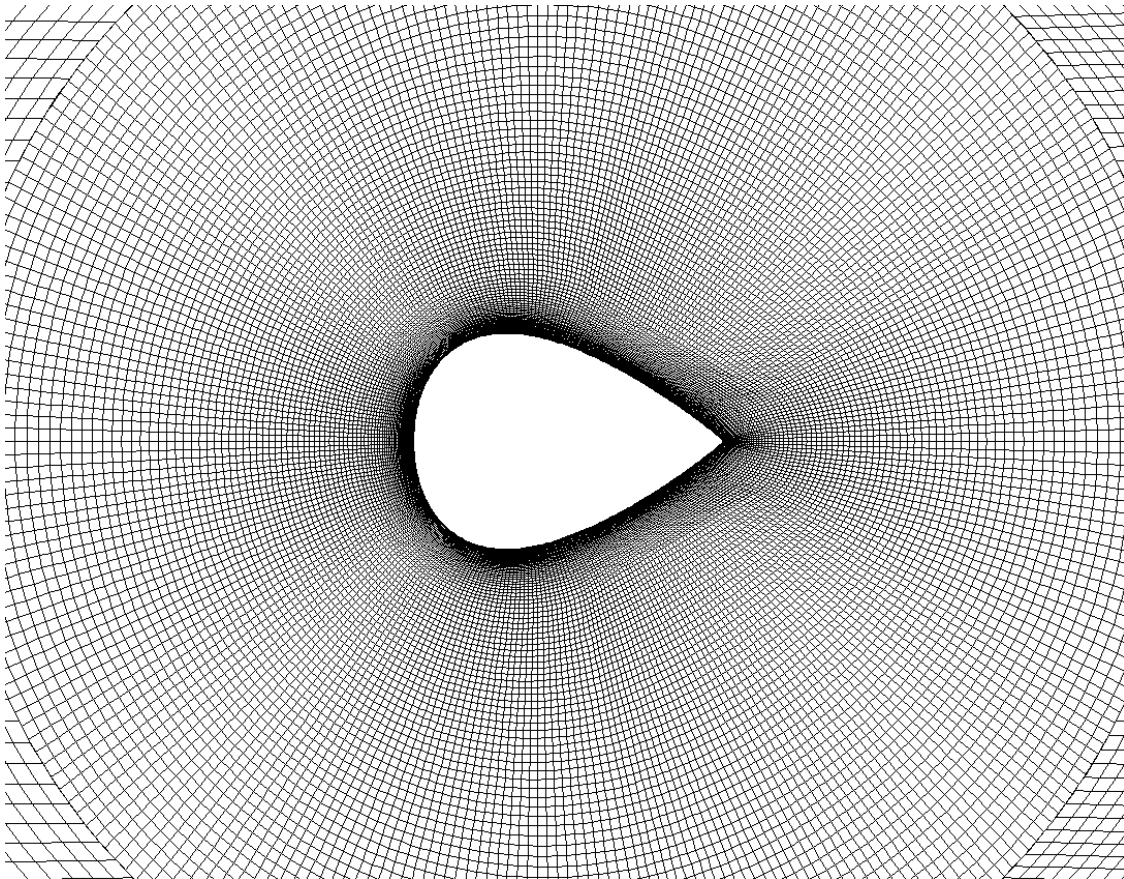


Figure A-3 Mesh Close To The Fairing.

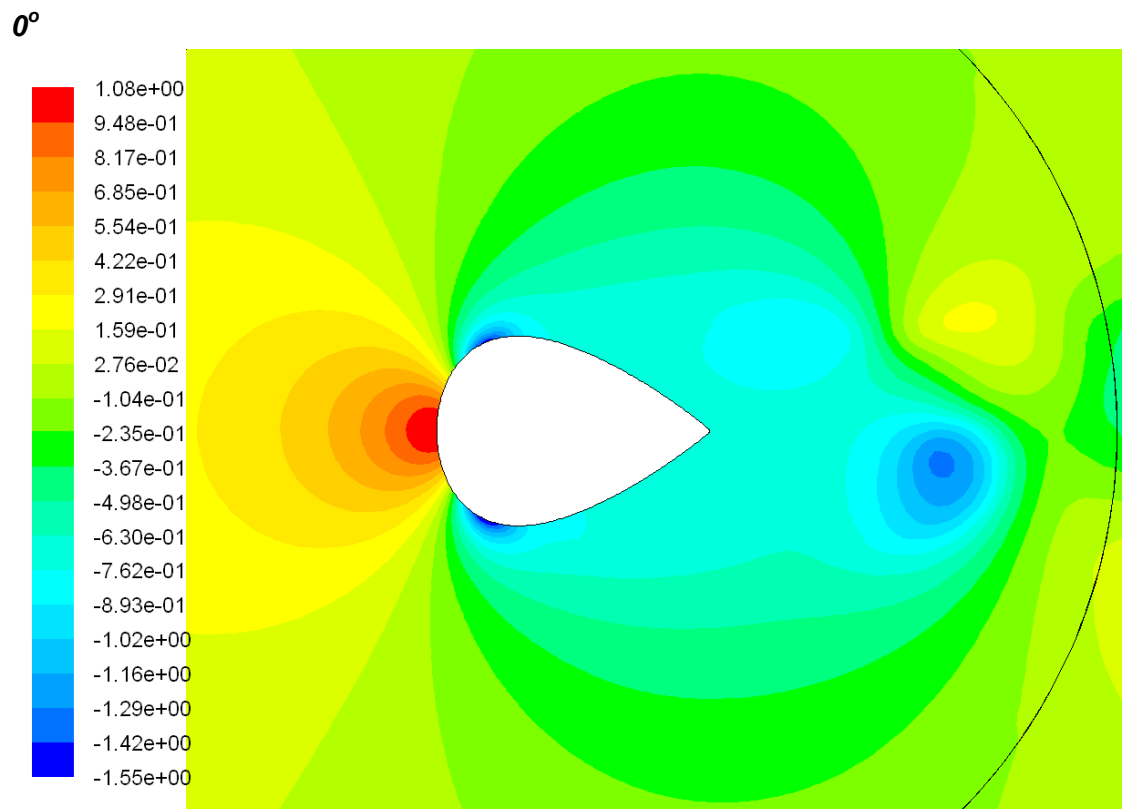


Figure A-4 Pressure Coefficient At 0° .

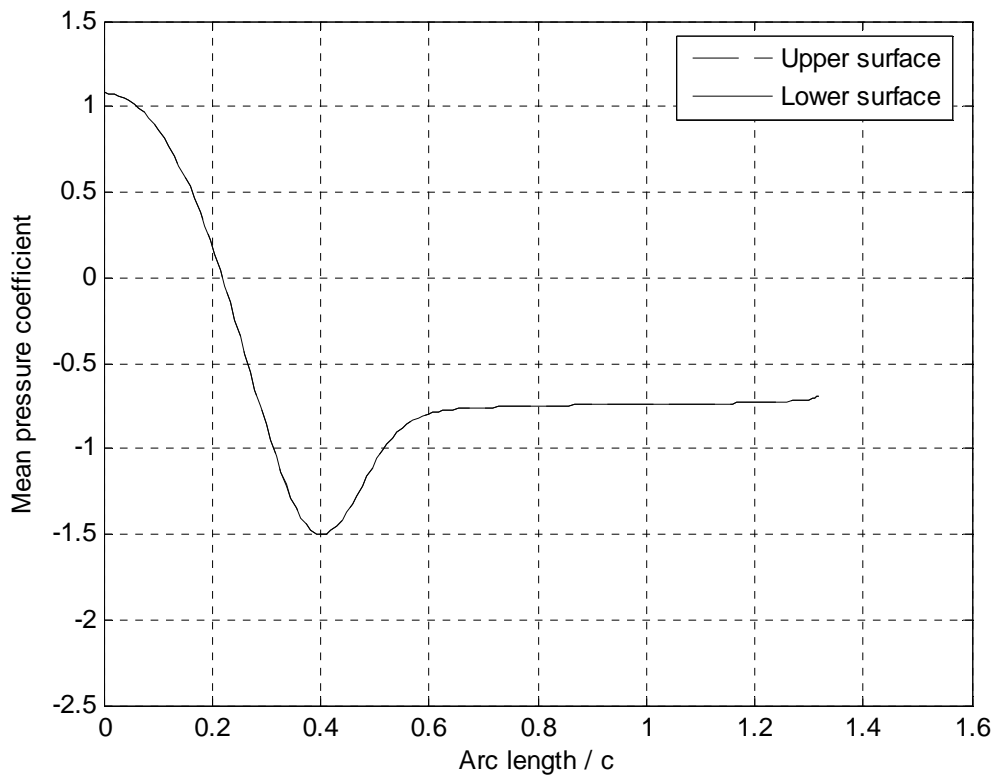


Figure A-5 Mean Pressure Coefficient Around The Fairing Surface At 0° .

5°

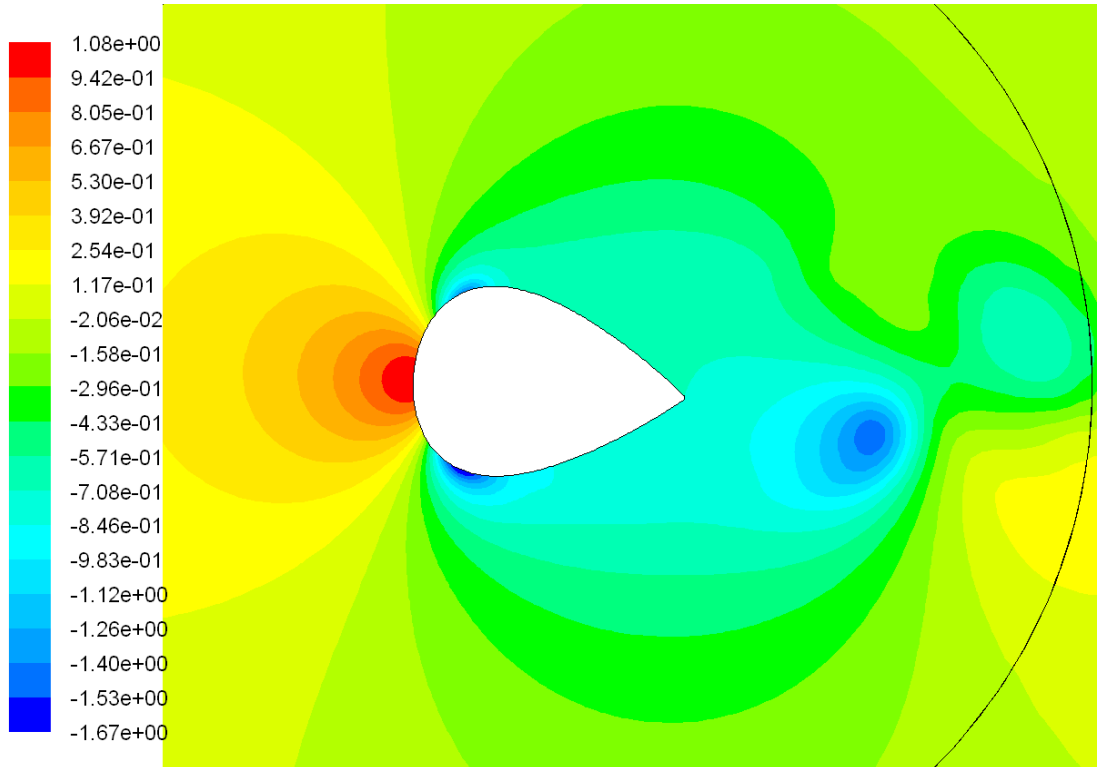


Figure A-6 Pressure Coefficient At 5°.

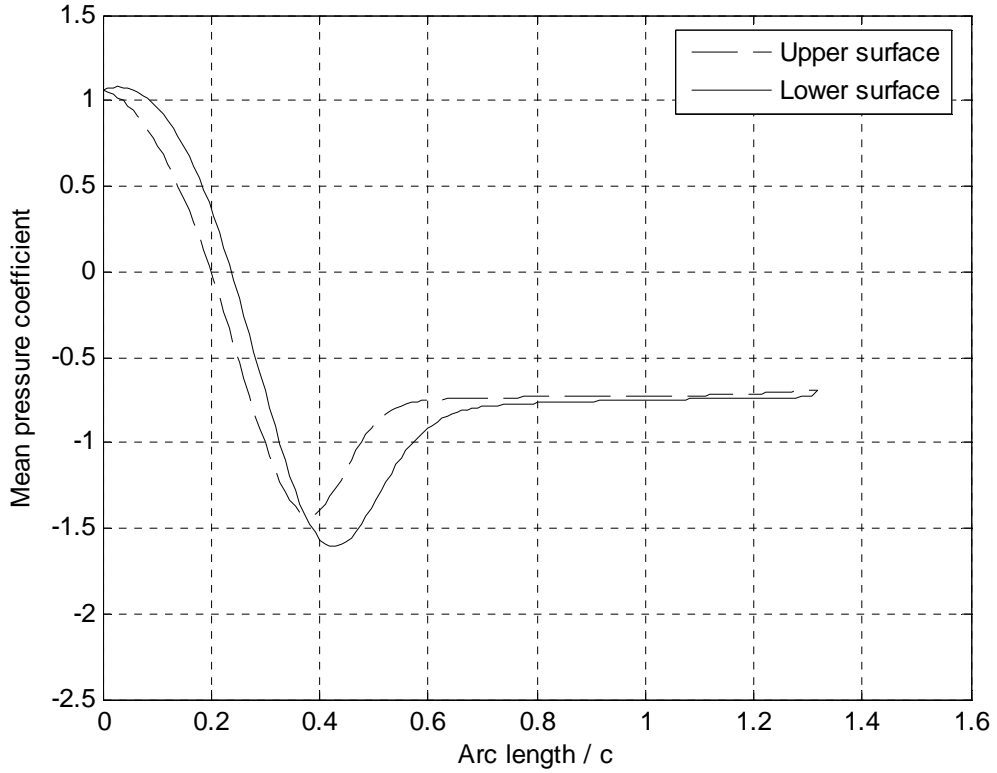


Figure A-7 Mean Pressure Coefficient Around The Fairing Surface At 5°.

10°

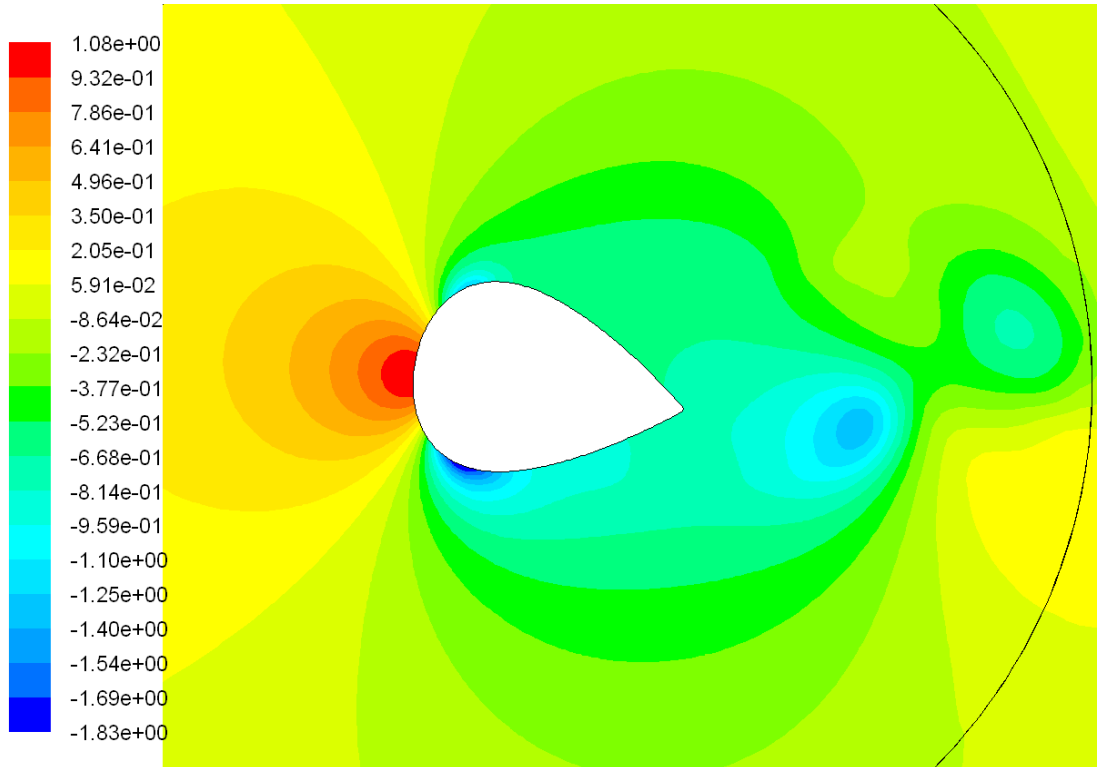


Figure A-8 Pressure Coefficient At 10°.

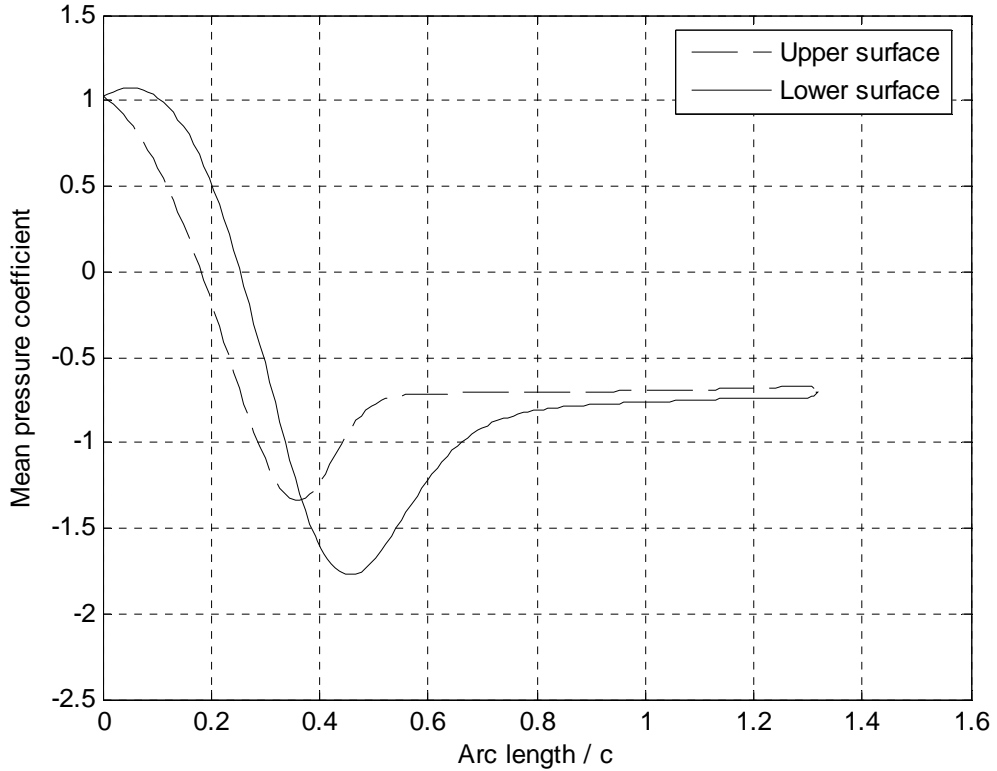


Figure A-9 Mean Pressure Coefficient Around The Fairing Surface At 10°.

15°

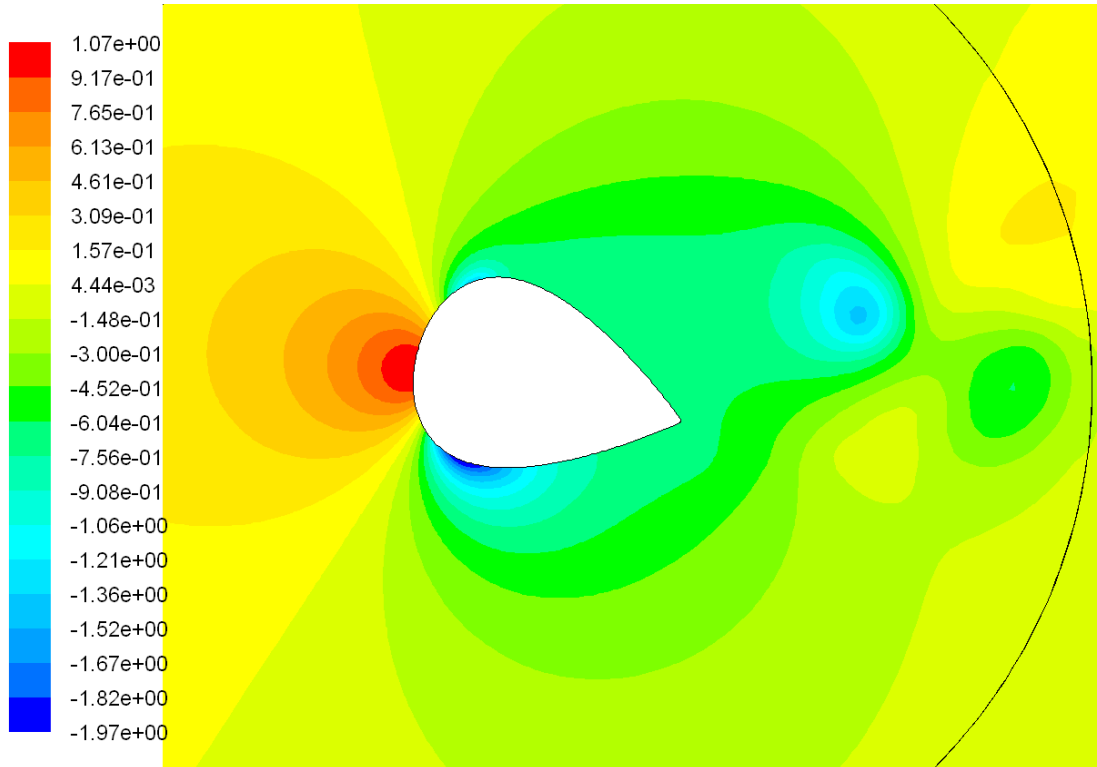


Figure A-10 Pressure Coefficient At 15°.

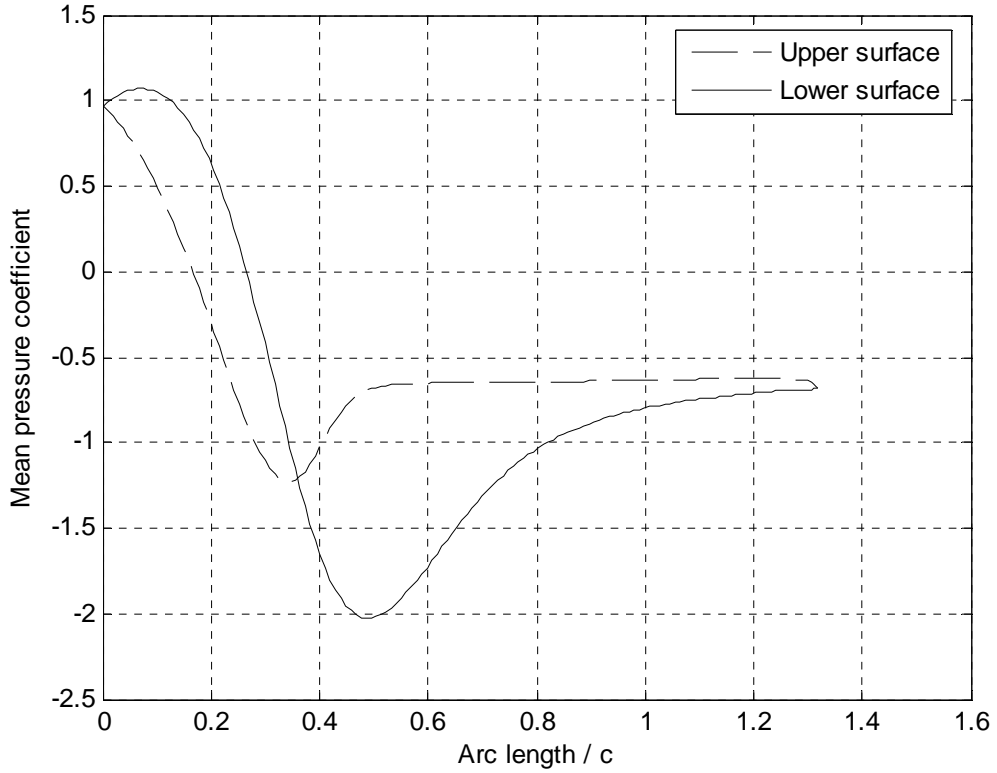


Figure A-11 Mean Pressure Coefficient Around The Fairing Surface At 15°.

Short Fairing

$$U = 0.08 \text{ (m/s)}$$

$$Re_c = 5 \times 10^4$$

$$Y^+ = 0.885$$

Turbulence model: Realisable $k - \epsilon$

Size of computational domain (L (upstream-downstream) x W): 25c (5c-19c) x 10c

Number of cells: 111284

Results

AoA	C_d	Amp(C_d)	C_L	Amp(C_L)	C_m	Amp(C_m)	St. No.	Run(s)
0°	0.549	0.001	0	0.110	0	0.018	0.21	1000
5°	0.550	0.006	-0.013	0.112	0.011	0.018	0.21	1000
10°	0.550	0.012	-0.032	0.107	0.021	0.018	0.21	1000
15°	0.551	0.016	-0.053	0.113	0.033	0.016	0.20	1000

$$\left. \frac{\partial C_L}{\partial \alpha} \right|_{\alpha=0} = -0.148$$

$$\left. \frac{\partial C_{M(CR)}}{\partial \alpha} \right|_{\alpha=0} = 0.126$$

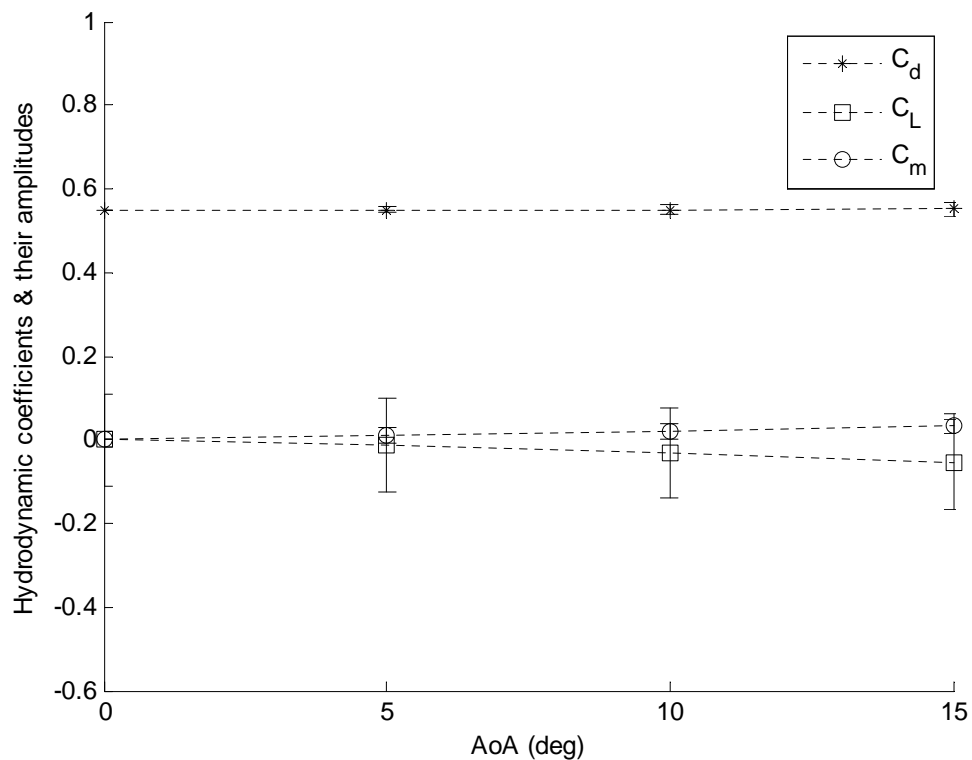


Figure A-12 Hydrodynamic Coefficients & Their Amplitudes.

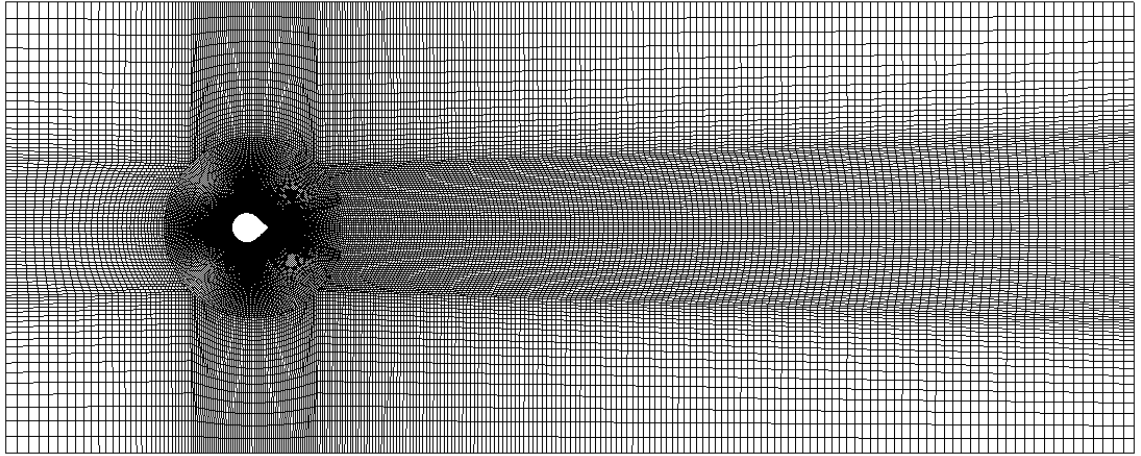


Figure A-13 Computational Domain And Mesh.

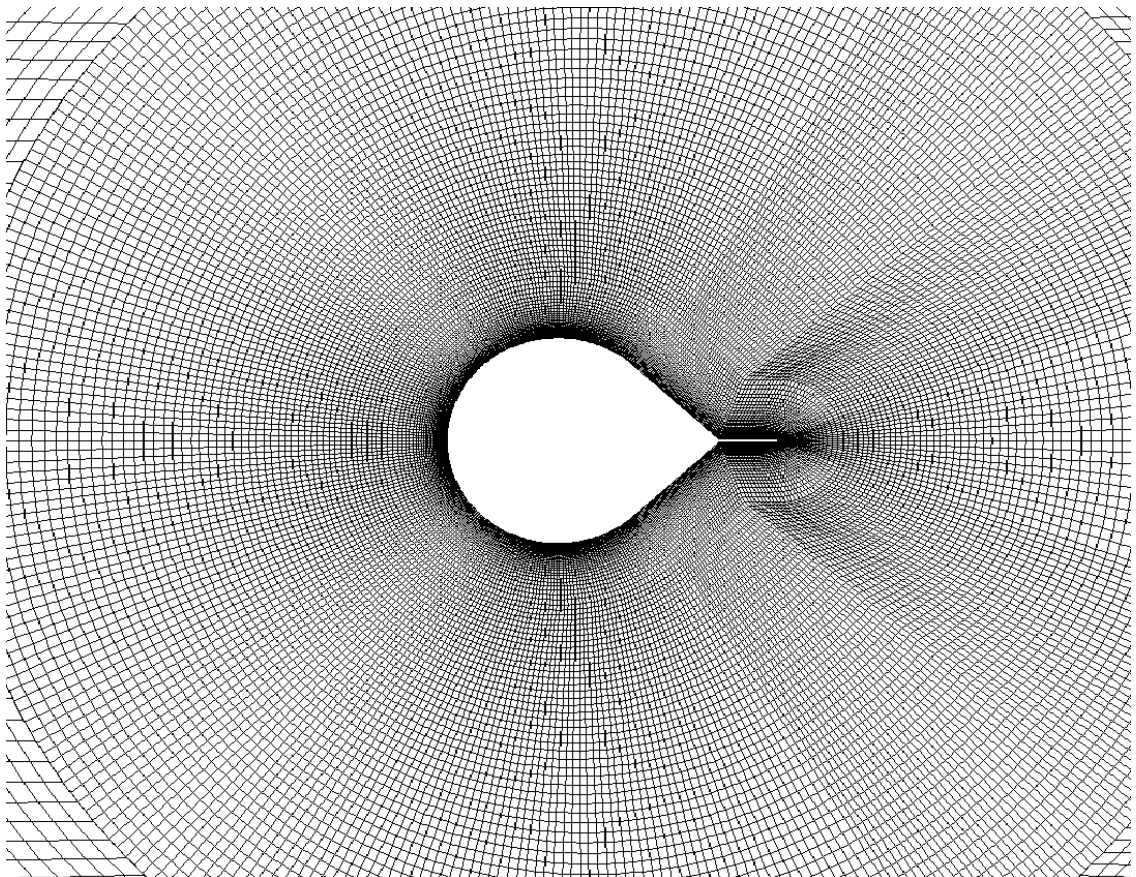


Figure A-14 Mesh Close To The Fairing.

0°

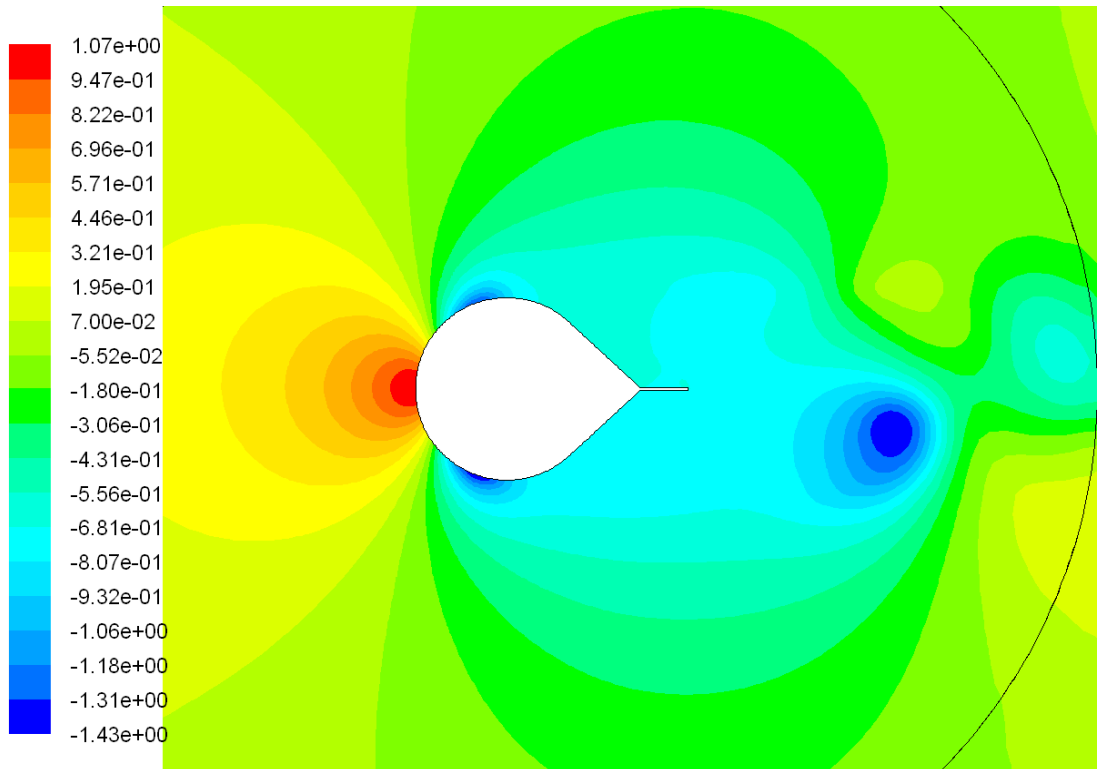


Figure A-15 Pressure Coefficient At 0°.

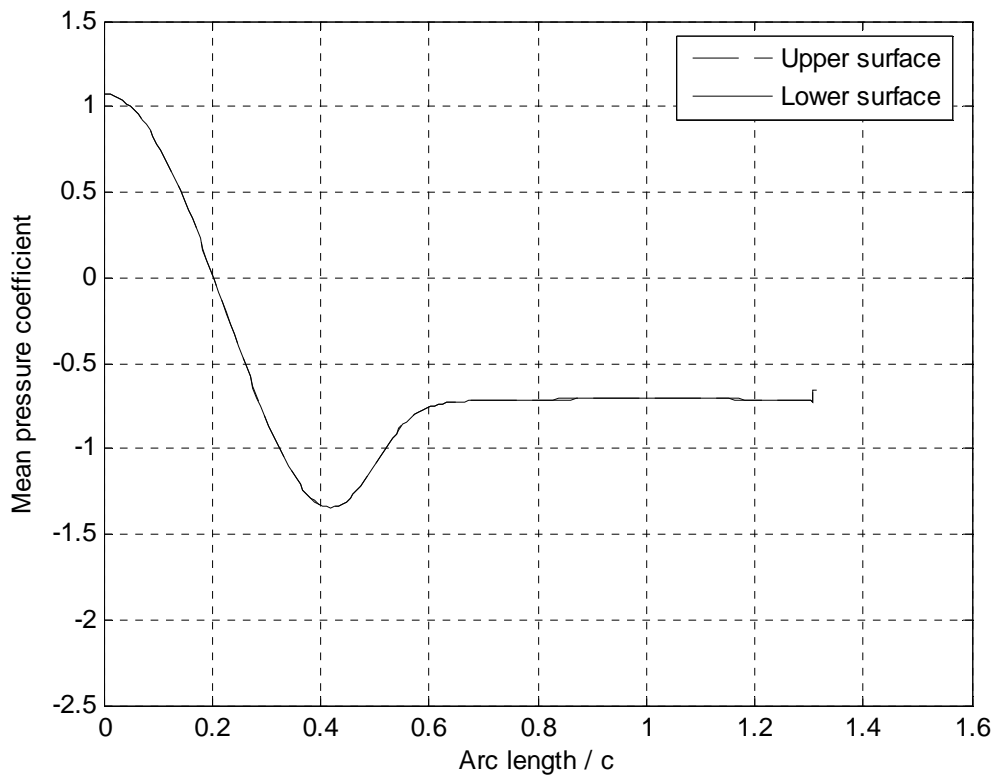


Figure A-16 Mean Pressure Coefficient Around The Fairing Surface At 0°.

5°

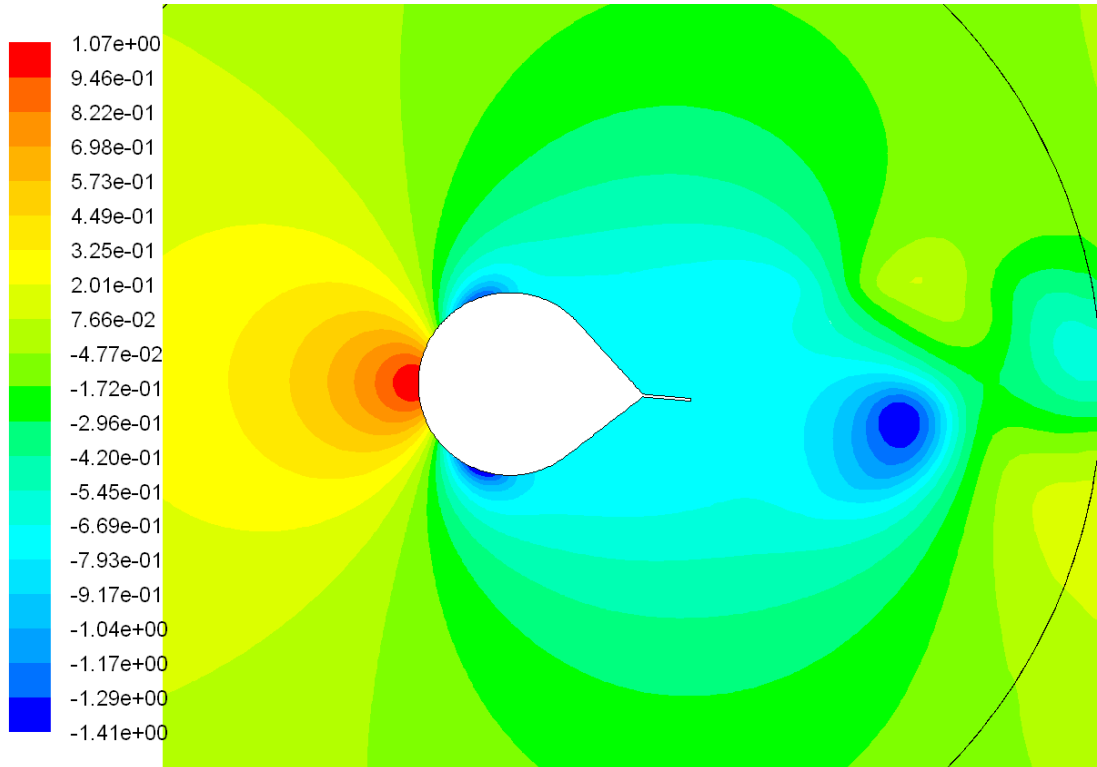


Figure A-17 Pressure Coefficient At 5°.

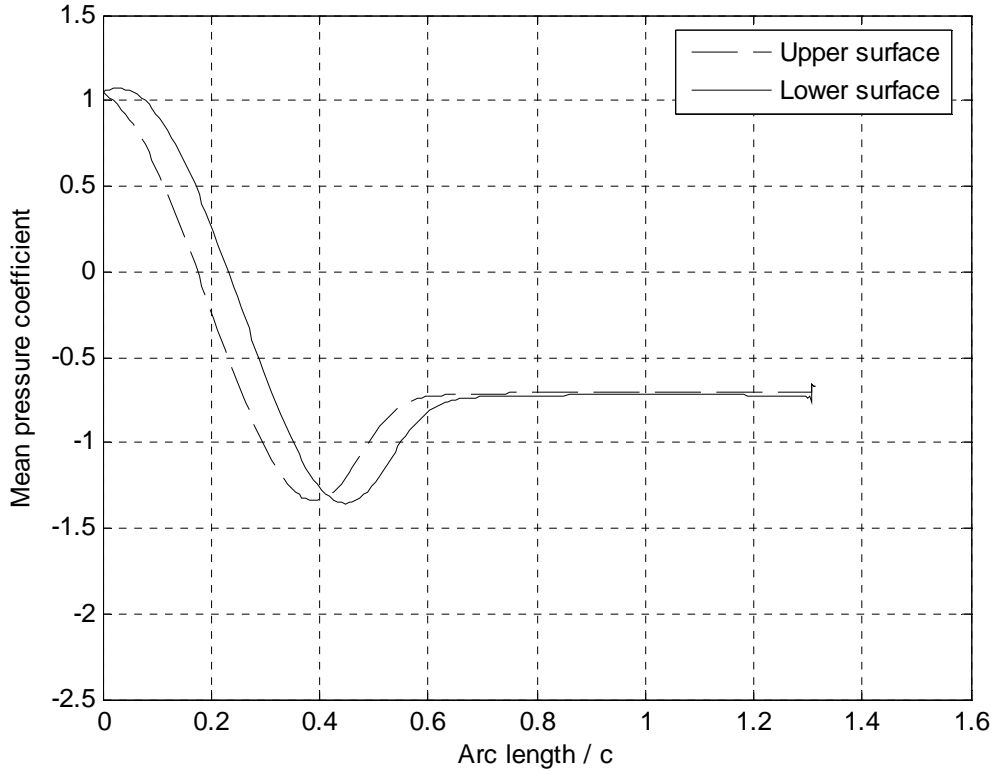


Figure A-18 Mean Pressure Coefficient Around The Fairing Surface At 5°.

10°

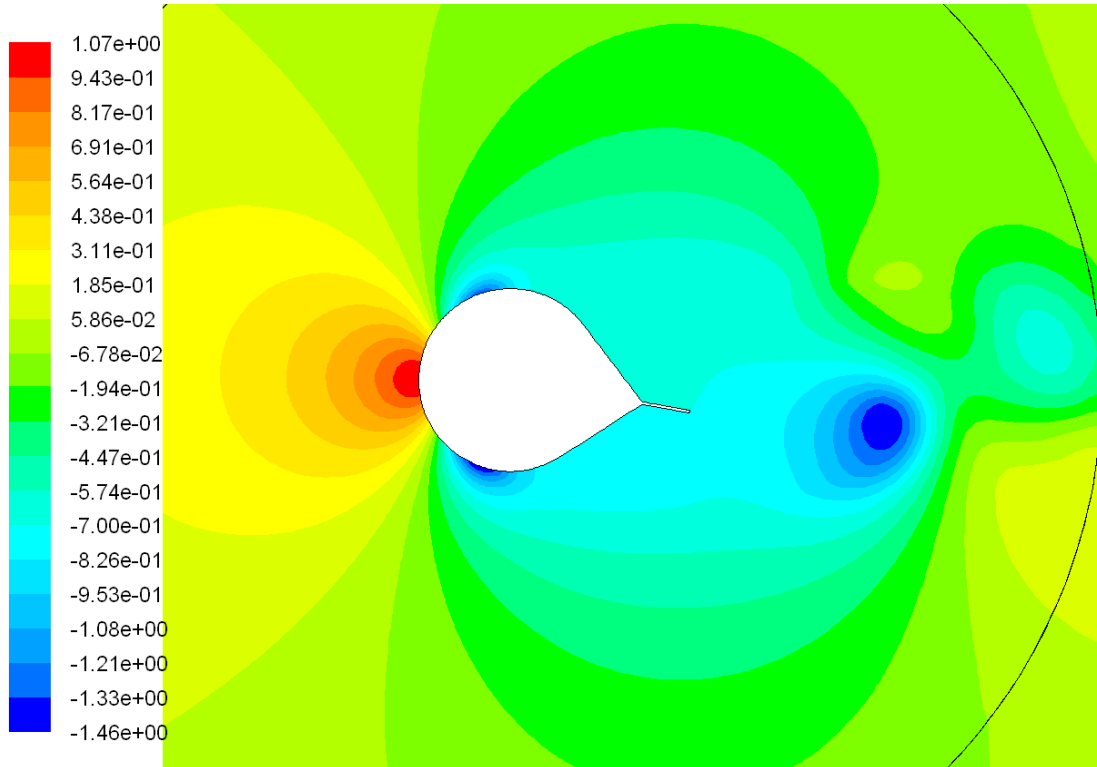


Figure A-19 Pressure Coefficient At 10°.

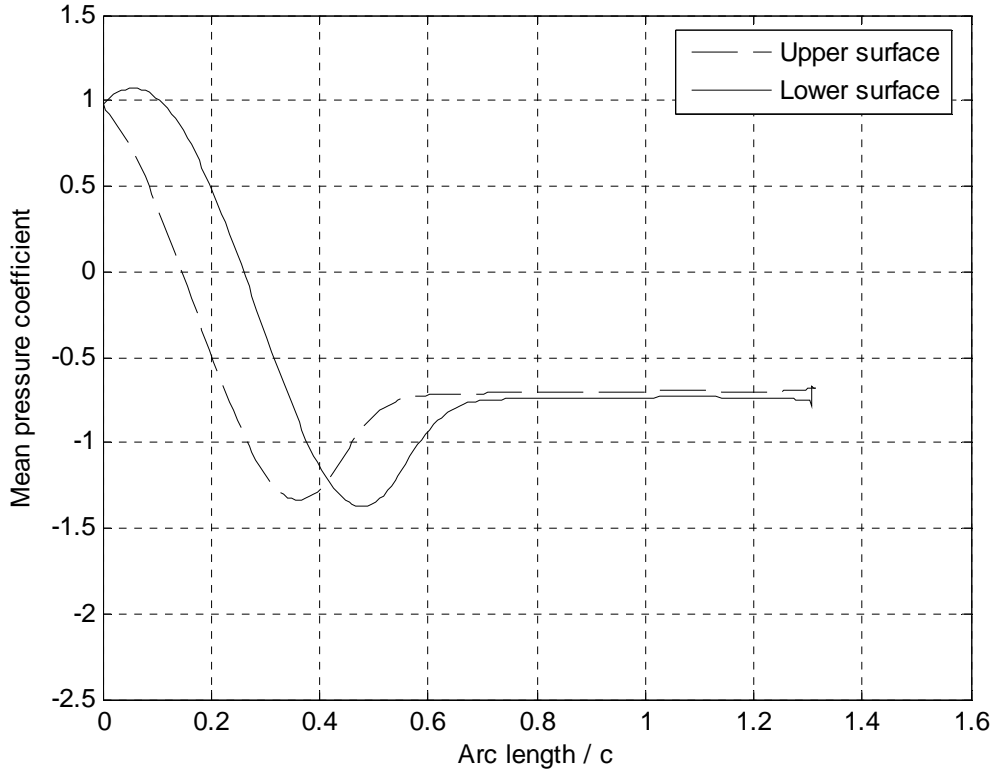


Figure A-20 Mean Pressure Coefficient Around The Fairing Surface At 10°.

15°

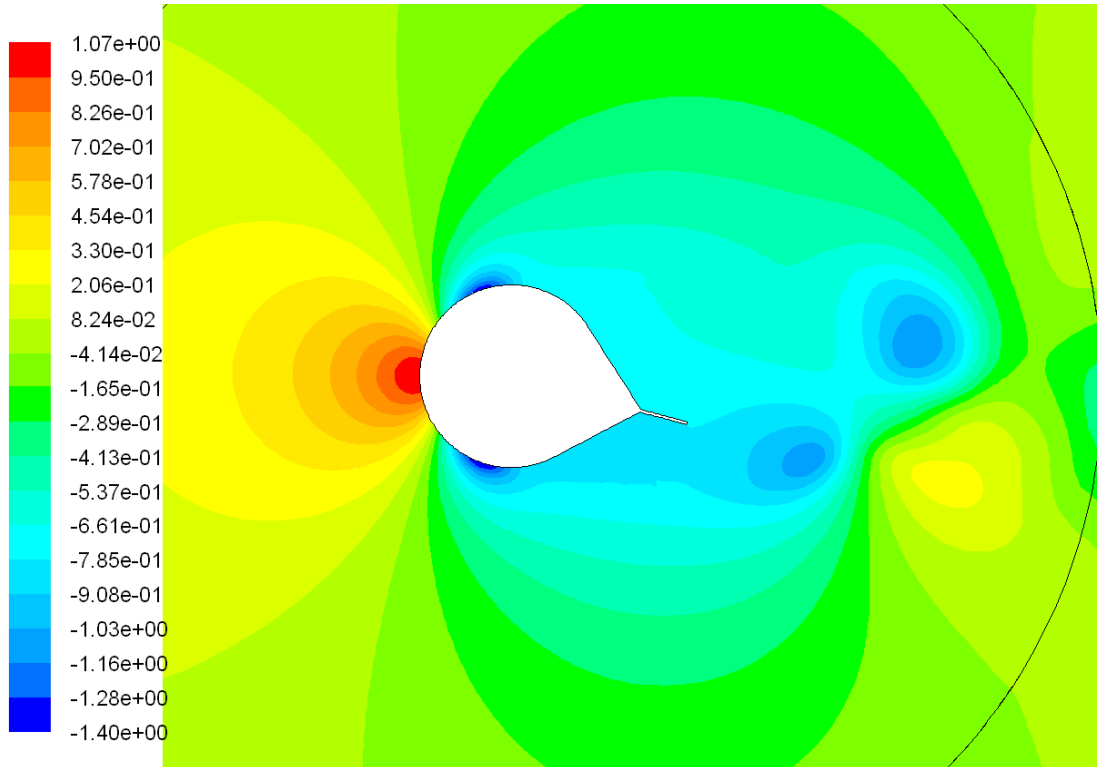


Figure A-21 Pressure Coefficient At 15°.

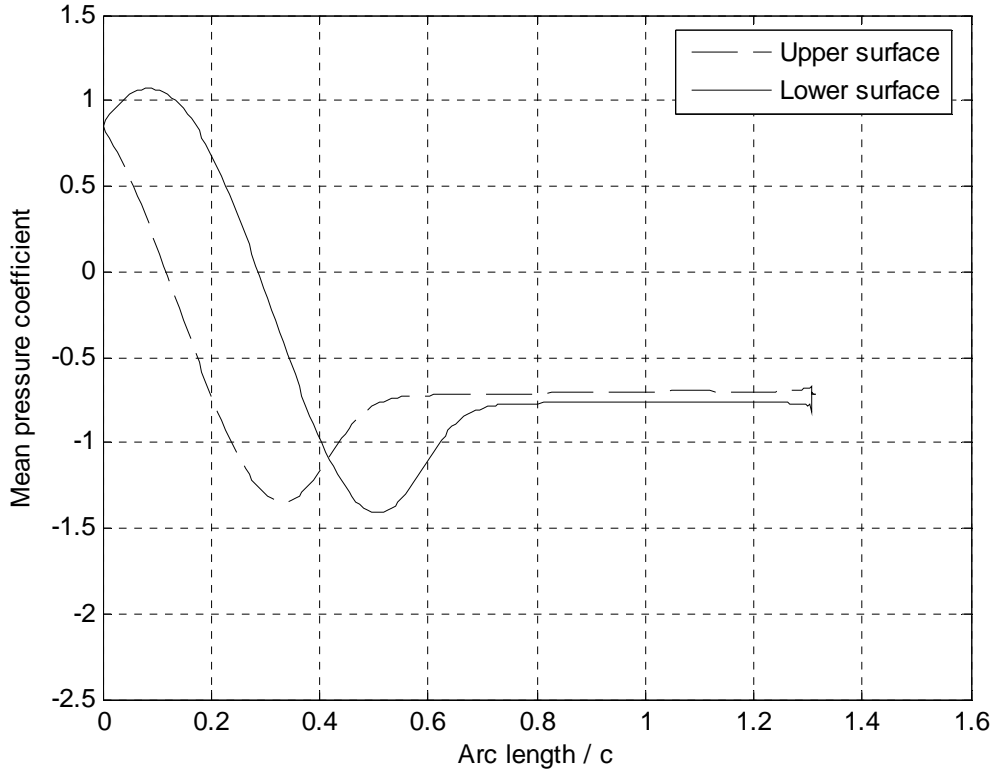


Figure A-22 Mean Pressure Coefficient Around The Fairing Surface At 15°.

Guide Vane

$$U = 0.08 \text{ (m/s)}$$

$$Re_c = 5 \times 10^4$$

$$Y^+ = 0.908$$

Turbulence model: Realisable $k - \varepsilon$

Size of computational domain (L (upstream-downstream) x W): 25c (5c-19c) x 10c

Number of cells: 147341

Results

AoA	C_d	Amp(C_d)	C_L	Amp(C_L)	C_m	Amp(C_m)	St. No.	Run(s)
0°	0.329	0.002	0	0.084	0	0.022	0.28	1000
5°	0.446	0.017	0.125	0.127	-0.027	0.036	0.23	1000
10°	0.597	0.043	0.250	0.240	-0.040	0.052	0.19	1000
15°	0.690	0.050	0.400	0.250	-0.045	0.055	0.17	1000

$$\left. \frac{\partial C_L}{\partial \alpha} \right|_{\alpha=0} = +1.432$$

$$\left. \frac{\partial C_{M(CR)}}{\partial \alpha} \right|_{\alpha=0} = -0.309$$

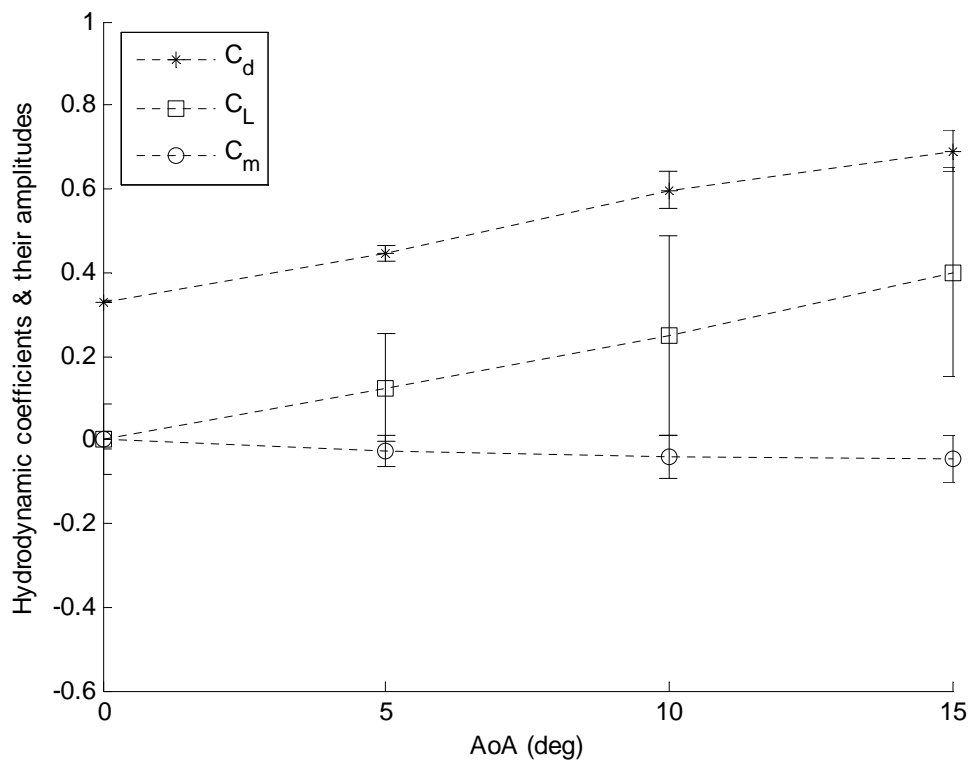


Figure A-23 Hydrodynamic Coefficients & Their Amplitudes.

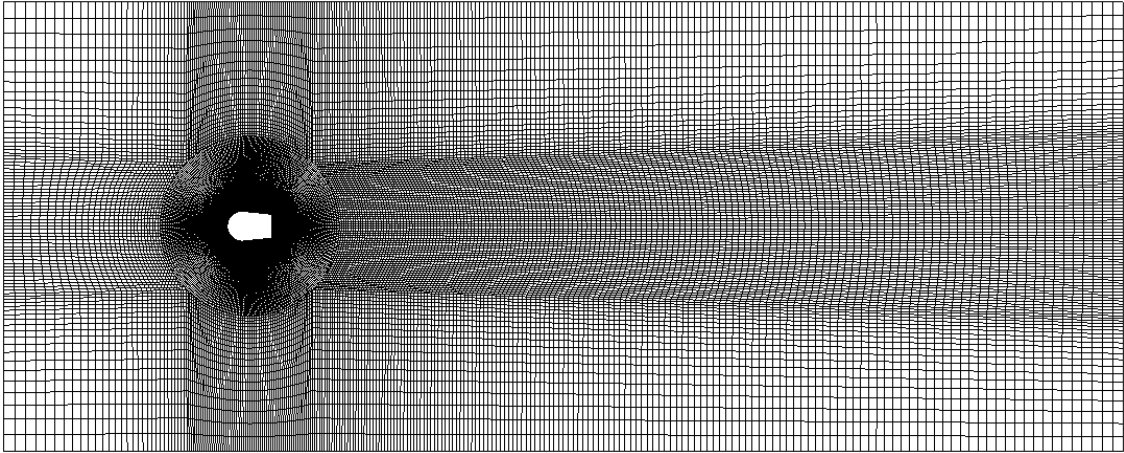


Figure A-24 Computational Domain And Mesh.

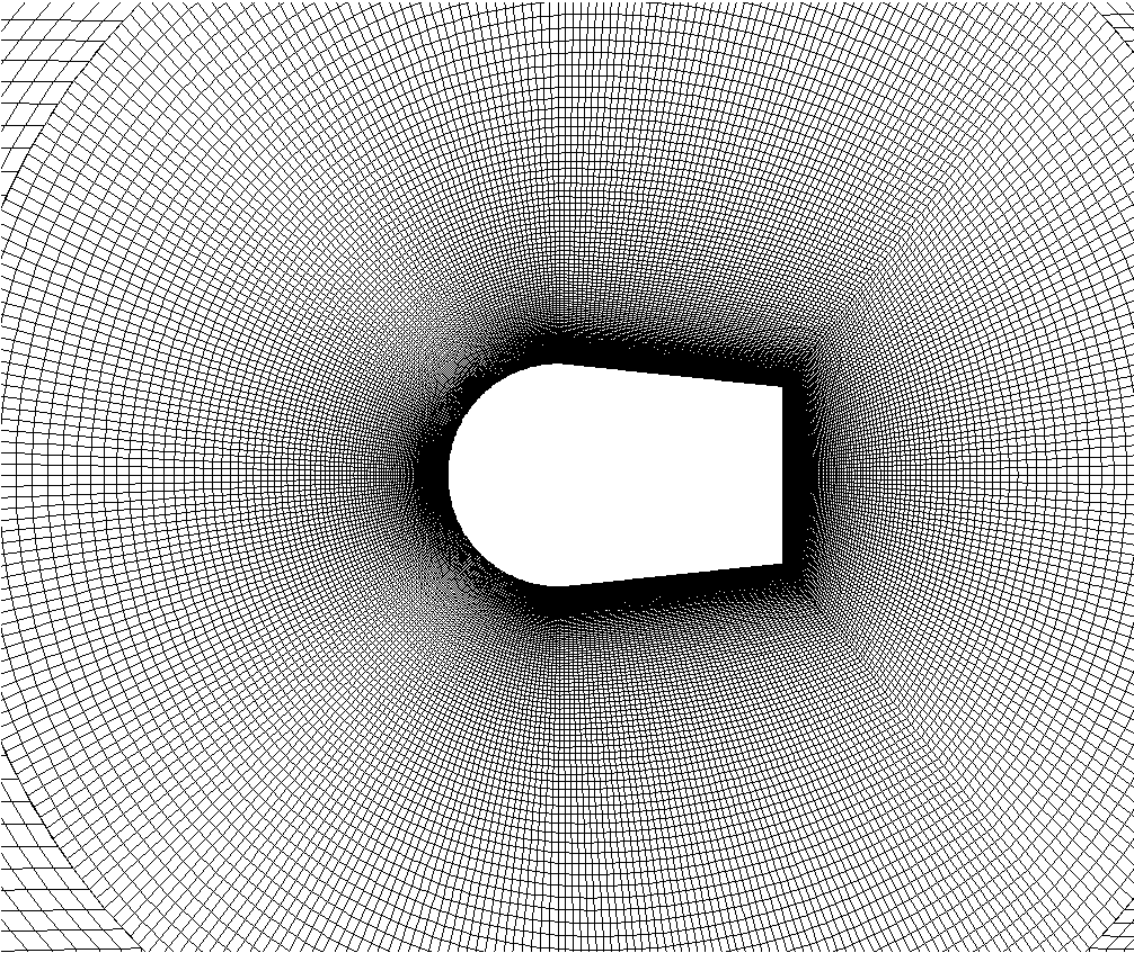


Figure A-25 Mesh Close To The Fairing.

0°

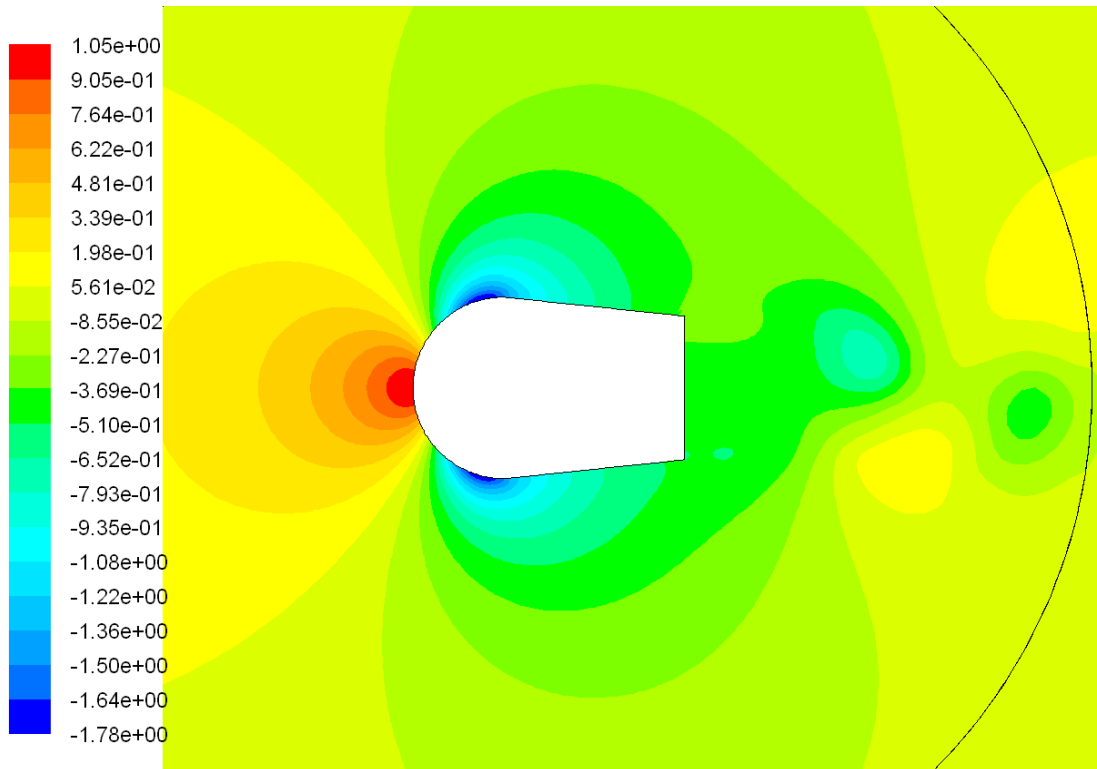


Figure A-26 Pressure Coefficient At 0°.

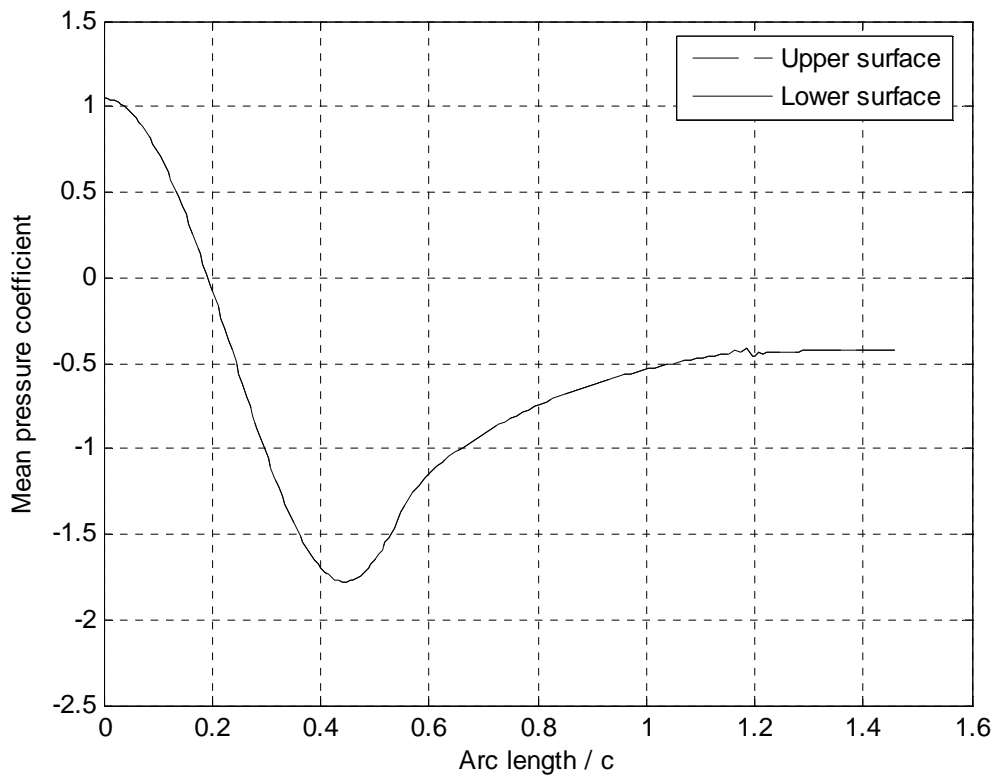


Figure A-27 Mean Pressure Coefficient Around The Fairing Surface At 0°.

5°

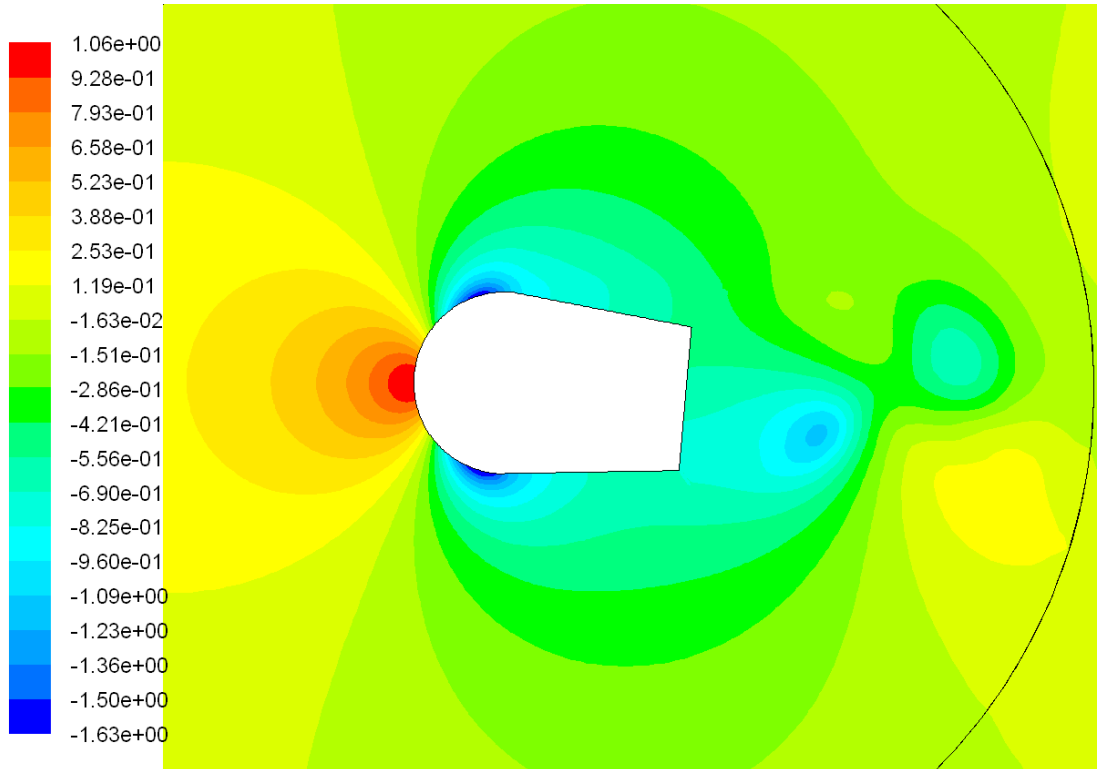


Figure A-28 Pressure Coefficient At 5°.

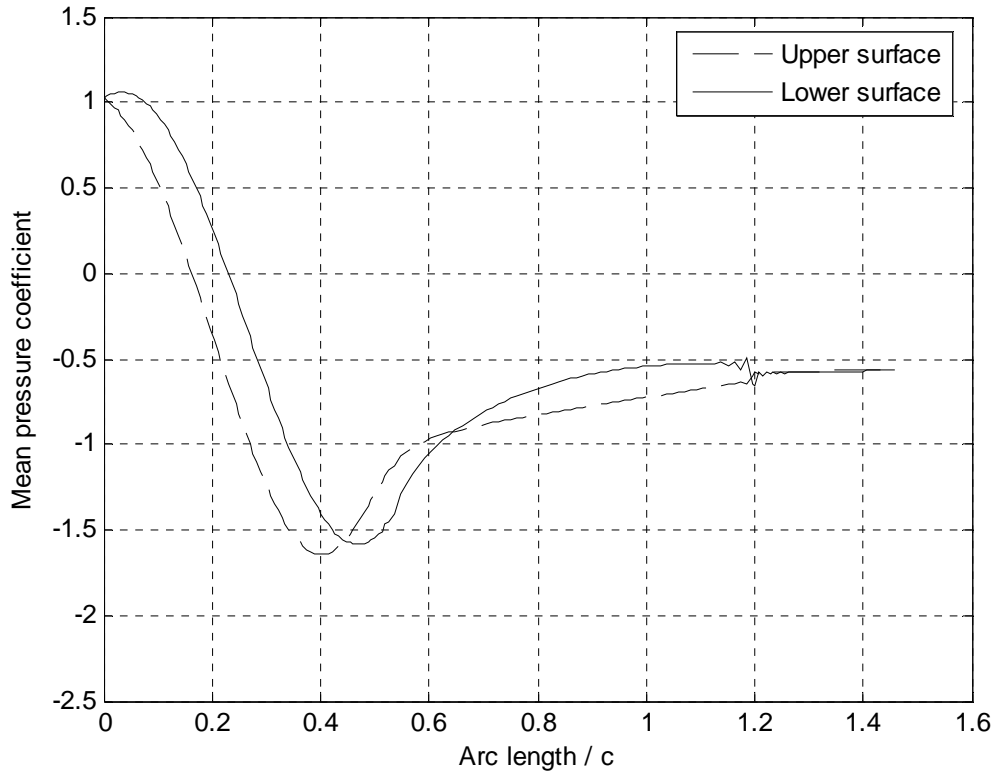


Figure A-29 Mean Pressure Coefficient Around The Fairing Surface At 5°.

10°

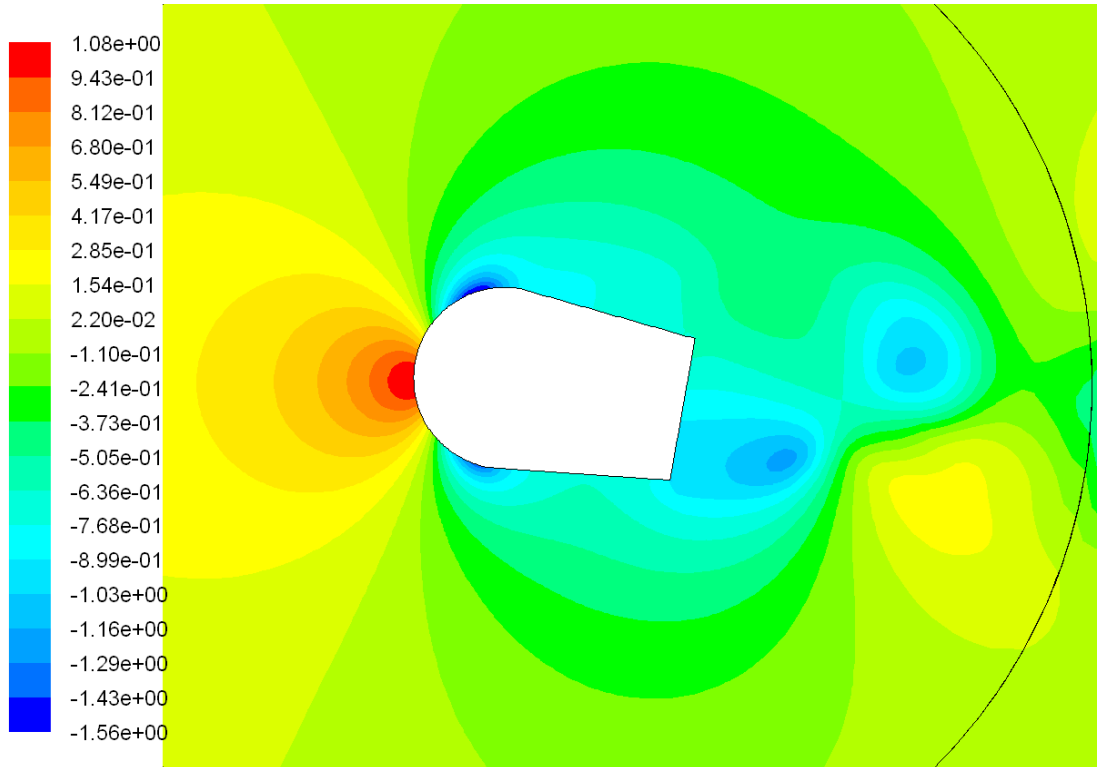


Figure A-30 Pressure Coefficient At 10°.

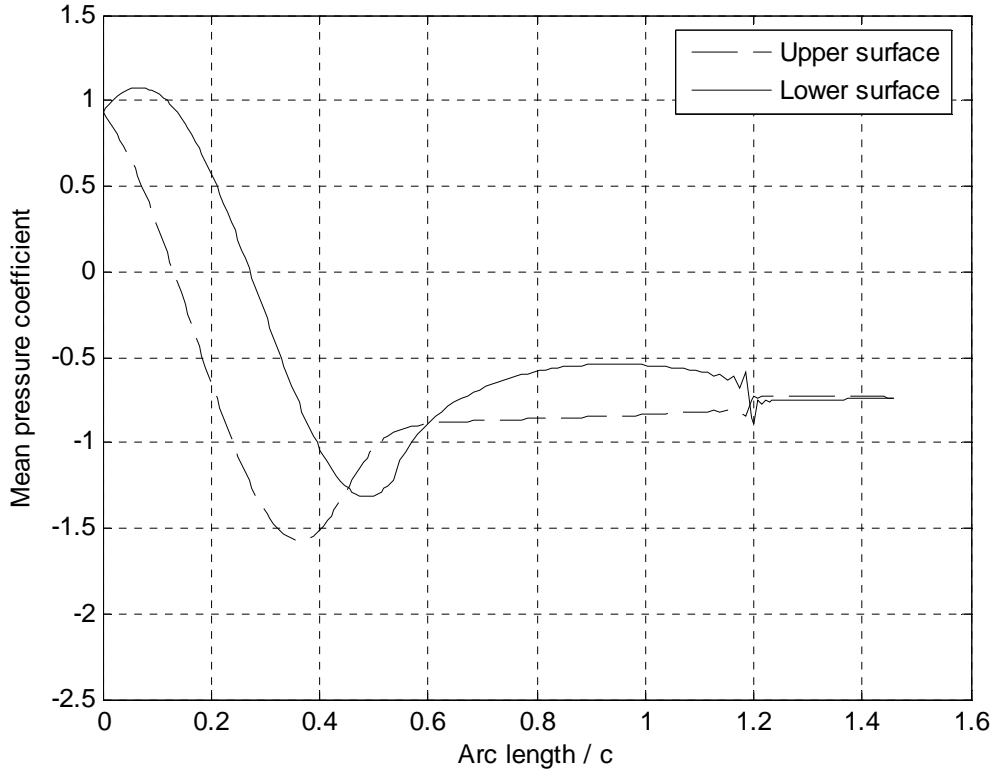


Figure A-31 Mean Pressure Coefficient Around The Fairing Surface At 10°.

15°

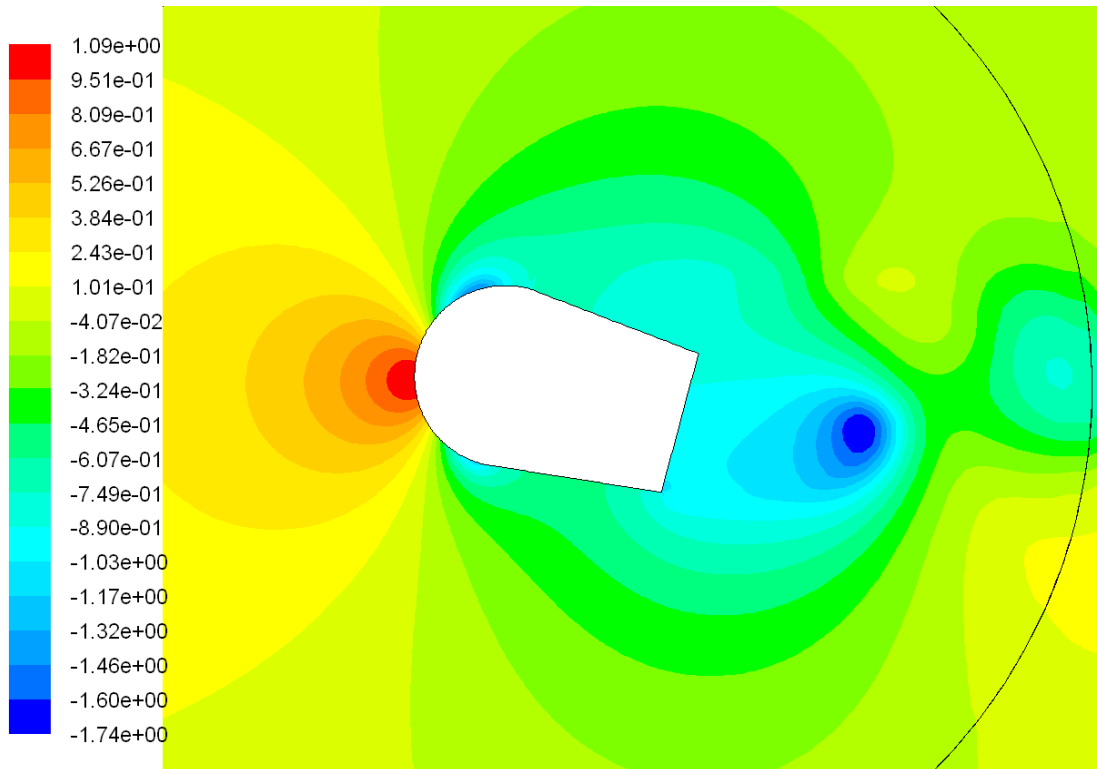


Figure A-32 Pressure Coefficient At 15°.

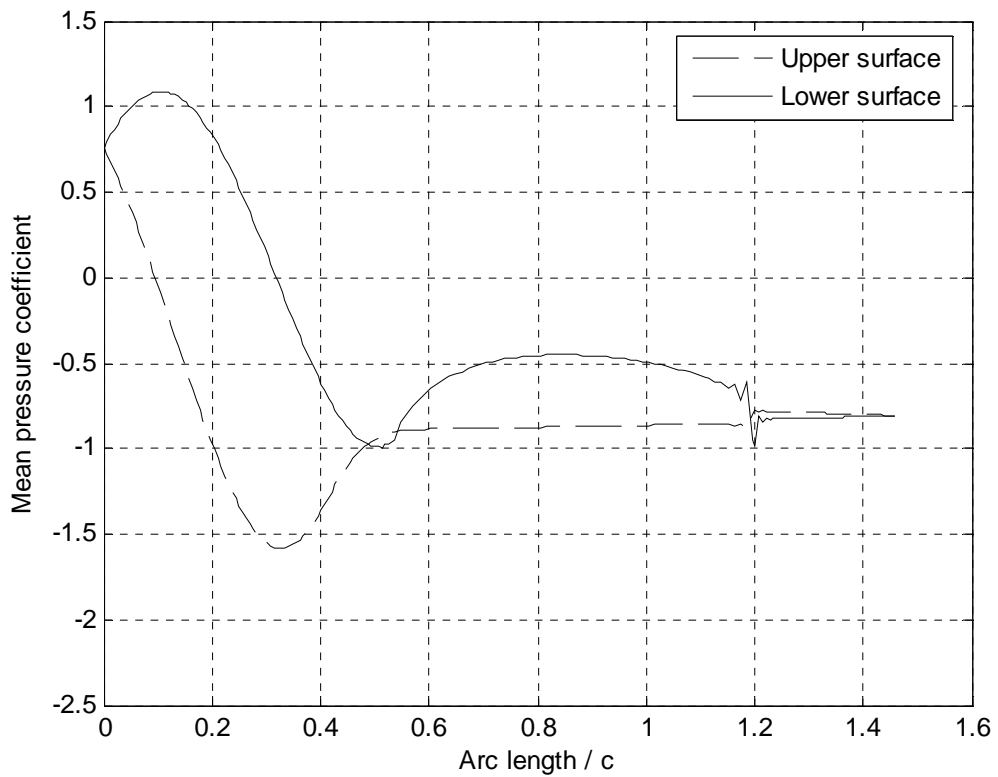


Figure A-33 Mean Pressure Coefficient Around The Fairing Surface At 15°.

Exxon's Fairing without Fin

$$U = 0.08 \text{ (m/s)}$$

$$Re_c = 5 \times 10^4$$

$$Y^+ = 0.839$$

Turbulence model: Realisable $k - \epsilon$

Size of computational domain (L (upstream-downstream) x W): 25c (5c-19c) x 10c

Number of cells: 130522

Results

AoA	C_d	Amp(C_d)	C_L	Amp(C_L)	C_m	Amp(C_m)	St. No.	Run(s)
0°	0.2716	0.0001	0	0.075	0	0.028	0.18	2200
5°	0.209	0.002	-0.545	0.060	0.065	0.025	0.21	1400
10°	0.285	0.006	-0.275	0.175	0.035	0.070	0.21	650
15°	0.365	0.015	0.005	0.175	0.005	0.063	0.19	600

$$\left. \frac{\partial C_L}{\partial \alpha} \right|_{\alpha=0} = -6.245$$

$$\left. \frac{\partial C_{M(CR)}}{\partial \alpha} \right|_{\alpha=0} = +0.745$$

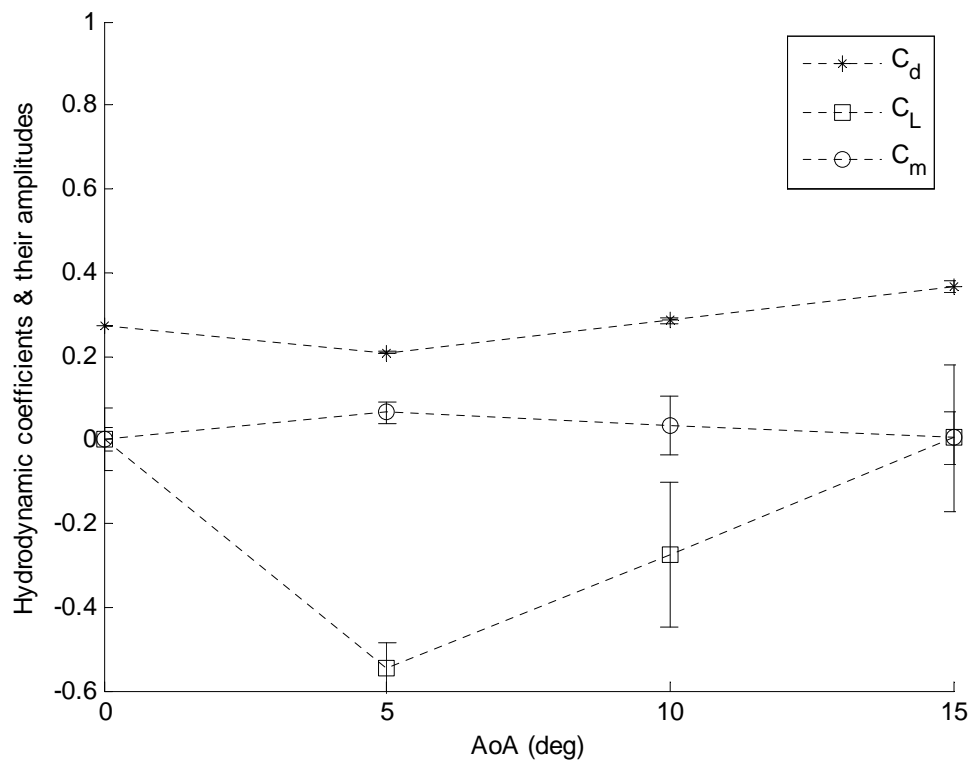


Figure A-34 Hydrodynamic Coefficients & Their Amplitudes.

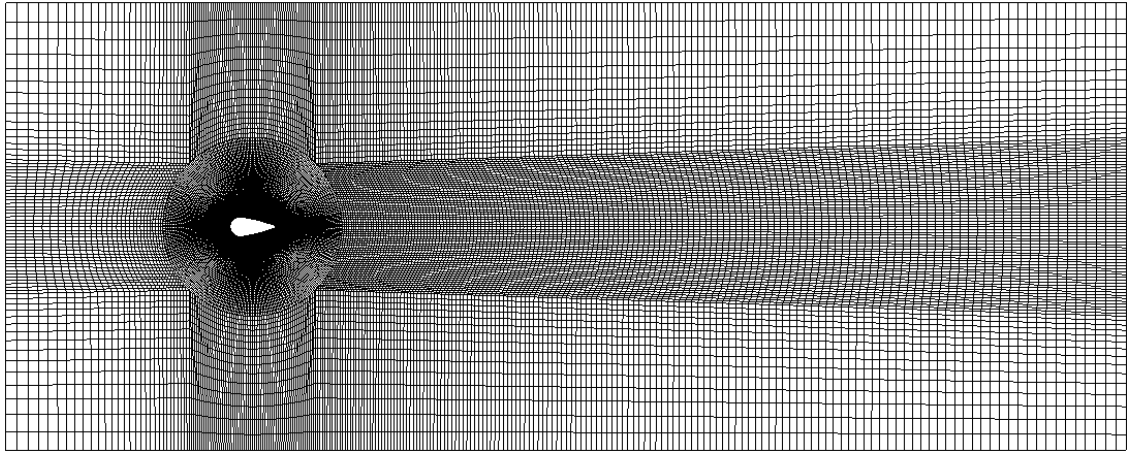


Figure A-35 Computational Domain And Mesh.

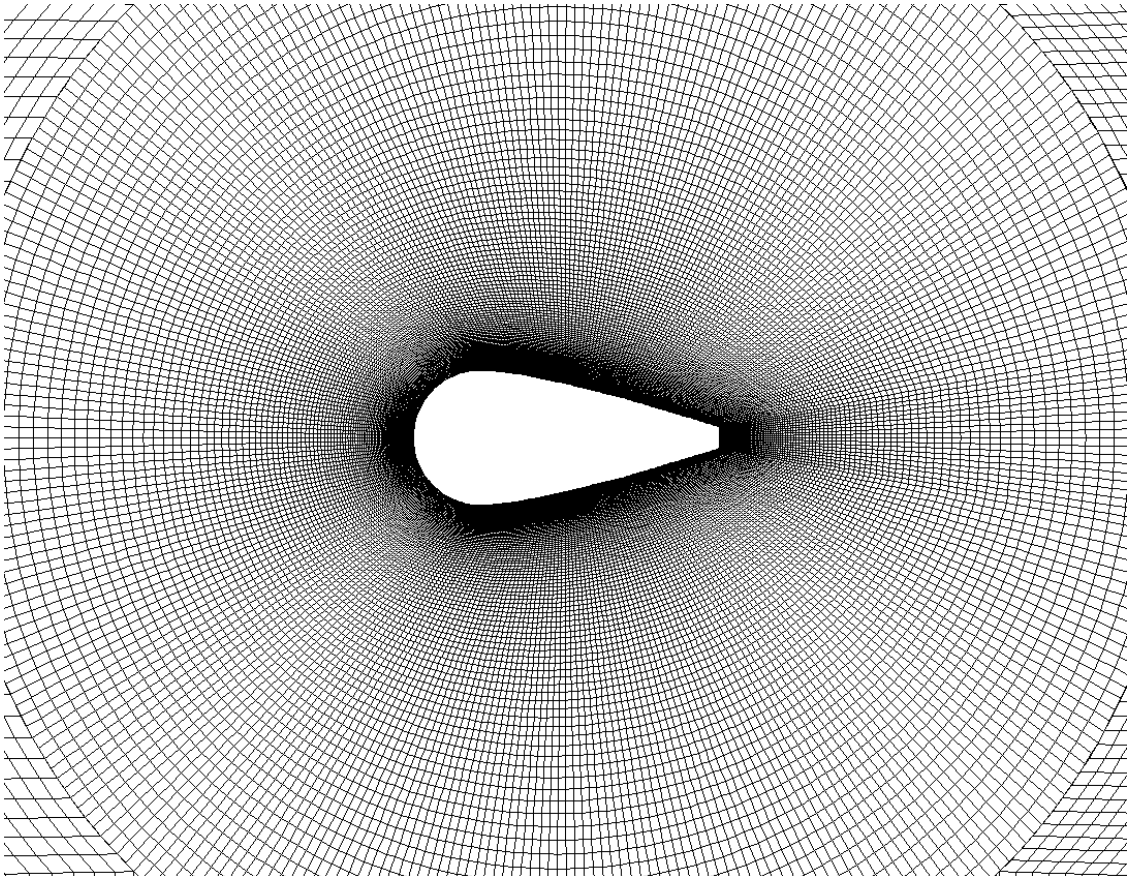


Figure A-36 Mesh Close To The Fairing.

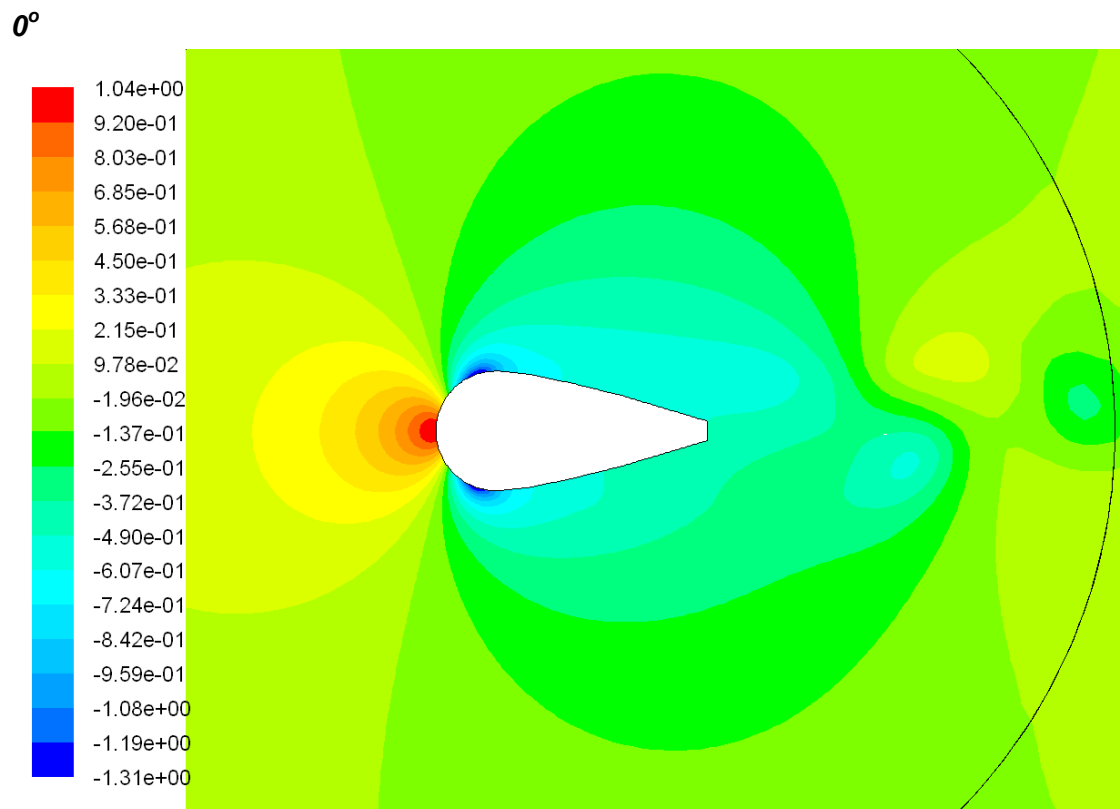


Figure A-37 Pressure Coefficient At 0° .

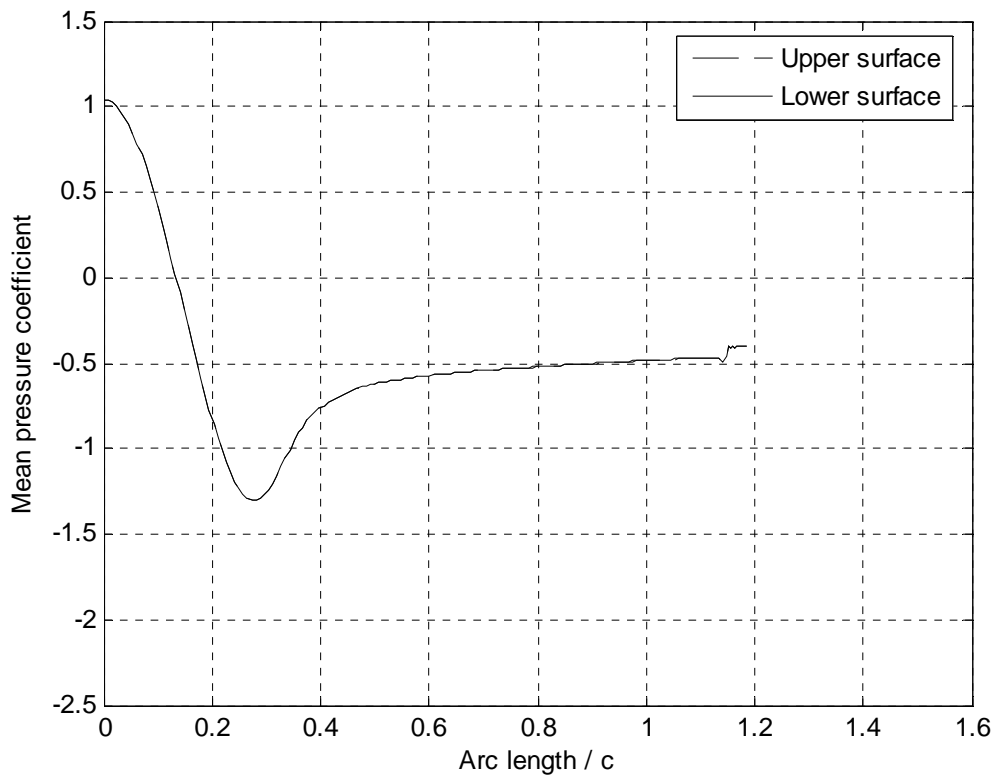


Figure A-38 Mean Pressure Coefficient Around The Fairing Surface At 0° .

5°

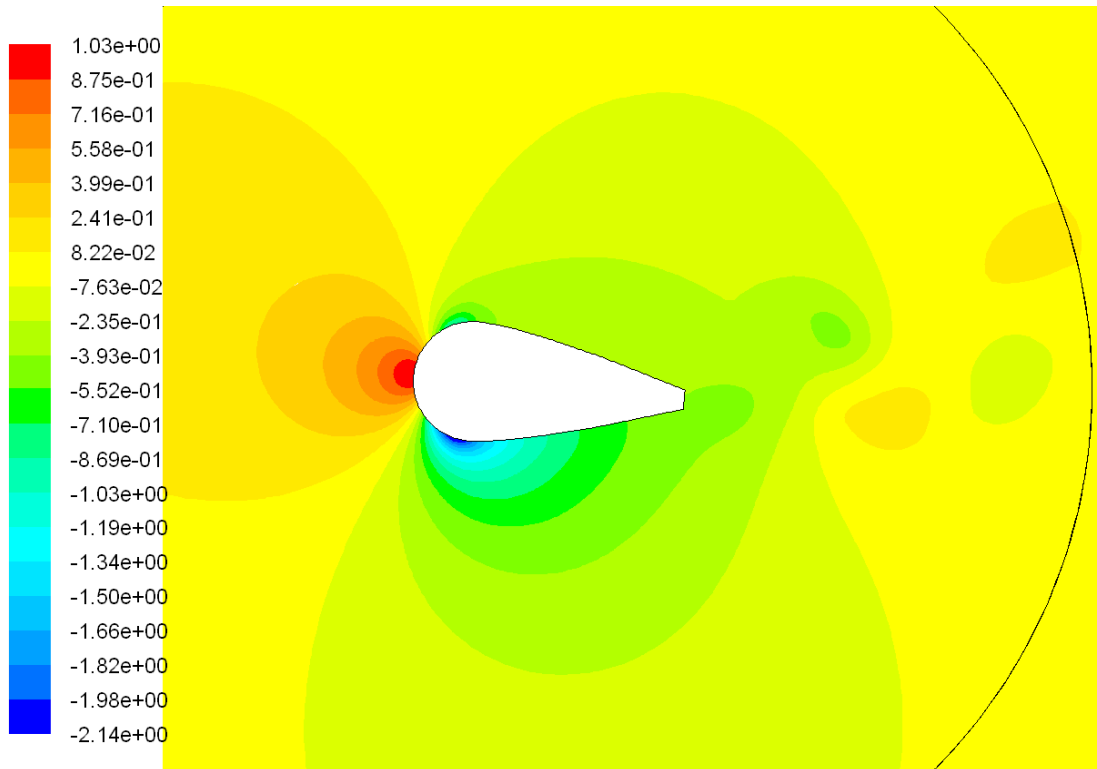


Figure A-39 Pressure Coefficient At 5°.

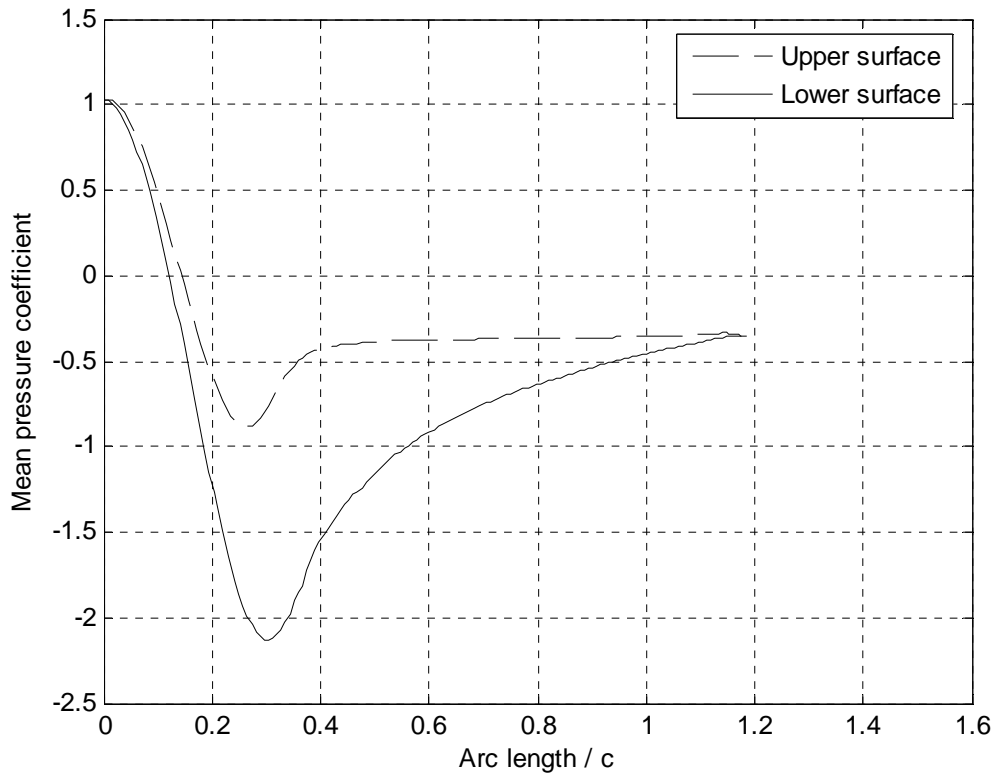


Figure A-40 Mean Pressure Coefficient Around The Fairing Surface At 5°.

10°

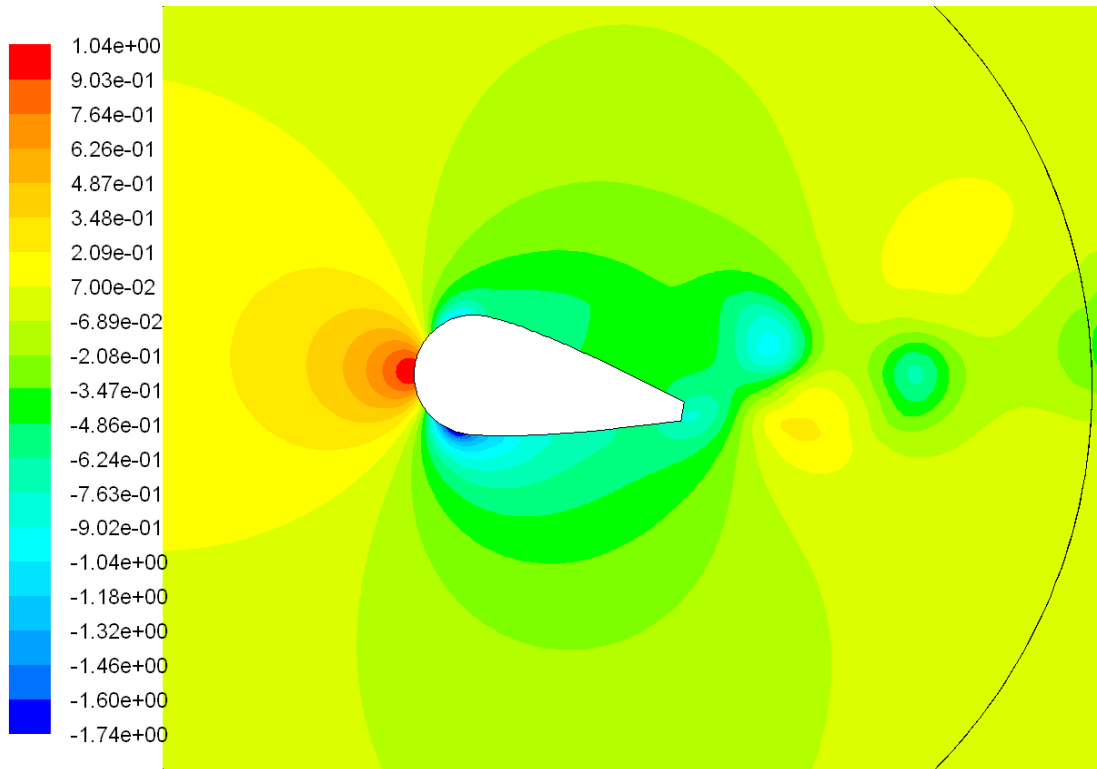


Figure A-41 Pressure Coefficient At 10°.

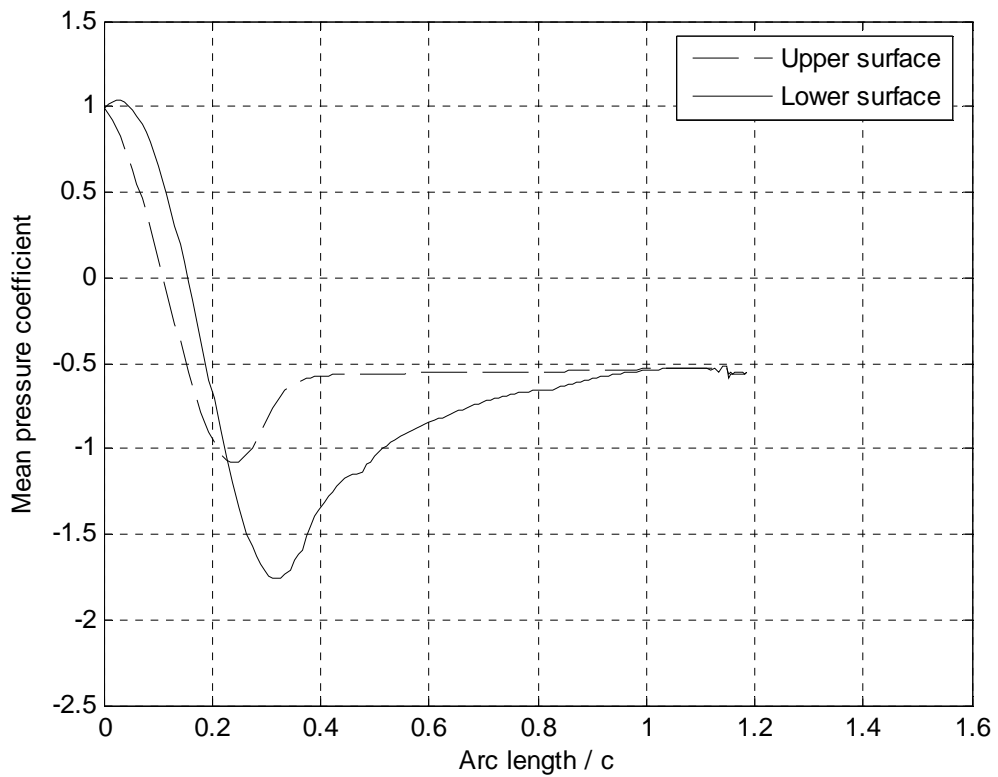


Figure A-42 Mean Pressure Coefficient Around The Fairing Surface At 10°.

15°

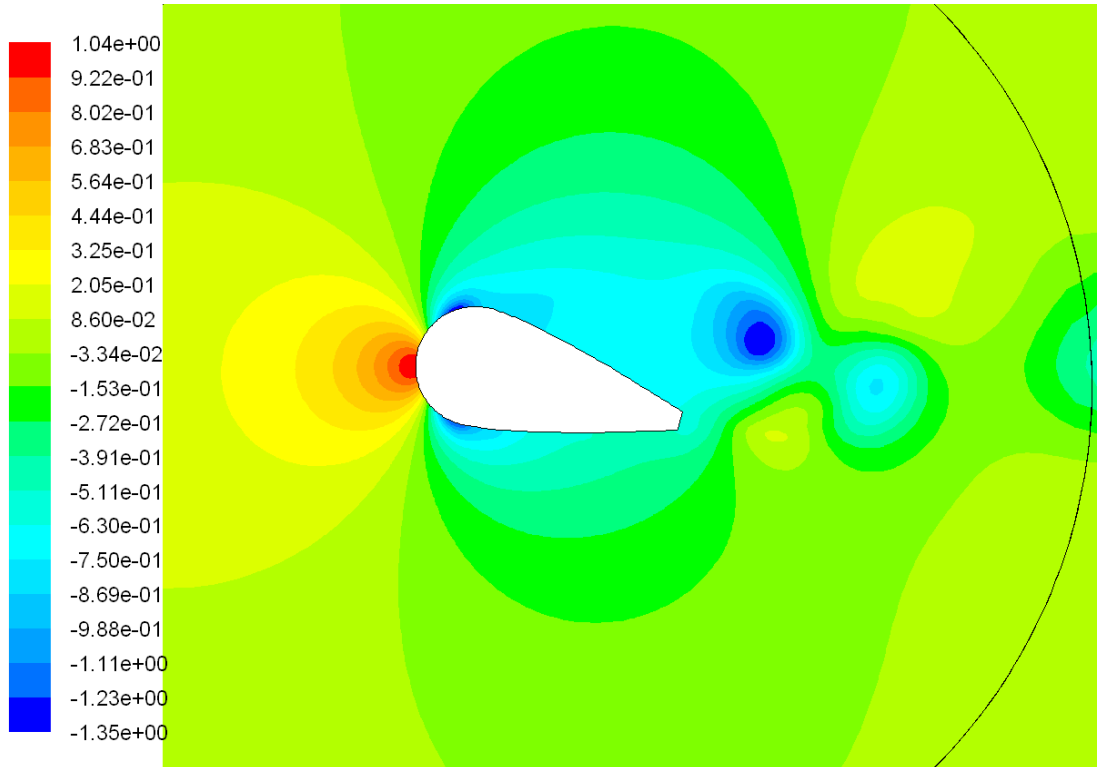


Figure A-43 Pressure Coefficient At 15°.

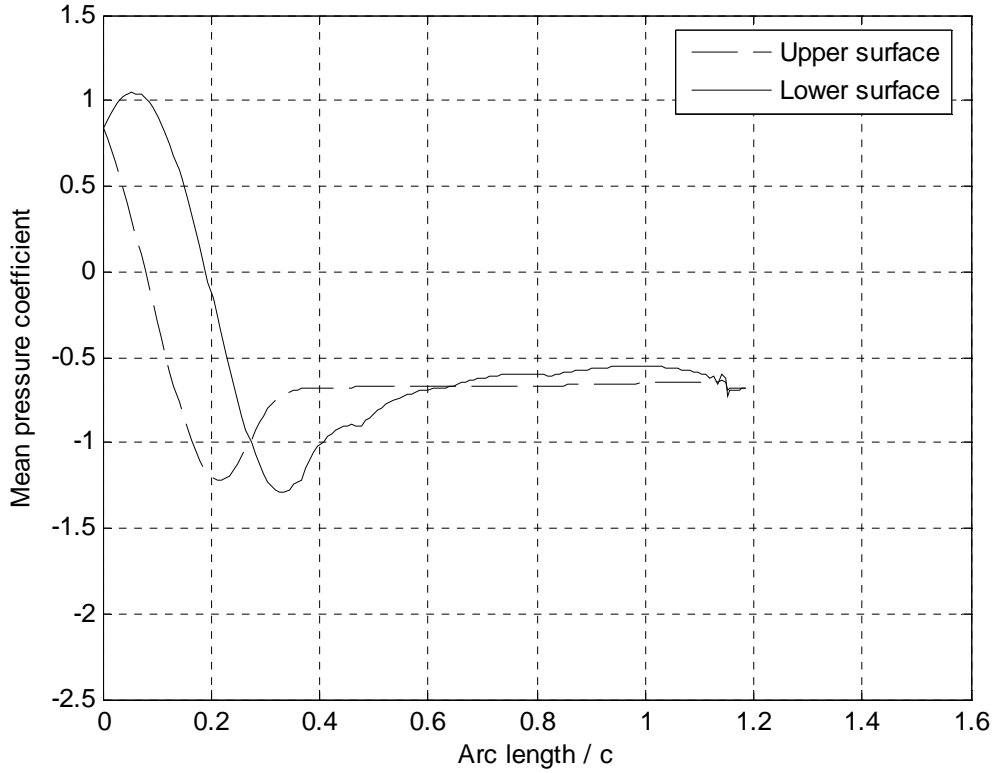


Figure A-44 Mean Pressure Coefficient Around The Fairing Surface At 15°.

Exxon's Fairing with Fin (3%)

$$U = 0.08 \text{ (m/s)}$$

$$Re_c = 5 \times 10^4$$

$$Y^+ = 0.935$$

Turbulence model: Realisable $k - \varepsilon$

Size of computational domain (L (upstream-downstream) x W): 25c (5c-19c) x 10c

Number of cells: 146164

Results

AoA	C_d	Amp(C_d)	C_L	Amp(C_L)	C_m	Amp(C_m)	St. No.	Run(s)
0°	0.2664	0.0002	0	0.058	0	0.023	0.18	2500
5°	0.241	0.006	-0.317	0.097	0.010	0.040	0.19	1000
10°	0.352	0.006	0.135	0.215	-0.085	0.085	0.18	1000
15°	0.445	0.006	0.425	0.200	-0.130	0.071	0.16	1000

$$\left. \frac{\partial C_L}{\partial \alpha} \right|_{\alpha=0} = -3.633$$

$$\left. \frac{\partial C_{M(CR)}}{\partial \alpha} \right|_{\alpha=0} = +0.115$$

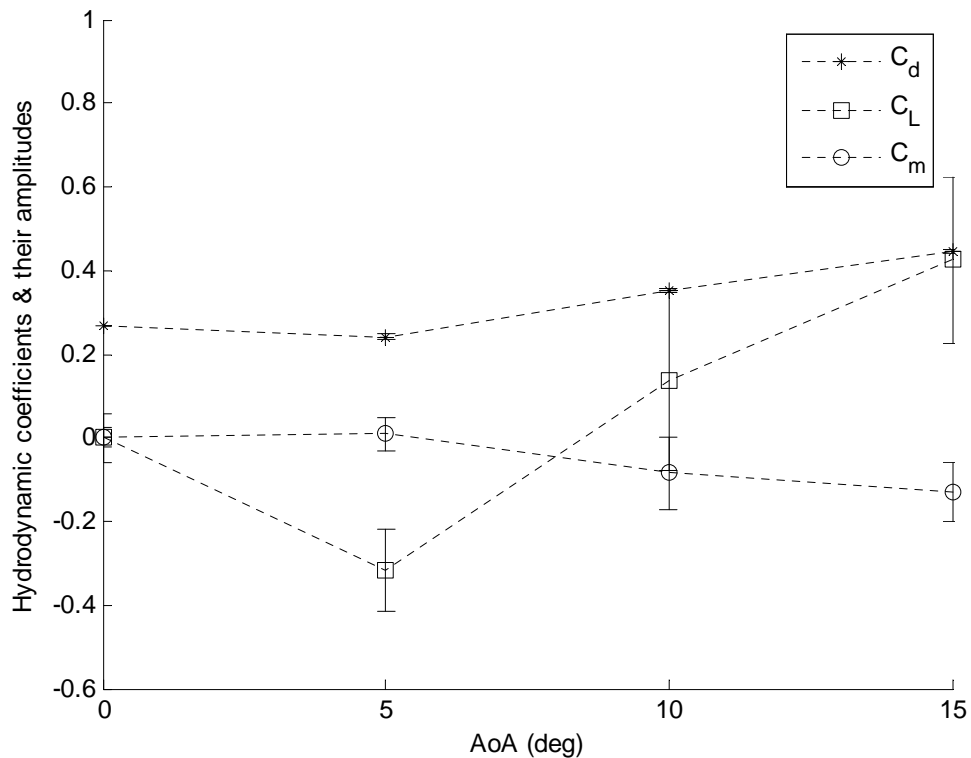


Figure A-45 Hydrodynamic Coefficients & Their Amplitudes.

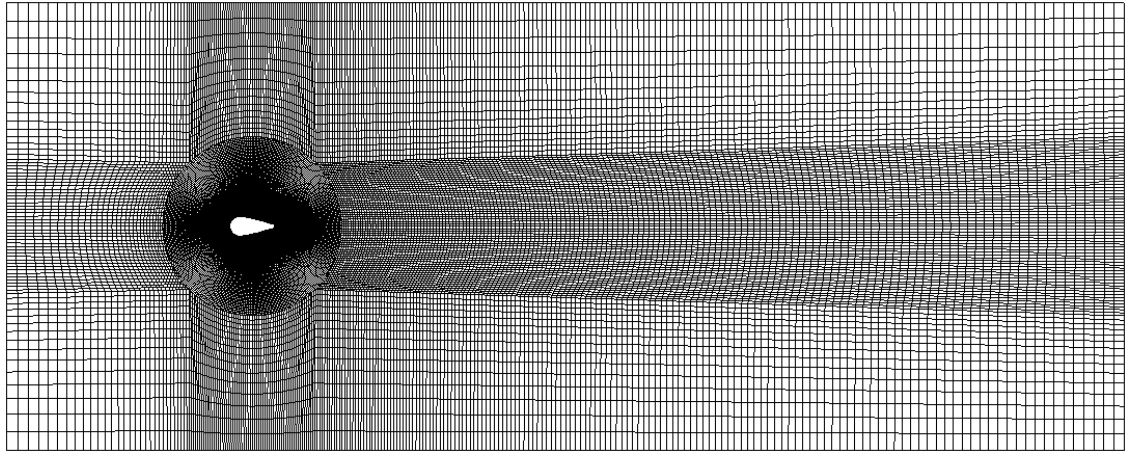


Figure A-46 Computational Domain And Mesh.

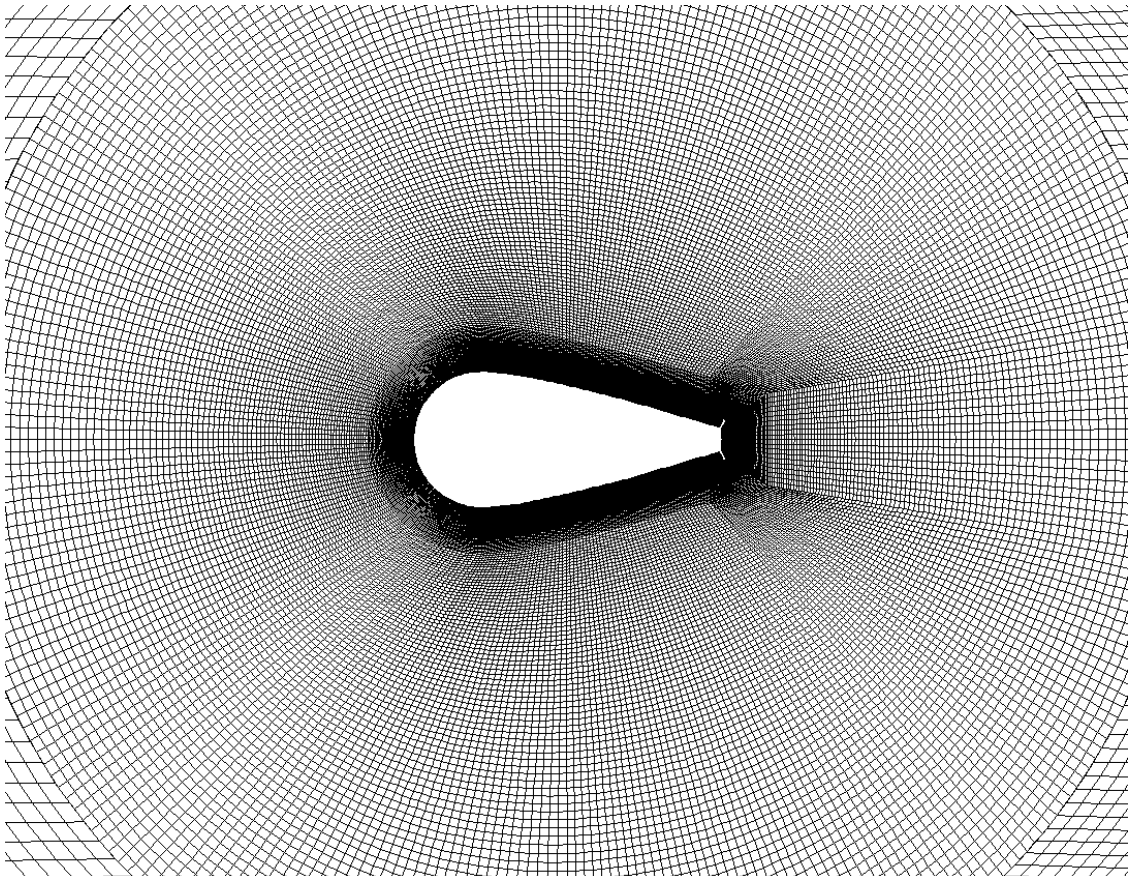


Figure A-47 Mesh Close To The Fairing.

0°

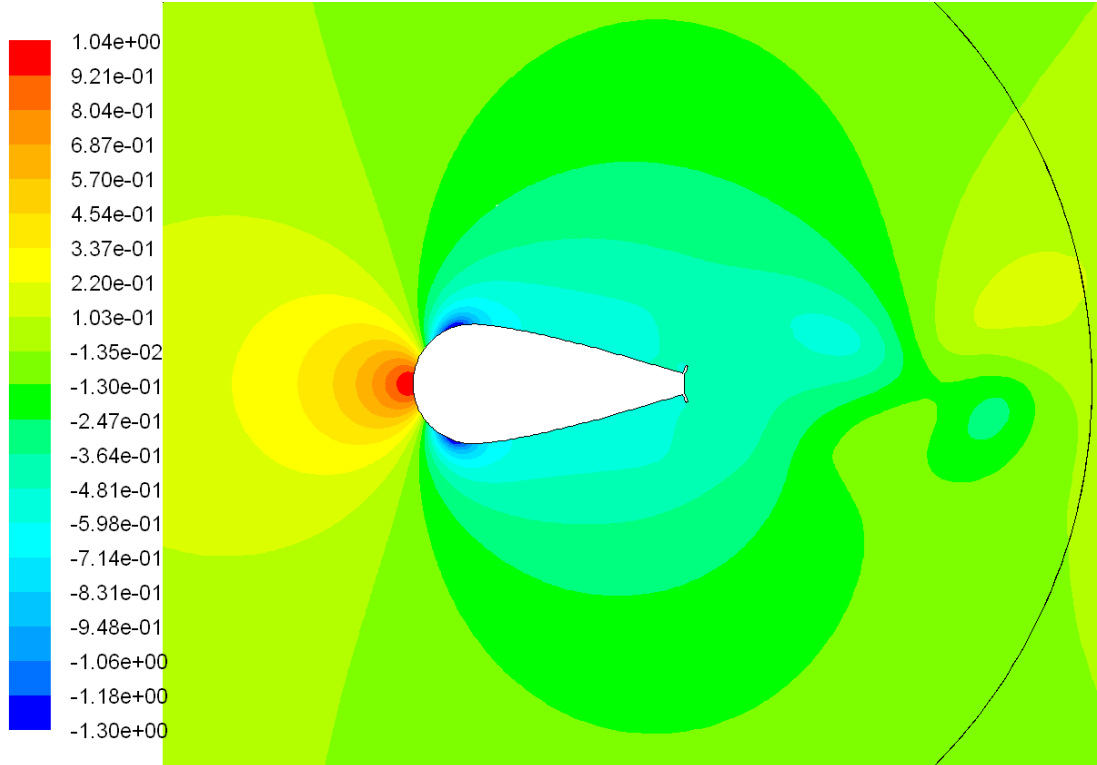


Figure A-48 Pressure Coefficient At 0°.

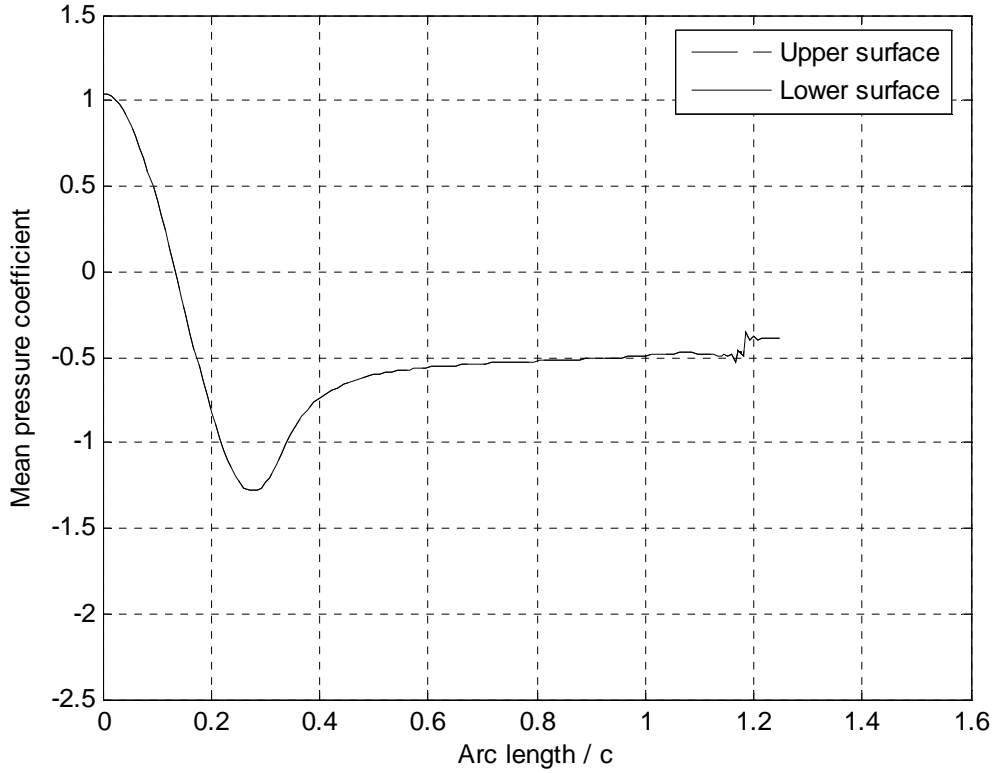


Figure A-49 Mean Pressure Coefficient Around The Fairing Surface At 0°.

5°

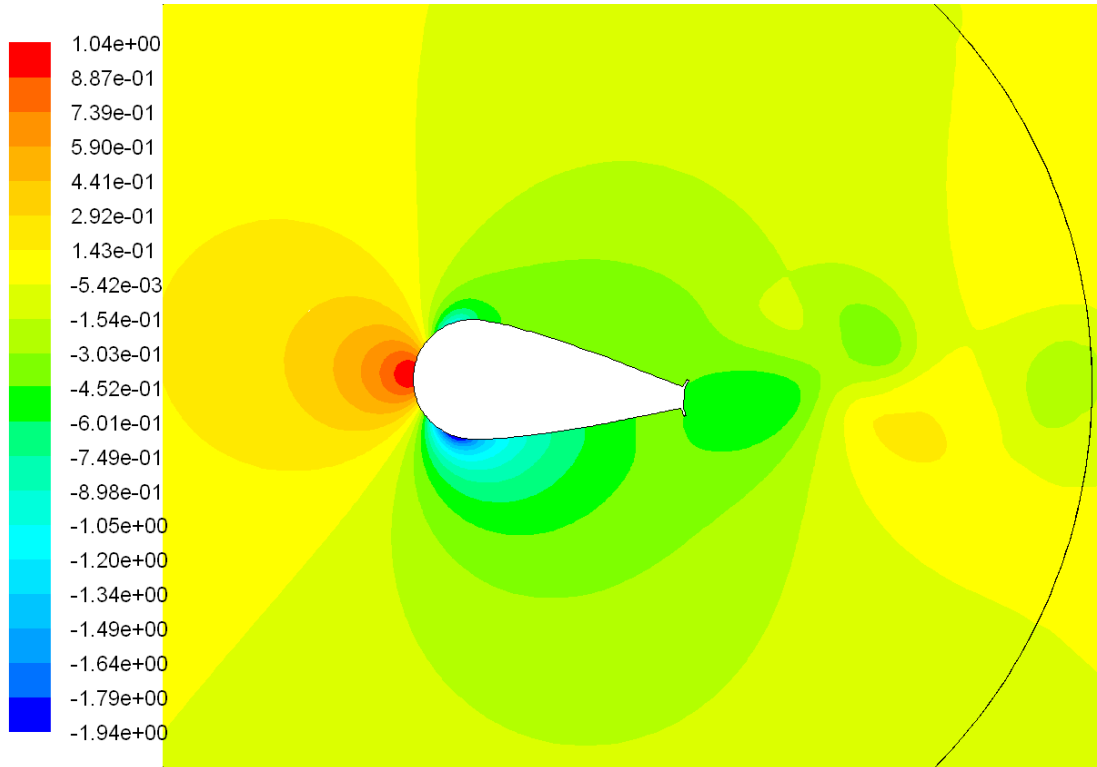


Figure A-50 Pressure Coefficient At 5°.

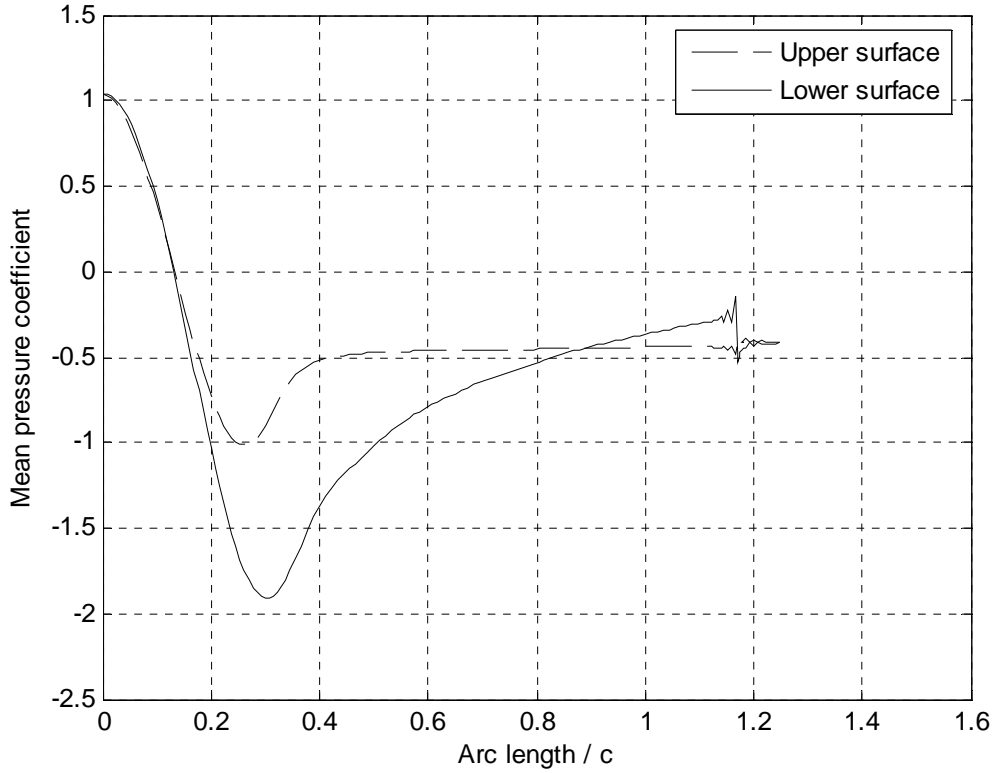


Figure A-51 Mean Pressure Coefficient Around The Fairing Surface At 5°.

10°

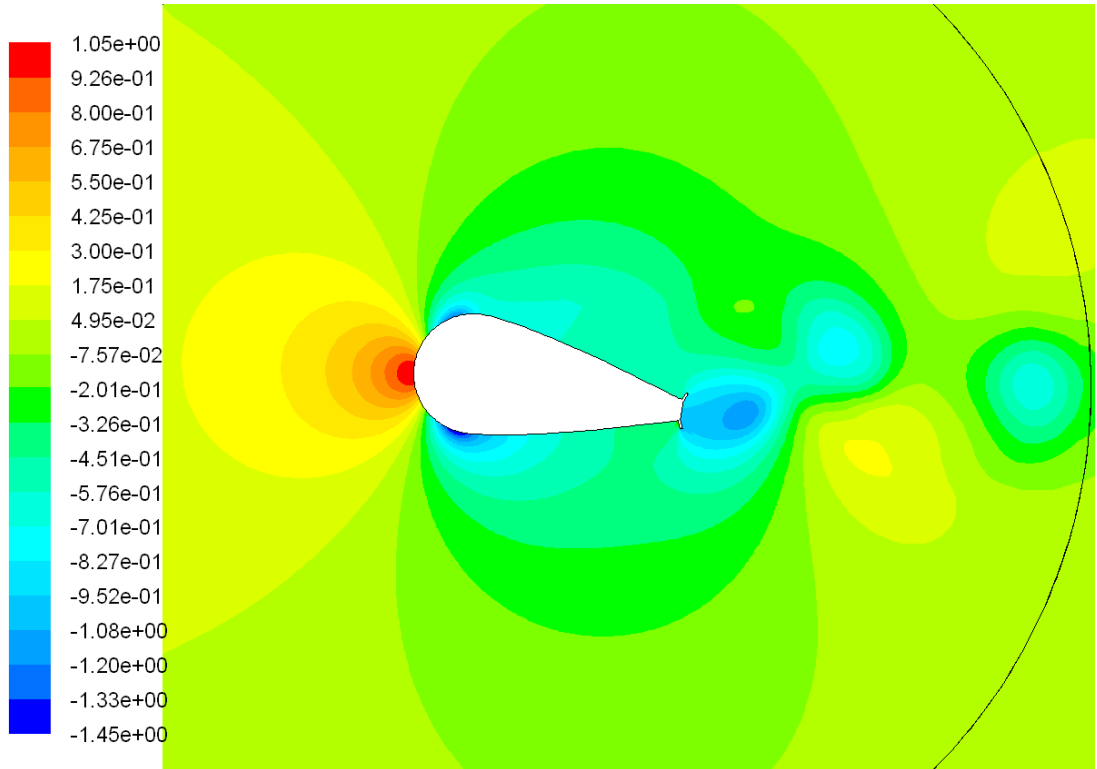


Figure A-52 Pressure Coefficient At 10°.

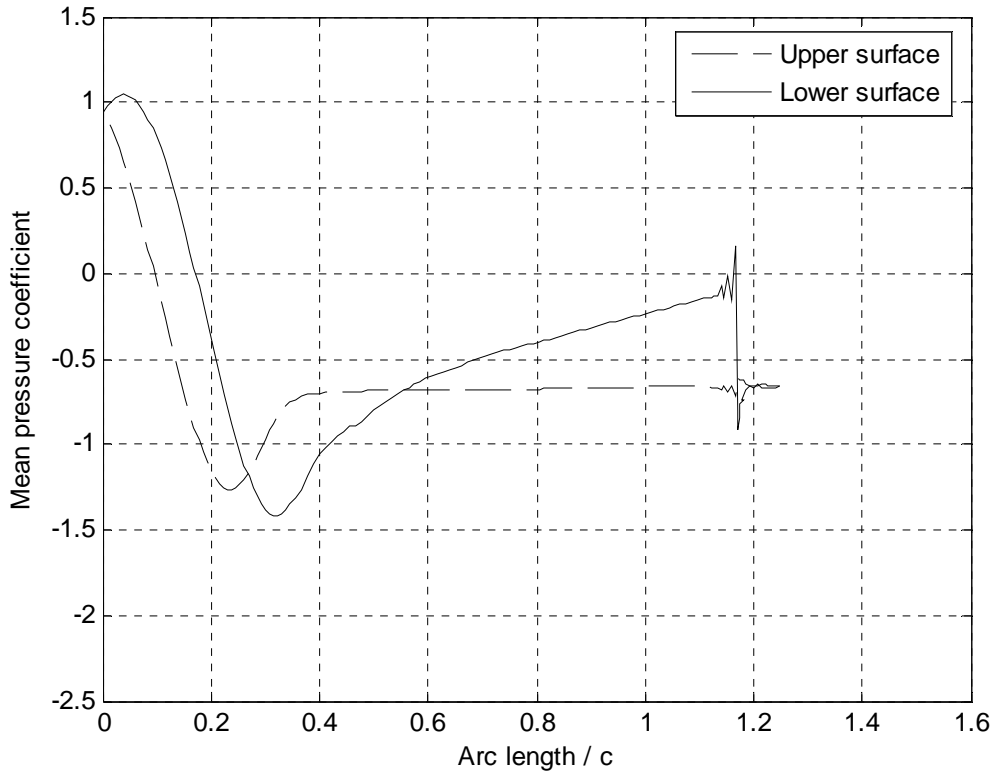


Figure A-53 Mean Pressure Coefficient Around The Fairing Surface At 10°.

15°

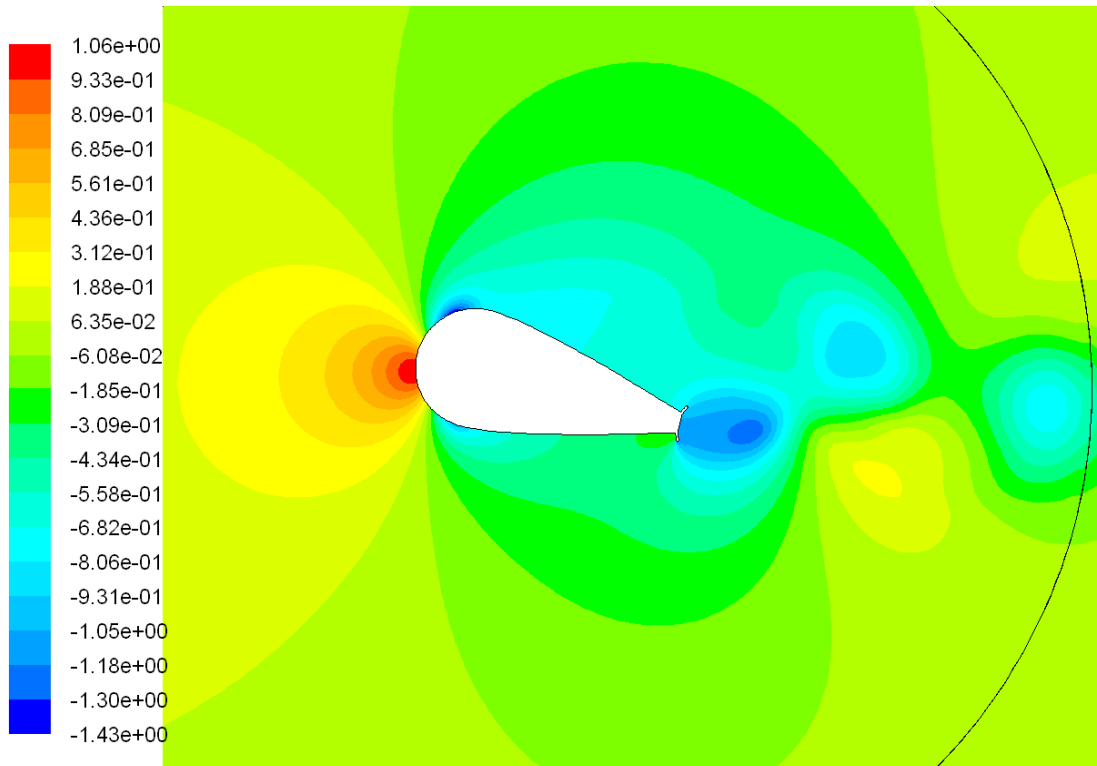


Figure A-54 Pressure Coefficient At 15°.

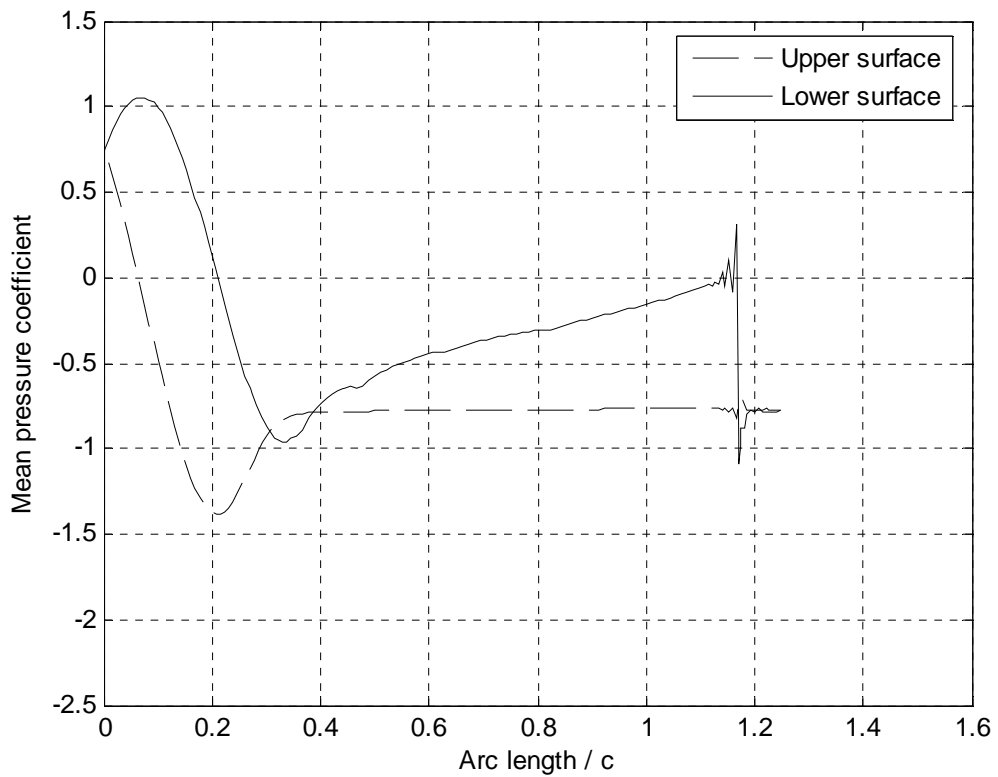


Figure A-55 Mean Pressure Coefficient Around The Fairing Surface At 15°.

Exxon's Fairing with Fin (5%)

$$U = 0.08 \text{ (m/s)}$$

$$Re_c = 5 \times 10^4$$

$$Y^+ = 0.934$$

Turbulence model: Realisable $k - \epsilon$

Size of computational domain (L (upstream-downstream) x W): 25c (5c-19c) x 10c

Number of cells: 146164

Results

AoA	C_d	Amp(C_d)	C_L	Amp(C_L)	C_m	Amp(C_m)	St. No.	Run(s)
0°	0.2542	0.0002	0	0.041	0	0.016	0.17	2700
5°	0.273	0.012	-0.090	0.013	-0.048	0.052	0.20	1000
10°	0.407	0.016	0.400	0.240	-0.160	0.095	0.18	1000
15°	0.510	0.011	0.650	0.225	-0.204	0.078	0.15	1000

$$\left. \frac{\partial C_L}{\partial \alpha} \right|_{\alpha=0} = -1.031$$

$$\left. \frac{\partial C_{M(CR)}}{\partial \alpha} \right|_{\alpha=0} = -0.550$$

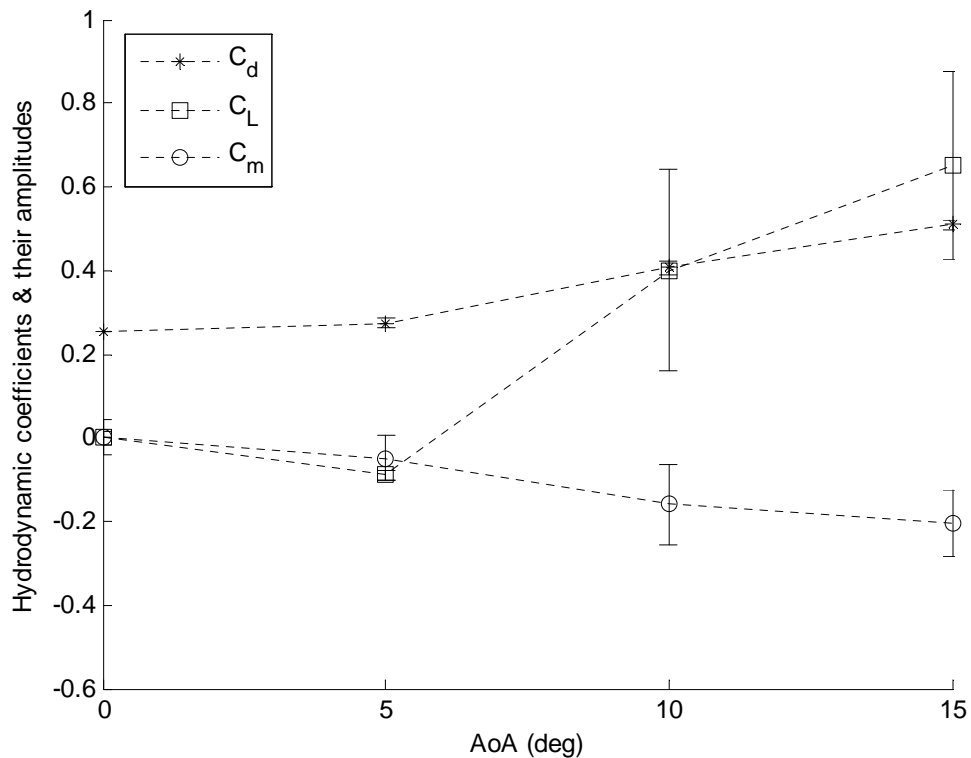


Figure A-56 Hydrodynamic Coefficients & Their Amplitudes.

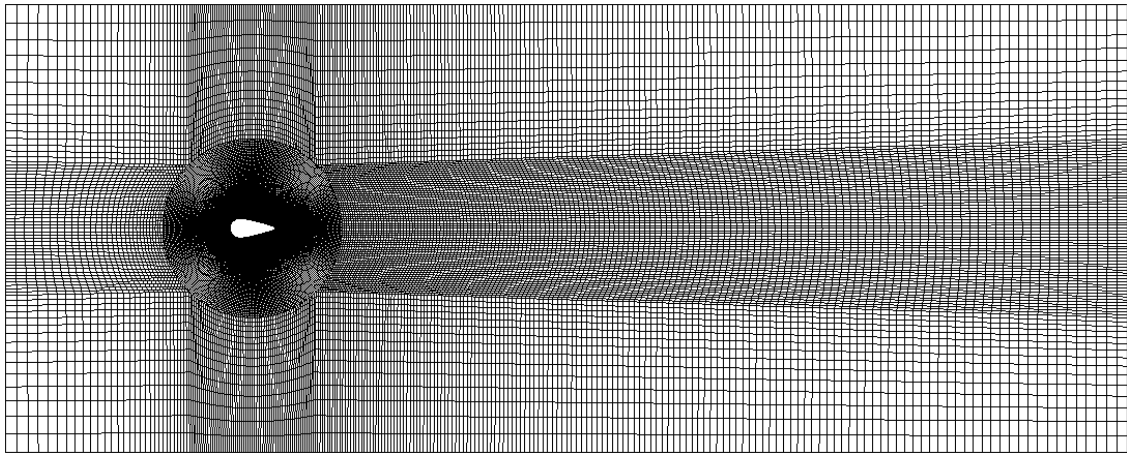


Figure A-57 Computational Domain And Mesh.

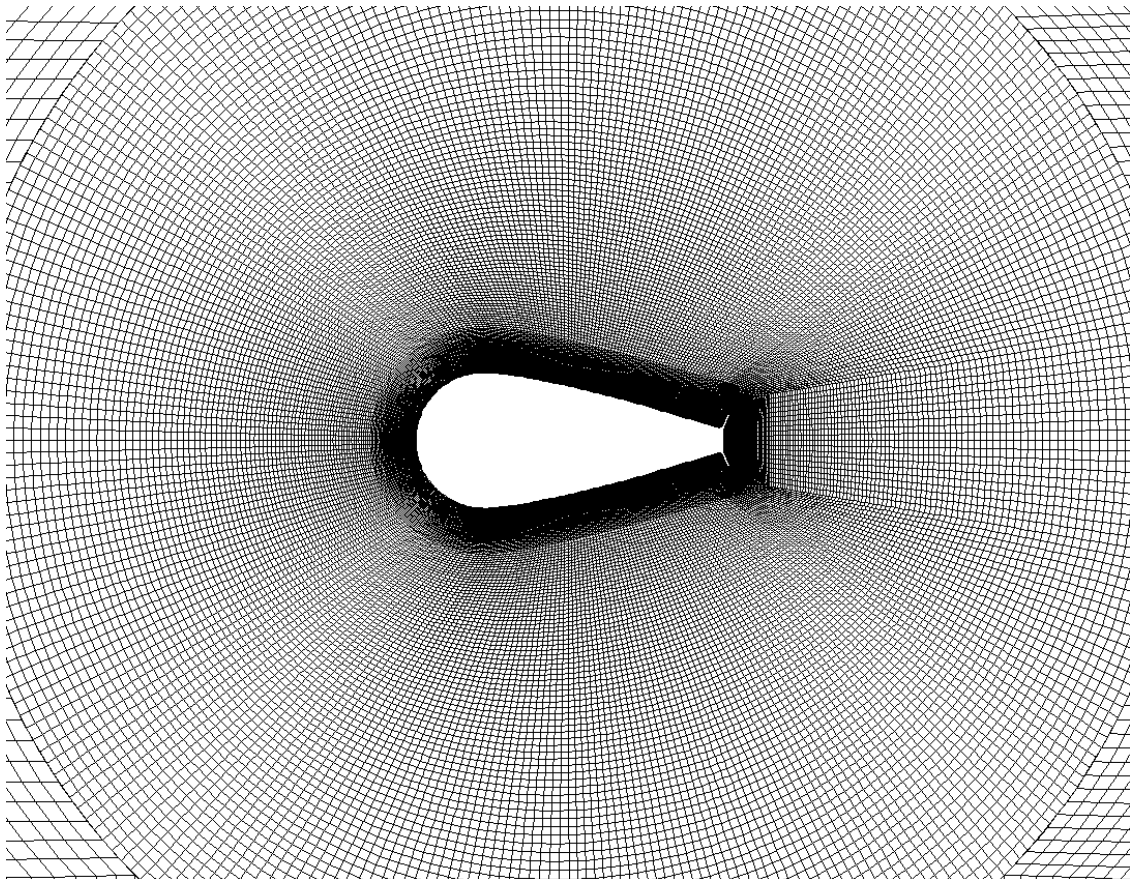


Figure A-58 Mesh Close To The Fairing.

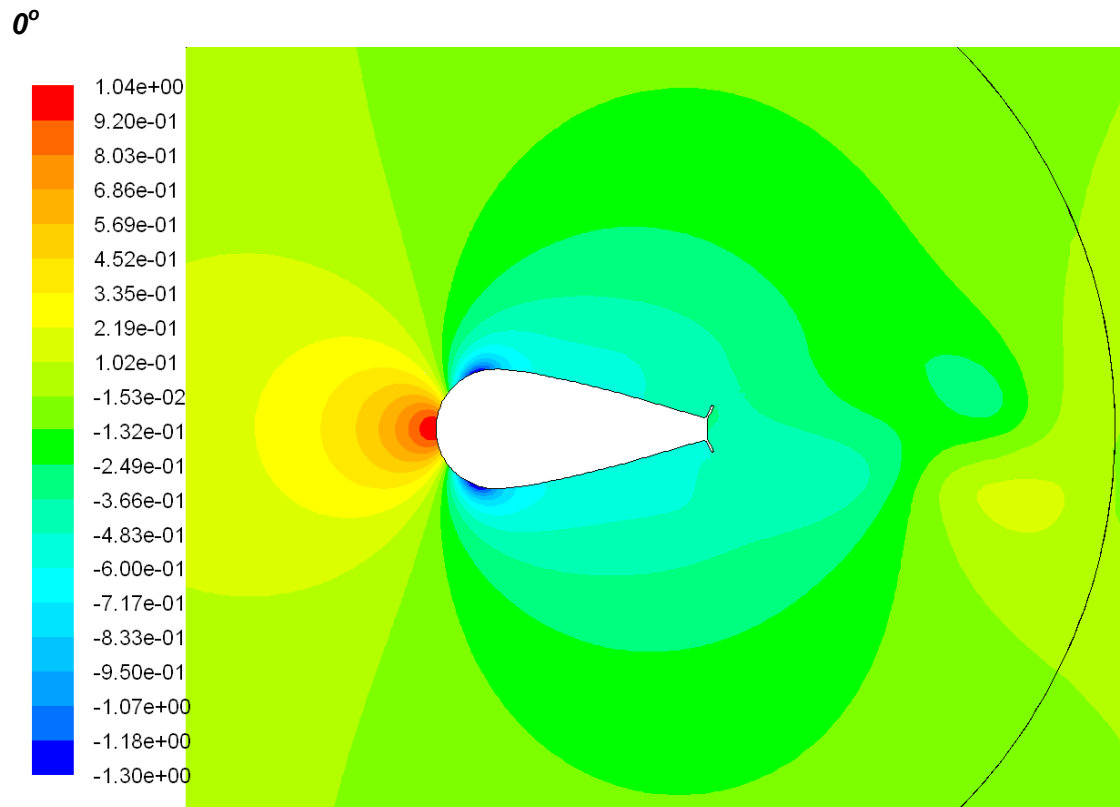


Figure A-59 Pressure Coefficient At 0° .

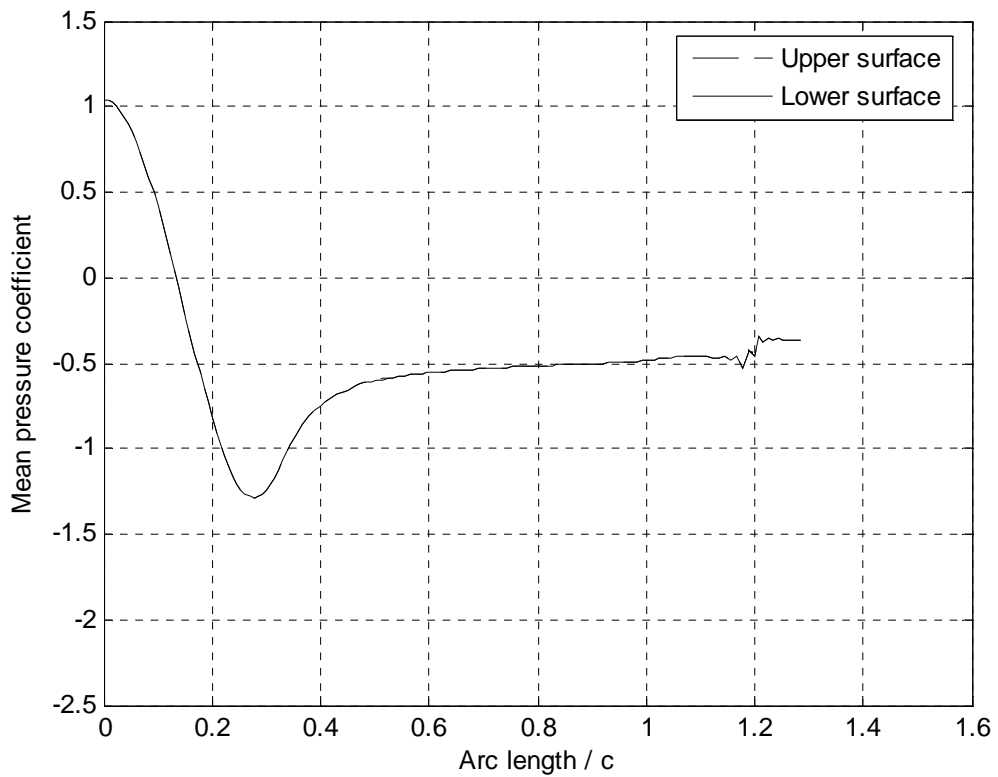


Figure A-60 Mean Pressure Coefficient Around The Fairing Surface At 0° .

5°

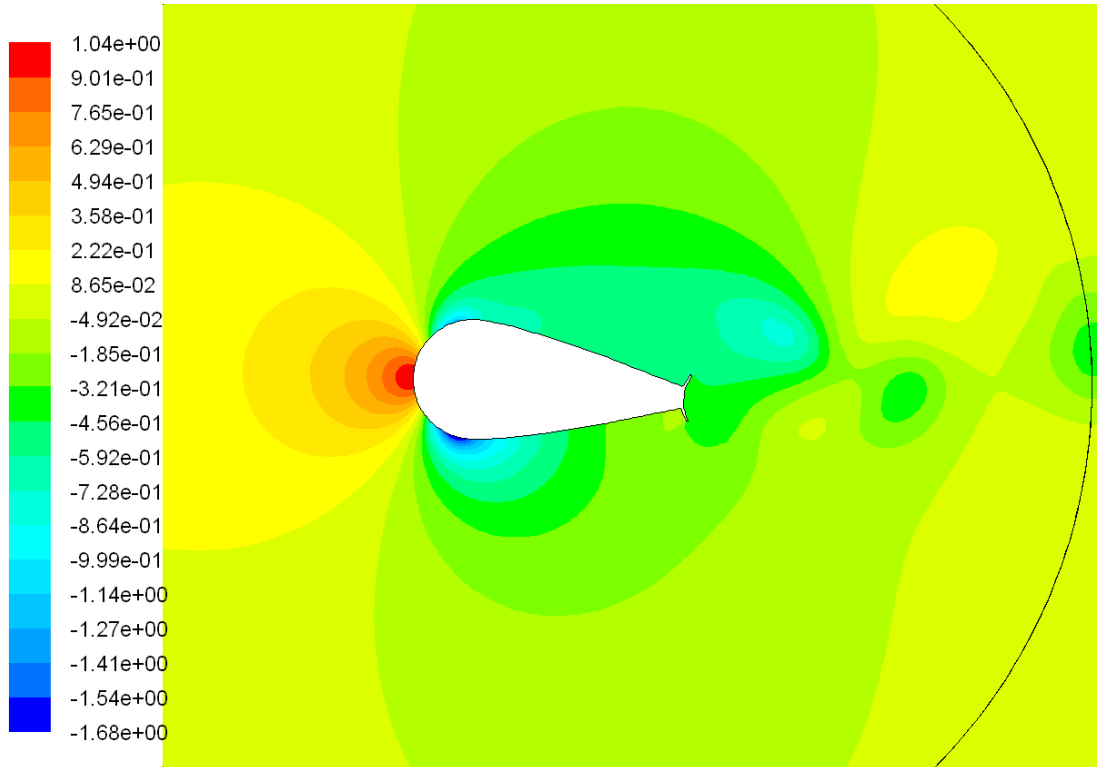


Figure A-61 Pressure Coefficient At 5°.

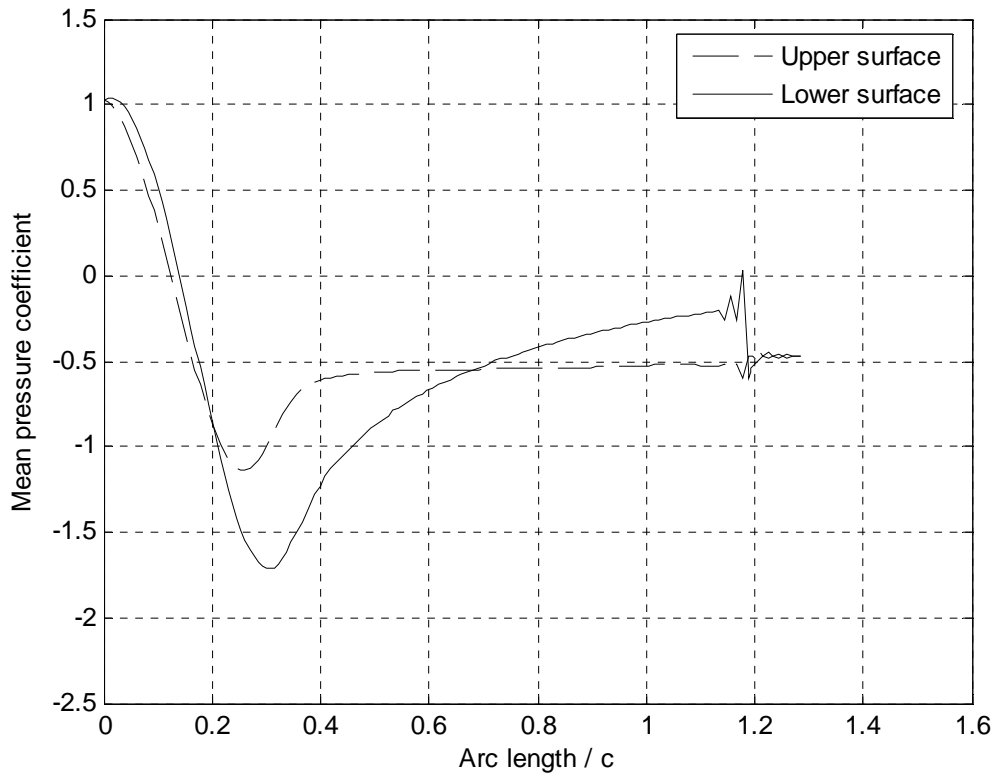


Figure A-62 Mean Pressure Coefficient Around The Fairing Surface At 5°.

10°

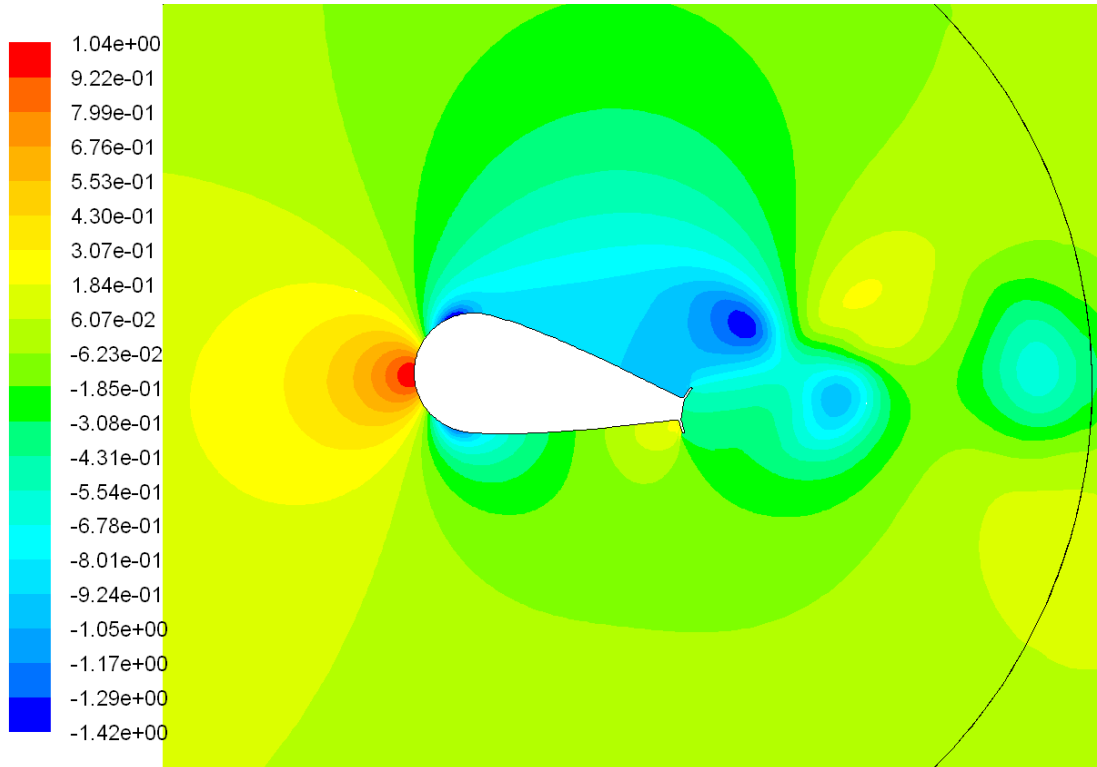


Figure A-63 Pressure Coefficient At 10°.

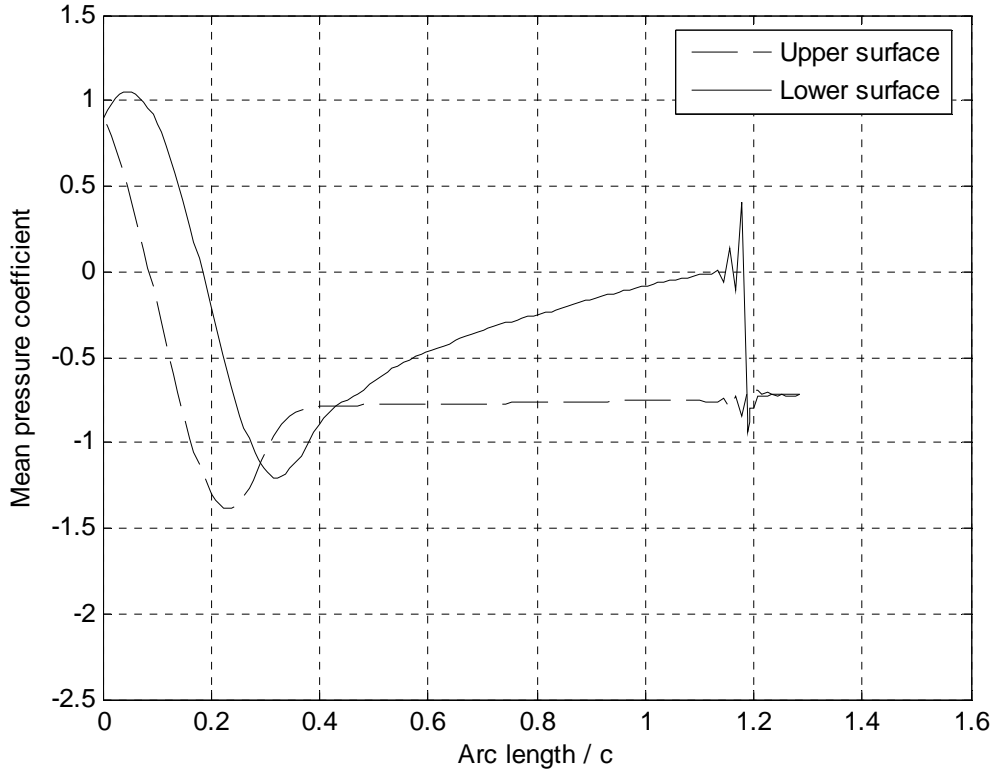


Figure A-64 Mean Pressure Coefficient Around The Fairing Surface At 10°.

15°

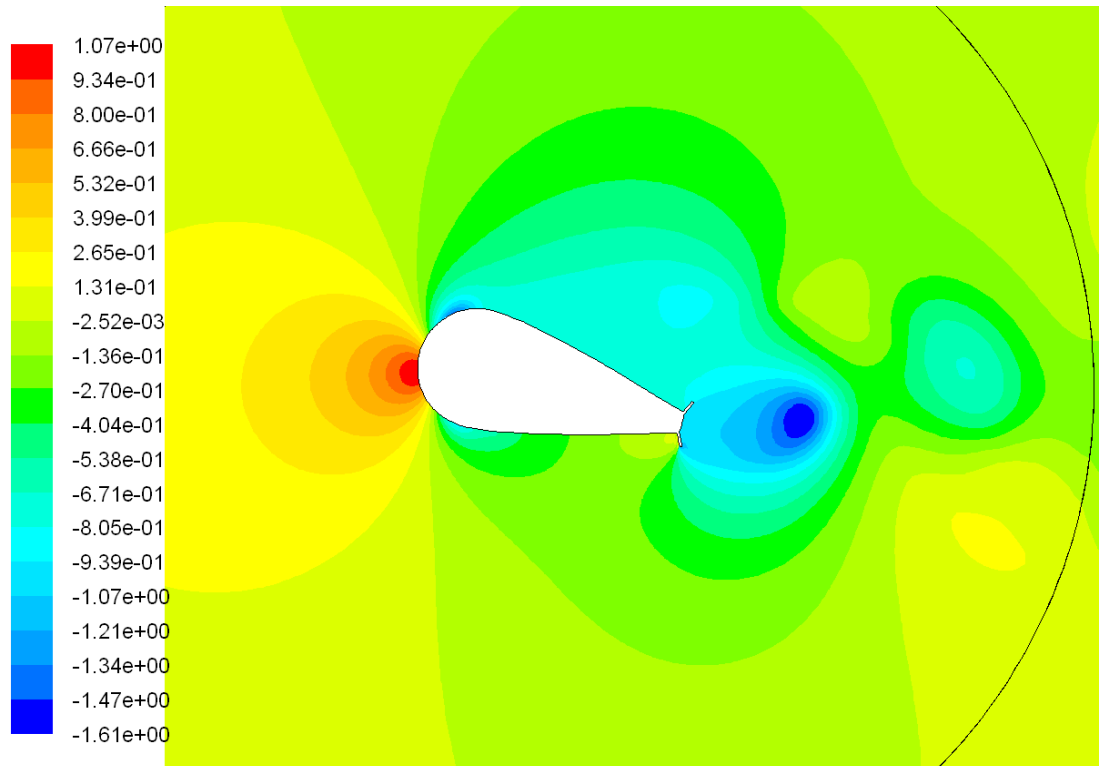


Figure A-65 Pressure Coefficient At 15°.

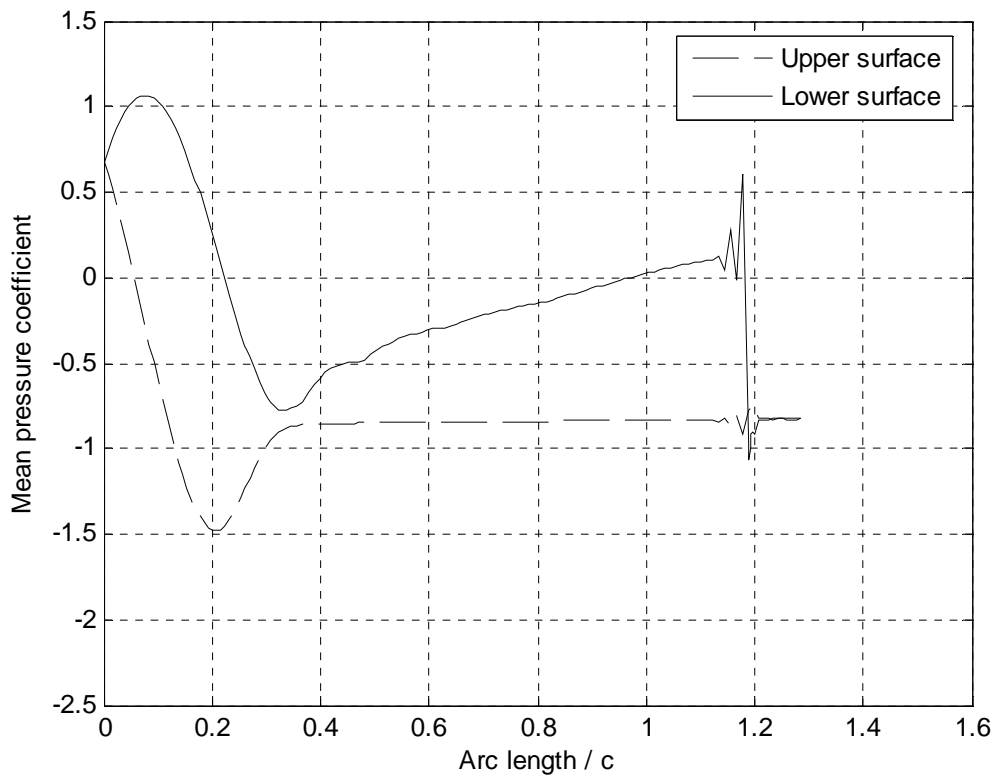


Figure A-66 Mean Pressure Coefficient Around The Fairing Surface At 15°.

Exxon's Fairing with Fin (7%)

$$U = 0.08 \text{ (m/s)}$$

$$Re_c = 5 \times 10^4$$

$$Y^+ = 0.935$$

Turbulence model: Realisable $k - \epsilon$

Size of computational domain (L (upstream-downstream) x W): 25c (5c-19c) x 10c

Number of cells: 153364

Results

AoA	C_d	Amp(C_d)	C_L	Amp(C_L)	C_m	Amp(C_m)	St. No.	Run(s)
0°	0.2477	0.0002	0	0.035	0	0.015	0.17	2700
5°	0.302	0.018	0.090	0.150	-0.095	0.065	0.19	1000
10°	0.448	0.025	0.585	0.245	-0.215	0.096	0.16	1000
15°	0.561	0.017	0.810	0.230	-0.257	0.081	0.14	1000

$$\left. \frac{\partial C_L}{\partial \alpha} \right|_{\alpha=0} = +1.031$$

$$\left. \frac{\partial C_{M(CR)}}{\partial \alpha} \right|_{\alpha=0} = -1.089$$

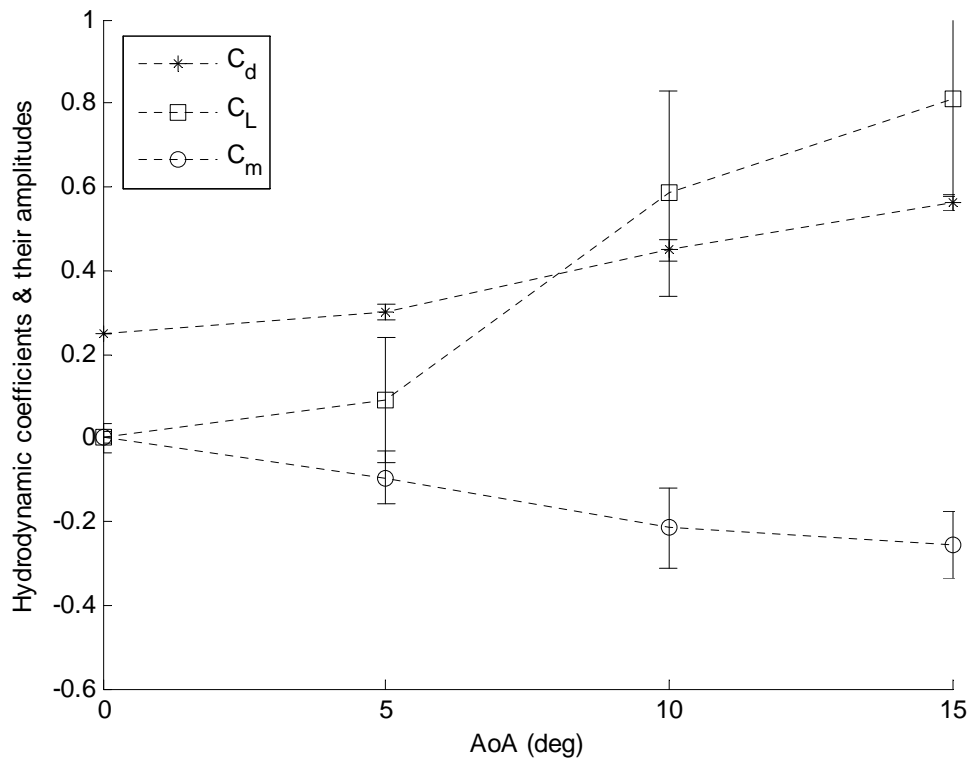


Figure A-67 Hydrodynamic Coefficients & Their Amplitudes.

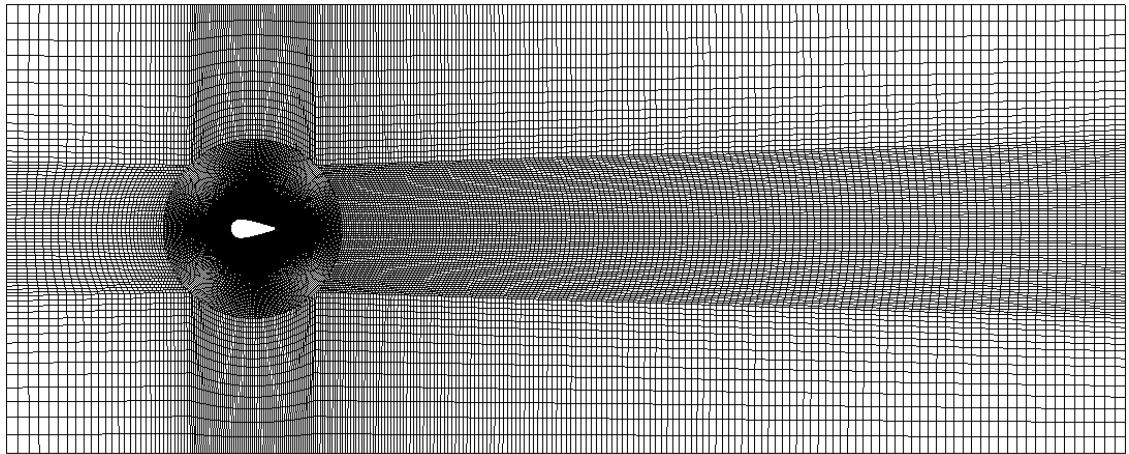


Figure A-68 Computational Domain And Mesh.

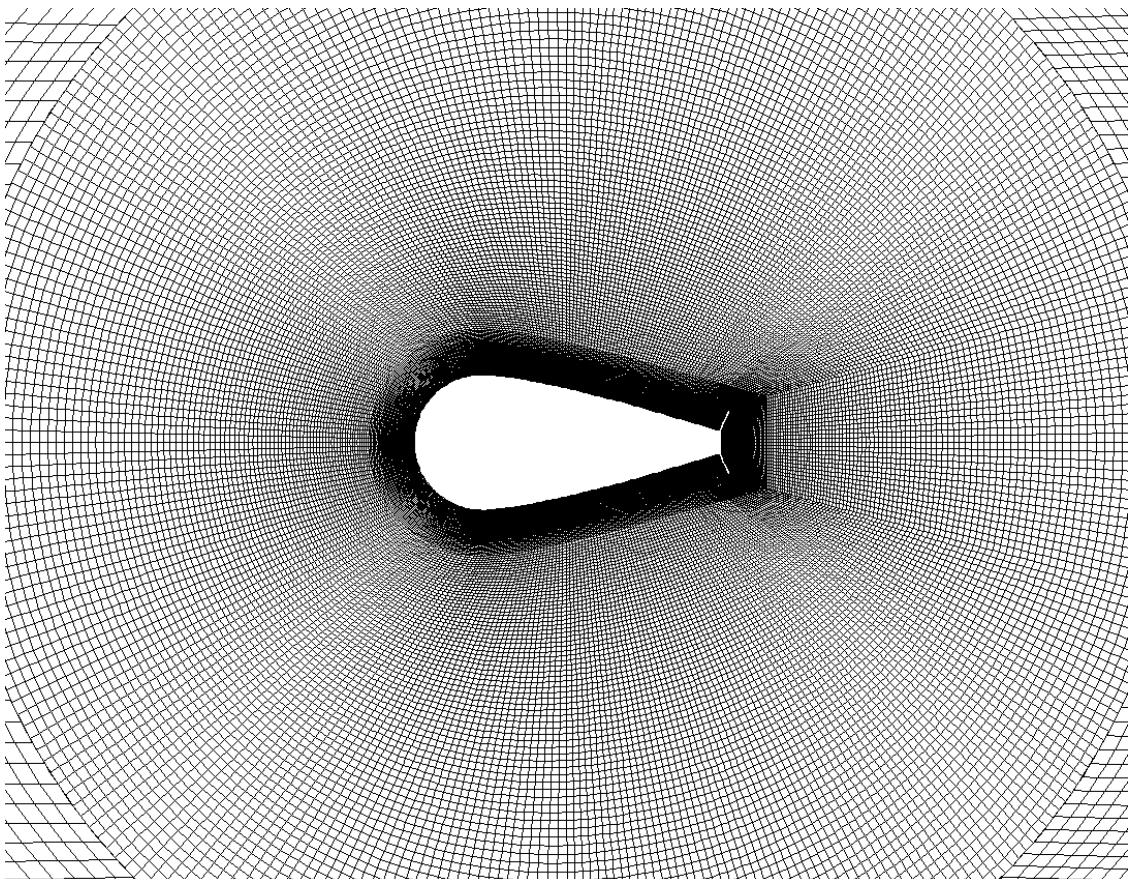


Figure A-69 Mesh Close To The Fairing.

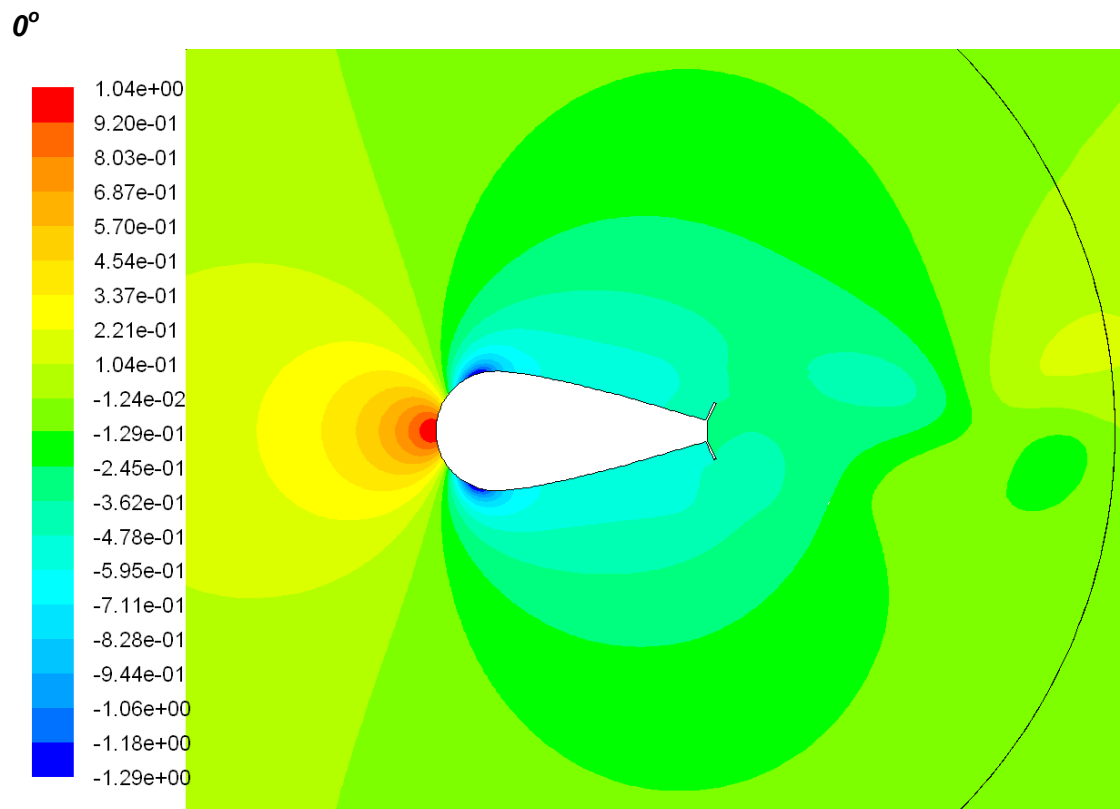


Figure A-70 Pressure Coefficient At 0° .

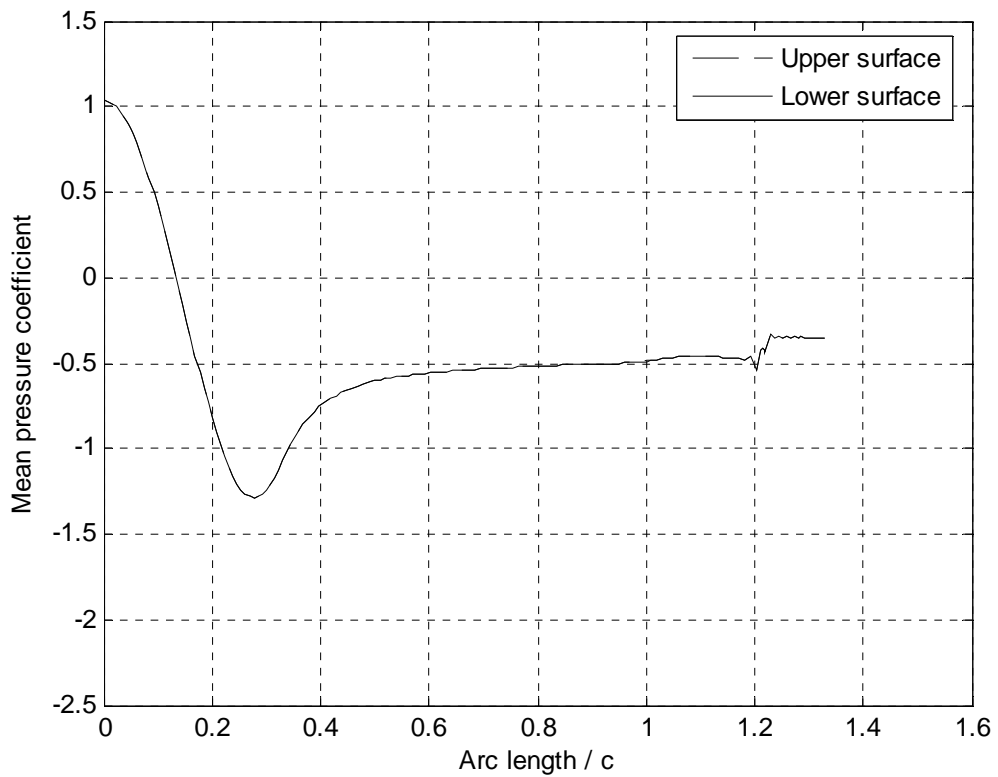


Figure A-71 Mean Pressure Coefficient Around The Fairing Surface At 0° .

5°

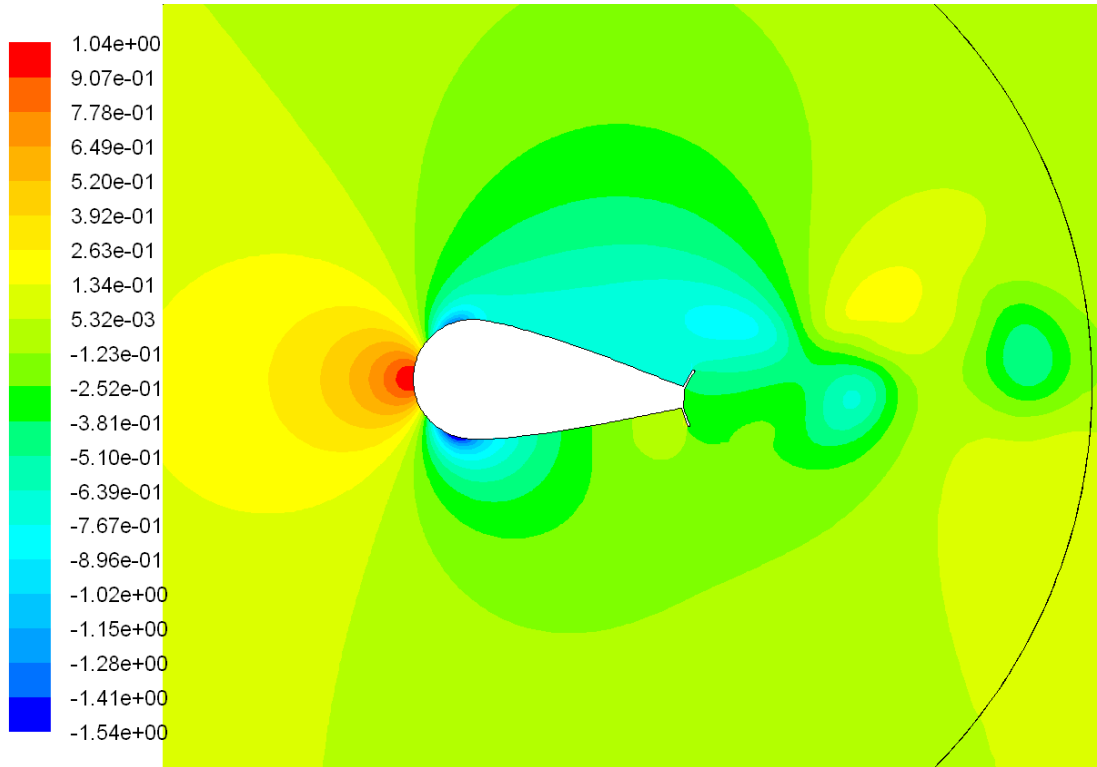


Figure A-72 Pressure Coefficient At 5°.

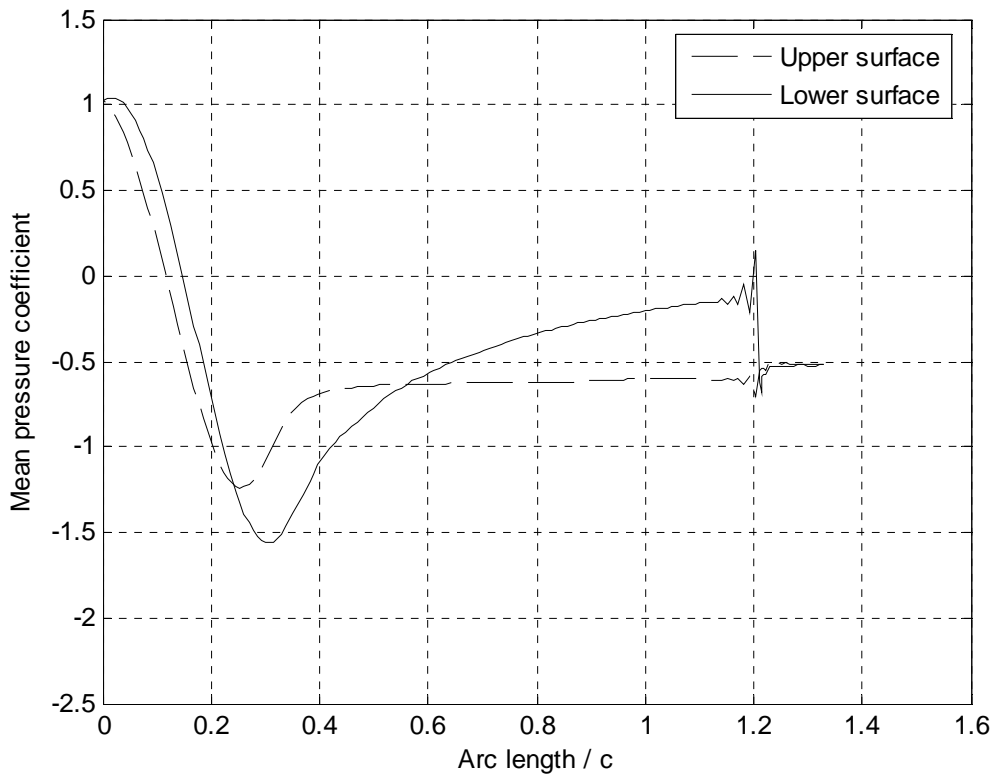


Figure A-73 Mean Pressure Coefficient Around The Fairing Surface At 5°.

10°

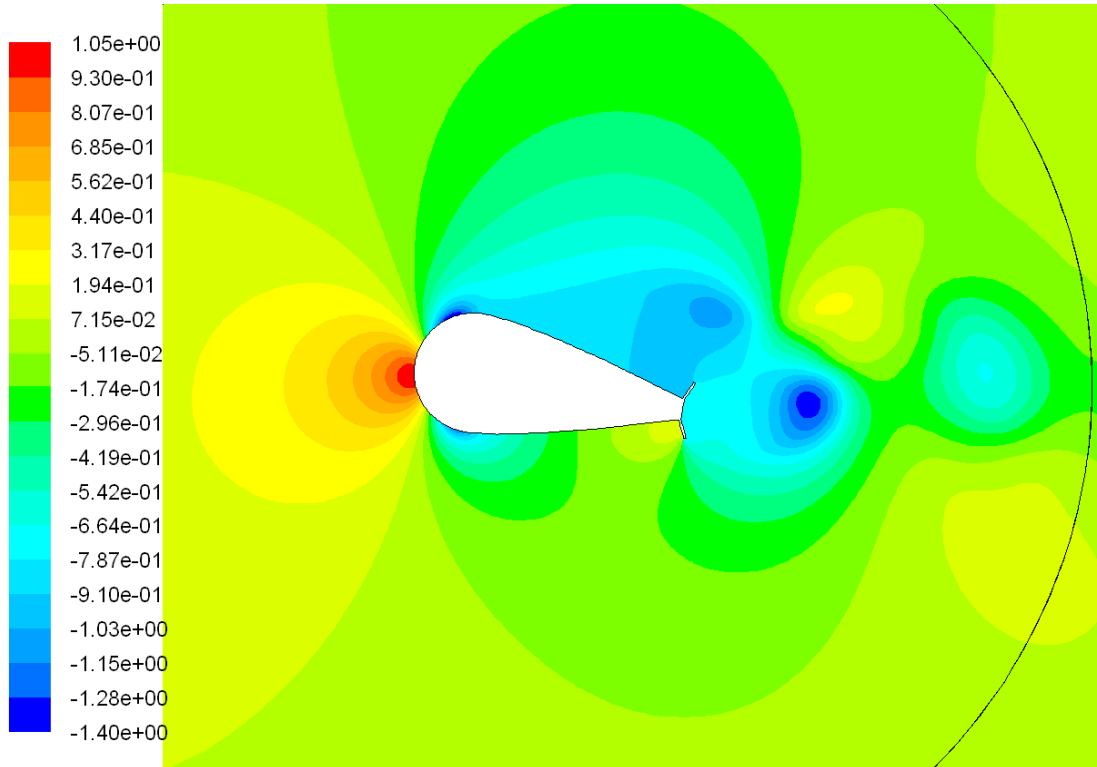


Figure A-74 Pressure Coefficient At 10°.

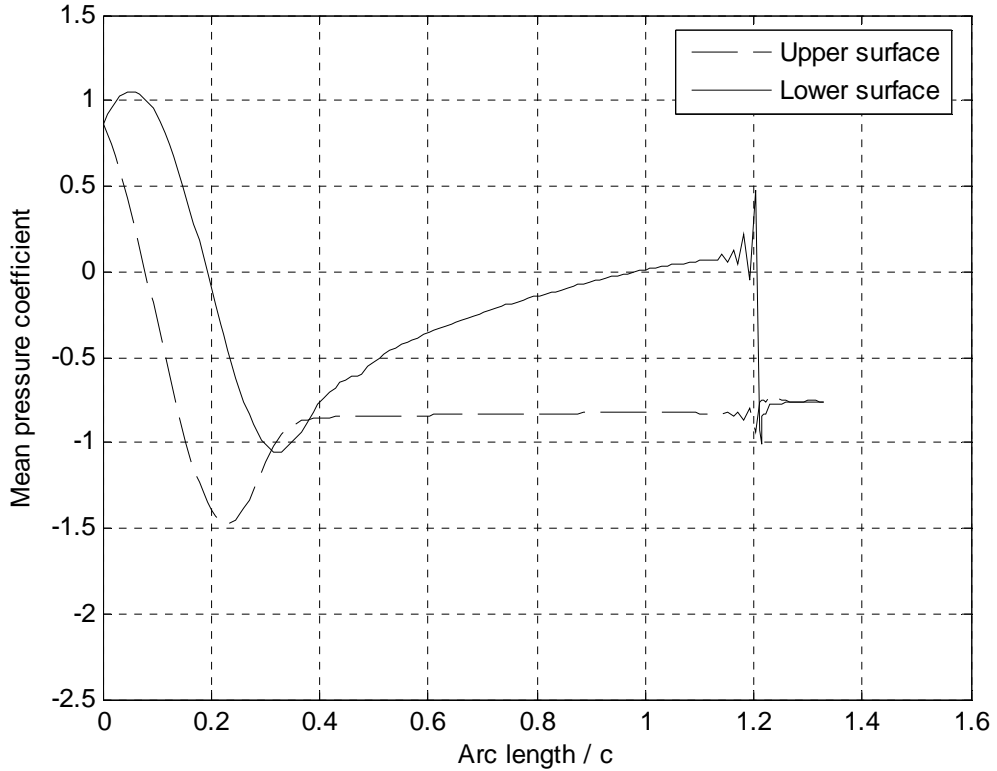


Figure A-75 Mean Pressure Coefficient Around The Fairing Surface At 10°.

15°

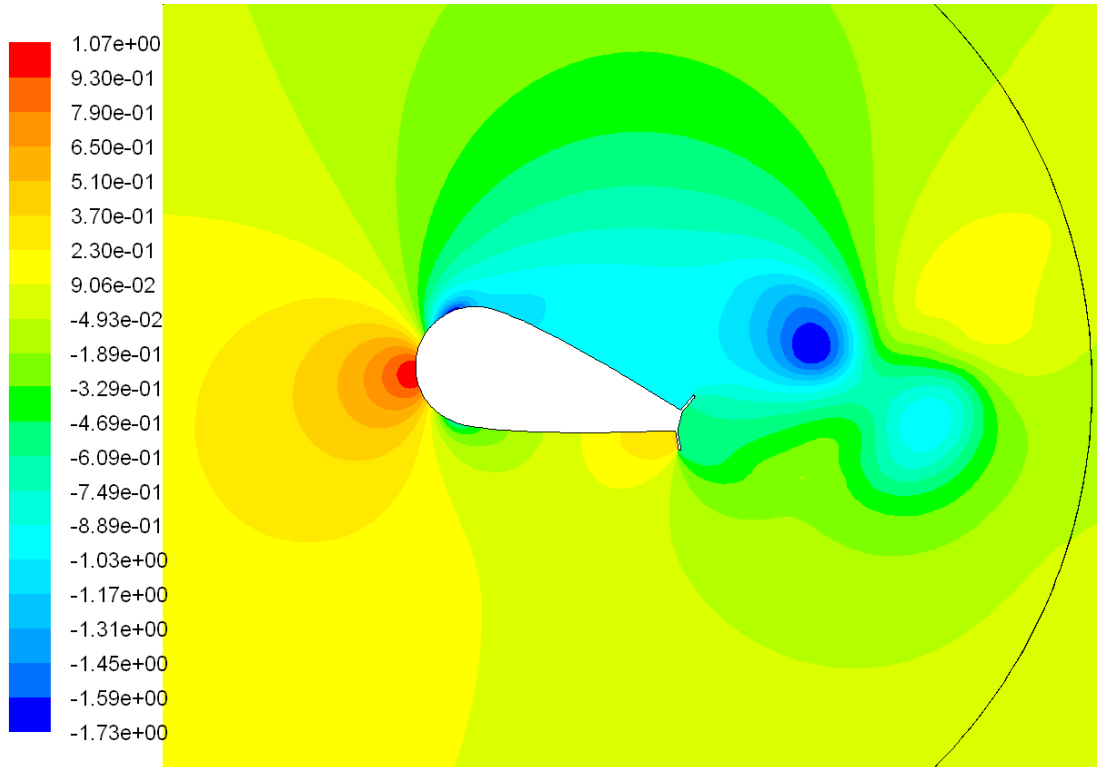


Figure A-76 Pressure Coefficient At 15°.

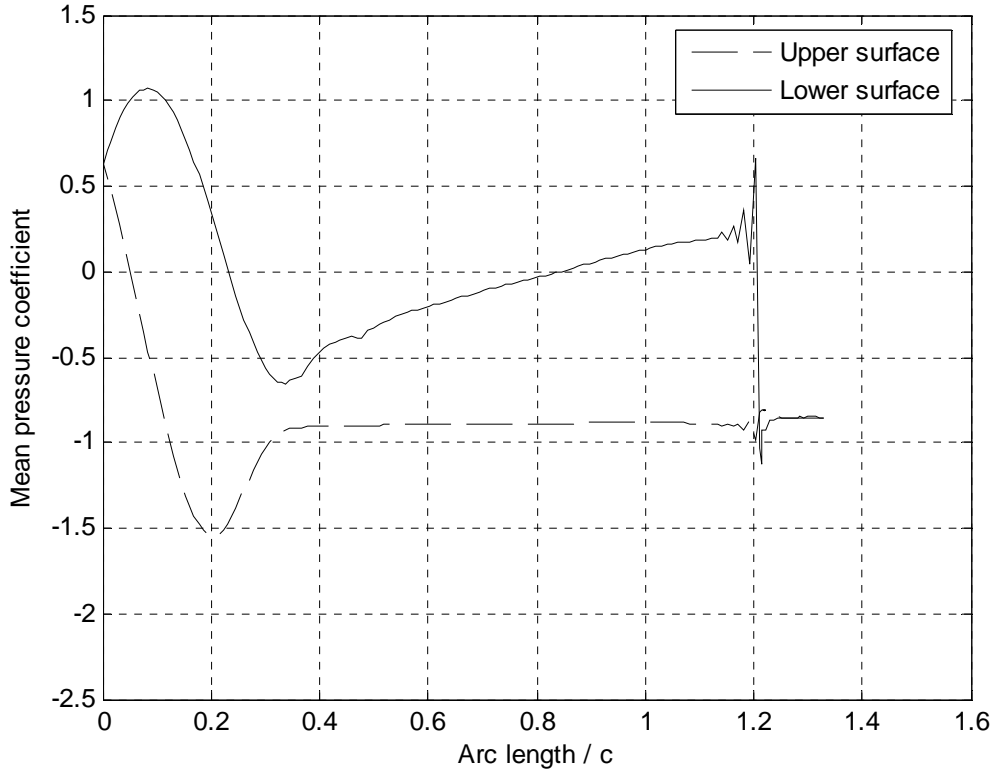


Figure A-77 Mean Pressure Coefficient Around The Fairing Surface At 15°.

Fairings Offset Table

NACA0070

X	Y	X	Y	X	Y	X	Y
0	0	22.0456	34.0815	63.8940	24.6149	99.7109	0.7818
0.0081	0.9336	22.9528	34.2941	64.7205	24.1839	99.8343	0.6089
0.0327	1.8669	23.8664	34.4776	65.5445	23.7482	99.9254	0.4169
0.0741	2.7995	24.7851	34.6326	66.3662	23.3079	99.9811	0.2118
0.1327	3.7313	25.7081	34.7597	67.1854	22.8631	100.0000	0
0.2090	4.6618	26.6344	34.8599	68.0023	22.4140		
0.3030	5.5906	27.5632	34.9338	68.8167	21.9606		
0.4153	6.5174	28.4937	34.9825	69.6288	21.5030		
0.5461	7.4418	29.4251	35.0068	70.4386	21.0413		
0.6958	8.3632	30.3568	35.0075	71.2462	20.5757		
0.8646	9.2814	31.2882	34.9858	72.0515	20.1061		
1.0531	10.1957	32.2189	34.9425	72.8545	19.6326		
1.2613	11.1057	33.1484	34.8784	73.6553	19.1553		
1.4897	12.0108	34.0763	34.7944	74.4539	18.6744		
1.7386	12.9105	35.0023	34.6915	75.2502	18.1897		
2.0081	13.8041	35.9263	34.5704	76.0444	17.7015		
2.2987	14.6912	36.8477	34.4320	76.8364	17.2097		
2.6106	15.5709	37.7664	34.2769	77.6262	16.7144		
2.9440	16.4426	38.6825	34.1063	78.4138	16.2157		
3.2994	17.3057	39.5955	33.9204	79.1993	15.7134		
3.6769	18.1592	40.5056	33.7201	79.9825	15.2078		
4.0766	19.0025	41.4124	33.5062	80.7636	14.6988		
4.4992	19.8346	42.3162	33.2790	81.5426	14.1865		
4.9443	20.6547	43.2167	33.0393	82.3193	13.6710		
5.4125	21.4619	44.1139	32.7876	83.0939	13.1521		
5.9037	22.2551	45.0078	32.5245	83.8663	12.6299		
6.4183	23.0334	45.8985	32.2505	84.6365	12.1045		
6.9561	23.7958	46.7859	31.9659	85.4044	11.5759		
7.5171	24.5411	47.6701	31.6714	86.1703	11.0441		
8.1016	25.2682	48.5509	31.3672	86.9338	10.5091		
8.7090	25.9760	49.4287	31.0538	87.6952	9.9709		
9.3395	26.6633	50.3031	30.7316	88.4542	9.4295		
9.9928	27.3290	51.1744	30.4009	89.2110	8.8849		
10.6683	27.9719	52.0427	30.0621	89.9657	8.3373		
11.3657	28.5909	52.9078	29.7155	90.7178	7.7864		
12.0846	29.1849	53.7698	29.3613	91.4678	7.2324		
12.8240	29.7529	54.6290	29.0000	92.2154	6.6752		
13.5833	30.2938	55.4852	28.6317	92.9607	6.1149		
14.3616	30.8069	56.3383	28.2567	93.7037	5.5514		
15.1581	31.2912	57.1887	27.8751	94.4442	4.9848		
15.9717	31.7462	58.0364	27.4875	95.1823	4.4151		
16.8012	32.1712	58.8812	27.0937	95.9179	3.8421		
17.6455	32.5660	59.7232	26.6941	96.6511	3.2661		
18.5033	32.9303	60.5626	26.2889	97.3819	2.6869		
19.3735	33.2638	61.3994	25.8782	98.1101	2.1045		
20.2548	33.5667	62.2335	25.4621	98.8358	1.5189		
21.1459	33.8391	63.0650	25.0410	99.5590	0.9302		

Short Faring

X	Y	X	Y	X	Y	X	Y
0	0	16.4388	28.8300	49.6219	29.3655	88.9625	0.5000
0.0075	0.7085	17.0524	29.1844	50.2394	29.0180	89.7418	0.5000
0.0300	1.4167	17.6733	29.5257	50.8494	28.6575	90.4840	0.5000
0.0674	2.1243	18.3014	29.8538	51.4516	28.2841	91.1909	0.5000
0.1198	2.8310	18.9362	30.1686	52.0458	27.8981	91.8641	0.5000
0.1872	3.5363	19.5775	30.4699	52.6317	27.4996	92.5052	0.5000
0.2694	4.2401	20.2251	30.7575	53.2090	27.0888	93.1159	0.5000
0.3665	4.9420	20.8786	31.0314	53.7776	26.6659	93.6974	0.5000
0.4785	5.6417	21.5377	31.2914	54.3370	26.2311	94.2512	0.5000
0.6052	6.3388	22.2022	31.5374	54.8871	25.7845	94.7787	0.5000
0.7466	7.0331	22.8718	31.7693	55.4277	25.3264	95.2811	0.5000
0.9027	7.7243	23.5461	31.9870	55.9585	24.8569	95.7595	0.5000
1.0733	8.4120	24.2248	32.1904	56.4792	24.3764	96.2152	0.5000
1.2585	9.0960	24.9077	32.3794	57.3399	23.5805	96.6491	0.5000
1.4581	9.7758	25.5945	32.5538	58.2006	22.7846	97.0624	0.5000
1.6720	10.4514	26.2848	32.7138	59.0613	21.9887	97.4560	0.5000
1.9002	11.1222	26.9783	32.8591	59.9219	21.1929	97.8309	0.5000
2.1425	11.7880	27.6747	32.9896	60.7826	20.3970	98.1879	0.5000
2.3988	12.4486	28.3738	33.1055	61.6433	19.6011	98.5279	0.5000
2.6691	13.1036	29.0751	33.2065	62.5040	18.8052	98.8517	0.5000
2.9531	13.7528	29.7784	33.2926	63.3647	18.0093	99.1601	0.5000
3.2508	14.3958	30.4834	33.3639	64.2254	17.2135	99.4539	0.5000
3.5621	15.0323	31.1897	33.4202	65.0861	16.4176	99.7336	0.5000
3.8867	15.6622	31.8971	33.4616	65.9468	15.6217	100.0000	0.5000
4.2246	16.2850	32.6052	33.4880	66.8075	14.8258	100.0000	0.4500
4.5756	16.9005	33.3136	33.4995	67.6682	14.0299	100.0000	0.4000
4.9395	17.5085	34.0222	33.4959	68.5289	13.2341	100.0000	0.3500
5.3162	18.1087	34.7305	33.4774	69.3896	12.4382	100.0000	0.3000
5.7055	18.7007	35.4383	33.4439	70.2503	11.6423	100.0000	0.2500
6.1072	19.2844	36.1452	33.3954	71.1110	10.8464	100.0000	0.2000
6.5212	19.8594	36.8510	33.3320	71.9717	10.0506	100.0000	0.1500
6.9473	20.4256	37.5552	33.2537	72.8324	9.2547	100.0000	0.1000
7.3853	20.9826	38.2576	33.1604	73.6931	8.4588	100.0000	0.0500
7.8349	21.5302	38.9579	33.0524	74.5538	7.6629	100.0000	0
8.2960	22.0683	39.6557	32.9296	75.4144	6.8670		
8.7684	22.5964	40.3508	32.7920	76.2751	6.0712		
9.2518	23.1144	41.0429	32.6398	77.1358	5.2753		
9.7461	23.6221	41.7315	32.4729	77.9965	4.4794		
10.2511	24.1192	42.4165	32.2916	78.8572	3.6835		
10.7664	24.6055	43.0975	32.0958	79.7179	2.8876		
11.2919	25.0809	43.7741	31.8856	80.5786	2.0918		
11.8273	25.5450	44.4462	31.6612	81.4393	1.2959		
12.3724	25.9976	45.1134	31.4226	82.3000	0.5000		
12.9270	26.4387	45.7754	31.1699	83.3966	0.5000		
13.4908	26.8679	46.4319	30.9033	84.4409	0.5000		
14.0635	27.2851	47.0826	30.6229	85.4356	0.5000		
14.6450	27.6900	47.7273	30.3288	86.3828	0.5000		
15.2348	28.0826	48.3656	30.0211	87.2850	0.5000		
15.8329	28.4627	48.9972	29.7000	88.1442	0.5000		

Guide Vane

X	Y
0	0
0.0065	0.6577
0.0258	1.3152
0.0581	1.9722
0.1033	2.6284
0.1613	3.2836
0.2322	3.9375
0.3159	4.5899
0.4124	5.2406
0.5217	5.8892
0.6437	6.5355
0.7783	7.1794
0.9256	7.8204
1.0854	8.4585
1.2577	9.0933
1.4425	9.7245
1.6396	10.3521
1.8490	10.9756
2.0706	11.5949
2.3043	12.2098
2.5500	12.8199
2.8077	13.4251
3.0772	14.0251
3.3584	14.6197
3.6513	15.2087
3.9556	15.7918
4.2714	16.3688
4.5984	16.9395
4.9366	17.5037
5.2857	18.0611
5.6458	18.6116
6.0166	19.1549
6.3979	19.6908
6.7898	20.2191
7.1919	20.7396
7.6041	21.2522
8.0264	21.7565
8.4585	22.2525
8.9002	22.7398
9.3514	23.2184
9.8119	23.6881
10.2816	24.1486
10.7602	24.5998
11.2475	25.0415
11.7435	25.4736
12.2478	25.8959
12.7604	26.3081
13.2809	26.7102
13.8092	27.1021

X	Y
14.3451	27.4834
14.8884	27.8542
15.4389	28.2143
15.9963	28.5634
16.5605	28.9016
17.1312	29.2286
17.7082	29.5444
18.2913	29.8487
18.8803	30.1416
19.4749	30.4228
20.0749	30.6923
20.6801	30.9500
21.2902	31.1957
21.9051	31.4294
22.5244	31.6510
23.1479	31.8604
23.7755	32.0575
24.4067	32.2423
25.0415	32.4146
25.6796	32.5744
26.3206	32.7217
26.9645	32.8563
27.6108	32.9783
28.2594	33.0876
28.9101	33.1841
29.5625	33.2678
30.2164	33.3387
30.8716	33.3967
31.5278	33.4419
32.1848	33.4742
32.8423	33.4935
33.5000	33.5000
34.6083	33.3833
35.7167	33.2667
36.8250	33.1500
37.9333	33.0333
39.0417	32.9167
40.1500	32.8000
41.2583	32.6833
42.3667	32.5667
43.4750	32.4500
44.5833	32.3333
45.6917	32.2167
46.8000	32.1000
47.9083	31.9833
49.0167	31.8667
50.1250	31.7500
51.2333	31.6333
52.3417	31.5167

X	Y
53.4500	31.4000
54.5583	31.2833
55.6667	31.1667
56.7750	31.0500
57.8833	30.9333
58.9917	30.8167
60.1000	30.7000
61.2083	30.5833
62.3167	30.4667
63.4250	30.3500
64.5333	30.2333
65.6417	30.1167
66.7500	30.0000
67.8583	29.8833
68.9667	29.7667
70.0750	29.6500
71.1833	29.5333
72.2917	29.4167
73.4000	29.3000
74.5083	29.1833
75.6167	29.0667
76.7250	28.9500
77.8333	28.8333
78.9417	28.7167
80.0500	28.6000
81.1583	28.4833
82.2667	28.3667
83.3750	28.2500
84.4833	28.1333
85.5917	28.0167
86.7000	27.9000
87.8083	27.7833
88.9167	27.6667
90.0250	27.5500
91.1333	27.4333
92.2417	27.3167
93.3500	27.2000
94.4583	27.0833
95.5667	26.9667
96.6750	26.8500
97.7833	26.7333
98.8917	26.6167
100.0000	26.5000
100.0000	25.8375
100.0000	25.1750
100.0000	24.5125
100.0000	23.8500
100.0000	23.1875
100.0000	22.5250

X	Y
100.0000	21.8625
100.0000	21.2000
100.0000	20.5375
100.0000	19.8750
100.0000	19.2125
100.0000	18.5500
100.0000	17.8875
100.0000	17.2250
100.0000	16.5625
100.0000	15.9000
100.0000	15.2375
100.0000	14.5750
100.0000	13.9125
100.0000	13.2500
100.0000	12.5875
100.0000	11.9250
100.0000	11.2625
100.0000	10.6000
100.0000	9.9375
100.0000	9.2750
100.0000	8.6125
100.0000	7.9500
100.0000	7.2875
100.0000	6.6250
100.0000	5.9625
100.0000	5.3000
100.0000	4.6375
100.0000	3.9750
100.0000	3.3125
100.0000	2.6500
100.0000	1.9875
100.0000	1.3250
100.0000	0.6625
100.0000	0

Exxon's Fairing without Fin

X	Y	X	Y	X	Y	X	Y
0	0	25.6238	21.8224	62.5408	14.4647	97.8433	4.1865
0.0138	0.7799	26.3991	21.7365	63.2692	14.2839	98.5622	3.9710
0.0552	1.5588	27.1744	21.6506	63.9975	14.1030	99.2811	3.7555
0.1241	2.3358	27.9497	21.5647	64.7259	13.9222	100.0000	3.5400
0.2204	3.1098	28.7250	21.4788	65.4543	13.7413	100.0000	3.1860
0.3440	3.8799	29.5003	21.3929	66.1827	13.5605	100.0000	2.8320
0.4949	4.6452	30.2756	21.3070	66.9111	13.3796	100.0000	2.4780
0.6726	5.4047	31.0510	21.2211	67.6394	13.1988	100.0000	2.1240
0.8772	6.1574	31.8263	21.1352	68.3678	13.0179	100.0000	1.7700
1.1082	6.9024	32.6016	21.0493	69.0876	12.8059	100.0000	1.4160
1.3654	7.6388	33.3769	20.9634	69.8065	12.5904	100.0000	1.0620
1.6486	8.3656	34.1522	20.8775	70.5254	12.3749	100.0000	0.7080
1.9572	9.0820	34.9170	20.7256	71.2443	12.1594	100.0000	0.3540
2.2910	9.7869	35.6809	20.5675	71.9632	11.9439	100.0000	0
2.6495	10.4797	36.4447	20.4093	72.6821	11.7284		
3.0323	11.1593	37.2085	20.2511	73.4010	11.5130		
3.4389	11.8250	37.9724	20.0929	74.1199	11.2975		
3.8688	12.4758	38.7362	19.9347	74.8388	11.0820		
4.3214	13.1111	39.5001	19.7765	75.5577	10.8665		
4.7962	13.7299	40.2639	19.6183	76.2766	10.6510		
5.2926	14.3316	41.0277	19.4601	76.9955	10.4355		
5.8100	14.9153	41.7916	19.3019	77.7143	10.2200		
6.3477	15.4803	42.5554	19.1437	78.4332	10.0046		
6.9051	16.0260	43.3193	18.9855	79.1521	9.7891		
7.4814	16.5517	44.0831	18.8273	79.8710	9.5736		
8.0759	17.0566	44.8470	18.6692	80.5899	9.3581		
8.6879	17.5402	45.6108	18.5110	81.3088	9.1426		
9.3167	18.0018	46.3746	18.3528	82.0277	8.9271		
9.9613	18.4409	47.1385	18.1946	82.7466	8.7116		
10.6211	18.8569	47.9023	18.0364	83.4655	8.4962		
11.2952	19.2494	48.6662	17.8782	84.1844	8.2807		
11.9828	19.6177	49.4300	17.7200	84.9033	8.0652		
12.6830	19.9615	50.1584	17.5392	85.6222	7.8497		
13.3948	20.2803	50.8868	17.3583	86.3411	7.6342		
14.1175	20.5737	51.6151	17.1775	87.0599	7.4187		
14.8502	20.8414	52.3435	16.9966	87.7788	7.2033		
15.5918	21.0830	53.0719	16.8158	88.4977	6.9878		
16.3416	21.2983	53.8003	16.6349	89.2166	6.7723		
17.0984	21.4868	54.5286	16.4541	89.9355	6.5568		
17.8615	21.6485	55.2570	16.2732	90.6544	6.3413		
18.6298	21.7831	55.9854	16.0924	91.3733	6.1258		
19.4024	21.8905	56.7138	15.9115	92.0922	5.9103		
20.1783	21.9704	57.4421	15.7307	92.8111	5.6949		
20.9565	22.0229	58.1705	15.5498	93.5300	5.4794		
21.7361	22.0478	58.8989	15.3690	94.2489	5.2639		
22.5162	22.0500	59.6273	15.1881	94.9678	5.0484		
23.2962	22.0500	60.3557	15.0073	95.6866	4.8329		
24.0732	21.9942	61.0840	14.8264	96.4055	4.6174		
24.8485	21.9083	61.8124	14.6456	97.1244	4.4019		

Exxon's Fairing with Fin (3%*c*)

X	Y	X	Y	X	Y	X	Y
0	0	26.3899	21.7376	78.3949	10.0717	100.7637	5.1708
0.0134	0.7695	27.4725	21.6176	79.4399	9.7643	100.4806	4.5662
0.0537	1.5381	28.5552	21.4977	80.4849	9.4569	100.1975	3.9617
0.1208	2.3049	29.6378	21.3777	81.5299	9.1495	100.0000	3.3380
0.2146	3.0688	30.7205	21.2577	82.5749	8.8421	100.0000	2.6704
0.3350	3.8289	31.8031	21.1378	83.6199	8.5347	100.0000	2.0028
0.4818	4.5845	32.8858	21.0178	84.6649	8.2273	100.0000	1.3352
0.6550	5.3344	33.9684	20.8979	85.7099	7.9199	100.0000	0.6676
0.8542	6.0778	35.0388	20.7004	86.7549	7.6126	100.0000	0
1.0792	6.8138	36.1054	20.4795	87.8000	7.3052		
1.3298	7.5415	37.1721	20.2586	88.8450	6.9978		
1.6056	8.2601	38.2387	20.0377	89.8900	6.6904		
1.9063	8.9685	39.3054	19.8168	90.9350	6.3830		
2.2316	9.6661	40.3720	19.5959	91.9800	6.0756		
2.5810	10.3518	41.4387	19.3750	93.0250	5.7682		
2.9541	11.0250	42.5053	19.1541	94.0700	5.4608		
3.3505	11.6847	43.5720	18.9332	95.1150	5.1534		
3.7697	12.3302	44.6386	18.7123	96.1600	4.8460		
4.2112	12.9607	45.7052	18.4914	96.7680	4.6672		
4.6744	13.5753	46.7719	18.2705	97.3760	4.4883		
5.1587	14.1735	47.8385	18.0496	97.9840	4.3095		
5.6637	14.7543	48.9052	17.8287	98.5919	4.1306		
6.1886	15.3172	49.9670	17.5867	99.1999	3.9518		
6.7328	15.8614	51.0242	17.3242	99.4918	4.4758		
7.2957	16.3863	52.0814	17.0617	99.7613	5.0493		
7.8765	16.8913	53.1386	16.7992	100.0309	5.6229		
8.4747	17.3756	54.1957	16.5367	100.3004	6.1964		
9.0893	17.8388	55.2529	16.2742	100.5700	6.7700		
9.7198	18.2803	56.3101	16.0117	100.5983	6.7555		
10.3653	18.6995	57.3673	15.7493	100.6274	6.7405		
11.0250	19.0959	58.4245	15.4868	100.6574	6.7251		
11.6982	19.4690	59.4816	15.2243	100.6883	6.7093		
12.3839	19.8184	60.5388	14.9618	100.7202	6.6929		
13.0815	20.1437	61.5960	14.6993	100.7530	6.6761		
13.7899	20.4444	62.6532	14.4368	100.7867	6.6588		
14.5085	20.7202	63.7104	14.1743	100.8215	6.6409		
15.2362	20.9708	64.7675	13.9118	100.8573	6.6225		
15.9722	21.1958	65.8247	13.6494	100.8942	6.6036		
16.7156	21.3950	66.8819	13.3869	100.9323	6.5841		
17.4655	21.5682	67.9391	13.1244	100.9714	6.5640		
18.2211	21.7150	68.9898	12.8383	101.0117	6.5433		
18.9812	21.8354	70.0349	12.5309	101.0533	6.5220		
19.7451	21.9292	71.0799	12.2235	101.0961	6.5001		
20.5119	21.9963	72.1249	11.9161	101.1401	6.4774		
21.2805	22.0366	73.1699	11.6087	101.1855	6.4541		
22.0500	22.0500	74.2149	11.3013	101.2323	6.4302		
23.1393	22.0500	75.2599	10.9939	101.2804	6.4055		
24.2246	21.9775	76.3049	10.6865	101.3300	6.3800		
25.3072	21.8575	77.3499	10.3791	101.0469	5.7754		

Exxon's Fairing with Fin (5%c)

X	Y	X	Y	X	Y	X	Y
0	0	26.2075	21.7578	76.0629	10.7577	101.4752	6.6831
0.0134	0.7695	27.2446	21.6429	77.0639	10.4632	101.1028	5.8896
0.0537	1.5381	28.2817	21.5280	78.0649	10.1688	100.7304	5.0962
0.1208	2.3049	29.3187	21.4131	79.0659	9.8743	100.3580	4.3027
0.2146	3.0688	30.3558	21.2981	80.0669	9.5799	100.0000	3.5060
0.3350	3.8289	31.3929	21.1832	81.0679	9.2854	100.0000	2.6295
0.4818	4.5845	32.4299	21.0683	82.0689	8.9910	100.0000	1.7530
0.6550	5.3344	33.4670	20.9534	83.0699	8.6965	100.0000	0.8765
0.8542	6.0778	34.4999	20.8120	84.0709	8.4021	100.0000	0
1.0792	6.8138	35.5216	20.6004	85.0720	8.1076		
1.3298	7.5415	36.5433	20.3888	86.0730	7.8132		
1.6056	8.2601	37.5651	20.1772	87.0740	7.5187		
1.9063	8.9685	38.5868	19.9656	88.0750	7.2243		
2.2316	9.6661	39.6085	19.7540	89.0760	6.9298		
2.5810	10.3518	40.6303	19.5424	90.0770	6.6354		
2.9541	11.0250	41.6520	19.3308	91.0780	6.3409		
3.3505	11.6847	42.6737	19.1192	92.0790	6.0465		
3.7697	12.3302	43.6955	18.9076	93.0800	5.7520		
4.2112	12.9607	44.7172	18.6960	94.1964	5.4236		
4.6744	13.5753	45.7389	18.4844	95.3128	5.0952		
5.1587	14.1735	46.7607	18.2728	96.4292	4.7668		
5.6637	14.7543	47.7824	18.0612	97.5456	4.4384		
6.1886	15.3172	48.8041	17.8496	98.6620	4.1100		
6.7328	15.8614	49.8224	17.6226	99.4789	4.4478		
7.2957	16.3863	50.8350	17.3711	99.9741	5.5009		
7.8765	16.8913	51.8477	17.1197	100.4694	6.5539		
8.4747	17.3756	52.8604	16.8683	100.9647	7.6070		
9.0893	17.8388	53.8730	16.6168	101.4600	8.6600		
9.7198	18.2803	54.8857	16.3654	101.4883	8.6455		
10.3653	18.6995	55.8984	16.1140	101.5174	8.6305		
11.0250	19.0959	56.9110	15.8625	101.5474	8.6151		
11.6982	19.4690	57.9237	15.6111	101.5783	8.5993		
12.3839	19.8184	58.9364	15.3597	101.6102	8.5829		
13.0815	20.1437	59.9490	15.1082	101.6430	8.5661		
13.7899	20.4444	60.9617	14.8568	101.6767	8.5488		
14.5085	20.7202	61.9744	14.6054	101.7115	8.5309		
15.2362	20.9708	62.9870	14.3539	101.7473	8.5125		
15.9722	21.1958	63.9997	14.1025	101.7842	8.4936		
16.7156	21.3950	65.0124	13.8510	101.8223	8.4741		
17.4655	21.5682	66.0250	13.5996	101.8614	8.4540		
18.2211	21.7150	67.0377	13.3482	101.9017	8.4333		
18.9812	21.8354	68.0504	13.0967	101.9433	8.4120		
19.7451	21.9292	69.0559	12.8188	101.9861	8.3901		
20.5119	21.9963	70.0569	12.5244	102.0301	8.3674		
21.2805	22.0366	71.0579	12.2299	102.0755	8.3441		
22.0500	22.0500	72.0589	11.9355	102.1223	8.3202		
23.0934	22.0500	73.0599	11.6410	102.1704	8.2955		
24.1334	21.9876	74.0609	11.3466	102.2200	8.2700		
25.1705	21.8727	75.0619	11.0521	101.8476	7.4765		

Exxon's Fairing with Fin (7%*c*)

X	Y	X	Y	X	Y	X	Y
0	0	26.1163	21.7679	74.8969	11.1007	102.9636	10.2341
0.0134	0.7695	27.1306	21.6555	75.8759	10.8127	103.0110	10.2102
0.0537	1.5381	28.1449	21.5431	76.8549	10.5247	103.0598	10.1855
0.1208	2.3049	29.1592	21.4307	77.8339	10.2367	103.1100	10.1600
0.2146	3.0688	30.1735	21.3183	78.8129	9.9487	102.8023	9.5051
0.3350	3.8289	31.1877	21.2060	79.7919	9.6608	102.4946	8.8501
0.4818	4.5845	32.2020	21.0936	80.7709	9.3728	102.1870	8.1952
0.6550	5.3344	33.2163	20.9812	81.7499	9.0848	101.8793	7.5403
0.8542	6.0778	34.2304	20.8678	82.7289	8.7968	101.5716	6.8853
1.0792	6.8138	35.2297	20.6609	83.7080	8.5088	101.2639	6.2304
1.3298	7.5415	36.2290	20.4539	84.6870	8.2209	100.9562	5.5754
1.6056	8.2601	37.2282	20.2470	85.6660	7.9329	100.6485	4.9205
1.9063	8.9685	38.2275	20.0400	86.6450	7.6449	100.3409	4.2656
2.2316	9.6661	39.2268	19.8331	87.6240	7.3569	100.0332	3.6106
2.5810	10.3518	40.2261	19.6261	88.6030	7.0689	100.0000	2.8944
2.9541	11.0250	41.2253	19.4192	89.5820	6.7810	100.0000	2.1708
3.3505	11.6847	42.2246	19.2122	90.5610	6.4930	100.0000	1.4472
3.7697	12.3302	43.2239	19.0053	91.5400	6.2050	100.0000	0.7236
4.2112	12.9607	44.2232	18.7983	92.5203	5.9166	100.0000	0
4.6744	13.5753	45.2225	18.5914	93.5005	5.6283		
5.1587	14.1735	46.2217	18.3844	94.4808	5.3399		
5.6637	14.7543	47.2210	18.1775	95.4611	5.0516		
6.1886	15.3172	48.2203	17.9705	96.4414	4.7632		
6.7328	15.8614	49.2196	17.7636	97.4216	4.4749		
7.2957	16.3863	50.2118	17.5259	98.4019	4.1865		
7.8765	16.8913	51.2023	17.2800	99.3029	4.0742		
8.4747	17.3756	52.1927	17.0341	99.7368	4.9993		
9.0893	17.8388	53.1831	16.7881	100.1707	5.9244		
9.7198	18.2803	54.1735	16.5422	100.6045	6.8495		
10.3653	18.6995	55.1639	16.2963	101.0384	7.7746		
11.0250	19.0959	56.1543	16.0504	101.4723	8.6998		
11.6982	19.4690	57.1447	15.8045	101.9061	9.6249		
12.3839	19.8184	58.1351	15.5586	102.3400	10.5500		
13.0815	20.1437	59.1255	15.3127	102.3687	10.5355		
13.7899	20.4444	60.1160	15.0668	102.3982	10.5205		
14.5085	20.7202	61.1064	14.8209	102.4286	10.5051		
15.2362	20.9708	62.0968	14.5750	102.4599	10.4893		
15.9722	21.1958	63.0872	14.3291	102.4921	10.4729		
16.7156	21.3950	64.0776	14.0831	102.5254	10.4561		
17.4655	21.5682	65.0680	13.8372	102.5596	10.4388		
18.2211	21.7150	66.0584	13.5913	102.5948	10.4209		
18.9812	21.8354	67.0488	13.3454	102.6311	10.4025		
19.7451	21.9292	68.0392	13.0995	102.6685	10.3836		
20.5119	21.9963	69.0229	12.8285	102.7070	10.3641		
21.2805	22.0366	70.0019	12.5406	102.7467	10.3440		
22.0500	22.0500	70.9809	12.2526	102.7875	10.3233		
23.0705	22.0500	71.9599	11.9646	102.8296	10.3020		
24.0878	21.9926	72.9389	11.6766	102.8730	10.2801		
25.1021	21.8802	73.9179	11.3886	102.9176	10.2574		

